Cromb, Marion (2023) *Quantum effects and novel physics in rotating frames.* PhD thesis.

https://theses.gla.ac.uk/83438/

Quantum Effects and Novel Physics in Rotating Frames

Marion Cromb

Submitted in fulfilment of the requirements for the
Degree of Doctor of Philosophy

School of Physics and Astronomy
College of Science and Engineering
University of Glasgow

February 2023

Abstract

The birth of quantum physics and general relativity were two revolutions in physics. But a century later, scientists have not yet united the two theories. Attempts to combine them are mostly theoretical; controlled experiments have historically been neglected due to the comparative weakness of gravity and the corresponding precision or extreme scales assumed needed to test quantum gravity effects.

We take a new approach, inspired by Einstein's equivalence of gravitational fields and accelerated frames. Non-inertial frames can be controlled in the lab, and allows us to experimentally test new frame-dependent effects *and* already-established quantum effects in new regimes. This frame-dependence is fundamentally interesting by itself, but also provides parallels to curved spacetime effects. To that effect, I have carried out experiments in rotating frames and shown new effects.

I have combined mechanical rotation with acoustics, sending sound waves through a rotating absorber. With this, I was the first to show experimental proof of the Zel'dovich effect: the amplification of waves carrying angular momentum by a rotating object. It is theorised the Zel'dovich effect should also generate *electromagnetic* waves out of the quantum vacuum, however the conditions are much harder to meet.

I have also done optics experiments to show how rotation can affect quantum entanglement. The Hong-Ou-Mandel effect was used as a witness for antisymmetric entanglement between photons. The symmetry of frequency entangled photon pairs can be manipulated by introducing path superpositions and controlling their phase difference. Through experiment I established that to witness antisymmetry with the Hong-Ou-Mandel effect it was much easier in the regime where the superposed paths had path length differences outwith the single-photon coherence length. Within a rotating frame, a rotation-dependent phase difference between counterpropagating beams of light appears, called the Sagnac effect. Combining Sagnac interferometers with a Hong-Ou-Mandel interferometer on a rotating platform, I have shown how rotation can control the entanglement symmetry of photon pairs.

The success of these experiments can be built on in future experiments exploring quantum effects in rotating frames and curved spacetimes. Identifying these effects has relevance in fundamental physics and to new technologies e.g. quantum communication, as it scales up to satellites in the curved spacetime around the rotating Earth.

Contents

List of Figures

Abbreviations

BBO beta barium borate.

COW Colella-Overhauser-Werner.

CW continuous-wave.

EM electromagnetic.

FWHM full-width-half-maximum.

GPS Global Positioning System.

GR general relativity.

GVM group velocity mismatch.

HOM Hong-Ou-Mandel (Section 3.1.3).

IOP Institute of Physics.

LCR liquid crystal retarder.

OAM orbital angular momentum.

OCT optical coherence tomography.

PMF polarisation-maintaining fibre.

Q-OCT quantum OCT.

QFT quantum field theory.

QFT/CS quantum field theory in curved spacetime.

QM quantum mechanics.

SLM spatial light modulator.

SNR signal-to-noise ratio.

SPADs single-photon avalanche diodes.

SPDC spontaneous parametric down-conversion (Section 3.1.2).

Acknowledgements

Thanks firstly to myself. I literally couldn't have done it without me. Thanks also to my un-earned white, English-as-a-first-language-speaking, middle-class privilege, without which life (dossing around with lasers for below-minimum wage) would have been a lot harder. There are many people pushed out of physics and academia through no fault of their own, I have had some protection from that.

Thanks to my family for their support. To the cats, for their lifetimes of service (cuddles).

Thanks to my friends, especially to those who bother to feign interest in my work, and the ones who keep me social.

Thanks to my supervisor Daniele Faccio, for enabling me to work on super interesting funda-mental physics problems, and the support, belief and advice over the years. An extra special thank you also for finding me an extra 6 months of money, to allow me to continue work in the group and complete my PhD without having to get a 'proper job' when a funded PhD extension to make up for months of disruption due to the pandemic was refused for inane bureaucratic reasons (yes I'm still bitter about it okay).

Thanks to my second supervisor Sonja Franke-Arnold for time spent proof-reading.

Thanks to Meraj Ahmad, for keeping me on track with thesis writing.

Thanks to my research group and my collaborators for their knowledge and wisdom. And also for when that knowledge is less than infinite, because it makes me feel less uniquely stupid when I realise that actually sometimes even the experts don't know, or disagree, because this is *research*.

Absolutely no thanks to the atmosphere of ever-rising moral-panic transphobia from the Brit-ish media. No thanks to COVID-19, or rather since a virus doesn't have a moral code and knows not what it does, no thanks particularly to the absolutely botched and late UK Gov-ernment response to a pandemic that lead to hundreds of thousands of unnecessary lives lost, and many more with long term health issues. And no thanks to the UK government response to anything else for that matter.

Hello to Jason Isaacs, down with the Nazis, and up with the workers and blue-haired feminists.

Declaration of Originality

I declare that, with the exception of Chapter 1, Section 2.1, Section 3.1, Section 4.1.1, Section 4.1.2, Section A1 and Section A2 which contain introductory material, and except where reference is made to the contribution of others, that this thesis is the result of my own work.

For example, the chapters in journal format (Chapter 2 and Chapter 4), the sections where the authors' versions of publications have been included (Section 2.2 and Section 4.2/Section 4.3), have been prefaced with a disclaimer stating the contribution of all named authors to the work. I confirm that my individual contribution to this work has been over 50%.

I declare that this thesis does not contain work submitted for any other degree at the University of Glasgow or any other institution.

Illustrations at the start of each chapter are copyright of the author.

Signature:
Printed Name: Marion Cromb

Date: 14/10/2022

List of Publications

The following is a list of papers I have written or contributed to during my PhD.

- [1] Marko Toroš, Sara Restuccia, Graham M. Gibson, <u>Marion Cromb</u>, Hendrik Ulbricht, Miles Padgett, and Daniele Faccio. 'Revealing and Concealing Entanglement with Noninertial Motion'. Physical Review A 101, no. 4 (April 2020): 043837. DOI: 10.1103/PhysRevA.101.043837.

- [2] <u>Marion Cromb</u>, Graham M. Gibson, Ermes Toninelli, Miles J. Padgett, Ewan M. Wright, and Daniele Faccio. 'Amplification of Waves from a Rotating Body'. Nature Physics, 22 June 2020. DOI:10.1038/s41567-020-0944-3.

- [3] <u>Marion Cromb</u>, Sara Restuccia, Graham M. Gibson, Marko Toros, Miles J. Padgett, and Daniele Faccio. 'Controlling Photon Entanglement with Mechanical Rotation'. arXiv, 11 October 2022. DOI: 10.48550/arXiv.2210.05628.

- [4] Marko Toroš, <u>Marion Cromb</u>, Mauro Paternostro, and Daniele Faccio. 'Generation of Entanglement from Mechanical Rotation'. Physical Review Letters, 21 December 2022. DOI: 10.1103/PhysRevLett.129.260401.

In this alternative format thesis, [2] and [3] have been reproduced within Chapter 2 and Chapter 4 respectively.

Note on the format of the thesis

This thesis contains two chapters that are in journal format: Section 2.2 (reproducing Ref. [2]) and Section 4.2/Section 4.3 (reproducing Ref. [3]). These have been included in the thesis with the same format as the rest of the thesis, and numbering of pages, references etc. are in sequence with the rest of the thesis. Part of the supplementary material of Ref. [3] has been moved to the Appendix (as Section A3) for improved readability, this is noted within the text.

Summary

Chapter 1: Introduction

The big-picture motivation is finding how can we unite quantum mechanics with general relativity. This chapter traces the history of these ideas, and gives broad context for the work.

Chapter 2: Amplification of Waves from a Rotating Body

This chapter relates the Zel'dovich effect (the amplification of waves with angular momentum from a rotating body) to ideas from quantum theory in curved spacetimes. Our work with acoustics shown here is the first experimental verification of this effect.

Chapter 3: Variations on the Hong-Ou-Mandel Effect

This chapter provides an introduction to the Hong-Ou-Mandel effect in photons, how it can be a witness for frequency entanglement, and how to do such an experiment is shown in practice.

Chapter 4: Controlling Entanglement with Rotation

This chapter introduces the Sagnac effect in a rotating frame, and describes how I have used it to control the symmetry of frequency-entangled photons, as witnessed by Hong-Ou-Mandel interference.

Chapter 5: Future Directions

This short chapter gives some ways in which the ideas in this thesis could be built upon in new experiments.

Chapter 6: Conclusions

The work presented, with its limitations and implications is summarised.

Appendix

Bonus content!

Physics of the future will hardly tolerate the strange and unsatisfactory division into quantum theory (microphysics that supervises nuclear phenomena) and the relativistic theory of gravitation that governed macroscopic bodies rather than individual atoms. Physics will not be divided into microscopic and cosmic physics - it should, and will, be united and undivided.

Matvei Petrovich Bronstein, 1930 [5, p. 89]

1

Introduction
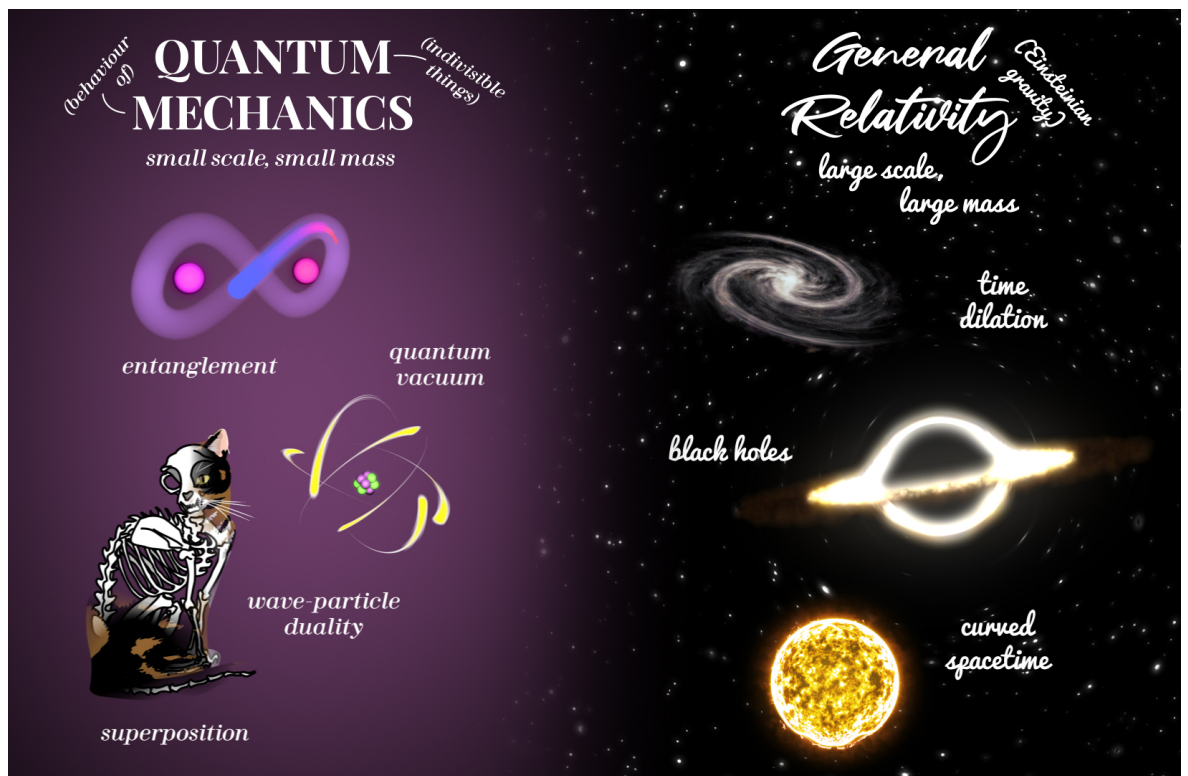
1.1 Revolutionary Physics: Quantum Physics and General Relativity

Around 100 years ago, there were two revolutions in our understanding of the physical universe. The theories of quantum physics and general relativity were born. These two pillars of modern physics have not yet crumbled, their predictions can be verified to staggering accuracy and remain our best methods to understand the nature of reality - within their respective realms.

1.1.1 Quantum Physics

Quantum theory initially emerged from an attempt to understand the measured spectrum of thermal radiation from a black body (a perfect absorber in thermal equilibrium). Classical theory predicted an 'ultraviolet catastrophe': that the energy emitted would become infinite at shorter wavelengths, something physically impossible. Failing to arrive at the correct spectrum with wave theories of radiation, in 1900 Max Planck conceptualised the black body as a cavity filled with hypothetical quantised oscillators. The energy of each individual oscillator could only take values that were integer multiples of a smallest energy quantum ϵ, proportional to the oscillator's frequency ν with a proportionality constant h: $\epsilon = h\nu$. This quantisation finally produced the correct spectrum of a body for its temperature. This hypothetical quantisation became more real when in 1905, Albert Einstein published an explanation of the photoelectric effect [6] that relied on light energy *truly* being carried in discrete quanta, with each packet (what we now call a photon) having an energy that was equal to its frequency ν multiplied by h.

Phenomenological quantum theory blossomed into quantum mechanics (QM) in the 1920s, with new mathematical models predicting and describing the behaviour of particles. The constant h became known as Planck's constant and is the fundamental physical constant at the heart of QM. It gives the proportionality between the momentum p and quantum wavelength λ of any particle: $\lambda = \frac{h}{p}$, underpinning the key quantum concept of wave-particle duality. It also provides the fundamental limit of precise knowledge of conjugate variables (such as position x and momentum p_x) in Werner Heisenberg's uncertainty principle:

$$\Delta x \Delta p_x \geq \frac{\hbar}{2} = \frac{h}{4\pi}. \tag{1.1}$$

These quantum aspects tend to manifest on the small scales of atoms or subatomic particles, or individual quanta of radiation (photons). Far beneath our everyday scale of solid matter, is a counter-intuitive quantum world. A world where particles can suddenly tunnel through walls, or be in a superposition of different states at the same time, or be entangled with another particle so that a measurement on one can affect the

outcome of a measurement of the other, no matter how far away [7, 8]. Nevertheless our precise understanding of these strange quantum effects now underpins much of the technology we take for granted everyday. Even the humble USB flash drive relies on quantum tunnelling!

As well as dealing with the quantum mechanical behaviour of light and matter, a quantum theory of fields and fundamental forces was also developed, quantum field theory (QFT). From this emerged the 'Standard Model' of physics, which covers three of the fundamental forces (electromagnetism as well as the strong and weak nuclear forces). However, it has so far been unable to incorporate the force of gravity.

1.1.2 General Relativity

To best understand gravity we must turn to Einstein's theory of general relativity (GR); gravity as the curvature of spacetime by matter and energy.

Principles of relativity have been around for a while. In the 1600s Galileo recognised that laws of motion (what we now refer to as Newtonian mechanics) would be the same in any inertial (non-accelerating) frame; he gives an example that if you were in a closed cabin in a uniformly moving ship, no amount of dropped objects, flying butterflies, etc would show that you were moving [9, p. 187].

In the late 1800s, extending this notion of relativity to electromagnetism was complicated by the assumed existence of the 'luminiferous aether'. The aether was a theorised medium considered essential to allow electromagnetic waves to propagate, just as mechanical waves required a medium. James Clerk Maxwell had shown that electromagnetic waves in empty space must travel at speed c, assuming this was a speed relative to the aether. This created a preferred frame for physics at which the aether was at rest. Experiments were set up to try and detect this aether, for example in 1887 Albert A. Michelson and Edward W. Morley tried to find a difference in the speed of light between a direction parallel to the Earth's movement through the stationary aether and a direction orthogonal to it. But whether the aether was proposed to be stationary or, when that hypothesis failed, dragged along with moving frames, the experiments gave null results [10, 11].

To protect the notion of the aether from the null result of the Michelson-Morley experiment among others, Hendrik Lorentz formulated the ideas of local time (time dilation) and length contraction along the direction of motion to ensure that observers moving relative to the aether make the same observations as an observer at rest [12]. To change variables between resting and moving frames required Lorentz transforms, given that name by Henri Poincaré who had incorporated them into his concepts of relativity [13].

This work by Lorentz and Poincaré meant, as Einstein himself noted, *"there is no doubt, that the special theory of relativity, if we regard its development in retrospect,*

was ripe for discovery in 1905." (Reprinted and translated in [14, p. 193]).[1] Neverthe-less, it was Einstein who got there first and properly brought electromagnetism into relativity by taking the speed of light c to be constant in all inertial frames; treating all inertial frames equally and dispatching with the 'superfluous' idea of the aether and its preferred aether reference frame:

> *Examples of [asymmetries in electromagnetic theory when applied to moving bodies], together with the unsuccessful attempts to discover any motion of the earth relatively to the "light medium," suggest that the phenomena of electrodynamics as well as of mechanics possess no properties corresponding to the idea of absolute rest. They suggest rather that [...] the same laws of electrodynamics and optics will be valid for all frames of reference for which the equations of mechanics hold good. We will raise this conjecture (the purport of which will hereafter be called the "Principle of Relativity") to the status of a postulate, and also introduce another postulate, which is only apparently irreconcilable with the former, namely, that light is always propagated in empty space with a definite velocity c which is independent of the state of motion of the emitting body. These two postulates suffice for the attainment of a simple and consistent theory of the electrodynamics of moving bodies based on Maxwell's theory for stationary bodies. The introduction of a "luminiferous ether" will prove to be superfluous inasmuch as the view here to be developed will not require an "absolutely stationary space" provided with special properties, nor assign a velocity-vector to a point of the empty space in which electromagnetic processes take place. ([15])*

The constant c is the characteristic constant of special relativity. At the time, it was just known as relativity, we now add the 'special' to refer to the fact it does not deal with gravity.[2]

Einstein then took the ideas of relativity further. In seeking a theory in which accelerating objects were subject to the same laws of physics as objects in non-inertial frames, incorporating the force of gravity by equating gravitational fields with non-inertial frames, and building on Hermann Minkowski's geometrical formulation of special relativity unifying space and time into a 4-dimensional spacetime [16], *general* relativity was quickly born. By 1915 Einstein had published his gravitational field equations [17], linking the structure of spacetime ($G_{\mu\nu}$) to the presence of matter and energy ($T_{\mu\nu}$):

$$G_{\mu\nu} = \frac{8\pi G}{c^4} T_{\mu\nu}, \tag{1.2}$$

where G is the constant of gravitation.[3]

---

[1]The idea that energy could also be seen as mass - perhaps the most famous equation associated with Einstein's special relativity $E = mc^2$ - was also forming within the wider physics community.

[2]Sometimes it is assumed that special relativity can only deal with inertial frames, this is a misconception, special relativity can deal with accelerated frames in flat 'Minkowski' spacetime perfectly well, albeit requiring curved co-ordinates to do so.

[3]We neglect the cosmological constant term $\Lambda g_{\mu\nu}$ which did not appear in Einstein's original equations, was put in by him in 1917, then removed again, then later added back in by cosmologists to explain the accelerating expansion of the universe [18]. It can generally be assumed to be zero under the scale of galaxies.
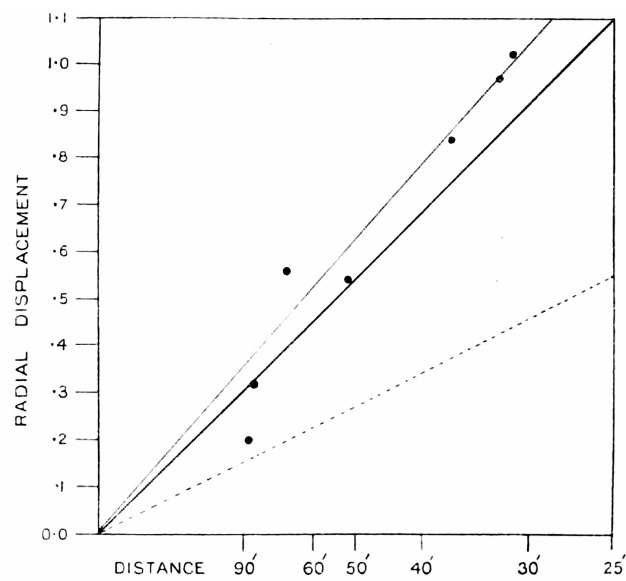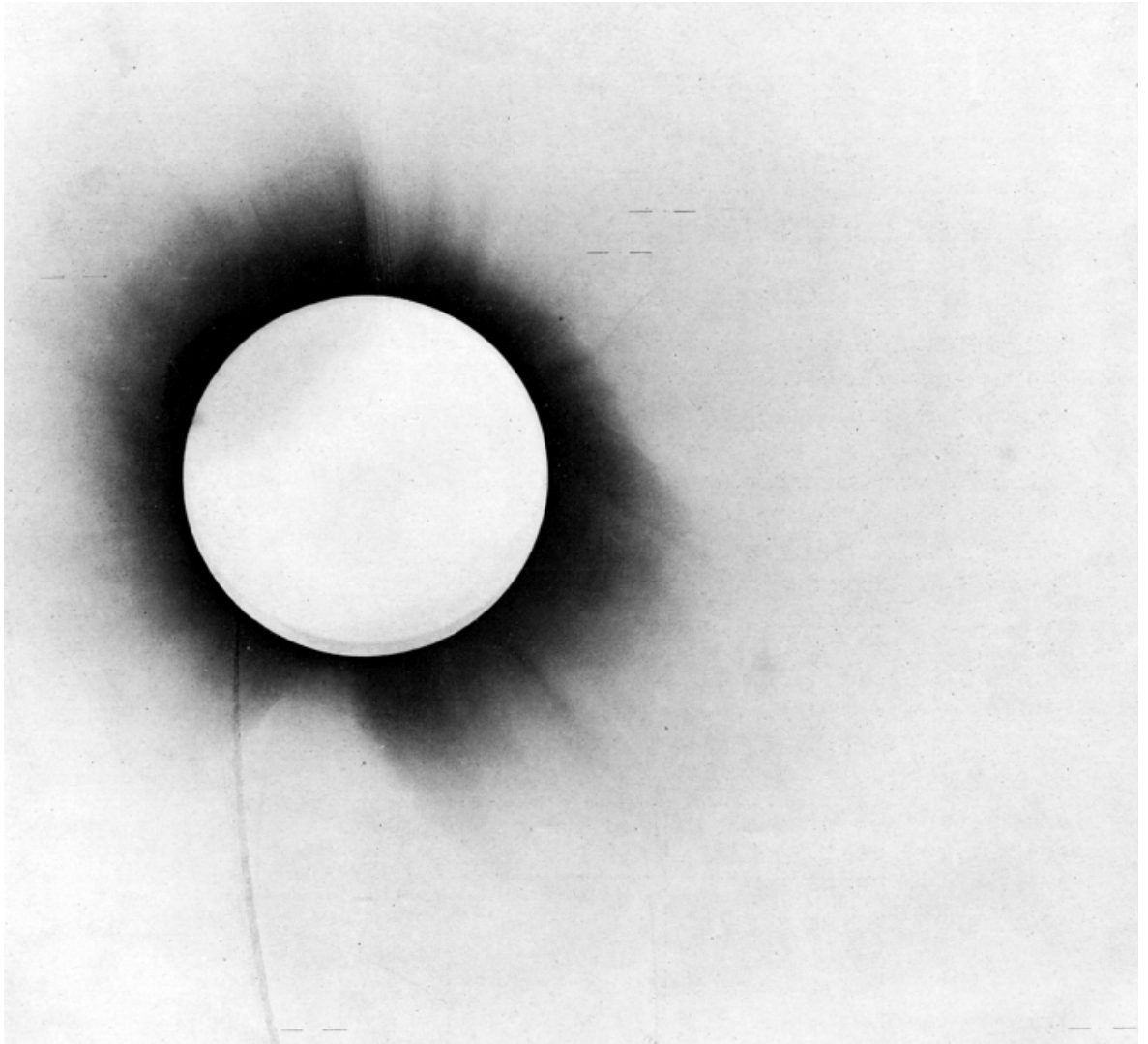
Figure 1.1: Above: Plate negative of the 1919 solar eclipse, from the expedition to Sobral, Brazil lead by Andrew Crommelin. Below: Measurements showing deflection of stars. The thick black line is Einstein deflection. The dashed line is Newtonian deflection. Dots and the thinner black line are star deflections and their best fit line. Reproduced from Ref. [19]

By 1919, GR had been verified by several tests, firstly it predicted the correct precession of Mercury [20], something that had previously baffled astronomers, secondly it predicted a greater deflection of light in gravitational fields than Newtonian gravity. The latter was put to the test by a team of astronomers: Frank Dyson, Arthur Eddington and Andrew Crommelin, who measured the deflection of stars whose light passed close to the sun during the solar eclipse of 29th May 1919 [19]. The measured deflection was greater than the Newtonian prediction and consistent with Einstein's prediction (Figure 1.1). Einstein had also proposed a third test of his theory, the gravitational redshift of light, which was not tested until 1960 in the Pound-Rebka experiment [21].[4] Gamma rays were emitted from the top of a 74 ft tower and detected at the bottom, (or vice versa), and the light at the bottom had higher frequency (by 5 parts in 10^{15}) than the light at the top, having gained energy from falling in the gravitational field (or alternatively, losing energy travelling against it). This experiment also effectively shows that clocks tick at different rates at different heights in the Earth's gravitational field - known as gravitational time dilation.

Once the theory was in place and had been verified as best it could at the time, the main advances in GR were in finding new solutions to the field equations (which is not trivial, due to their nonlinearity), and interpreting what those solutions meant. The solutions predicted new phenomena, such as gravitational waves and black holes, and even in theory allowing wormholes and time travel [23].

Tests of the details of GR can be extreme technical challenges because gravity is an extremely weak force. A simple small magnet can hold up a nail even when the entire (6×10^{24} kg) mass of the Earth is pulling it down. Consider the force between a proton and an electron at the distance of the diameter of an atom ($\sim 1 \times 10^{-10}$ m), the magnitude of the electric force is:

$$F = k_e \frac{|q_1||q_2|}{r^2} = 8.99 \times 10^9 \,\mathrm{N\,m^2\,C^{-2}} \frac{(1.60 \times 10^{-19} \,\mathrm{C})^2}{(1 \times 10^{-10} \,\mathrm{m})^2} = 2.3 \times 10^{-8} \,\mathrm{N} \qquad (1.3)$$

whereas the gravitational force (the Newtonian approximation being more than adequate here) is:

$$F = G \frac{m_1 m_2}{r^2} = (6.67 \times 10^{-11} \,\frac{\mathrm{m^3}}{\mathrm{kg\,s^2}}) \frac{1.67 \times 10^{-27} \mathrm{kg}\ 9.11 \times 10^{-31} \mathrm{kg}}{(1 \times 10^{-10} \mathrm{m})^2} = 1.01 \times 10^{-47} \mathrm{N}.$$
$$(1.4)$$

Because of this weakness, GR only usually becomes relevant on the most (literally) massive scales, which usually also translates to the biggest scales, that of planets, stars, solar systems, and galaxies. Nevertheless, the extra precision of general relativity is still needed in our everyday life here on Earth. Global navigation satellite systems (such as the United States' Global Positioning System (GPS)) would quickly lose accuracy

---

[4]In order to detect the tiny redshift present on a human scale, a source (and receiver) of photons with a very 'sharply defined energy' was required, which had to wait until Rudolf Mössbauer's 1958 discovery of recoil-free γ ray emission and absorption from solids [22].

and become completely useless without compensating for gravitational time dilation. There'd be no Pokémon Go without Einstein!

1.2 The problem

These two theories are super successful within their respective domains (small scale vs. high mass) and between them they cover almost everything. Yet we know these theories are not complete, because they seem to be fundamentally, mathematically, incompatible. To over-simplify (massively) QM is a theory of discrete quanta, whereas GR is smooth and continuous on all scales. QM is probabilistic, events can have multiple random outcomes, while GR is deterministic. Our knowledge of where the two domains truly merge is very poor, for example in the centres of black holes where there is a lot of mass trying to collapse into an infinitely small point, both theories should come into play, but since our mathematics breaks down at that point we can only deem it a singularity - usually a sign of an incomplete theory.[5] As Michio Kaku puts it: *"for half a century any physicist who tried to mediate a shotgun wedding between the quantum theory and general relativity found that the theory blew up in their faces, producing infinite answers that made no sense."* ([24, p. 236])[6] Other phenomena unexplained by QM and GR - deviations from the Standard Model [26, 27], the apparent existence of dark matter and dark energy in the universe [18] - also indicate weaknesses in these two cornerstones of our physical understanding.

1.2.1 Quantum gravity?

Even from the early days of QM and GR, physicists have recognised a need to unite them [28]. Initially there was (in hindsight, very naive) optimism, in 1929 Werner Heisenberg and Wolfgang Pauli dismissively asserted: *"quantization of the gravitational field, which is indispensable for certain physical reasons, may be carried out without any new difficulties"* ([29, p. 3]).[7]

One of the first to take a stab at it was Soviet physicist Matvei Petrovich Bronstein, who believed in 1930 *"it is a task of the nearest future to identify the ties between quantum mechanics and the theory of gravitation"* ([5, p. 88])), and in 1933 that *"after relativistic quantum theory is formulated, the next task would be to realize the third step, [...] to merge quantum theory (ℏ constant) with special relativity (c constant) and the theory of gravitation (G constant) into a single whole"* ([5, p. 90]). His $cG\hbar$-framework (an up to date version mapped out in Figure 1.2), that recognises the significance of these fundamental constants, is still useful today to map out the state of fundamental

---

[5]Just like the 'ultraviolet catastrophe'.

[6]For example, calculating the vacuum energy density - the cosmological constant Λ - with QM [25], infamously has given answers up to 120 orders of magnitude bigger than observed.

[7]Physicists continue to be optimistic, in 2002 Kip Thorne predicted *"by 2020 physicists will understand the laws of quantum gravity"* ([30, p. 20]). Sorry, Kip.
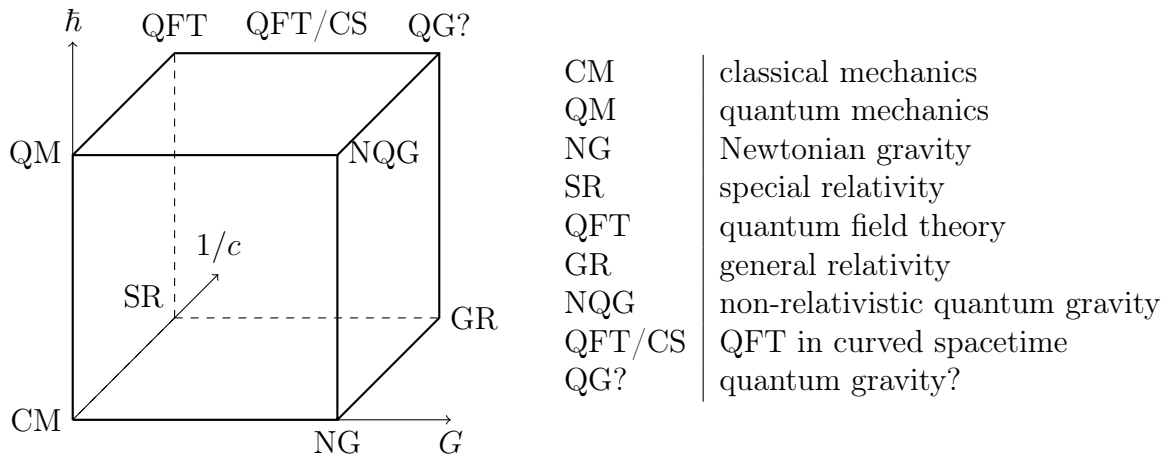
Figure 1.2: $cG\hbar$ map of fundamental physics theories, sometimes known as a 'Bronstein cube'. We use $1/c$ as an axis rather than c as one can consider special relativity emerging from the speed of light being finite, rather than infinite. Although the variance of the axes is not to be taken too literally! Non-relativistic quantum gravity is not a fleshed out physical theory of its own (although one can include research into the Schrödinger-Newton equation as part of it), so this either indicates a neglected area of physics, or maybe just the limitations of this simplified cube metaphor.

physics so far, and where it still has to go. By 1936, Bronstein was perhaps the first to really grasp the conceptual difficulties, in his paper in which he quantised the linearised equations of Einstein's theory he wrote *"without a deep revision of classical notions it seems hardly possible to extend the quantum theory of gravity also to this domain [of strong gravitational fields]"* ([31]). Sadly he did not live to pursue the problem much further; in 1937 he was arrested in Stalin's Great Purge, and executed the next year.

Einstein and Eddington both worked on trying to find grand theories of everything until their deaths in 1955 (Figure 1.3) and 1944 respectively. Einstein from the perspective of trying to find a classical unified field theory of gravitation and electromagnetism - a further generalisation of general relativity - from which quantum mechanics could naturally emerge [32], and Eddington veering off into numerology [33], both becoming increasingly isolated from the wider scientific community.[8] Most[9] physicists were much more interested in unravelling the secrets of QM than dealing with GR, or their combination, which didn't seem to have much practical application.[10]

It was not until the 1960s that general relativity entered its 'golden age' and became mainstream [23]. Various approaches to, and the unique difficulties of, combining quantum theory and general relativity into a consistent theory of quantum gravity then

---

[8]The general public was still obsessed with Einstein's work though, Eddington in 1929 wrote to Einstein with this account: *"You may be amused to hear that one of our great department stores in London (Selfridges) has posted on its window your paper (the six pages pasted up side by side) so that passers-by can read it all through. Large crowds gather around to read it!"* ([34]) One struggles to imagine such interest in a theoretical physics paper today!

[9]But not all, as Carlo Rovelli notes in Ref. [35], by the end of the 1950s the main conceptual approaches to quantum gravity had all been conceived.

[10]A very notable exception was Chandrasekhar, whose balancing of quantum-mechanical electron-degeneracy pressure and gravitational attraction in 1930 lead to the limiting mass of a white dwarf before its self-gravity becomes too much and it must collapse into what we now accept as a black hole.

Figure 1.3: Einstein's desk in Princeton, taken hours after Einstein's death and captured exactly as the Nobel Prize-winner had left it, Princeton, New Jersey, 18th April 1955. (C) Ralph Morse/The LIFE Picture Collection/Shutterstock. Reprinted with written permission from the copyright holder.

Figure 1.4: My page from my sixth form leavers' yearbook, in which I (over-)confidently state that one of my next steps in life is to 'unite quantum physics and general relativity'. The rest has been blurred out of irrelevance to this thesis, and from vague embarrassment.

began to be fleshed out (for a history of approaches to quantum gravity see Ref. [35]). While promising iterations of string theory and loop quantum gravity begin to address the problems inherent in their foundations of combining QM and GR, here in the early 2020s we still do not yet have complete unification of the two.

1.3 An experimentalist's approach

This difficult question of how to unite our two most fundamental theories has also interested me since I was a teenager (as evidenced by a rather confident statement in my sixth form yearbook, Figure 1.4). So, what's my approach now as a PhD researcher? It's a very big field, and naturally there are some aspects of it that interest me and others that don't. I don't have the theoretical background to make a headway in the mathematics of string theory or loop quantum gravity or to invent a new quantum gravity theory of everything. But when faced with uncharted territory, you shouldn't only theorise about what's out there, you must also step out and see. As someone with a non-binary gender, I'm rather familiar with the middle ground between *supposedly* 'opposite' things; just because it makes *some* people uncomfortable and confused, that middle ground doesn't simply stop existing! There is little consensus on *how* to make gravity quantum, yet we don't need a theory of everything to test situations where both QM and GR are relevant, to start mapping this uncharted territory. We can seek experimental facts, and gather evidence independent of any particular quantum gravity theory.[11]

---

[11]The lack of a theory unifying electricity and magnetism at the time didn't stop Hans-Christian Ørsted and Michael Faraday from experimentally advancing our knowledge of electromagnetism!

It has previously been regarded that quantum gravity is almost impossible to test due to the extreme conditions at which our current theories break down. Certainly if we try to go straight into the thick of it, *directly* probing physics at the Planck scales at which quantum gravity *must* rear its head, such as the Planck length (10^{-35} m), or the Planck energy (10^{28} eV), is still about 15 orders of magnitude outside our current technological abilities. However, new effects that dominate at those scales should still be present at more accessible scales, just likely suppressed [36]. There may be ways to amplify these small effects in other ways, or find small corrections to our current theories, or do indirect tests of the quantumness of gravity. We can start skirting the edges of the unknown, and slowly pushing back the boundaries of ignorance - there might be surprises! This should be within the limits of current and near term technology, Ian Percival and Walter Strunz [37] note that atom interferometers can place bounds on Planck-time (10^{-44} s) scale fluctuations, akin to the way Einstein's Brownian motion experiment could probe atomic scales with microscopic effect through diffusion processes. In a similar way, Giovanni Amelino-Camelia points out that LIGO gravitational wave detectors (which successfully detect the classical counterpart to the graviton) are already placing bounds on the magnitude of inherent quantum gravity noise (akin to quantum shot noise) from potential 'fuzziness' of spacetime [38].

One way some headway could be made in quantum gravity phenomenology is from the general relativity side, on astronomical and cosmological scales. For example, looking for signatures of quantum effects in the very early universe in the cosmic microwave background, or in gamma ray bursts [39]. However, coming from an undergraduate background in quantum mechanics and experimental quantum optics, I prefer a hands on approach, of controlled, repeatable experiments rather than observations.

From the quantum side, our current confidence in quantum mechanics is almost entirely from tests where gravitational effects are irrelevant. Starting to move quantum experiments into a regime where gravity cannot be ignored is essential for a greater understanding of the interplay between QM and GR. One early and significant experiment that takes this approach is the 1975 Colella-Overhauser-Werner (COW) experiment [40] which tested the effect of the gravitational potential on the de Broglie wavelengths of neutrons. By changing the relative height of the two arms of a neutron interferometer, interference patterns were observed due to the gravitational potential difference creating a difference in the quantum mechanical matter-wave phase. This matched predictions of the Schrödinger-Newton equation, which is just the Schrödinger wave equation with a Newtonian gravitational potential added.[12] In this sense it is very much a non-relativistic test, and one in which gravity also remains classical, not quantised. Nevertheless this combination of quantum wave-particle duality with gravity shows the potential of elegantly simple tabletop experiments to test quantum aspects of gravity.

Tests of quantum mechanics in gravitational fields and curved spacetimes may not

---

[12]One point of interest is that this gravitational quantum interference is dependent on mass, once $\hbar$ appears, the mass no longer cancels and gravity is no longer purely geometric [41, pp. 127–129].

simply reinforce what has already been verified, the interplay between the two could generate new effects, that any successful theory of quantum gravity would also have to explain. Quantum effects of (classical) curved spacetimes have been theorised within the framework of quantum field theory in curved spacetime (QFT/CS). While QFT/CS does not treat gravity in a quantum way, and struggles to incorporate the dynamics of gravitational fields, it has been very influential in quantum gravity. In a 2015 review of the developments in quantum gravity, Carlip et al. refer to Hawking's 1974 discovery using QFT/CS techniques that black holes emit thermal radiation [42, 43] as *"perhaps the most notable achievement in the study of quantum gravity so far"* ([44, p. 11]). In 1976, Bill Unruh connects this effect to accelerating frames [45], showing that observers accelerating through a vacuum in flat spacetime will not see a vacuum, but will detect a thermal bath of particles, this prediction is called the Unruh effect. In a curved spacetime, this means different observers, even if none are accelerating, can have different ideas of what is vacuum and what is particles. But which are the true particles whose energy actually contributes to the gravitational field? About this paper Rovelli muses: *"The paper points out the existence of a general relation between accelerated observers, quantum theory, gravity and thermodynamics. Something deep about nature should be hidden in this tangle of problems, but we do not yet know what."* ([35, p. 12])

So far tests of QFT/CS have mainly been via analogue effects. Somewhat before his time, in 1981 Unruh showed that an analogue of Hawking radiation would be present in moving fluids [46]. According to Barceló et al.'s review paper on analogue gravity [47], it took about ten years before others such as Ted Jacobson picked up on this idea, and the field of analogue gravity was born. This was a way of using isomorphisms to transform gravitational metrics onto the physics of other systems, firstly to gain new perspectives on gravity and allow cross-fertilisation of ideas with other fields of physics [48], and more recently because they are more accessible for experiments. Such experiments have mainly focused on Hawking radiation and black hole thermodynamics in water flow, Bose-Einstein condensates and nonlinear optics [49, 50, 51, 52, 53, 54, 55]. Analogue gravity has shown that curved spacetime effects like Hawking radiation can now be considered as a specific formulation of more general classical and quantum processes; in a review of the new directions analogue gravity is taking, Grace Field points out:

> *The phenomenon [of Hawking radiation] was originally predicted in an astrophysical context, but more and more authors in the analogue gravity literature are emphasizing that this was pure accident. Hawking radiation, they write, is in fact a much more general effect that could have been derived in any number of contexts. And — even if their ability to confirm the existence of astrophysical radiation is unclear — analogue systems are perfectly capable of detecting genuine instances of this more general notion of Hawking radiation, a kinematic effect which some authors dub the Hawking process. ([56, p. 12])*

While there is scope for direct tests of QFT/CS, only a few have been performed, such as the observation of the dynamical Casimir effect (a way to amplify photons out of the vacuum with a moving mirror [57]) in a superconducting circuit [58]. Regardless, the fact that this framework of QFT/CS leads to the discovery of new generalised effects in analogue systems speaks to the transformative effect attempting to understand quantum aspects of gravity could have on our understanding of everyday physics.

There should also be ways to test whether gravity is quantum at all, without having a complete answer to *how* gravity is quantum. Within our current understanding of quantum theory, two separated systems can only become entangled through the mediation of a quantum field, not from local operations on those systems and/or classical forms of communication between them [59]. If gravitational interaction alone could entangle two initially separable systems, that would mean that gravity must be quantum in some way, not classical [60, 61]. This is the aim of the experimental QGEM (quantum gravity induced entanglement of masses) project, and will be a huge technical challenge, but experimentally feasible. These sorts of experiments are akin to the suggestion made by Richard Feynman at the 1957 Chapel Hill conference [62] - does a quantum superposition of masses create a quantum superposition of spacetimes?

Combining undeniably quantum elements with curved spacetimes and gravitational effects seems like a fruitful way to make experimental progress in answering these big questions. In particular I am interested in quantum entanglement, and how that can be controlled or produced with curved spacetimes. With a background in quantum optics, for me quantum photonics is a natural system in which to explore entanglement, as the technology to create and control photon entanglement is quite mature in some aspects.[13] So what are the ways we can start to bring gravity and curved spacetime into it? One option would be to use the Earth itself, it curves spacetime around it and creates a noticeable gravitational field, this is the method of e.g. the COW experiment. The frame at rest within the gravitational field on the surface of the Earth is also the regime in which most of quantum optics has been tested, albeit most of the time this fact has not been considered relevant to the outcome of the experiment. If we want to take control of this aspect of the experiment without blasting off into space, we can look to lessons from the equivalence principle.

1.3.1 Revolutionary physics: Rotating frames

Einstein's Equivalence Principle posits the physical equivalence of a homogeneous gravitational field to a corresponding uniformly linearly accelerated reference system without gravity. It means that the laws of physics are locally the same when you stand on the surface of the Earth in the Earth's gravitational field, 'feeling' the mass of the entire planet pulling you down, to if you were out in empty space, standing in a rocket

---

[13]Recognising this, the 2022 Nobel Prize in Physics [63] has been awarded to John Clauser, Alain Aspect and Anton Zeilinger for their pioneering quantum optics tests of entanglement [64, 65, 66].
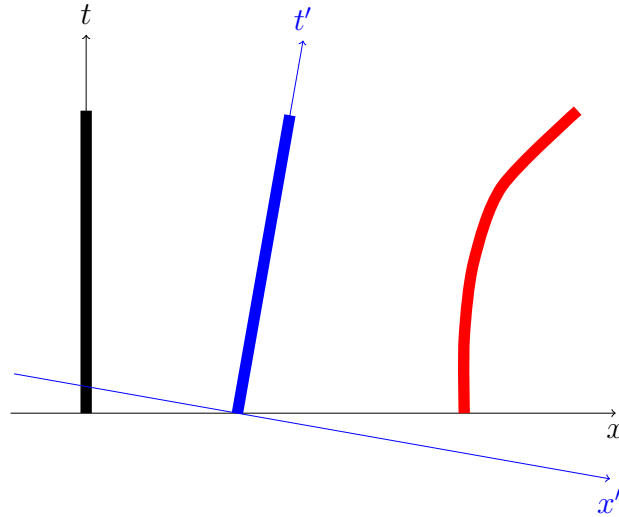
Figure 1.5: Worldlines in flat spacetimes. The left and central lines (black and blue) represent trajectories of inertial objects. The red line on the right is an accelerating object. In the unprimed frame (x, t), the black object is stationary and the blue object is moving. but in the primed frame, the blue object is stationary, and the black object is moving. The motion is only relative. However, in both frames the red object is accelerating - there is no rotation of the space and time axis that will straighten that worldline.

linearly accelerating at 1g. Free fall and inertial motion are equivalent, encompassing the idea of the universality of free fall.[14] In curved spacetime, when not in a freely falling (inertial) frame and instead say standing on the surface of the Earth, gravity manifests akin to fictitious forces that arise in non-inertial frames.

In flat spacetime, trajectories ('worldlines') of inertial objects are straight lines[15], and objects undergoing forces accelerate, leading to curved (deformed) trajectories in spacetime (Figure 1.5). No axis tilting into another inertial viewpoint will stop that deformed trajectory looking curved, which is why absolute acceleration is always detectable. Within a non-inertial frame, the co-ordinate system itself becomes curvilinear - this curvature from the non-inertial motion becomes encoded in its metric tensor.[16] The change of co-ordinate system changes how equations of motion are expressed,

---

[14]Universality of free fall is the idea that e.g. dropping two different masses (neglecting air resistance) from the Leaning Tower of Pisa at the same time, they will both reach the ground at the same time, as their acceleration due to gravity is independent of mass. This equivalence of inertial and gravitational mass is also known as the weak equivalence principle. Einstein's equivalence principle encompasses the weak equivalence principle and also states any local non-gravitational test in a freely falling frame is independent of the frame velocity *and* its location in spacetime. There is also a strong equivalence principle, which extends that principle also to local gravitational tests.

[15]Along the time axis for an object that is stationary in an observer's reference frame, tilted partly along the space axis for objects that appear moving at constant velocity in the observer's reference frame. Of course in special relativity, an equally valid inertial viewpoint is the tilted one of the 'moving' object, whose own trajectory is along its time axis and the other object now is moving partially along the space axis.

[16]The metric tensor g_{ij} is a way of defining invariant distances and angles that generalises to non-Euclidean spaces, and is a way of encoding the structure of the space. An infinitesimal invariant distance d_s in the space is defined by $ds^2 = g_{ij}dx^i dx^j$, where repeated indices are summed over. This is akin to the way we can find the distance between two co-ordinates in 2D flat space with Pythagoras' theorem.

giving rise to extra terms we refer to as fictitious forces, such as the centrifugal and Coriolis forces [67] in rotating frames. The Cartesian straight-line worldline of an inertial object seen from within a non-inertial frame will - with respect to the frames curved co-ordinate system - appear deformed in comparison. Such an inertial object, to observers in the non-inertial frame, appears to be accelerated under these fictitious forces, yet cannot detect its own acceleration.

In curved spacetime, the only inertial frames are local ones moving along geodesics - the worldlines of freely falling particles - which we can think of as tracing the shortest spacetime distance between two points in a curved spacetime. There are no straight lines with which to define a globally inertial frame, globally the frames are non-inertial. That means that two freely falling objects will appear to accelerate relative to each other. This relative acceleration is very different to absolute acceleration, which would occur when a worldline is deformed away from a geodesic [68]. The latter can be detected locally, the former cannot.[17]

We can create different non-inertial frames in the lab, allowing us to test quantum mechanics in different curved metrics, and new regimes. One way would be to use linear acceleration, but for the simplest case of constant linear acceleration this can be a pain as your experiment doesn't stay in the same place. For circular motion, you can build an experiment that spins. For example, researchers in Vienna used a drop tower and a centrifuge to simulate different gravitational field strengths and showed that quantum entanglement stays constant in uniform accelerations from milli-g to hyper-g [70].[18]

In rotating frames, we have *curved space*, and time also goes a bit weird[19], although *spacetime* is still flat. Nevertheless, this allows us to draw parallels with curved space-times. Using rotating frames also allows us to explore effects associated with those frames, such as the special relativistic Sagnac effect. Within a non-inertial frame, the global speed of light in a vacuum can differ from c (although its *local* speed of light will always be c). Light circling in opposite directions in a rotating frame will complete a common path loop (within the rotating co-ordinate system) in different times. This is called the Sagnac effect. The difference in times can be used as a measure of the rotation speed of the frame. In what ways might rotating frames also affect quantum states? If the equivalence principle holds, then quantum effects in superpositions of rotating frames could provide evidence of quantum gravity [72].

By developing experiments along these lines we start to tread paths towards quantum gravitational tests. With this motivation in mind, within my PhD, I have shown new effects with experiments in rotating frames. In one project I have verified a 50 year old

---

[17]Interestingly, whilst nowadays we see general relativity as gravitation from geometry, arguably [69] Einstein didn't think of it that way, instead seeing it as a unification of gravitation with inertia, that happens to use geometric tools to describe it.

[18]There are also non-inertial frames other than linear acceleration and circular motion, in which observers at rest experience a time-independent co-ordinate system, such as motion along a catenary or a helix [71].

[19]It is impossible to synchronise clocks around a closed loop in a rotating frame, for the same reason as the Sagnac effect: that light takes different times to circle in different directions.

prediction that waves can be amplified through interaction with a rotating absorber, albeit in the more initially achievable case of a classical, rather than quantum, system (Chapter 2 and Ref. [2]). This effect links strongly to rotational superradiance effects in curved spacetimes [73]. I have also investigated how to detect and manipulate quantum entanglement in Hong-Ou-Mandel interferometry (Chapter 3), combining this with the Sagnac effect in a rotating frame to devise and experimentally verify the successful control of photon pair entanglement symmetry with mechanical rotation (Chapter 4 and Ref. [3]). From these investigations, we have envisioned ways to build on these ideas (Chapter 5) to tread a little further still on the paths to quantum gravity.

An experiment is a question which we ask of Nature, who is always ready to give a correct answer, provided we ask properly, that is, provided we arrange a proper experiment

<div align="right">Charles Vernon Boys, 1889 [74]</div>

2

Amplification of Waves from a Rotating Body
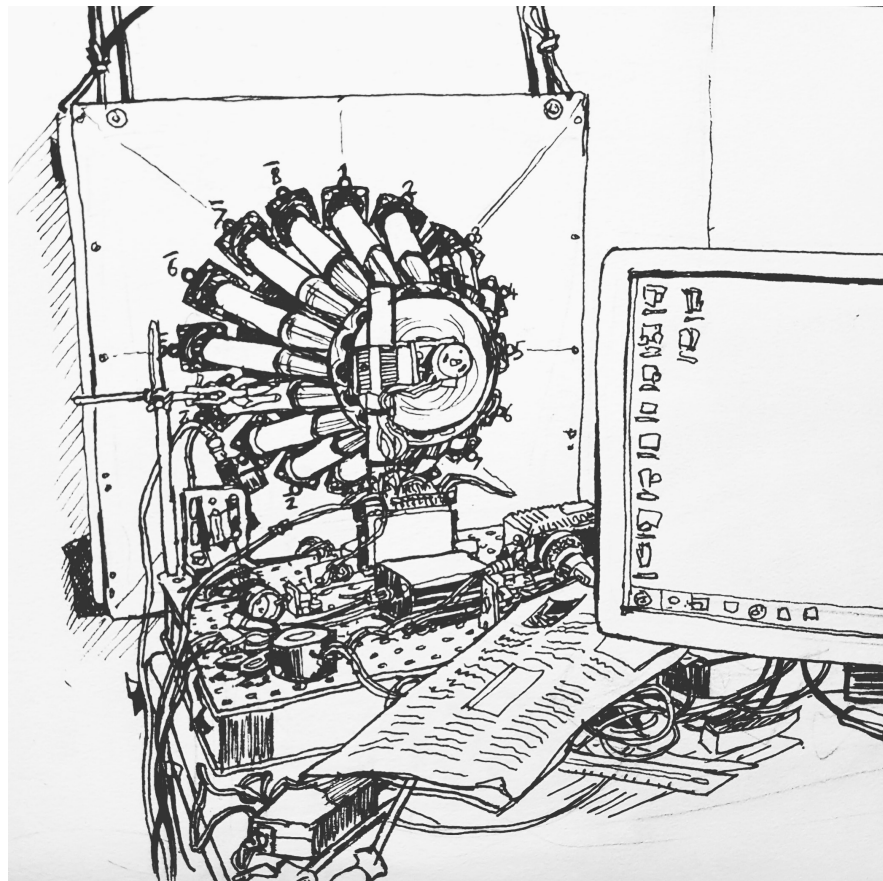
2.1 Introduction to the Acoustic Zel'dovich Effect

The Zel'dovich effect is a fundamental effect which details how waves with angular momentum can be amplified through interactions with rotating absorbers [75, 76]. For electromagnetic (EM) waves it should also spontaneously amplify radiation out of the quantum vacuum. The condition to produce the effect requires the rotation frequency Ω of the absorbing object to be greater than the frequency of the waves ω divided by their angular momentum order ℓ:

$$\omega/\ell < \Omega. \tag{2.1}$$

This allows the angular frequency of the object to outpace the angular phase velocity of the wave. This condition gives the waves a rotational Doppler shifted *negative frequency* within the object's rotating frame, forcing a sign change of the absorption of the waves by the object into amplification. Within the history of physics, the theoretical discovery of this effect is closely linked to results concerning curved spacetimes, such as black hole superradiance and Hawking radiation [23, 77]. These related effects have been tested in generalised forms in analogue experiments [54, 49, 51, 52, 53, 55], yet the Zel'dovich effect, which could be put to direct test, had not - until my work. Perhaps the main reason this effect had been overlooked is that this condition is very difficult to obtain with electromagnetic waves on a technical level. However, recent work had translated the effect into more amenable geometries [78], and into the regime of sub-wavelength acoustics [79, 80]. A previous experiment at the University of Glasgow that had been constructed to measure the reversal of orbital angular momentum (OAM) with extreme rotational-Doppler shifted sound waves [81] had required meeting the negative-frequency condition that is also needed for the Zel'dovich effect. We could add absorption to the same experimental set-up to search for experimental verification of the Zel'dovich effect - and indeed, we found it! The measurements and analysis I performed proving the amplification effect I wrote up (with input from my brilliant colleagues) in the paper (Ref. [2]) reproduced in Section 2.2. While acoustic waves belong to the domain of classical physics and certainly won't be amplified out of the vacuum (*"In space, no-one can hear you scream"* ([82])), we hope this verification of a general Zel'dovich effect will provide extra motivation to test this effect in a much more technically challenging quantum regime.

2.1.1 Relation of the Zel'dovich effect to effects in curved spacetimes

The Zel'dovich effect was inspired by work by Roger Penrose on the extraction of energy from black holes. In 1969, Penrose found from the solutions of general relativity that energy could be extracted from black holes if the black hole was rotating [83, 84], via a classical process involving particles now known as the Penrose process. Perhaps inspired

by the idea of a Dyson Sphere[1], a hypothetical structure an advanced civilisation could build around a star to fully use it as a power source [86], Penrose imagined a civilisation which has built structures surrounding a rotating black hole to extract its energy.

The curvature of spacetime around a rotating black hole is characterised by the Kerr metric [87]. In general relativity, the metric tensor $g_{\mu\nu}$ defines an invariant scalar interval ds^2 in spacetime.[2] The amount and way that space curves is encoded in how this spacetime distance is formed:

$$ds^2 = g_{\mu\nu}dx^\mu dx^\nu \tag{2.2}$$

The Kerr metric is an exact solution to the Einstein field equations of general relativity which describes the region around a rotating black hole of mass M and angular momentum J in a spherical spatial co-ordinate system (r, θ, ϕ).[3]

$$\begin{aligned} ds^2 = -c^2 d\tau^2 = &- \left(1 - \frac{r_s r}{\Sigma}\right) c^2 dt^2 + \frac{\Sigma}{(r^2 - r_s r + a^2)} dr^2 + \Sigma\, d\theta^2 \\ &+ \left(r^2 + a^2 + \frac{r_s r a^2}{\Sigma} \sin^2\theta\right) \sin^2\theta\, d\phi^2 - \frac{2r_s r a \sin^2\theta}{\Sigma} c\, dt\, d\phi \end{aligned} \tag{2.3}$$

Here $r_s = \frac{2GM}{c^2}$ is the Schwarzschild radius (the radius of the black hole event horizon, beyond which even light cannot escape), $\Sigma = r^2 + a^2 \cos^2\theta$ and $a = \frac{J}{Mc}$[88].

The important feature of this metric is the appearance of the cross term $dt\, d\phi$: it couples time t and space ϕ co-ordinates, blending movement through time with movement in space. This means the spacetime is not static. Here this results in an effect called 'frame dragging'; a rotating mass spins spacetime around with it. Around the event horizon of such a black hole is a region called the ergosphere, in which the frame dragging effect is so extreme that even travelling at the speed of light is not fast enough to stop you rotating with the black hole, from the point of view of an observer (infinitely) far away from the black hole. While particles can still escape from this region with a subluminal speed, they will be dragged round the black hole to some extent. Within this ergoregion it is even possible for particles to have a negative energy.

Penrose imagined an advanced civilisation, that has built two structures around a black hole, one that is far away and is stationary (S), and a closer one that rotates with the black hole (S*), see Figure 2.1. Inhabitants at S lower an object to S* gaining gravitational energy, at S* it is further lowered into the ergosphere of the black hole. They split the object in half once its in the ergosphere such that one part has a negative energy (as seen by S), this part they allow to cross the event horizon, never to be seen

---

[1]Named after Freeman Dyson who popularised the idea, however he took the idea [85, p. 211] from science fiction writer Olaf Stapledon's 1937 novel 'Star Maker'.

[2]The sign of ds^2 indicates causality - whether it is possible to transmit information between two events in spacetime, limited by the speed of light. If $ds^2 \leq 0$ yes, if $ds^2 > 0$, no.

[3]The Kerr metric can also be adapted to be used to describe spacetime around rotating massive bodies that aren't black holes, such as the Earth.
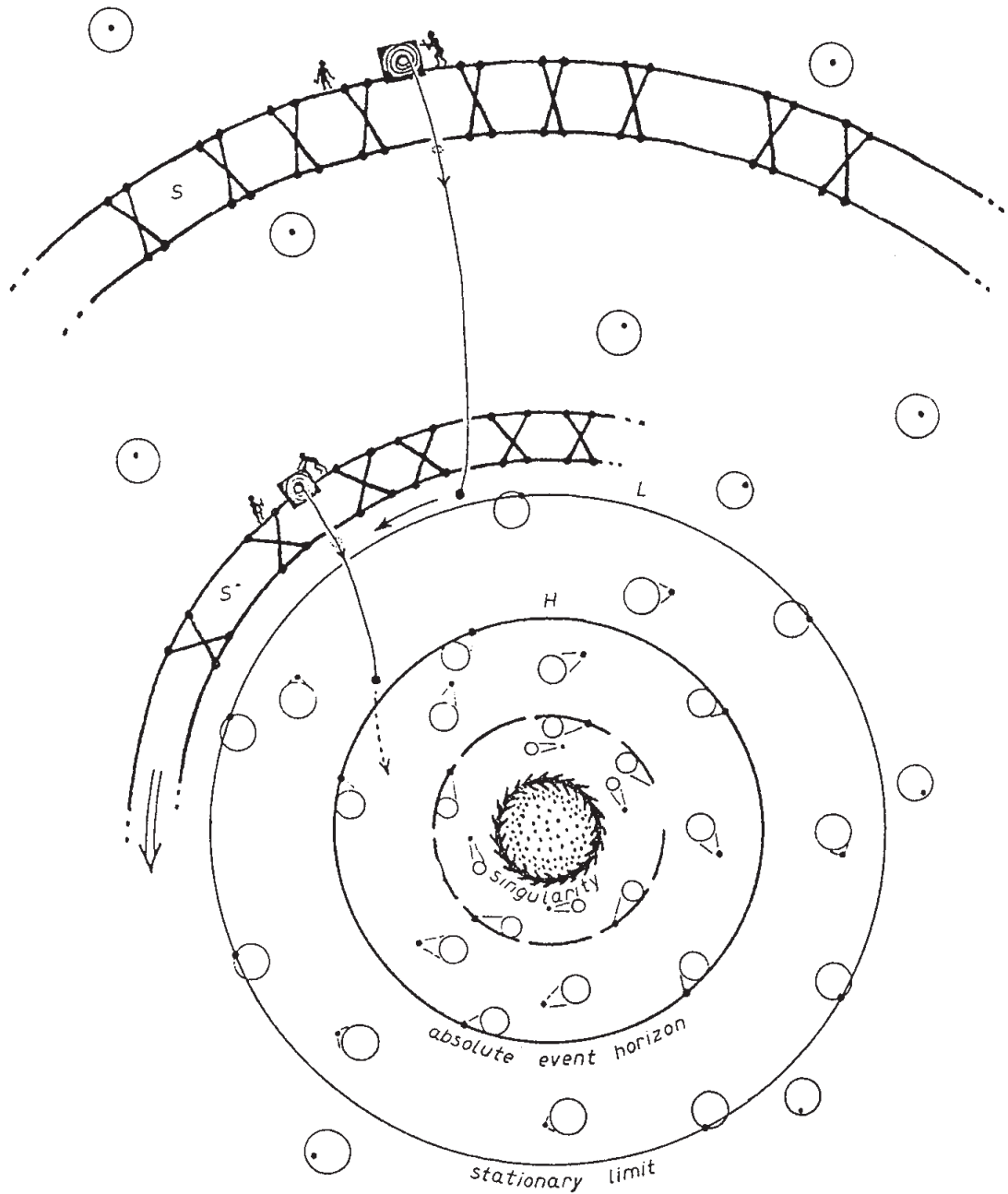
Figure 2.1: The Penrose Process. Between the stationary limit and the event horizon of a rotating black hole is the ergosphere, where moving with the rotation of the black hole is unavoidable. In this region, objects can have negative energy. By dropping negative energy masses into the black hole, the inhabitants at S (infinity) lose negative energy, i.e. gaining more energy than they put in, having extracted it from the rotational energy of the black hole. Reprinted from '"Golden Oldie": Gravitational Collapse: The Role of General Relativity' by Roger Penrose, General Relativity and Gravitation, Vol 34, pages 1141–1165 (2002) Springer Nature. [83] Copyright © 2002, Plenum Publishing Corporation. Reused with permission from the publisher.

again. Having lost negative energy, the remaining part brought back to S now carries more energy than the original object dropped in, essentially having extracted energy from the black hole. 29% of the mass of the black hole could be extracted as energy in this process - much more efficient than fission or even fusion [89]! It has been shown by Reva Kay Williams [90, 91] that this extremely efficient process can explain the production of the extremely high energy relativistic particle jets that shoot out of the poles of quasars.[4] The idea of the Penrose process has caught the imagination of scientists and non-scientists alike. Recently 2018's 'High Life', a critically acclaimed science fiction film by Claire Denis, imagines a near future mission of the first crew sent to extract energy from a black hole [96].

Hearing about the Penrose process from Kip Thorne, Charles Misner and John Wheeler [23], in 1971 Yakov Zel'dovich translated this effect from particles to waves, and generalised it to any rotating absorber. The wave analysis allowed the result to be extended to the quantum regime, allowing the generation of radiation from the vacuum:

> *The foregoing pertains to a body made of a material that absorbs waves when at rest; the conditions for amplification and generation are obtained after transforming the equations to the moving system. A similar situation can apparently arise also when considering a rotating body in the state of gravitational relativistic collapse. The metric near such a body is described by the well-known Kerr solution. The gravitational capture of the particles and the waves by the so-called trapping surface replaces absorption [...] Finally, in a quantum analysis of the wave field one should expect spontaneous radiation of energy and momentum by the rotating body. The effect, however, is negligibly small. ([75])*

He found that for waves of frequency ω and angular momentum ℓ interacting with an absorber rotating at frequency Ω, electromagnetic waves (and/or quantum vacuum fluctuations!) would be amplified, taking energy from the absorber, if they satisfied the condition that we refer to as the Zel'dovich condition:[75, 76, 97]

$$\omega - \ell\Omega < 0. \tag{2.4}$$

In the most rigorous treatment he specifically considered the amplification of electromagnetic waves on reflection from a rotating metallic cylinder, but the principle of this idea of 'rotational superradiance' is rooted in more general thermodynamics, and has strong links to many different superradiant phenomena in physics, such as Mach cones and the Čerenkov effect [73].

---

[4]Williams has not received appropriate credit for this work [92]; women are routinely undercited for their work in physics [93], and this was no doubt likely compounded by racism towards her as a Black person, as has been evidenced in other scientific fields [94]. Sadly the 1909 comment by Hertha Ayrton that *"an error that ascribes to a man what was actually the work of a woman has more lives than a cat"* ([95]), sparked by the misattribution of the discovery of radium to Marie Curie's husband, still has validity today. Aryton was the first woman to win the Royal Society Hughes Medal in 1906, shockingly there's only been two other female winners of this annual award in the 100+ years since!

The general thermodynamic argument is as follows. Considering conservation of energy, if the cylinder has total energy E, the change in E with respect to time t is the difference between the incident wave energy flux W and the reflected wave energy flux W_1:

$$\frac{dE}{dt} = W - W_1. \tag{2.5}$$

From the conservation of angular momentum, the change in total angular momentum J of the cylinder is the difference between the incident and reflected wave's angular momentum:

$$\frac{dJ}{dt} = \frac{\ell}{\omega}(W - W_1). \tag{2.6}$$

Using the thermodynamic identity $dE = TdS + \Omega dJ$ (which relates the change in energy to the change in entropy S and change in angular momentum via temperature T and rotation rate Ω, keeping other properties like volume of the cylinder constant), to make sure we obey the 2nd Law of Thermodynamics ($dS \geq 0$) we require:

$$\frac{dE}{dt} - \Omega\frac{dJ}{dt} \geq 0, \tag{2.7}$$

i.e.

$$(W - W_1)(1 - \frac{\ell\Omega}{\omega}) \geq 0. \tag{2.8}$$

This means when Eq. 2.4 is satisfied, the reflected wave must have more energy than the incident wave - it will be amplified by its interaction with the cylinder!

Moving back to the rotating black hole system, the equivalent case of the Penrose process for wave amplification is often referred to as Penrose superradiance, and it requires the same condition as Eq. 2.4, sometimes called the Zel'dovich-Misner condition in that context, incorporating Misner's consideration of reflection from rotating black holes [98]. Zel'dovich's suggestion that rotating black holes should amplify and radiate was further elucidated by Starobinskii in 1973 [99], and it was this work by Zel'dovich and Starobinskii that prompted Hawking's discovery that all black holes should radiate and eventually evaporate, as summarised by Carla Rodrigues Almeida:

> *In [Hawking's] hotel room, with Zel'dovich and Thorne as witnesses, Starobinskii presented his and his supervisor's results to Hawking, who was unaware of them. To [Werner] Israel [100, p. 264][5], Hawking recalled that he liked the idea but was not convinced by the calculations. He mentioned Starobinskii had told him about spontaneous radiation—a phenomenon which Starobinskii himself had not discussed in his paper. Hawking reportedly thought their arguments had physical ground, but he remained skeptical. Inspired by Zel'dovich's and Starobinskii's ideas, Hawking worked on this problem back home. His conclusion, he said, really annoyed him: all black holes must radiate. ([77])*

---

[5]I have corrected the reference for Werner Israel's statement [100, p. 264], from the original article by Almeida it is numbered incorrectly.

The famous prediction of Hawking radiation [42] and black hole evaporation kick-started research that tried to incorporate both general relativity and quantum mechanics, particularly the field of quantum field theory in curved spacetimes (QFT/CS).[6]

Direct tests of QFT/CS predictions have been difficult, and instead focus has been on analogue tests of the astrophysical phenomena. For example, analogue Hawking radiation has been shown in many systems [49, 51, 52, 53, 54], while analogue Penrose superradiance has been shown in water flows [50] and nonlinear optics [55]. All these effects share the same requirement as the Zel'dovich effect of needing negative frequency modes. However, Zeldovich's direct claims about rotating absorbers has mainly been overlooked until recently.

2.1.2 Use of acoustics

Zel'dovich himself was quick to point out [76] that because the linear velocity of the rotating body from which energy is extracted must exceed the phase velocity of the incident waves, it would be impossible to satisfy this condition (Eq. 2.4) for plane EM waves in vacuum, as the body could not move faster than the speed of light! For an EM beam with OAM (Figure 2.2) it is at least physically possible, as the OAM order reduces the angular phase velocity below c, but for optical frequencies of hundreds of trillions of Hz, an extremely high order OAM would be required to bring down the rotational frequency of the object to something mechanically possible. Low frequency radio waves also would not be feasible as they require very large antennas to generate, due to the huge wavelengths involved (wavelength = velocity/frequency, e.g. a 30 Hz EM wave has a wavelength of around 10,000 km, roughly the same size as the entire Earth), which would be very impractical outside of military applications. Not to mention the fact that one would have to both control the OAM and direct the beam in a certain way towards a rotating object likely many magnitudes smaller than the wave.[7]

Essentially the speed of light makes seeing this effect with EM waves difficult. However, acoustic waves offer an alternative. The speed of sound in air is about 300 m/s, about a million times slower than that of light. This means that low acoustic frequencies are easily accessible, they can match practical mechanical rotation speeds on the order of tens of Hz. However, Zel'dovich's original proposal had an odd geometry, it concerned the amplification of modes with a spiral phase structure that propagated radially inwards, i.e perpendicular to the rotation axis of the absorber, and scattered off radially. This would make the required modes hard to generate and hard to detect to prove amplification. Thankfully, theoretical models showed that the effect would also

---

[6]The fact that the predicted radiation from a black hole had a thermal spectrum, also vindicated Jacob Bekenstein's ideas [101] that black holes were truly thermodynamic objects, not just analogous with them, thus starting the field of black hole thermodynamics. Ted Jacobson has even shown Einstein's equation can be derived from thermodynamic principles [102].

[7]But who knows, maybe there is some far fetched possibility of finding a clever way to use radio waves to extract energy from tornadoes or hurricanes using the Zel'dovich effect.
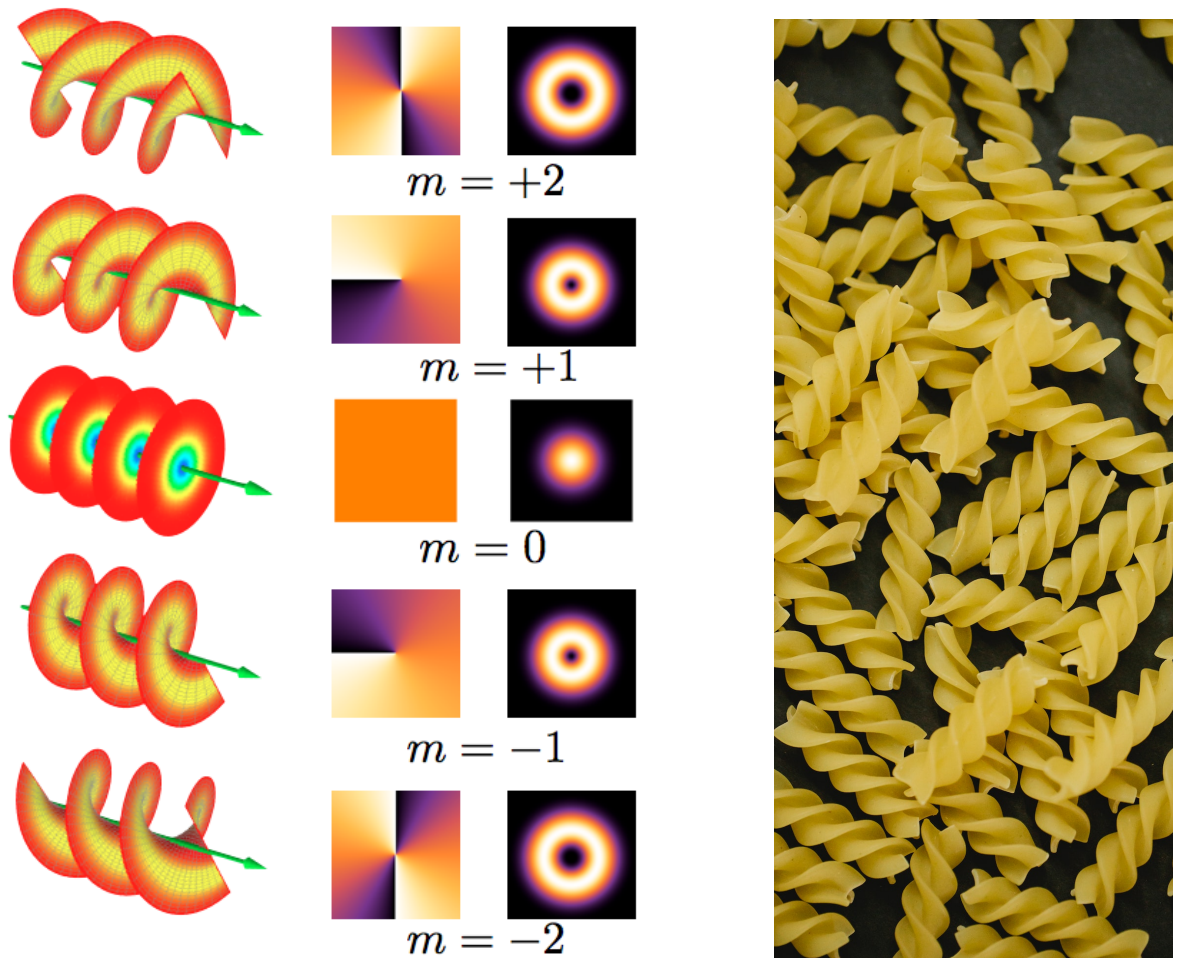
Figure 2.2: Spot the difference: (left) OAM modes. m refers to the mode number, referred to elsewhere in this thesis as ℓ. Columns show the helical structures, phase-front and intensity of the beams. By Wikimedia user E-karimi. Reproduced under CC BY-SA 3.0: creativecommons.org/licenses/by-sa/3.0/ **(right)** Fusilli pasta.

occur for waves propagating along the rotation axis, whether EM waves [78] or sound waves [80]. In particular, Faccio and Wright showed that the effect should work with sound waves in transmission, and with rotating sound absorbers much thinner than the wavelength [79], which meant rotation speeds of 10s of Hz could be used without needing an absorber on the scale of several metres.

Propagating sound waves with OAM can be produced by using a ring of speakers which put out the same frequency signal but with set phase delays between neighbouring speakers in the ring. This can create helical phase fronts and the order of OAM can be changed depending on the size of the phase delay [81].

The Zel'dovich condition coincides with the condition required to rotationally Doppler-shift waves so that their frequencies become negative, linking back to the negative energy condition in the Penrose process. The well-known linear Doppler effect creates a frequency shift between a source and a receiver who have relative linear velocity. The lesser known rotational Doppler effect creates a frequency shift of waves with angular momentum ℓ between a source and a receiver who have relative angular velocity Ω.

The rotational Doppler shifted frequency $\omega_{Doppler}$ is given by:

$$\omega_{Doppler} = \omega + \ell\Omega \qquad (2.9)$$

For sufficient $\ell\Omega$, the shifted frequency can become negative. The total angular momentum of the wave can have both spin and orbital angular momentum components, however for acoustic waves, the waves are longitudinal not transverse, so they do not have a spin degree of freedom, only the OAM contributes to the angular momentum. The negative frequency Doppler regime was observed in sound waves [81], where in practice the negative frequency waves were observed as positive frequency waves that had flipped sign in their OAM i.e. the phase front was rotating in the opposite direction. While in the linear Doppler case, extreme shifts to negative frequencies create a time inversion of the signal, this does not happen in the rotational Doppler case because there is no relative motion along the source-receiver axis. With the necessary condition already achieved in the lab, by adding absorption to the system, the Zel'dovich effect could finally be tested in experiment.

2.2 Amplification of Waves from a Rotating Body

This section (Section 2.2) reproduces the author's version of the accepted, peer reviewed manuscript published in *Nature Physics* on 22nd June 2020 as 'Amplification of Waves from a Rotating Body' by Marion Cromb, Graham M. Gibson, Ermes Toninelli, Miles J. Padgett, Ewan M. Wright, and Daniele Faccio. DOI: 10.1038/s41567-020-0944-3 [2] and does not violate the copyright of the publisher.

The majority of the research and the writing of the paper was undertaken by myself. I performed all the measurements and data analysis included in the paper, with the exception of fitting to the theoretical model, which was mostly done by Ewan Wright and Daniele Faccio. Figures generated by myself, with theoretical fits added by Daniele Faccio. The experimental set-up and the LabVIEW code for data acquisition had already been built and developed by Graham Gibson and Ermes Toninelli for a previous experiment to measure negative rotational Doppler shifted frequencies [81]. The adaptations to the experiment and the code required to generate and detect Zel'dovich amplification were formulated and carried out by myself, with technical help from Graham Gibson. The idea behind the experiment was conceived by Daniele Faccio, Miles Padgett and Ewan Wright, based on the theory work by Daniele Faccio and Ewan Wright [79]. Fruitful discussions with Graham Gibson, Daniele Faccio, Ewan Wright and Miles Padgett happened throughout the undertaking of the research. I drafted and rewrote the paper, with edits and corrections provided by Graham Gibson, Daniele Faccio, Ewan Wright and Miles Padgett.

Text included in { this format } has been added to the original text to explicitly indicate contributions of others.

2.2.1 Abstract

In 1971 Zel'dovich predicted that quantum fluctuations and classical waves reflected from a rotating absorbing cylinder will gain energy and be amplified. This key conceptual step towards the understanding that black holes may also amplify quantum fluctuations, has not been verified experimentally due to the challenging experimental requirements on the cylinder rotation rate that must be larger than the incoming wave frequency. Here we experimentally demonstrate that these conditions can be satisfied with acoustic waves. We show that low-frequency acoustic modes with orbital angular momentum are transmitted through an absorbing rotating disk and amplified by up to 30% or more when the disk rotation rate satisfies the Zel'dovich condition. These experiments address an outstanding problem in fundamental physics and have implications for future research into the extraction of energy from rotating systems.

2.2.2 Introduction

In 1969, Roger Penrose proposed a method to extract the rotational energy of a rotating black hole, now known as Penrose superradiance [83]. Penrose suggested that an advanced civilisation might one day be able to extract energy from a rotating black hole by lowering and then releasing a mass from a structure that is co-rotating with the black hole. Yakov Zel'dovich translated this idea of rotational superradiance from a rotating black hole to that of a rotating absorber such as a metallic cylinder, showing it would amplify incident electromagnetic waves, even vacuum fluctuations, that had angular momentum [75, 76, 97]. These notions involving black holes and vacuum fluctuations converged in Hawking's 1974 prediction that non-rotating black holes will amplify quantum fluctuations, thus dissipating energy and eventually evaporating. Analogue laboratory experiments have been carried out that confirm these physical ideas: Penrose superradiance, or superradiant scattering, in classical hydrodynamical vortices in the form of 'over-reflection' [103, 50] and Hawking's predictions classically in flowing water [49] and in optics [104, 105], plus a quantum analogue in superfluids [51, 52, 53]. However, experimental verification of Zel'dovich amplification in the form of amplification of waves from an absorbing cylinder is still lacking.

Zel'dovich found the general condition for amplification from an absorbing, rotating body:

$$\omega - \ell\Omega < 0 \tag{2.10}$$

where ω is the incident wave frequency, ℓ is the order of (what it is referred to in the current literature as) the orbital angular momentum, OAM [106, 107, 108] and Ω is the rotation rate of the absorber. When this is satisfied, the absorption changes sign and the rotating medium acts as an amplifier. Outgoing waves then have an increased amplitude, therefore extracting energy from the rotational energy of the body in the same spirit of Penrose's proposal.

Satisfying the condition in Eq. (2.10) with electromagnetic waves is extremely challenging. For $\ell = 1$ we would need rotation speeds Ω in the GHz to PHz region (microwave to optical frequencies) which is many orders of magnitude faster than the typical 100-1000 Hz rotation speeds available for motor-driven mechanically rotating objects. The highest OAM reported to date in an experiment is of order $\ell \sim 10,000$ in the optical domain [109], yet still leaves little hope of closing the rotation frequency gap required to satisfy Eq. (2.10) [110, 78].

However, recent work has shown that this condition and the observation of gain is theoretically achievable with acoustic waves [79, 111, 112]. The proposed interaction geometry requires sending an acoustic wave in transmission through a rotating absorbing disk. This provides a strong technical advantage compared e.g. to sending the waves radially inwards towards the outer surface of a cylinder, as it allows us to use relatively low frequencies for both the waves and the disk rotation whilst keeping the dimensions sufficiently compact (the disk can be made very thin). An acoustic wave with OAM order ℓ will experience a rotational Doppler shift [113, 114] due to the disk rotation, such that the wave frequency is shifted by a quantity $\omega - \ell\Omega$. This implies that the acoustic wave frequency will become negative when the Zel'dovich condition Eq. (2.10) is satisfied, which is precisely the pre-requisite physical condition outlined by Zel'dovich in his original work. This condition was recently observed by Gibson et al. [81] by measuring the acoustic frequency with a rotating microphone. Although one cannot directly measure negative frequencies, the switch in sign of the acoustic wave frequency manifested itself as a switch in the sign of the wave orbital angular momentum, which was measured by tracking the phase difference between two closely spaced, co-rotating microphones.

In this work we experimentally demonstrate that Zel'dovich amplification is readily observable with acoustic waves with relatively low OAM ($\ell = 3, 4, 5$) and at low acoustic frequencies of order of 60 Hz, i.e. readily accessible rotation rates for the absorbing disk such that spurious signals (for example, due to noise) are also minimised. Our acoustic measurements are resolved as a spectrogram and analysed as a function of disk rotation frequency, showing an intensity gain of $\sim 30\%$ of acoustic energy over a range of orbital angular momenta. These measurements represent a significant step forward in our understanding of Zel'dovich amplification, a fundamental wave-matter interaction that lies at the heart of a series of physical processes in condensed matter systems, superfluids and black holes.

2.2.3 Model

{ This section (Section 2.2.3) was mainly contributed by Ewan Wright and Daniele Faccio, based on previous work [79]. }

An acoustic conical wave carrying OAM ℓ is normally incident onto an absorbing material rotating at frequency Ω, and which is surrounded on both sides by non-rotating
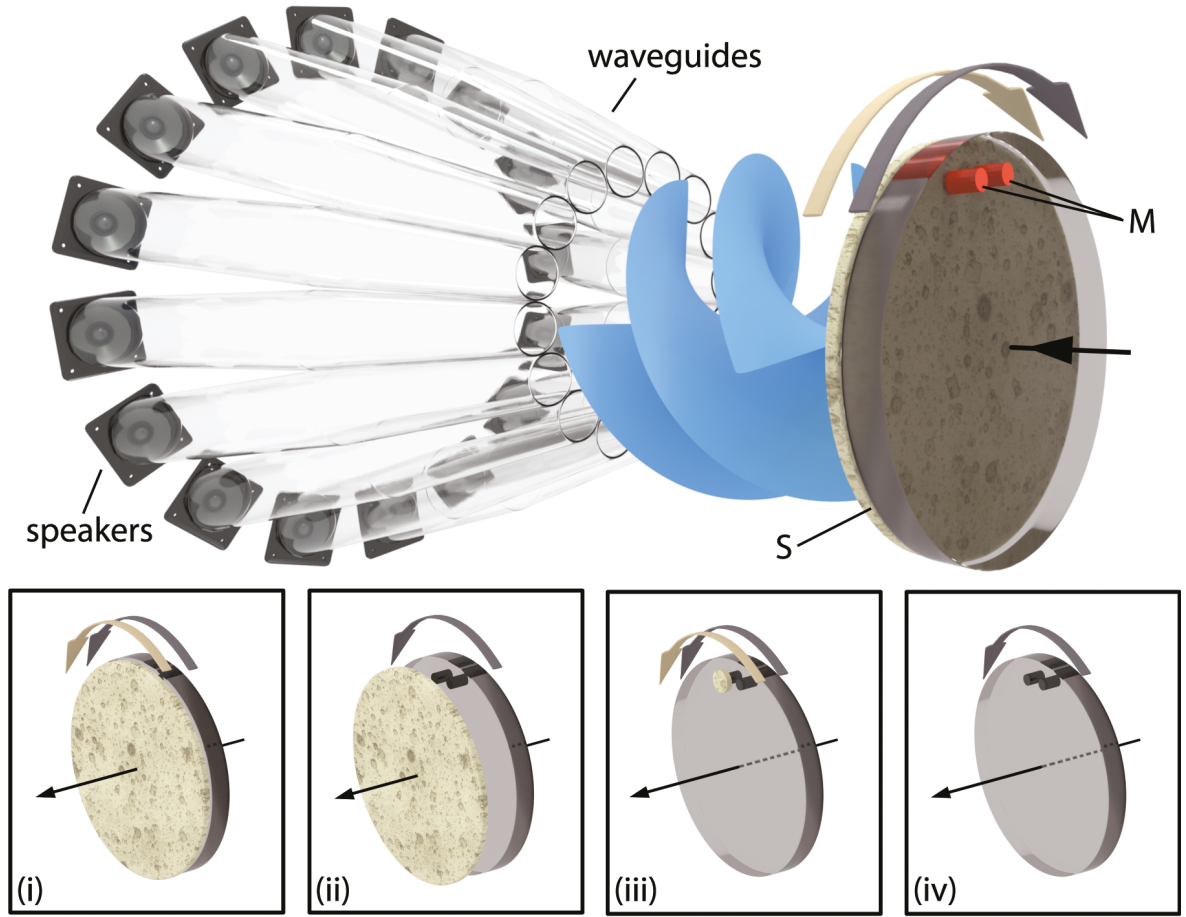
Figure 2.3: Schematic outline of experiment. 16 loudspeakers (Visaton; SC 8N) are arranged in a ring (diameter ≈0.47m) to create an OAM acoustic field, channelled by acoustic waveguides to a smaller area (diameter ≈0.19 m) and incident on a rotating disk of sound-absorbing foam (S). The absorbing disk also carries two closely spaced (2 cm distance) microphones (M). The microphones transmit their data via Bluetooth (Avantree; Saturn Pro), for live data acquisition whilst in rotation. The set-up is adapted from that used by Gibson et. al. [81]. Insets indicate the various configurations used in the experiments for the rotating disk and absorbing foam: (i) supporting disk with microphones and absorber are co-rotating; (ii) absorber is detached and remains static, whilst microphones rotate; (iii) an absorber is placed in front of only one of the two microphones; (iv) absorber is completely removed, microphones rotate.

air. The acoustic wave equation for density variations $\tilde{\rho}$ in a frame rotating with the medium is [115]:

$$\frac{\partial^2 \tilde{\rho}}{\partial t^2} - \Gamma' \nabla^2 \frac{\partial \tilde{\rho}}{\partial t} - v^2 \nabla^2 \tilde{\rho} = 0, \tag{2.11}$$

where v is the sound velocity and Γ' the damping parameter: A similar wave equation applies in the surrounding air with sound velocity v_0 and $\Gamma' = 0$. Under the condition that the medium length L is much less than the acoustic wavelength, the transmission of the beam incident from air onto the rotating medium may be solved by treating the effects of the medium absorption term in (2.11) within the first Born approximation. The details of this model have been worked out previously (supplementary material in

[79]) and lead to the following expression for the acoustic beam transmittance:

$$T = \left[1 - \frac{L\omega^2}{k_z v^4}\Gamma'(\omega - \ell\Omega)\right] C(\omega), \tag{2.12}$$

where $k_z = (\omega/v)\cos\theta$ is the longitudinal component of the sound wavevector and can be controlled through the conical beam focusing angle, θ. We underline that it is the term $(\omega - \ell\Omega)$ in the transmittance that can change the sign of the absorption and lead to gain in correspondence with the Zel'dovich condition in Eq. (2.10).

Equation (2.12) also includes the frequency response of the microphones, $C(\omega)$. Standard microphones exhibit a roll-off in sensitivity starting below ~ 100 Hz. We model this response with a function $C(\omega) = 1 - \exp[-(\omega - \ell\Omega)^2/\sigma^2]$, where σ determines the rate at which the sensitivity drops as a function of frequency. However the precise form of this function is not critical to our main conclusions, as the experiments described below compare between two microphones with the same frequency response.

2.2.4 Experiments

We generate an acoustic wave with orbital angular momentum using a ring of speakers and tubes that guide the sound directly onto the rotating disk, as shown in Fig. 2.3. The ring of 16 loudspeakers are all driven at the same frequency ($\omega = 60$ Hz), each with a specific phase delay in order to approximate a helical phase front, generating a beam carrying OAM [81]. Depending on the phase delay between adjacent speakers, different OAM states can be produced. For example, a phase delay of $\pi/2$ radians between adjacent speakers creates an OAM beam of topological charge $\ell = 4$.

A motor (RS Components; 536-6046) is used to rotate the disk fitted with two closely spaced microphones. Sound absorbing material can be placed in front of both, one or neither of the microphones (as illustrated in Fig. 2.3 (i), (iii) and (iv) respectively). Test measurements are taken with the two microphones under experimental conditions in order to ensure that they exhibit the same acoustic response, with and without the absorbing material placed in front of them (see Methods). The data from the microphones is communicated via Bluetooth to a computer.

Fig. 2.4 shows an example of a measured spectrogram. The acoustic frequency is set to 60 Hz on all of the speakers and phase delays are set to generate waves with $\ell = 4$ - other ℓ modes are expected to also be generated as a result of the imperfections in speaker uniformity and the limited number of speakers used [81]. The Zel'dovich condition and inversion from absorption to gain is therefore expected for a disk rotation of 15 Hz. The disk is therefore rotated in the 0 to 30 Hz range, which also corresponds to the linear response range of our motor (i.e. linear increase of rotation speed with driving voltage). The spectrogram exhibits a series of features: as the disk rotation rate increases, the input 60 Hz frequency splits into a series of signals, depending on
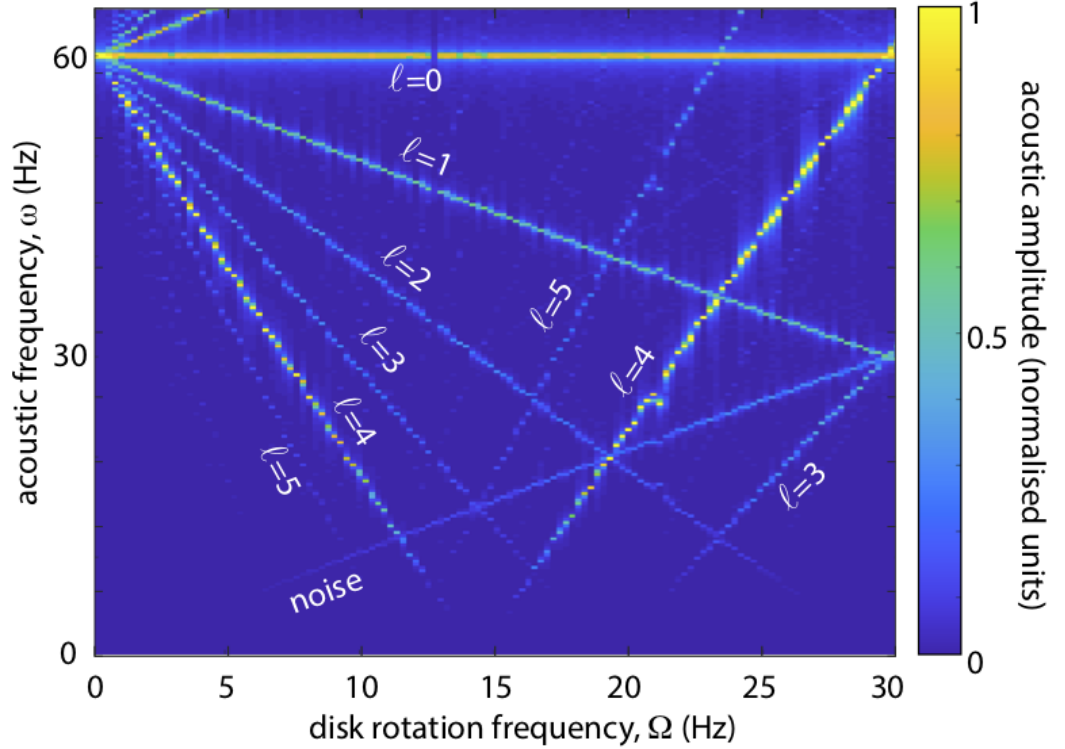
Figure 2.4: Spectrally resolved acoustic measurements. An example of a measured spectrogram showing the measured acoustic frequency (ω) spectrum in the rotating frame for increasing rotation frequencies (Ω). The OAM beam is generated in the lab frame at 60 Hz at a constant volume, with the speaker output phases optimised for the $\ell=4$ mode. For each value of Ω, the data shows an independent spectrum, obtained from the Fourier transform of the measured signal from one of the two microphones on the rotating disk. The data clearly shows the input 60 Hz signal split into multiple components, corresponding to the various OAM modes (indicated in the graph) as a result of a rotational Doppler shift, $\omega - \ell\Omega$, that leads to linearly varying frequency as a function of Ω, for each ℓ-mode. The microphone response decreases for decreasing measured ω and below 4 Hz is zero (i.e. below the noise level). The supplementary video shows an animation with the overlaid acoustic signal that is recorded with increasing Ω.

the OAM value ℓ with a clear signal measured for $\ell = 0 - 5$ (as labelled in the figure). We can also clearly see an additional signal that is due to the noise generated by the rotation and therefore appears at the same frequency as the rotation rate.

All of the observed OAM modes shift in frequency due to the rotational Doppler shift ($\Delta\omega = -\ell\Omega$) and after the labelled OAM modes have gone through zero frequency they satisfy their Zel'dovich condition. Beyond zero, the rotational Doppler shift formula predicts negative frequencies, which results in an inversion of the sign of ℓ (i.e. positively sloped traces in the spectrogram) when measured in the rotating frame [81]. In order to verify the presence of gain in this Zel'dovich regime, we proceed to extract the amplitude for each ℓ value from the spectrograms.
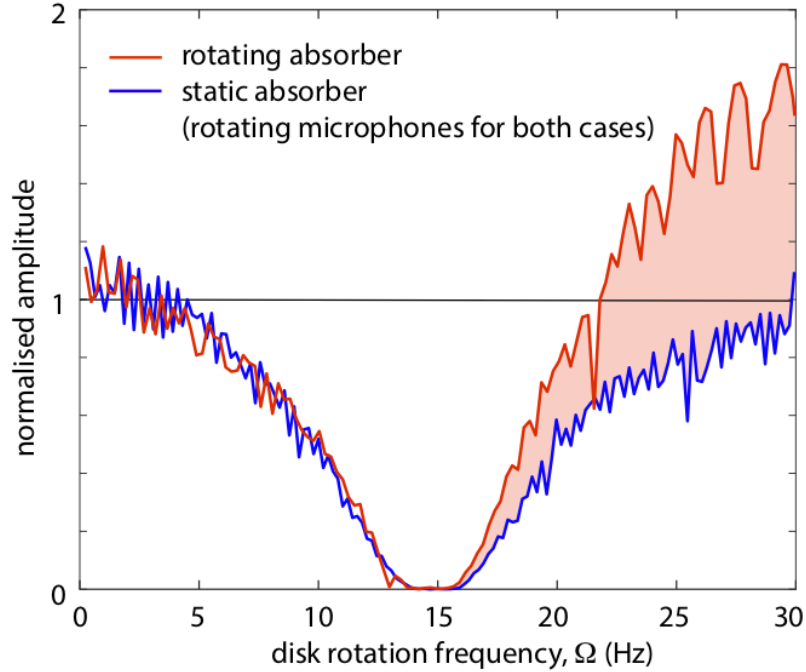
Figure 2.5: The effect of rotation. A measurement of the acoustic amplitude for $\ell = 4$ for the case of a rotating absorber (red curve) and for the case in which the absorber is detached from the rotating disk holding the microphones, and hence is static (blue curve). The rotating absorber case shows a clear increase of the transmitted acoustic amplitude above the Zel'dovich condition ($\omega - \ell\Omega < 0$ is satisfied for this case when $\Omega > 15$ Hz).

2.2.5 Results

In Fig. 2.5 we show the effect of rotation on transmitted acoustic signal for the $\ell=4$ mode as the disk rotation rate is increased from 0 to 30 Hz. The two curves indicate two different cases: the absorbing disk is co-rotating with the microphones (red curve) and the absorbing disk is slightly detached from the motor mount so that the microphones rotate whilst the disk remains static (blue curve). As the rotation speed is increased, the modes are Doppler shifted and the measured signal from both microphones decreases due to the lower microphone response at lower acoustic frequencies. As the mode is Doppler shifted through zero frequency (at $\Omega = 15$ Hz), the measured acoustic frequency increases again and the transmitted signal increases. In the non-rotating case, no increase is observed in the transmitted signal for the same rotational Doppler shift (i.e. for symmetric points around $\Omega = 15$ Hz). Conversely, when the absorber is in rotation with no other changes to the experiment, we observe a clear increase in the transmitted signal at high rotation rates that satisfy the Zel'dovich condition (shaded area).

In Fig. 2.6 we show evidence of absolute gain in the acoustic signal, i.e. evidence that the transmitted energy is larger than the incident energy. One microphone (microphone 1, red curve) in the rotating frame has absorbing foam in front of it, the other microphone next to it (microphone 2, blue curve) does not. We observe that at low rotation speeds (2-5 Hz), the transmitted signal is lower compared to microphone 2, as it has been
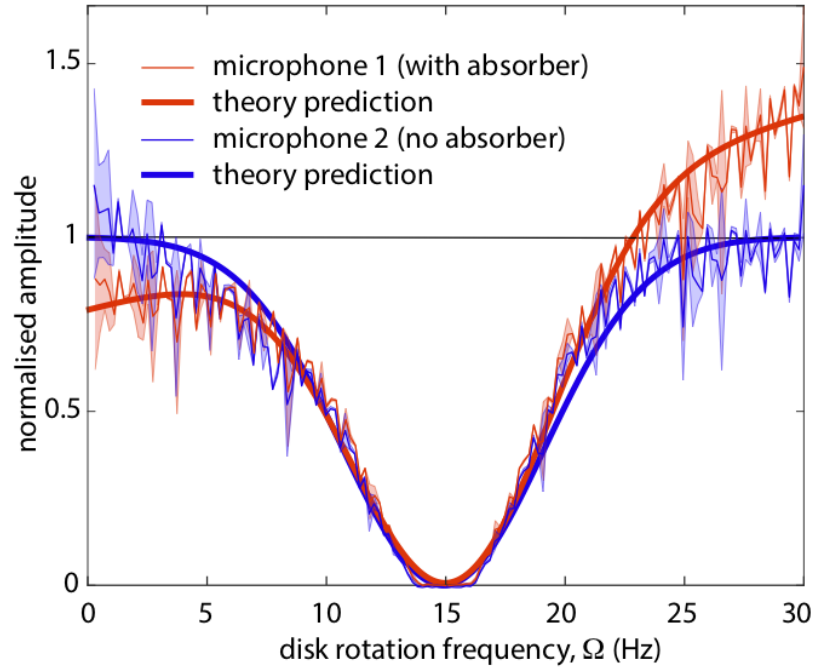
Figure 2.6: Evidence of absolute gain. The measured acoustic amplitude with $\ell = 4$ and with the absorber placed on one of the microphones (red curve) but not on the other (blue curve) shows clear differences in the signals. For rotation rates $\Omega < 15$ Hz (i.e. such that $\omega - \ell\Omega > 0$) absorption is observed in particular at the lowest frequencies (blue shaded area). Conversely, at the highest frequencies (where $\omega - \ell\Omega < 0$), a clear gain in the transmitted signal is observed. The ~ 1.3x higher signal at $\Omega \sim 30$ Hz compared to $\Omega \sim 0$ Hz highlights the presence of absolute gain of the acoustic signal. Theoretical predictions from Eq. (2.12) are shown with the damping parameter $\Gamma' = 0$ m^2/s (no absorber, thick blue curve) and $\Gamma' = 8 \cdot 10^4$ m^2/s (thick red curve) The shaded areas show the standard deviation of the measured signals across 7 sets of data (2 seconds of acquisition each). { Data and error bars analysed and plotted by myself, theoretical fits to Eq. (2.12) were done by Ewan Wright and Daniele Faccio. }

absorbed by the foam. Conversely, rotating faster than $\Omega = 15$ Hz and thus satisfying the Zel'dovich condition leads to clear increase in the transmission signal compared to the non-absorbing case. The amplification is such that the signal transmitted through the absorber above $\Omega = 25$ Hz is greater by about 30% than the signal at the slowest rotation speeds that did not pass through the absorber. This indicates absolute gain: we measure more sound with the rotating absorber than without it.

{ Theoretical fits to Eq. (2.12) were done by Ewan Wright and Daniele Faccio. }

The thick solid curves in Fig. 2.6 show the theoretical predictions from Eq. (2.12). We first proceed to fit Eq. (2.12) to the data from microphone 2 that has no absorber present ($\Gamma' = 0$) thus obtaining the shape of $C(\omega)$, the frequency response of the microphones. This determines the frequency sensitivity parameter, $\sigma = 22$ Hz. We then refer to the data from microphone 1 and use the low rotation frequency (2-5 Hz) data to determine the value of the dissipation parameter, $\Gamma' = 8 \cdot 10^4$ m^2/s. We notice that the same theoretical curve provides a quantitatively accurate prediction of the full behaviour for all Ω, including the 30% gain measured at high rotation frequencies,

thus further corroborating the interpretation of the gain originating from the Zel'dovich effect.

Further analysis shown in Fig. 2.7 of multiple OAM modes transmitted through the rotating absorber reveals amplification for all the OAM modes analysed that satisfy the Zel'dovich condition, not just the strongest $\ell = 4$ mode. In more detail, if we consider in Fig. 2.7 a fixed Doppler shifted frequency, e.g. $\omega - \ell\Omega = -30$ Hz for all ℓ (corresponding to $\Omega = 30$, 22.5 and 18 Hz for $\ell = 3$, 4 and 5, respectively), we note that all curves within the experimental error show the same gain of $\sim 10\%$. If instead we consider a fixed disk rotation frequency, e.g. $\Omega = 30$ Hz we see that the gain, i.e. transmitted acoustic energy, increases linearly with ℓ. Both of these observations are in agreement with the theoretical prediction Eq. (2.12).
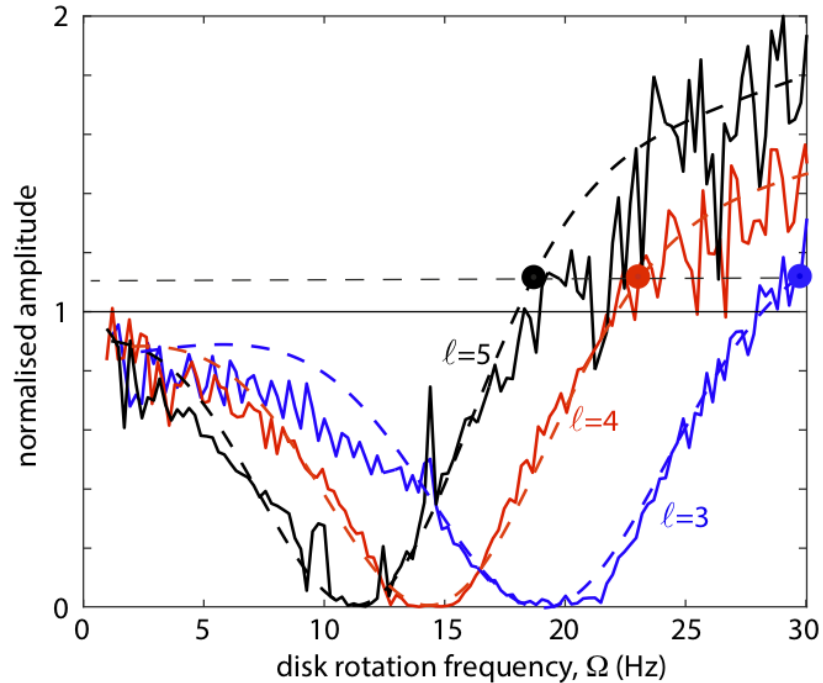
Figure 2.7: Comparison for different OAM beams. The spectrograms show signals for a range of ℓ that can also be analysed and compared. For all ℓ that pass through the Zel'dovich condition we see evidence of transmittance greater than 1 as a result of rotation. Comparing the transmission values for the same rotational Doppler shifted frequency (i.e. -30 Hz, corresponding to $\Omega = 30$, 22.5 and 18 Hz (indicated as solid circles) for $\ell = 3$, 4 and 5, respectively), the gain in transmittance appears, within the experimental error, to be constant, ~ 1.1 (horizontal dashed line) for all ℓ and increases linearly with ℓ for a fixed Ω (compare e.g. at $\Omega = 30$ Hz). Both observations confirm the predictions of Eq. (2.12). Theoretical fits from Eq. (2.12) are also shown as dashed lines, with no varying parameters (other than ℓ). { Data analysed and plotted by myself, theoretical fits to Eq. (2.12) were done by Ewan Wright and Daniele Faccio. }

2.2.6 Conclusions

Amplification of waves from a rotating absorber as predicted by Zel'dovich is a foundational prediction in fundamental physics that lies somewhere between the proposition by Penrose that energy can be extracted from rotating black holes and Hawking's prediction that static black holes will evaporate as a result of the interaction with quantum vacuum. Zel'dovich's original model indeed referred to amplification of vacuum modes from a rotating metallic cylinder but was also extended to include the amplification of classical waves. Whilst very hard to verify with optical or electromagnetic waves, acoustic waves allow direct measurements of significant amplification of waves due to a rotating absorber. A key step in achieving this result is the use of a geometry where the waves are transmitted through a thin absorbing cylinder [79, 111, 112] rather than in reflection from an extended cylinder. This relaxes the experimental constraints and limitations that arise in the original proposal due to the requirement that the cylinder length be larger than the wavelength, in order to ensure interaction and reflection of the incident waves. For example, this would have required a cylinder with a length of several meters for the conditions used here, which would have been very challenging to rotate at 30 Hz.

Similar concepts could in principle be extended to electromagnetic waves [78] thus possibly extending our results also to amplification of electromagnetic modes from the quantum vacuum.

2.2.7 Methods

The rotation speed of the absorber was increased in steps of (approximately) 0.2 Hz. Various forms of sound absorbing foam were tested with varying yet similar porosity (e.g. cellular ethylene propylene diene monomer, EPDM, soundproofing rubber, RS Components, 5% absorption at 60 Hz). All cases showed similar results, in line with our expectation that details in the medium 4-5 orders of magnitude smaller than the sound wavelength will not significantly influence the dynamics.

Figure 2.8 shows a photograph of the sound-absorber interaction region. The acoustic waveguides can be seen on the left, conducting the sound towards and directly on to the rotating absorber. The absorbing foam is held in place with a support structure, which is made of a plastic disk with no air gaps or possibility for sound to reach the microphones (5 mm diameter, embedded in the supporting plastic disk) without passing through the foam. This setup ensures that all sound reaches the microphones only through the foam.

For each rotation speed, sound was recorded for short time intervals, e.g. 2 to 3 seconds. The microphone signal was then Fourier transformed (and averaged over 2 to 3 separate measurements) so as to decompose the signal into its frequency spectrum. The frequency spectrum for each rotation speed was then used to create a single matrix

of the full spectrogram (e.g. Fig. 2.4). In MATLAB the 'tfridge' range of functions was used to extract the signal amplitude (in arbitrary units) along each OAM mode in this spectrogram. The highest neighbouring frequency bin for each rotation speed was added to the signal in order to reduce noise from the discretisation of the Fourier-transformed data.

We also verified that the two microphones in our setup are calibrated so as to provide the same response for the same incident signal, for all rotation speeds. Fig 2.9 shows two graphs with measurements of the two microphone responses (black and green curves) when both are uncovered (absorber removed) or both have an absorber placed in front of them. Both graphs show a nearly identical response for the two microphones under the operating conditions of our experiments.
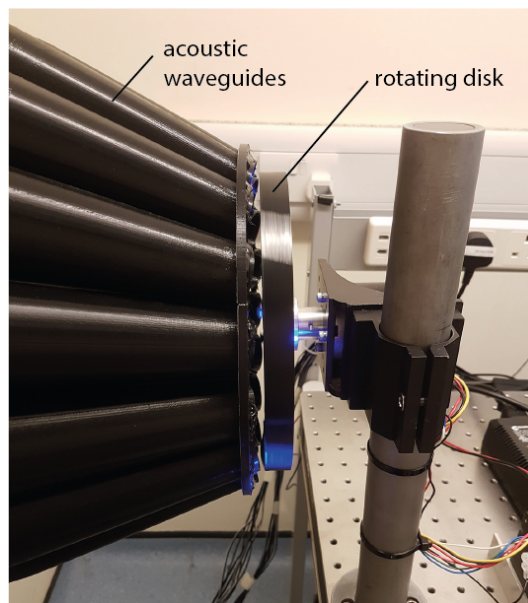
Figure 2.8: Photograph of the setup showing the detail of the interaction region where the acoustic waveguides conduct the sound directly on to the absorber, supported by a plastic disk.
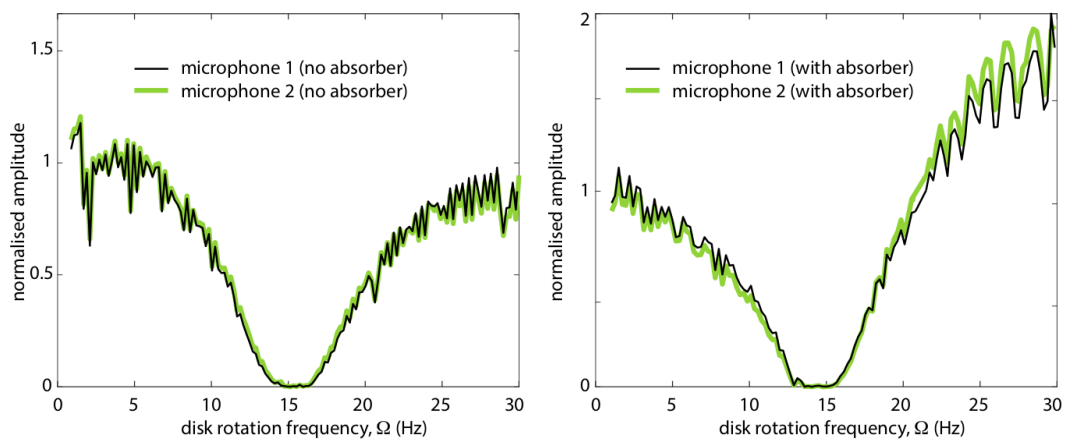
Figure 2.9: Microphone calibration: measurements of response when both microphones have no absorber or both have absorbers placed in front of them, showing that the microphones are both calibrated and measure, as desired, the same signal.

2.3 Additional Methodology

2.3.1 Choice of measurement frame

The amplification effect should not depend on the reference frame the sound is measured in [79], so it can be measured in the rotating frame, or in the lab frame. However, experimental considerations made it easier for us to observe the effect in the rotating frame. Measuring in the rotating frame means the absorbing foam can be directly placed over the microphones, ensuring only sound transmitted through the foam is measured when it is rotating. Various distorting factors [81], for example the discreteness of the array, mean the 60 Hz OAM beam generated is not completely pure. These factors mean the acoustic energy spreads over multiple OAM modes, as well as exciting higher harmonics (120 Hz, 160 Hz, etc), to which the microphone is more sensitive (early data showing these higher harmonics is shown in Figure 2.10). In the lab frame the whole discrete spectrum of OAM modes generated are degenerate in acoustic frequency, so are more complicated to separate when measuring with static microphones. Detecting all the OAM modes generated at once means that amplification of one mode which satisfies the Zel'dovich condition (Eq. 2.10) could be hidden amongst a greater absorption of the whole beam due to other OAM modes present that do not satisfy Eq. 2.10. Measuring in the rotating frame, as the rotation speed is increased from zero, the rotational Doppler effect means that the single Fourier peak at the lab frame frequency of 60 Hz spreads out into a number of clearly defined frequency peaks corresponding to the OAM modes present (Figure 2.4), as each has a characteristic rotational Doppler shift. By using the rotational Doppler effect to separate these modes in Fourier space, the sound present in a single mode satisfying the Zel'dovich condition (Eq. 2.10) can be isolated, extracted and analysed. The exception to this is then only at individual (ω, Ω) points where the modes cross.

2.3.2 Optimising the effect

To see a strong effect in transmission, it was found to be critical to keep the absorbing foam and microphones as close to the waveguide outputs as possible. This was due to the large diffraction of OAM modes (Figure 2.11) away from the waveguide output and to avoid detecting sound that had been reflected from other objects or walls in the room.

The thickness of the foam also should not be too large, to keep the microphones close to the waveguide outputs, and as some sound needs to get through. An example of the absorbing foam used is shown in Fig. 2.12.
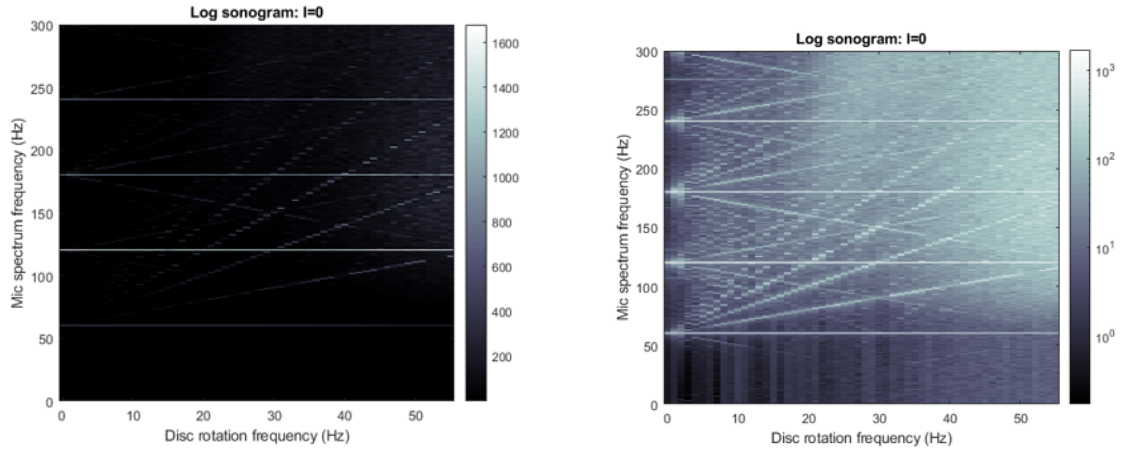
(a) Linear scale, PC with poor microphone input at low frequencies

(b) Log scale, PC with poor microphone input at low frequencies
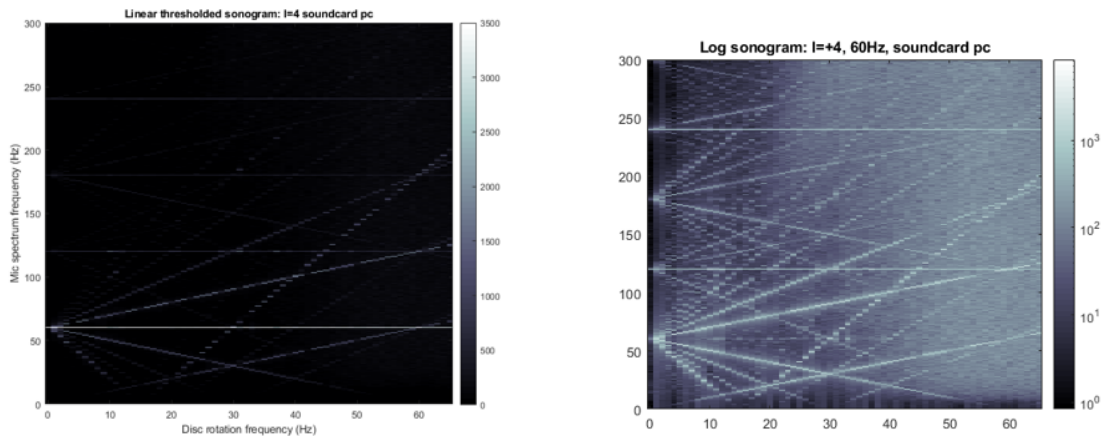
(c) Linear scale, PC with better low frequency response

(d) Log scale, PC with better low frequency response

Figure 2.10: Sonograms using rotation to separate out different OAM modes with the rotational Doppler shift. Using both linear (a,c) and logarithmic scales (b,d). Shows the difference in mode output between target modes of l=0 and l=+4, and difference in frequency response between different PCs (using the same microphones). One PC has poor frequency measurements under about 80 Hz (a,b), the other below about 20 Hz (c,d). Shows the presence of higher harmonics and additional OAM modes present in the sound, when the aim is to generate a 60Hz sound wave in a single OAM mode. The strong $\ell=0$ harmonics at 60, 120, 180, 240 Hz don't always show up on the rendered pixel figures because they're horizontal lines only one frequency bin thick, but they are there. The log scale shows just how many other components there are other than $\ell = 4$ (these other faint components also show up when generating a l=0 acoustic beam).
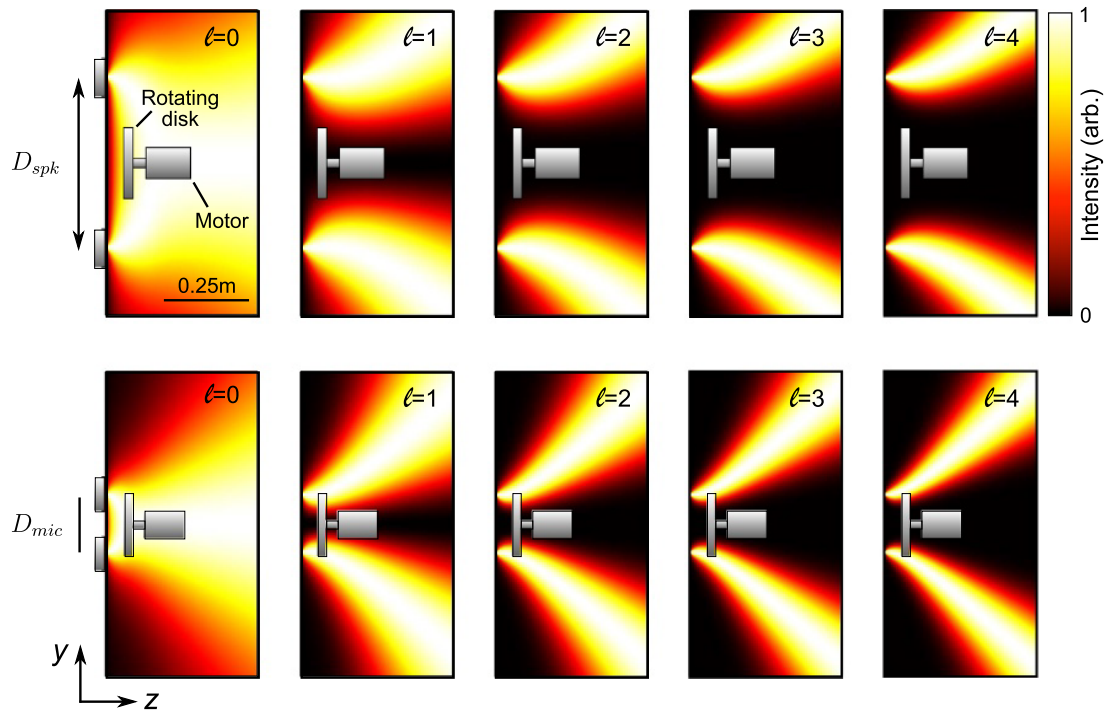
Figure 2.11: Diffraction of OAM modes. Supplementary Figure 2 from Ref. [81] Copyright © 2018 the Author(s). Published by PNAS. Reused under the conditions of the Creative Commons Attribution-NonCommercial-NoDerivatives License 4.0 (CC BY-NC-ND)

Figure 2.12: Example of sound-absorbing foam: An example of the foam used as absorbing material in the experiments. The full disk is shown here (diameter 20 cm, thickness 1 cm)

2.4 Conclusions

2.4.1 Impact

The experiment was generously described in the accompanying Nature Physics News & Views article by Bruce Drinkwater as *"a masterpiece of elegant simplicity"* ([116]), explaining:

> *There are two reasons why this experiment is so elegant. The first is that it is performed in such a way that other effects are minimized so that the Zel'dovich amplification was clearly and irrefutably observed. [...] The second justification for elegance is less tangible, but I would suggest that it fulfils an experimentalist's version of beauty. Once described and — better still — once seen, it is immediately obvious that it has the minimum number of parts arranged in the simplest possible way to produce a conclusive result. This second aspect means that it is repeatable and will allow others to extend this line of thinking further. If you would like a black hole in your lab, here is the recipe! ([116])*

Drinkwater also points out the importance of the experiment in the context of work with acoustic OAM waves, which are becoming increasingly popular for their applications, for example in acoustic manipulation at everyday length scales. The significance of the work in the field was further emphasised when the Institute of Physics (IOP) awarded the paper the 2021 Bob Chivers Prize in Physical Acoustics: 'this annual prize promotes research in physical acoustics by recognising the best paper by a PhD student at a UK university' [117].

Within two years of the paper, a research group at Zhejiang University in China was able to replicate the experimental setup and published work where they also observed amplification of sound waves due to interaction with a rotating absorber [118]. [8] This work they see as *"a great prospect in practical applications such as amplifying the information-carrying OAM waves for high-speed acoustic communication"* ([118]), which is an essential technology in regimes where there is high electromagnetic absorption and optical scattering [119] such as underwater: i.e. situations where sonar is used rather than radar.

The research also inspired interest from non-scientists, particularly with the link to black hole physics. To present the work in an accessible way to the public, I created an animated video [120] that explained the research and its context, released when the paper was published along with a press release. Journalists picked up on the work both online and in national print media, [121, 122, 123, 124] as a result of this media buzz I gave interviews on several radio shows, including BBC Radio [125], and together with

---

[8]However, as they were motivated more by seeing strong amplification than certifying the Zel'dovich effect, it seems clear that there are additional amplification effects at play in their work. By adding periodic holes to the rotating absorber, which is likely to introduce resonance effects, they engineer it to obtain high amplification, even at a rotation frequency too low to satisfy the Zel'dovich condition. As they use non-rotating microphones there is an air gap between the absorber and the microphones so they could also be picking up sound that is not transmitted through the absorber.

my supervisor wrote an article for The Conversation [126]. The extent of this outreach was even such that I even received some "fanmail" from an inmate in a United States prison, who had heard the segment on the BBC World Service! In recognition of the success of this public outreach, I was awarded the 2021 University of Glasgow Physics and Astronomy Outreach prize.

2.4.2 Further research

2.4.2.1 Energy loss of the absorber

Further work not included in the paper is to observe the effect from a different perspective; that is, as well as measuring the amplification of the waves, to observe the correlating loss of rotational energy of the absorber. I made some progress on this, however the way that the motor was constructed to lock in to a stable, constant frequency made the results a little unclear and not always consistent, there were too many spurious mechanical forces to take into account. To avoid this, measurements on the changes to the rotation slowing rate were tried when the disc was freely spinning and the motor power turned off, but this also had problems. The lack of purity of the OAM mode produced by the speakers made it hard to pinpoint exactly what the expected response on the absorber would be for all the modes making up the sound waves at different rotation frequencies, and extracting the damping effect of the Zel'dovich effect from the larger damping produced by the general sound pressure and normal OAM torque in these conditions would have been tricky. However with a different motor with a smoother linear response, or improvement to the purity and characterisation of the OAM waves [127], this avenue could be pursued for further research.

2.4.2.2 The Electromagnetic Zel'dovich effect

The proof of this Zel'dovich effect in acoustics, as well as the large size of the effect should provide extra motivation to tackle an experiment showing the effect in electromagnetic waves, even potentially in the quantum regime. One experimental proposal to achieve the very tricky electromagnetic frequency-matching conditions is to construct an electric (super-conducting) circuit that interacts with a freely levitating rotating conducting microsphere that can spin up to MHz frequencies, and measure the effect on the EM mode of the circuit [128]. If noise sources can be suppressed, then it may even be possible to measure generation of EM modes with such a system. This would draw an even closer link between this research and quantum effects in rotating frames and curved spacetimes.

Despite its long history, going back to Thomas Young at the beginning of the 19th century, optical interference still challenges our understanding, and the last word on the subject probably has not yet been written

Leonard Mandel, 1999

3

Variations on the Hong-Ou-Mandel Effect

3.1 Introduction

3.1.1 Motivation

The endgame target experiment was to use rotational motion to alter a quintessentially quantum property. With my experimental background in quantum optics, using photons seemed a natural choice, as did investigating quantum entanglement, for the non-classical element. Photons, especially entangled photons, are the workhorses of quantum optics [129, 130], easily created and adapted to test out different quantum phenomena, particularly in quantum information theory [131]. The Hong-Ou-Mandel (Section 3.1.3) (HOM) effect [132] is another probe of non-classicality of light; indistinguishable single photon states interfere differently to classical states of light due to quantum statistics. A previous experiment done at the University of Glasgow [133] used rotation to change the delay between two photons, detecting the time difference with HOM interference. HOM measurements can also act as an entanglement witness for antisymmetric entangled states [134]. For antisymmetric input states, an inversion of the usual Hong-Ou-Mandel 'dip' signal is observed, turning into a peak. If we could use rotational motion to alter photon entanglement into an antisymmetric state, this should be verified by a dip turning into a peak. Adapting the experimental design to change the quantum properties of the photons with rotational motion was a natural next step.

Before attempting the experiment in a rotating frame, it made sense to first become familiar with generating entangled photons, setting up a Hong-Ou-Mandel interferometer, and investigating the conditions required to generate and witness an antisymmetric entangled state, in a non-rotating experiment. While similar static experiments had been done using cavities [135] or birefringence [136] to manipulate the symmetry of frequency-entangled photon pairs in a HOM experiment, we believe we were the first to use a Michelson interferometer in our static setup. This choice also allowed us to probe different coherence length regimes of the photons: both outside the single photon coherence length (which had already been investigated [137]) and inside (which had not been done in experiment). This was particularly important as the initial theoretical plan for the rotating experiment [1] proposed using a balanced Sagnac interferometer, requiring investigation inside the single photon coherence length regime.

Creating a Hong-Ou-Mandel experiment where we can create dips and peaks requires general knowledge of the different aspects of the experiment. Firstly, how to generate entangled photon pairs with the common method of spontaneous parametric down-conversion (Section 3.1.2) (SPDC), secondly, a general understanding of HOM interference, and thirdly, how to use optics to manipulate the entangled state of the produced photon pairs to create peaks.

3.1.2 Spontaneous Parametric Down Conversion (SPDC)

The most common method for producing photon pairs and heralded single photon states for quantum optics experiments is using SPDC [138, 139, 140, 141].

In general, the optical properties of a material depend on the strength of electrical, magnetic and acoustic fields present. Light, being an electromagnetic wave, also has the potential to change the optical properties of the material it passes through; at sufficiently high light intensities, nonlinear optical effects can occur. The optical response of a nonlinear material is described by a polarisation P which is a nonlinear function of the electric field E:

$$P_i = \epsilon_0 \left(\sum_j \chi^{(1)}_{ij} E_j + \sum_{jk} \chi^{(2)}_{ijk} E_j E_k + \sum_{jk\ell} \chi^{(3)}_{ijk\ell} E_j E_k E_\ell + \cdots \right) \tag{3.1}$$

and characterised by nonlinear optical susceptibilities of different orders $\chi^{(2)}, \chi^{(3)}, \dots$. When light propagates through such a material, it excites a wave in the material polarisation. The nonlinear polarisation wave contains frequency components which are not present in the incident light, and light at these new frequencies can be generated in the medium [142]. This is the basis of processes such as frequency doubling, sum-frequency generation and parametric amplification, as well as SPDC. These processes usually require high input intensities for the nonlinear contributions to be significant.

SPDC can occur in materials (usually crystals) with a second-order ($\chi^{(2)}$) nonlinear susceptibility. Within such a nonlinear crystal, a pump photon of frequency ω_p can spontaneously down-convert into two photons of lower energy (historically denoted the 'signal' and the 'idler'). This spontaneity means photon pair production events (and the times between them) are independent. The spontaneity arises from the fluctuations of the quantum vacuum, making the process very inefficient: the highest generation rates are of one pair per 10^6 pump photons [143], but typical rates are much lower (one pair per 10^{12}). However this does mean that heralded SPDC photons are a good approximation of the completely non-classical single photon Fock states (although not perfect, because there is a non-zero possibility of four photons being produced rather than two [144, 145]).

SPDC is a parametric process, which means that it does not change the quantum state of the medium itself. Because no energy or momentum can be transferred to the material, the photons involved obey energy and momentum conservation laws [146]:

$$\omega_p = \omega_s + \omega_i \tag{3.2}$$

$$\vec{k}_p = \vec{k}_s + \vec{k}_i \tag{3.3}$$

If $\omega_s = \omega_i$ the process is 'degenerate', if $\vec{k}_s = \vec{k}_i$ the process is 'collinear'. These conservation laws ensure time-energy and position-momentum entanglement between
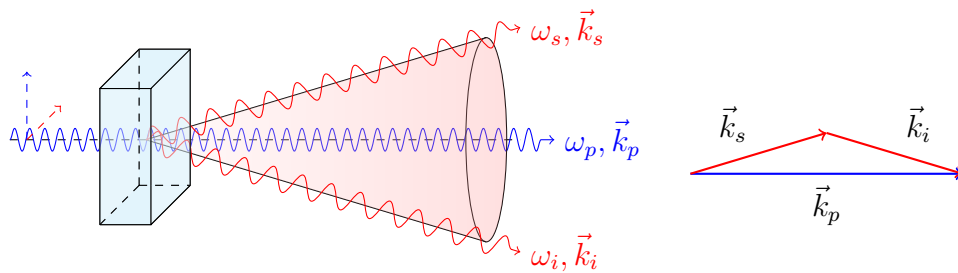
Figure 3.1: Type-I crystal SPDC generation. The higher frequency pump is shown in blue, signifying vertical polarisation and propagates along the horizontal axis. The lower frequency signal and idler are shown in red, signifying horizontal polarisation.

the pair of photons produced [147].

Parametric processes are generally coherent, so require phase matching between the pump and the down-converted beams to be efficient, to ensure amplitude contributions from different parts of the crystal constructively interfere along the propagation direction. Chromatic dispersion[1] generally causes a phase mismatch, but the phase matching is often achieved by utilising a different polarisation in a birefringent material so that the refractive indices match e.g $n_e(\lambda_p) = n_o(\lambda_s)$.

There are two types of phase matching: critical and non-critical phase matching. Critical phase matching relies on careful (within a finite 'acceptance angle') alignment of the angle of the beams with respect to the crystal's optic axes. Non-critical phase matching relies on careful temperature control to match refractive indices along the optic axes, this makes it less sensitive to alignment, but may require high temperatures of 200 °C or more.

The use of polarisation in phase matching leads to different types of SPDC [129]. In Type I, the generated photons share the same polarisation (orthogonal to the pump) i.e. H → VV, V → HH (Figure 3.1). In Type II the generated photons have perpendicular polarisations, i.e. H → HV, V → VH. Type 0 (V → VV, H → HH) can be achieved in periodically poled materials [148], where quasi-phasematching occurs due to the periodic nature of the material and birefringence is not required.

There are certain other effects that reduce the efficiency of nonlinear processes, these are known as temporal and spatial walk-off. Temporal walk-off occurs when there is a group velocity v_g mismatch between the e- and o-waves, or between different frequencies in the crystals [149]. This limits the useful interaction length within the crystal and different photons become temporally separated by $L\sigma$ after propagating through a crystal of length L, where the group velocity mismatch (GVM) σ is:

$$\sigma = \frac{1}{v_g^1(\lambda)} - \frac{1}{v_g^2(\lambda)}. \tag{3.4}$$

Spatial walk-off occurs because in birefringent crystals the Poynting vector (the direc-

---

[1]Chromatic dispersion: noticeable frequency dependence of phase and group velocity on the medium the light is travelling through.

tion of the flow of energy) is not necessarily in the same direction as the wave vector $\vec{k}$ (which is normal to the wavefronts), there can be an angle ρ between them [150]:

$$\rho = -\frac{1}{n_e}\frac{\partial n_e}{\partial \theta}.\tag{3.5}$$

This creates a deflection towards decreasing refractive index for e-polarised waves propagating at an angle θ to the crystal optical axis, due to the angle dependence of its refractive index $n_e(\theta)$. As as e- and o- beams separate it limits the useful interaction length in the crystal, and is a problem for critical phase matching.

3.1.2.1   Polarisation-entangled SPDC

To generate polarisation-entangled pairs (e.g. to create the Bell states in Section A2.0.1) with SPDC requires the generation of H-polarised down-converted photons to be otherwise indistinguishable from the V-polarised down-converted photons. This can be done with any SPDC type. For Type II by partly overlapping the H and V emission rings generated from a single Type II crystal, and post-selecting the two overlap spots in the far field for the signal and idler beams, the $|\Psi\rangle$ state is generated [151]. The symmetry of the two-photon polarisation Bell state $|\Psi\rangle$ can be altered (between $|\Psi^+\rangle$ and $|\Psi^-\rangle$) simply by using a birefringent wave plate to adjust the phase between the polarisations [152]. For Type I, by using two thin Type I crystals stacked at right angles, the emission cones from each crystal overlap completely, and a $|\Phi\rangle$ state is generated for diametrically opposed photons over the whole ring [153], meaning nearly every pair generated is hyperentangled (energy, momentum and polarisation). Type 0 polarisation entangled SPDC is also possible [154]. Walk-off effects can degrade the entanglement if they introduce distinguishing information between the processes, and are often combated with compensating crystals.

3.1.3   The Hong-Ou-Mandel (HOM) Dip

The Hong-Ou-Mandel effect [132, 155], also known as photon coalescence or photon bunching[2], is often regarded as one of the essential experiments in quantum optics [129]. Originally, the technique was used to measure the length of a photon wave-packet at a single photon level, as an alternative to nonlinear effects with high energy pulses [157]. More generally, a HOM interferometer tells you about the distinguishability of photons.

The HOM effect is a quantum effect that occurs when two indistinguishable single photons are incident at the same time on orthogonal input ports of a lossless 50:50 beamsplitter, which has an equal probability of reflecting or transmitting light [156]. A beamsplitter (Figure 3.2) can be represented by matrix transformation M mapping input ports a, b to output ports c, d.

---

[2]Although the effects are related [156], it is not to be confused with the photon bunching in time within the statistics of light from a thermal source compared to a coherent light beam.
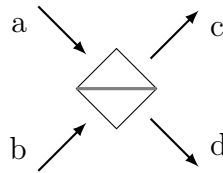
Figure 3.2: Beamsplitter input and output ports
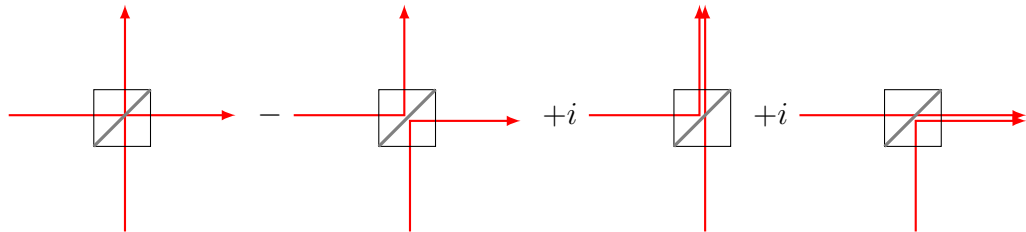
Figure 3.3: HOM interfering probability amplitudes.

$$\begin{pmatrix} c \\ d \end{pmatrix} = M \begin{pmatrix} a \\ b \end{pmatrix} \tag{3.6}$$

For a lossless beamsplitter, the form of the matrix M is constrained by unitarity ($MM^\dagger = \mathbf{1}$), and for a lossless 50:50 beamsplitter there are two commonly used conventions for the transformation, a symmetric form and an asymmetric form.[3]

$$M = \frac{1}{\sqrt{2}} \begin{bmatrix} 1 & i \\ i & 1 \end{bmatrix} \qquad (3.7) \qquad\qquad M = \frac{1}{\sqrt{2}} \begin{bmatrix} 1 & 1 \\ 1 & -1 \end{bmatrix} \qquad (3.8)$$

The only difference between them is an arbitrary phase, equivalent experimentally to putting a thin piece of glass in front of one input and one output port [159]. Within this thesis we will generally use the symmetric form (Eq. 3.7).

Consider two independent single photons arriving at different input ports a and b of a beamsplitter; there are four classically possible outcomes as shown in Figure 3.3: both transmitted, both reflected, photon from a reflected while the photon from b is transmitted, and photon from a transmitted while the one from b is reflected. The first two outcomes result in the photons exiting in different paths, whilst for the last two outcomes the photons take the same path, they 'coalesce' (or 'bunch').

If the photons are completely indistinguishable, both in their photon properties and their timing, the first two situations (both transmitted and both reflected) become indistinguishable themselves; you cannot tell which happened from looking at the out-

---

[3]The symmetry we refer to here represents the spatial symmetry - for temporal symmetry it is the opposite. For Eq. 3.7 both inputs acquire the same phase shift upon reflection, but running time backwards from the output, you need its Hermitian conjugate to obtain the original input. Whereas Eq. 3.8 is spatially asymmetric - one beam when reflected gets a phase change, the other beam does not. However it is temporally symmetric - it is its own Hermitian conjugate. [158] One can think of Eq. 3.7 as representing a cube beamsplitter and Eq. 3.8 as representing a plate beamsplitter, but in practice quirks of manufacturing make the actual phases somewhat arbitrary.

come. The unitarity of the lossless beamsplitter transformation[4] combined with the photons' bosonic commutation relations results in complete destructive interference between the outcomes where the photons exit in separate paths, cancelling each other out, and so the indistinguishable photons must always coalesce and take the same exit path. Which exit path this is is completely random.

Mathematically speaking, our initial input state $|\Psi_i\rangle$ is a single photon in input a and a single photon in input b, which we can also represent as creation mode operators $a^\dagger, b^\dagger$ acting on the vacuum $|0\rangle$:

$$
\begin{aligned}
|\Psi_i\rangle &= |1\rangle_a |1\rangle_b |0\rangle_c |0\rangle_d \\
&= a^\dagger |0\rangle_a \, b^\dagger |0\rangle_b |0\rangle_c |0\rangle_d
\end{aligned}
\tag{3.9}
$$

To find the final output state $|\Psi_f\rangle$ we apply the beamsplitter transformation (Equations 3.6 and 3.8) on the mode creation operators:

$$
\begin{pmatrix} a^\dagger & b^\dagger \end{pmatrix} = \frac{1}{\sqrt{2}} \begin{pmatrix} c^\dagger & d^\dagger \end{pmatrix} \begin{bmatrix} 1 & i \\ i & 1 \end{bmatrix},
\tag{3.10}
$$

$$
\begin{aligned}
|\Psi_f\rangle &= \frac{1}{\sqrt{2}}(c^\dagger + id^\dagger)|0\rangle_a \, \frac{1}{\sqrt{2}}(ic^\dagger + d^\dagger)|0\rangle_b |0\rangle_c |0\rangle_d \\
&= \frac{1}{2}|0\rangle_a |0\rangle_b \, (c^\dagger + id^\dagger)(ic^\dagger + d^\dagger)|0\rangle_c |0\rangle_d \\
&= \frac{1}{2}|0\rangle_a |0\rangle_b \, (ic^\dagger c^\dagger + c^\dagger d^\dagger - d^\dagger c^\dagger + id^\dagger d^\dagger)|0\rangle_c |0\rangle_d .
\end{aligned}
\tag{3.11}
$$

Bosonic mode operators obey commutation relations:

$$
[a_1, a_2^\dagger] = a_1 a_2^\dagger - a_2^\dagger a_1 = \delta_{12}, \quad [a_1, a_2] = [a_1^\dagger, a_2^\dagger] = 0,
\tag{3.12}
$$

i.e. $c^\dagger d^\dagger = d^\dagger c^\dagger$, $c^\dagger c^\dagger = c^\dagger c^\dagger$, $d^\dagger d^\dagger = d^\dagger d^\dagger$. So

$$
\begin{aligned}
|\Psi_f\rangle &= \frac{1}{2}|0\rangle_a |0\rangle_b \, (ic^\dagger c^\dagger + id^\dagger d^\dagger)|0\rangle_c |0\rangle_d \\
&= \frac{i}{2}|0\rangle_a |0\rangle_b \, (|2\rangle_c |0\rangle_d + |0\rangle_c |2\rangle_d) .
\end{aligned}
\tag{3.13}
$$

The final state is a quantum superposition of both photons in port c and both photons in port d. This occurs regardless of the choice of phase in the beamsplitter transformation; the quantum HOM effect is a phase insensitive effect as photon number states ('Fock states': $|1\rangle$, $|n \in \mathbb{N}_1\rangle$ ...) have maximally uncertain phase [162], and which output path they bunch into is random, it is not determined. For classical light (e.g. coherent states $|\alpha\rangle$) interfering at the beamsplitter, the final state depends on the phase between the two beams, and the choice of phases for the beamsplitter (see Section A1 for the mathematics). The relative phases tune between complete destructive to constructive

---

[4]For a lossy beamsplitter, this unitarity no longer holds and the photon statistics can be tuned by the complex reflectivity and transmissivity [160, 161]
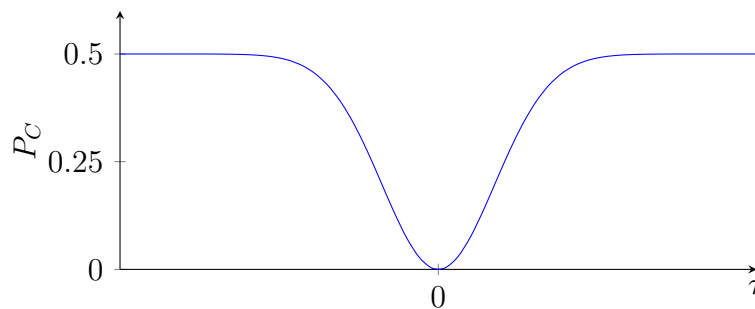
Figure 3.4: An example of a HOM dip for a Gaussian wavepacket (typical when interference filters are placed in front of the detectors), showing the probability P_C of a coincidence count against the delay τ between two photons interfering at a beamsplitter.

interference in one arm and vice versa in the other. This occurs even if the average photon number is one ($|\alpha = 1\rangle$); there is a fundamental 'quantumness' in the single photon state not present in a weak classical light beam.

To observe the HOM effect, because it is technically difficult to 'photon number resolve' [163, 164] - to detect whether you have one photon or two (or three, etc.) in a single output port - instead of measuring an increase in coalescence, the complementary decrease in anti-coalescence is almost always measured instead. If a detector of single photons is placed in each output path, if one detects a photon (a 'singles' count) at the same time as the other (in practice within a short coincidence window of a few nanoseconds) then together they register a 'coincidence count', meaning the photons have exited in different paths. If you measure coincidence counts C while you change the delay τ between the two input photons (i.e. adjusting temporal distinguishability), you get a dip in coincidences when the delay τ goes to zero and their arrival times overlap, known as a HOM dip. An example is shown in Figure 3.4. As the output port is random, the total singles counts in each arm should stay constant over all delays. The effect is independent of phase, so it is phase stable and measures the group delay between photons rather than the phase delay. The width of a HOM dip indicates the coherence length of the single photon wavepacket [156], and the visibility of the dip V_{HOM} indicates overall indistinguishability in all photon properties, such as frequency and polarisation.

$$V_{\text{HOM}} = 1 - \frac{C(\tau = 0)}{C(\tau = \infty)} \tag{3.14}$$

A HOM dip can be observed with classical light if the phase of the light is uniformly randomised to make it incoherent (for example with a rotating ground glass diffuser), to remove the first-order interference. However the visibility of such a dip cannot exceed 50%, and so a dip visibility greater than 50% is commonly accepted to indicate quantum light.[5]

---

[5]This 50% classical limit can however naturally be exceeded if the randomised phase is *not* uniform, if it's heavily controlled and limited only to certain values where strong classical constructive interference occurs in one of the output ports, this would create a high visibility dip in coincidences without a dip in singles counts in each arm, see [165] and [166] for a discussion.

The quantum HOM effect detailed above is a specific case of more general two-photon quantum interference effects [156]. These extensions to the HOM effect pinpoint the heart of the effect to the properties of the overall two-photon state. To recognise the importance of seeing an entangled photon pair state as one overall (by definition non-separable) unit, we refer to such a pair as a single 'biphoton'. If the overall biphoton amplitudes are indistinguishable, the photons themselves do not have to be identical [167], nor is temporal overlap at a beamsplitter necessary or sufficient to see HOM interference [168].

3.1.4   Hong-Ou-Mandel peaks

While the HOM effect is most usually associated with a dip in coincidences, there are cases where it can generate a peak in coincidences.

3.1.4.1   Fermions

One of these cases is where instead of doing HOM interferometry with bosons such as photons, an analogous experiment would be performed with fermions such as electrons [169, 170, 171]. Pauli's exclusion principle, a consequence of the fermionic anti-commutation relations, means identical fermions cannot be in exactly the same state, and so they won't exit in the same path at the same time, and must 'anti-bunch' instead, creating a peak in coincidences [172].

From Eq. 3.11, if we apply the fermionic mode operator anti-commutation relations:

$$\{a_1, a_2^\dagger\} = a_1 a_2^\dagger + a_1^\dagger a_2 = \delta_{12}, \quad \{a_1, a_2\} = \{a_1^\dagger, a_2^\dagger\} = 0, \tag{3.15}$$

i.e. $c^\dagger c^\dagger = d^\dagger d^\dagger = 0$, $d^\dagger c^\dagger = -c^\dagger d^\dagger$. So

$$
\begin{aligned}
|\Psi_f\rangle &= \frac{1}{2} |0\rangle_a |0\rangle_b \left(i c^\dagger c^\dagger + c^\dagger d^\dagger - d^\dagger c^\dagger + i d^\dagger d^\dagger \right) |0\rangle_c |0\rangle_d \\
&= \frac{1}{2} |0\rangle_a |0\rangle_b \left(c^\dagger d^\dagger + c^\dagger d^\dagger \right) |0\rangle_c |0\rangle_d \\
&= |0\rangle_a |0\rangle_b \left(c^\dagger d^\dagger \right) |0\rangle_c |0\rangle_d \\
&= |0\rangle_a |0\rangle_b |1\rangle_c |1\rangle_d .
\end{aligned}
\tag{3.16}
$$

Identical independent fermions should always exhibit perfect anti-coalescence arriving at the same time at a lossless 50:50 beamsplitter, almost as if the beamsplitter was not there.

3.1.4.2   Entangled bosons

For bosons, such as photons, a 'fermionic' peak in coincidences at a lossless beamsplitter only occurs with entanglement (for the basics of entanglement see Section A2), specifically antisymmetric entanglement [173], and as such can be used like an entanglement

witness [134, 174]. As independent single photons are bosons, they cannot have an antisymmetric wavefunction by themselves, so can only create HOM dips, they cannot anti-coalesce to create a peak.[6] However if two photons are entangled then together they can have an antisymmetric wavefunction in one or more degrees of freedom, including polarisation, spatial modes, and frequency, and so produce a 'fermionic' HOM peak.[7]

For example, anticoalescence can be observed with a polarisation-entangled photon pair in the antisymmetric $|\Psi^-\rangle$ Bell state [176, 161] (see Section A2.0.1 for a definition of Bell states). The symmetry of such an entangled state, where each photon always has the opposite polarisation to its pair regardless of the polarisation basis, can be changed between symmetric $|\Psi^+\rangle$ and antisymmetric $|\Psi^-\rangle$ simply by using birefringent wave plates to adjust the phase between the polarisations [176, 161]. Antisymmetry in the spatial biphoton wavefunction can be induced by engineering the spatial mode of the SPDC pump beam [177, 178].

For frequency-time entangled photons one method to observe a photonic HOM peak is to add additional paths to one or both of the HOM interferometer arms, for example with a birefringent quartz rod [136], a cavity [135, 179], or a layered reflective sample [180, 181]. These additional paths create multiple dips for each distinct delay present, as well as cross-interference dips between them. By tuning the modulo 2π phase between the additional paths the symmetry of the biphoton entangled state is altered and these cross interference features can change between dips and peaks. Intriguingly these extra interference features render the normally phase-insensitive HOM effect sensitive to phase [156] through the state (anti-)symmetry.[8] The extra interference features occur when two photons do not actually 'meet' within their coherence lengths at the beamsplitter, arising instead from the temporal indistinguishability of the overall biphoton state when the detector 'coincidences' actually have a specific time gap, leading some to call it 'non-local' interference [156, 137]. This temporal indistinguishability leading to the extra interference features degrades outside the biphoton coherence length inherited from the pump, and the features correspondingly disappear outside this regime [137].

---

[6]One experiment seems to show anti-coalescence between independent single photons [175], however this only occurs with post-selection on certain detection events, where they essentially project onto an entangled state)

[7]To maintain the global bosonic wavefunction of the biphoton, an antisymmetric wavefunction in one degree of freedom, e.g. polarisation, must be compensated with antisymmetric behaviour in the beamsplitter spatial modes, i.e. anticoalescence [156]. Correspondingly, 'bosonic' HOM dips would be observed for entangled fermions by preparing the fermions with an antisymmetric entangled wavefunction.

[8]This phase sensitivity could be used for other applications. For example, combining the phase sensitivity (from the flip) and HOM group delay sensitivity (from a shift of the dip) could provide a way to do depth estimations with large dynamic range from tens of nanometers to millimeters, without running into phase wrapping issues usually present in interferometric techniques [182].
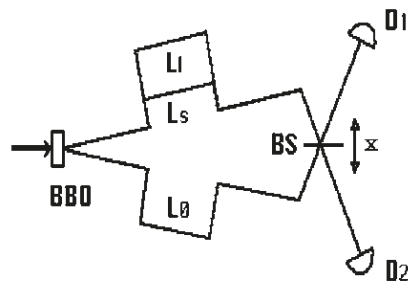
(a) Schematic diagram
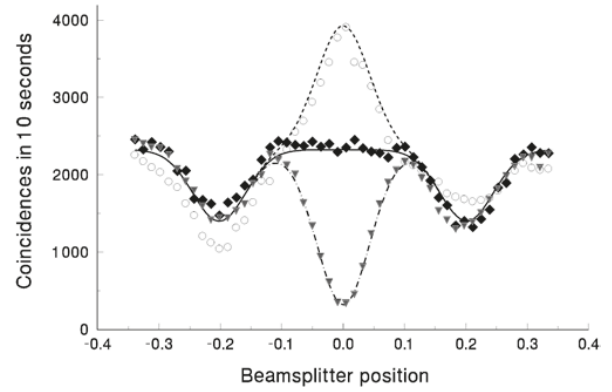
(b) HOM interference pattern. The triple dip-peak pattern corresponds to different phases $\phi = 0, \pi/2$, and π (triangles, diamonds, and circles, respectively)
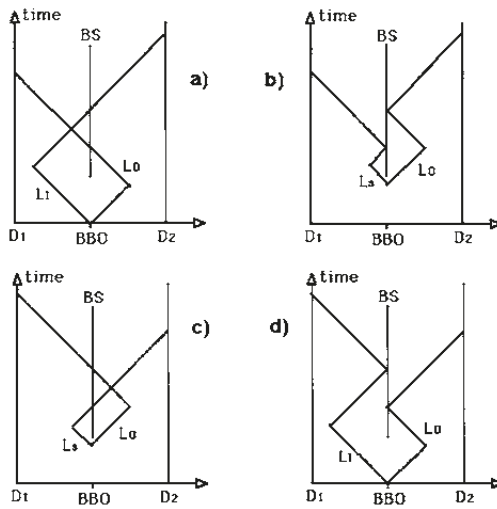
(c) Feynman diagram of interfering possibilities
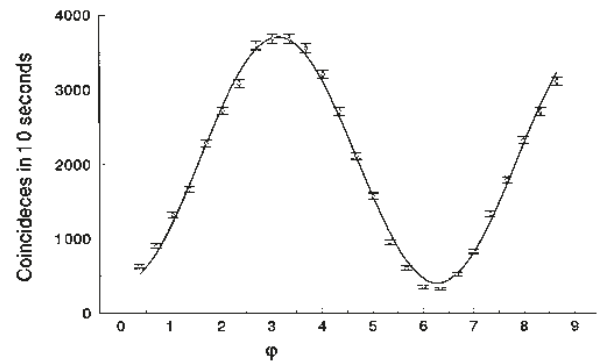
(d) Coincidences at the central beamsplitter position oscillate when changing the phase between L_s and L_l with a Pockels cell

Figure 3.5: Non-local HOM interference. Figures reproduced from Strekalov, D. V., T. B. Pittman, and Y. H. Shih. 'What We Can Learn about Single Photons in a Two-Photon Interference Experiment'. Physical Review A 57, no. 1 (1 January 1998) [136] with permission of the journal.

3.1.5 Creating non-local Hong-Ou-Mandel interference

To detect photon entanglement with a Hong-Ou-Mandel measurement, an antisymmetric entangled state between the photons is required [134, 174, 173], which creates a peak in measured coincidence counts instead of the more common dip (for symmetrically entangled or independent photons). As mentioned in Section 3.1.4, one way to create such a HOM peak from SPDC photons, which are usually produced with a symmetric biphoton spectrum, is to add additional paths to one or both of the HOM interferometer arms. Here I shall outline how the effect occurs with a qualitative description, with the help of previous experimental realisations as examples.

The method of Strekalov et al. (Ref. [136]), is shown in Figure 3.5. The schematic (Figure 3.5a) shows two paths of lengths L_l and L_s within the signal arm of the interferometer. The diagram suggests an unbalanced Mach-Zehnder interferometer, but the

experimental implementation was actually a birefringent quartz rod. This was aligned at 45° to the input polarisation, splitting the light into two path delays by polarisation, with a polariser placed after the quartz rod to regain the original polarisation before interfering at the beamsplitter. There is also a Pockels cell [183] placed before the polariser to finely tune the phase ϕ between the two paths. The delay induced by the birefringent crystal ($L_l - L_s = 2\Delta L$) was larger than the single photon coherence length in the experiment so we can think of it as splitting the light into two distinct temporal packets, rather than changing the overall polarisation of the light. The idler arm has a path length of L_0, which is halfway between L_l and L_s when the beamsplitter is at the $x = 0$ position. The coincidence measurements taken as the beamsplitter position is varied are reprinted in Figure 3.5b. Two dips are expected at $x = \pm\Delta L/2$ as at these positions half the signal photons temporally overlap with the idler photons on the beamsplitter, and this results in the standard HOM interference but with a maximum of 50% visibility as each idler photon has a 50% chance of meeting its signal pair. There is an additional interference feature in the centre, outside of the single photon coherence length, and where no photons meet at the beamsplitter (thus we refer to it as 'non-local'). How does this occur? To comprehend this feature, which can be a peak, a dip or inbetween we have to understand the entangled photon pairs as a single biphoton wavepacket. It is interference between indistinguishable probability amplitudes of the biphoton as a whole which results in this interference. The Feynman-type diagrams in Figure 3.5c help illuminate these interfering possibilities. In Figure 3.5c a) and b), detector 1 (D1) fires $\Delta L/c$ before detector 2 (D2). This can occur when both photons are transmitted for the signal photon taking path L_l (Figure 3.5c a)), and when both photons are reflected if the signal photon takes path L_s (Figure 3.5c b)). Similarly in Figure 3.5c c) and d) D2 fires $\Delta L/c$ before D1. The coincidence window (10 ns) is much larger than time $\Delta L/c \approx 0.6$ ps so these events are still considered coincidences. While the time between photon pair production and detection is different between e.g. Figure 3.5c a) and b), if there is no clock-like distinguishing information, such as from a pulsed pump laser (or any other pump with a shorter coherence length than the relevant path difference ΔL), then the photon pair production time is impossible to recover, and so Figure 3.5c a) and b) become indistinguishable possibilities for the biphoton and interfere. The phase between these possibilities, determining whether they interfere destructively or constructively, then depends on the phase ϕ between L_l and L_s. Figure 3.5d shows how the coincidence rate at the central beamsplitter position $x = 0$ depended on this phase - oscillating between a dip ($\phi = 0, 2\pi, ...$) and a peak ($\phi = \pi, 3\pi, ...$), and thus changing the photon entanglement from symmetric to antisymmetric with the phase.

Sagioro et al. [135] performed a similar experiment, but added additional paths to their HOM interferometer with a cavity. By tuning the cavity length, they too could control the phase difference that could turn the biphoton state antisymmetric. The
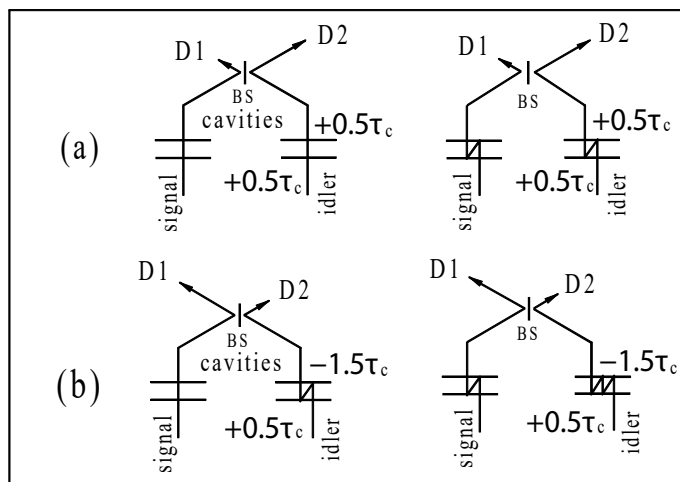
Figure 3.6: Feynman path diagrams explaining background interferences for two-cavity HOM. Photon idler begins $0.5\tau_c$ (τ_c = cavity crossing time) advanced in relation to photon signal. In (a) it remains $0.5\tau_c$ advanced, after both twin photons cross their cavities. In (b), photon signal, after both photons cross their cavities, is advanced $1.5\tau_c$ in relation to photon idler. It is known which photon (signal or idler) arrives first from the detection time, but there is indistinguishability in which process has happened before the photons arriving. Processes in line (a) interfere, processes in line (b) interfere and so on. Fig. 12 in Ref. [179]. Reprinted with permission of the publisher.

same research group also showed in 2015 using a femtosecond pulsed pump laser that the non-local interference correspondingly disappeared outside of the pump coherence length [137]. In that paper they also mention that by putting a cavity in each arm, there is no longer a requirement to be within the pump coherence length to allow (some) forms of non-local interference, as the symmetry can retain the key indistinguishability of when the photons were produced. They explore both the one-cavity and the two-cavity cases theoretically in Ref [179], where they also point out how in the two-cavity case, the background level of coincidences can fluctuate, even when the cavity length is outside of the single photon coherence length. This new form of interference occurs at delay times between the main interference features, where it is possible to know which photon (signal or idler) arrived first, depending on the time delay between the detections, but crucially not what happened to them on the way. For example, as shown in Figure 3.6 there is interference between the possibilities where both photons pass straight through the cavity, and when they both take a round trip through each cavity, (and when they both take two round trips, etc). As the indistinguishability of this background interference depends on not knowing when the photon pair was initially produced, this background interference should be diminished by a limited pump coherence length in the two-cavity case[9] (although this is not explicitly stated in Ref. [179]). This background interference is of a similar origin to Franson interference [184].

---

[9]This is what Marko Toroš found in our theoretical calculations for the rotating experiment in Section A3.

3.1.6 On the quantum-ness of flippy dips

While researchers state that seeing any HOM peak is unambiguous proof of (antisymmetric) photon entanglement [134, 174], and thus acts as an entanglement witness, it is interesting to note that the oscillating cross-interference HOM dips also show up in some classical analogues to HOM interference. The field of optical coherence tomography (OCT) measures the depths and thicknesses of various reflecting layers within a sample by interfering low coherence light [185]. By scanning a reference arm of an interferometer against the sample arm, interference features occur only when the time taken in the reference arm matches the timing of the light reflected from the different depth layers in the sample. Quantum OCT techniques use frequency-time entangled photons, single photon detection, and the HOM effect to do the same thing, with added dispersion cancellation and higher resolution than traditional OCT techniques, observing HOM dips corresponding to the depth of each layer surface. In quantum OCT (Q-OCT) experiments they naturally also observe extra oscillating cross-interference features due to using entangled photon pairs and having multiple paths in one of the HOM interferometer arms. But intriguingly, OCT researchers, in striving to replicate the 'quantum' advantages of Q-OCT with classical light in classical experiments, have also sometimes managed to (unintentionally) replicate these extra 'artifacts'. For example by using oppositely chirped pulses and sum-frequency detection (a sort of classical 'time reversed HOM' [186]), or spectral intensity interferometry [187, 188]. These classical analogues may be surprising but nevertheless, it is the single-photon (and two-particle) nature of the HOM effect (and the HOM detection), that is key to its quantum nature, and the existence of classical *analogues* do not make HOM effects any less quantum. For example the standard 50% visibility limit of a standard HOM dip is also exceeded by a chirped pulse analogue [189], because the classical limit is set by the *coincidence detection method* which measures intensity correlations, rather than the electric field correlations of sum frequency generation.

3.2 Methods: How to build a HOM interferometer

3.2.1 Photon pair production and detection

The first step was to get a source of frequency-entangled photons, and build a standard HOM interferometer. Frequency-time entangled photon pairs centred at 804 nm with matching polarisations were produced through Type I SPDC by pumping a beta barium borate (BBO) crystal with a 402 nm, 100 mW continuous-wave (CW) laser (Coherent OBIS LX 405). The linewidth of the laser was not given in the manufacturer specifications as it is not a narrow-linewidth laser, by measurement its full-width-half-maximum (FWHM) was ≤ 1.15 nm (Figure 3.7). Initially a 1 mm long BBO crystal was used, but was later changed when using the nested interferometer (which added a
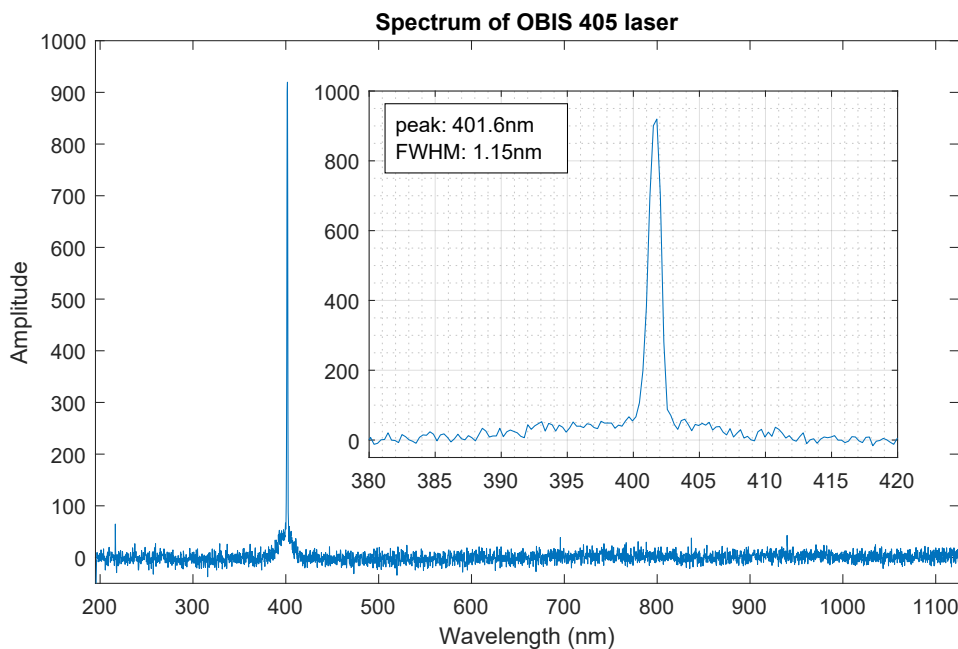
Figure 3.7: OBIS laser spectrum. Data taken by Charles Altuzarra, data plotted by myself.

lot of loss to the system) for a 3 mm long crystal to increase the nonlinear interaction time and so produce more photons.

The SPDC photons are produced in a cone, representing the possible $\vec{k}$ vectors allowed, so in the far field of the crystal a ring of down-converted photons was observed (Figure 3.8). The face of the crystal had been cut along the optic axes such that a cone with 3° angle from the pump axis would be produced when pumped with 405 nm light at normal incidence. Changing the angle of the crystal to the pump alters the angle at which the signal and idler photons are produced, and change the diameter of the ring. A diagram of the optics used to create the photon pair source is shown in Figure 3.9a. A longpass filter at 633 nm was placed after the crystal to block the 402 nm pump beam in the centre of the ring, as it is much much brighter than the 804 nm down conversion. A lens was placed in the far field of the crystal to collimate this ring.

As the entangled photon pairs are produced with equal and opposite transverse momenta, photons from diametrically opposed positions on the ring of down-converted photons were separated (using a D-shaped mirror in half of the beam) and coupled into separate single mode (and polarisation maintaining) optical fibres. Those fibres couple into single-photon avalanche diodes (SPADs) (Figure 3.9b), which send an electrical signal each time a photon is detected to a coincidence counting machine (ID900 Time Controller, IDQ), specially designed to be able to process and keep track of the timing of signals in rapid succession. Detection events are recorded with precise timestamps (down to 13 ps time resolution) and counted as 'singles', and coincidences are counted when both SPADs record a photon within a short coincidence window (usually 1-5 ns). These machines send data via USB cable to a computer, and a LabVIEW program was developed to communicate with the coincidence machine. This gave customisable
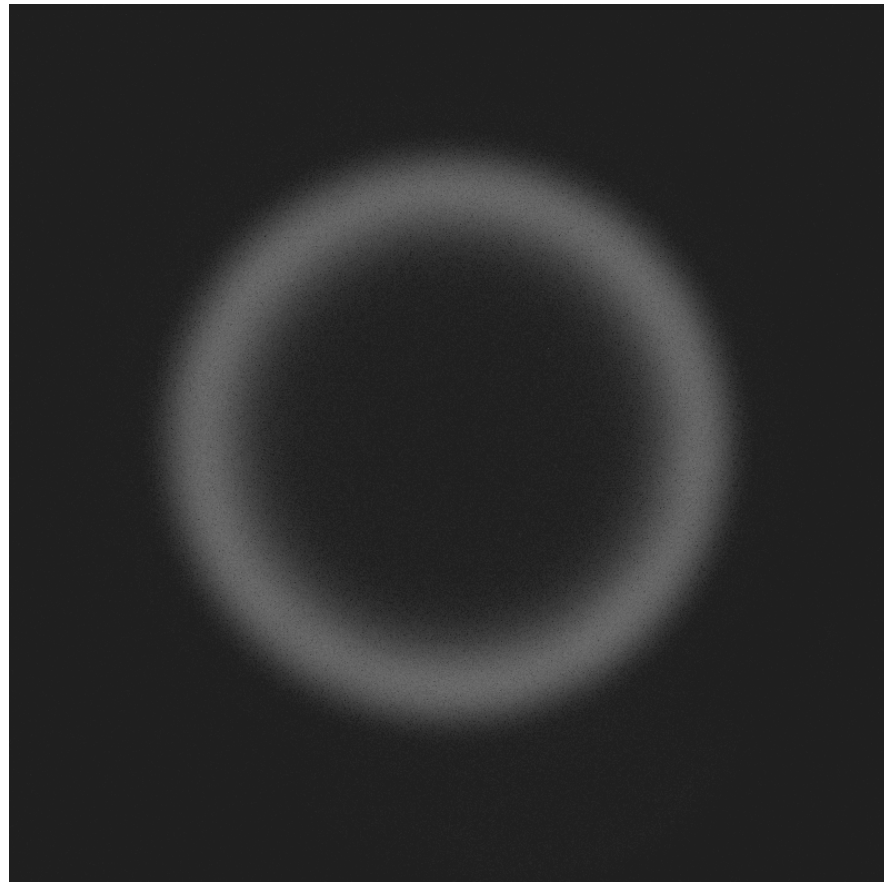
Figure 3.8: SPDC output from the BBO crystal, imaged in the far field. The pump beam that would propagate through the centre has been spectrally filtered out. The ring represents the possible $\vec{k}$ vectors allowed. A pair of entangled photons will sit diametrically opposed on this ring, as they are produced with equal and opposite momenta from the pump beam. The cutting of the crystal with respect to the optic axis is designed so produced photon pairs have a certain angle between them. Changing the angle of the crystal to the pump beam changes the phase matching conditions, which collapses or expands the ring.

(a) Photon pair source   **(b)** Coincidence detection to select correlated spatial modes   **(c)** Hong-Ou-Mandel interference and coincidence measurement
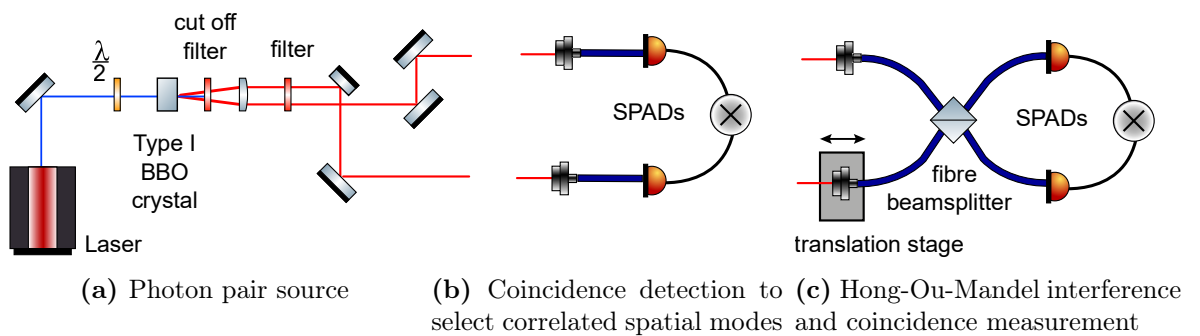
Figure 3.9: Photon pair source (a) and the detection schemes for coincidence measurement for (b) alignment and (c) Hong-Ou-Mandel interference

control of the settings on the coincidence machine, such as the coincidence window used and the delays required to synchronise the two detectors to look for coincidences in the right time window. This also allowed measurement in real-time of the singles and coincidences count rates.

The coupling positions and angles were aligned to maximise the coincidence counts. This alignment is very sensitive, the phase matching conditions required to allow the process of SPDC mean that the photon pairs produced are highly correlated in position and momentum, so if the spatial modes coupled into the fibres don't match, then both photons of the pair will not be picked up, and most photons detected will not be correlated in time. When the modes coupled into the detectors match, there's a strong peak in the histogram of coincidences per timebin, as the photons detected were produced at the same time and so are detected in both SPADs with correlated times.

By chance, coincidences can also occur even if the detectors are picking up independent sources of photons, rather than SPDC pairs. These are called accidentals (A) and can be estimated from the rates of the singles counts at each detector and the coincidence window Δt used, assuming independent events:

$$A = S_s S_i \Delta t, \tag{3.17}$$

where S_s, S_i are the signal and idler detector single count rates. The shorter the window, the fewer accidentals, but if you cut too far, then you start throwing away lots of true coincidences, as there will be a certain spread in the relative photon detection times due to the photon bandwidth, and (to a lesser extent in this setup) the resolution and jitter of the timing system.

To assess the strength of the true coincidences, a useful measure can be the 'quantum contrast' QC, the ratio of the coincidence rate C over the expected accidental rate:

$$QC = \frac{C}{A} = \frac{C}{S_s S_i \Delta t}. \tag{3.18}$$

3.2.2 'Normal' HOM

The fibres to the detectors were then replaced by a fibre-coupled beamsplitter to create a HOM interferometer (Figure 3.9c). To observe the HOM dip in the coincidence signal between the output ports of the beamsplitter, the path lengths of the input interferometer 'arms' have to be matched exactly, to within hundreds, or even tens of microns. The lengths can usually normally be matched to within a few millimeters using a tape measure to measure optical paths between the BBO crystal and each fibre coupler. Asymmetry in the lengths of the optical fibre arms of the fibre-coupled beamsplitter also has to be accounted for. The precise delay required can be found by placing one fibre optic coupler onto a motorised translation stage (the 'HOM stage'), then scanning the stage slowly whilst measuring coincidences at the outputs of the

beamsplitter to find a dip. The stage itself also has to be aligned precisely to move parallel with the photon propagation axis, otherwise the light becomes decoupled and all counts reduce when the stage moves. Finding the dip with the stage can take a while because there are trade offs between speed, resolution, acquisition time, signal-to-noise ratio (SNR), the width of the dip, and rate of photons detected. For example, putting a narrower bandpass filter (centred at the down-converted photon wavelength) in front of the couplers widens the HOM dip and allows the dip to be scanned with a larger step resolution and so greater speed. However, this will also reduce the number of photons detected, reducing SNR, and may necessitate an increase in acquisition time at each step to combat that, which then makes the scan slower again. In general I found it was slightly quicker and easier to find a dip when the dip was quite wide, even amongst the increased noise.

3.2.2.1 Actually not-so-normal HOM

Once a HOM dip was found, it was unusually irregular. Figure 3.10 shows the shapes of the 'wiggly' HOM dip through different wavelength filters, and Figure 3.11 shows the HOM interference without filtering the SPDC.[10] Normally with wider bandwidth filters, small peaks either side, or on one side of the dip, are relatively common in HOM experiments [156] but not the large peak I was seeing with the 40 nm filter (Figure 3.10a), nor are such side peaks usually as pronounced with 10 nm filters (Figure 3.10b and c) as I was seeing. Nevertheless, filtering the spectrum of the SPDC strongly with a 3 nm bandwidth filter, thus making the smaller number of photons remaining highly indistinguishable, did result in a high visibility, symmetric dip (Figure 3.10d).

I did not manage to identify the aspect of my experiment that was contributing the spectral and phase distortions that caused the irregular shape of the interference. It did not qualitatively improve changing the length or tilt of the crystal, nor the alignment of the filters or couplers (Figure 3.11). Similar distortions can arise from chromatic dispersion[11]. The dip from the 810/10 nm filter in particular (Figure 3.10c) is reminiscent of dip shapes from highly 3rd order dispersive media [190] which also correspondingly disappear with highly filtered SPDC [191]. Chromatic dispersion is often a problem in optical fibres, although usually only becomes apparent in much longer lengths of fibres than I was using.[12] The geometry of an optical component can also cause dispersion, for example in prisms and lenses. Another possibility could be multiple spatial modes in the pump beam, which can affect the HOM dip shape [178]. Various phase functions applied to a spatial light modulator (SLM) can be used to both simulate and nullify distorting effects on HOM dips such as dispersion, as shown

---

[10]Except for filtering out the pump.

[11]Chromatic dispersion is also what causes rainbows through, so we can't get too annoyed at chromatic dispersion as a concept.

[12]Typical values of second order dispersion as a function of length in optical fibre: $d_f^{(2)} \approx 35 \text{ fs}^2/\text{mm}$, and third order dispersion: $d_f^{(3)} \approx 30 \text{ fs}^3/\text{mm}$ [191].
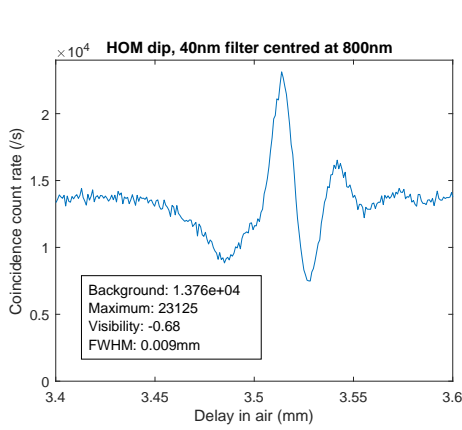
(a) HOM dip, 40nm bandwidth filter, centred at 800nm
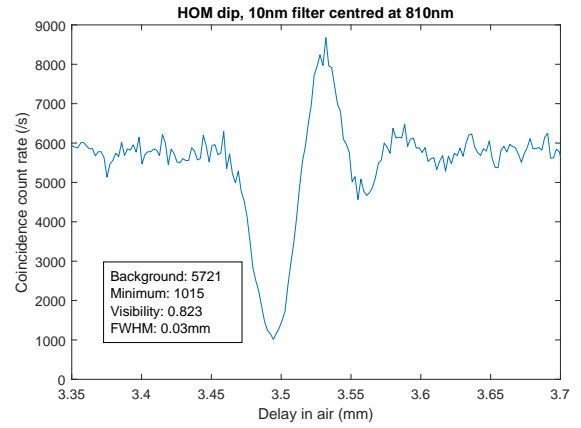
(b) HOM dip, 10nm bandwidth filter, centred at 810nm
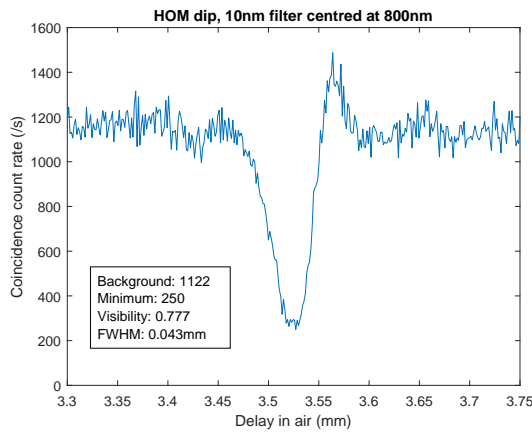
(c) HOM dip, 10nm bandwidth filter, centred at 800nm
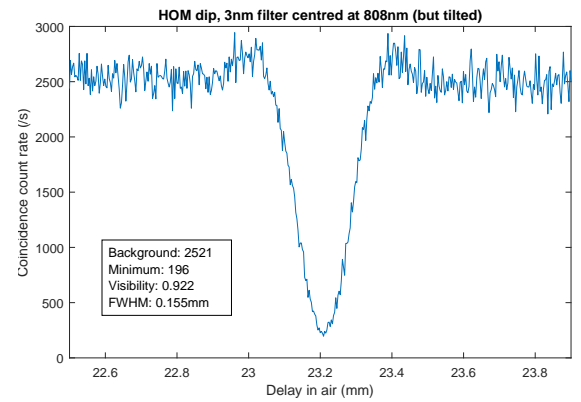
(d) HOM dip, 3nm bandwidth filter, centred at 808nm, but tilted to lower the centre wavelength for a higher count rate.

Figure 3.10: HOM dip measurements, photon pairs from the 3 mm BBO crystal, which gave a brighter SPDC source. The shape of the interference for different bandwidths did not qualitatively depend on whether the 1 mm or 3 mm crystal was used. The HOM dip delay is different for (d) as it was measured at a later time, after the delay stage had been replaced.
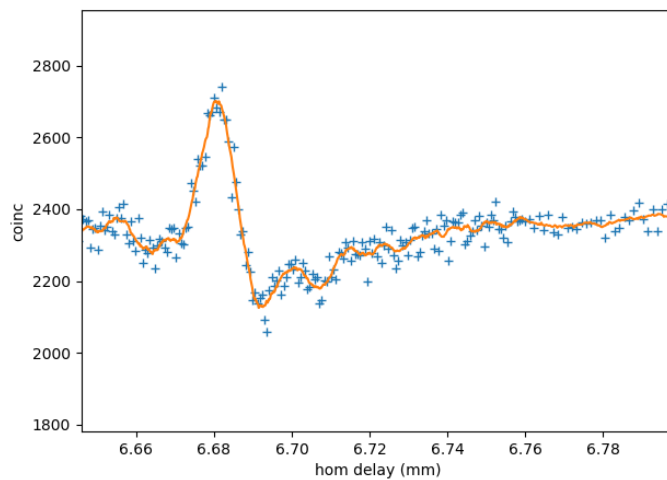
Figure 3.11: #nofilter. The full SPDC spectrum from the crystal already has a strong antisymmetric component, producing a HOM peak. This HOM measurement is from the nested interferometer experiment with one of the extra paths blocked, which is why the counts are pretty low compared to Figure 3.10 despite the lack of spectral filter.
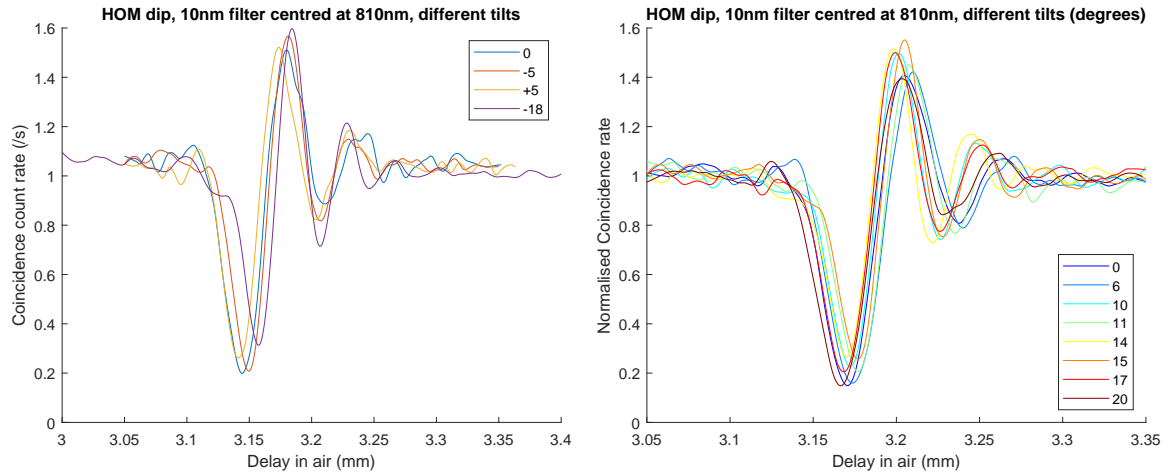
Figure 3.12: Changing the tilt of the SPDC filter
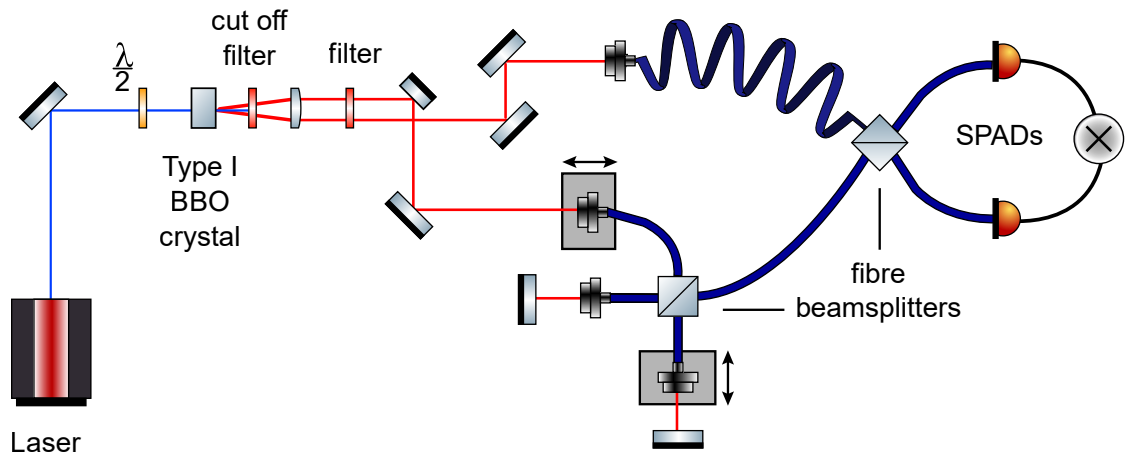
Figure 3.13: Diagram of HOM with nested Michelson interferometer. There are two translation stages; one controls the overall delay between the signal and idler paths, we refer to this as the 'HOM delay'. The other controls the difference between the nested paths in the Michelson interferometer.

by Mazzotta et al. [191]. So if the shape of the dip is really important, this method can be used to correct for issues in the setup.

It was frustrating not to uniquely identify the cause, but the shape of the dip was not actually that important to the task, which was to see how by adding in extra delays to the system, non-local interference features could be observed and controlled in various coherence length regimes.

3.2.3 HOM with Michelson nested interferometer

By adding another fibre beamsplitter, I could add a nested Michelson interferometer in a modular way (Figure 3.13, [1]), and change between the nested HOM configuration and the normal HOM configuration without realigning optics. This would create the short and long paths needed to see the non-local interference described in Section 3.1.5, and allow the effect to be explored in the regimes from where the nested path length difference is matched (inside the single photon coherence length) to very unbalanced
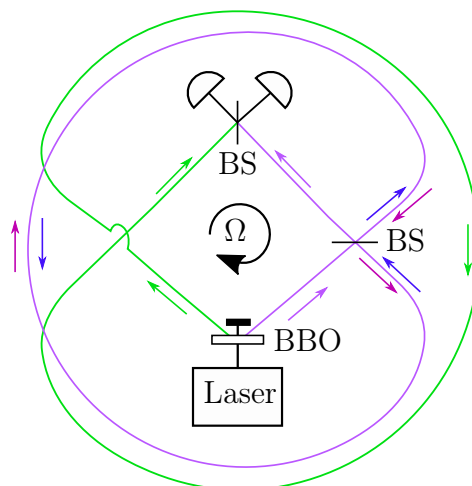
Figure 3.14: Layout of proposed quantum Sagnac/Hong-Ou-Mandel interferometer on a rotating platform. Two entangled photons are emitted from the BBO crystal: Photon a (purple arrow) enters a Sagnac interferometer using the lower 50:50 beamsplitter (BS) and exits towards the upper 50:50 beamsplitter where two-photon HOM interference occurs with photon b (green arrow) that circles around the setup (in order to maintain the same overall path length as photon a). Coincidence counts are measured between detectors PD1 and PD2 as a function of the rotation frequency. Reprinted Figure 3 from Ref. [1] with permission from the publisher.

(outside the biphoton coherence length). The initial theoretical plan for altering entanglement symmetry with rotation proposed a balanced Sagnac interferometer in one arm (Figure 3.14), so a Michelson interferometer in one arm was a flexible way to approximate and troubleshoot this proposal in a static regime, allowing control over the phase difference without rotation.

The Michelson interferometer, when unbalanced, creates a loss of 50% in the signal photon arm, which degrades the SNR of the experiment. At this point I decided to swap the 1 mm BBO crystal for a longer (3 mm) one, to have a brighter SPDC source to start with, mitigating some of that loss.

The Michelson interferometer consisted of a 50:50 fibre beamsplitter with the reflection and transmission arms each connected to a fibre collimator, where the light propagated in air, hit a mirror at normal incidence, and reflected back into the fibre beamsplitter through the coupler again (Figure 3.13). The mirror for one arm was fixed, whilst the other was mounted on a translation stage (the 'nested stage') to change the path length. In this setup the fibre beamsplitter used for the Michelson was the one previously used to get the normal HOM dip measurements, with fibres around 30 cm long. I then used another fibre beamsplitter available in the lab with fibres around 1 m long for the HOM beamsplitter. The overall extra path length from the nested interferometer was matched on the other side with an extra length of optical fibre, to match the delays between signal and idler to within the range of the translation stages, so that each Michelson arm could produce a HOM dip.

Despite measuring the lengths of the fibres and air gaps precisely, the coincidence histogram clearly showed a mismatch of signal and idler photons of around 800 pico-
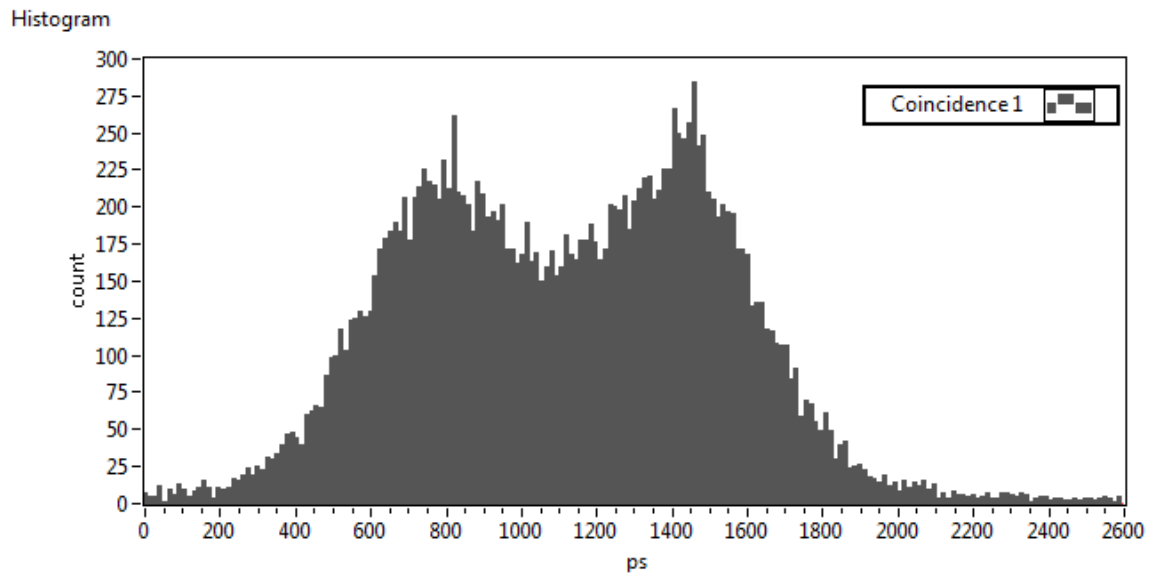
Figure 3.15: Histogram showing large mismatch of delays between signal and idler arms, when the calculated delays from the length of the fibres and free-space paths are supposedly matched. There are two peaks in the histogram separated by 700-800 ps.

seconds - a mismatch equivalent to 16cm of fibre unaccounted for, out of about 2.5 metres total (Figure 3.15). There was clearly something a bit off with the fibres in the 1 m fibre beamsplitter, as when I tested them in a simple HOM experiment (Figure 3.9c) the dip could not be found within the range of the stage, meaning the arms were quite mismatched, despite seemingly being the same length. This made it difficult to even start to find the path lengths required in the Michelson interferometer when the delay stages only had 1 or 2 cm range. I replaced the translation stages so that using both translation stages, an overall range of 5 cm could be scanned over to find the HOM dip.

By offsetting the mirrors in the Michelson until the broad peaks in the coincidence histogram (Figure 3.15) completely overlapped I could match the delays to within about 100 ps (about 3 cm in air), which could be scanned slowly with the translation stages whilst measuring coincidences to find the HOM dips. Once the dips were found, the experiment was adjusted so the range of both the HOM delay stage and the nested stage encompassed several mm either side of the dip associated with the fixed Michelson arm. This allowed the dip associated with the variable Michelson arm to be moved through the fixed dip and measurements to be taken both in the balanced regime and in the unbalanced regime. Figure 3.16 gives an example of how the measurements for a fixed path difference in the nested Michelson were taken in the LabVIEW program.

3.2.3.1   Liquid Crystal Variable Retarder

Some measurements (Figures 3.20 and 3.21) were taken just using the nested stage to vary the separation of the HOM dips, and if the exact path length difference was not so relevant, to investigate the effect of phase as well (Figure 3.24). However, the
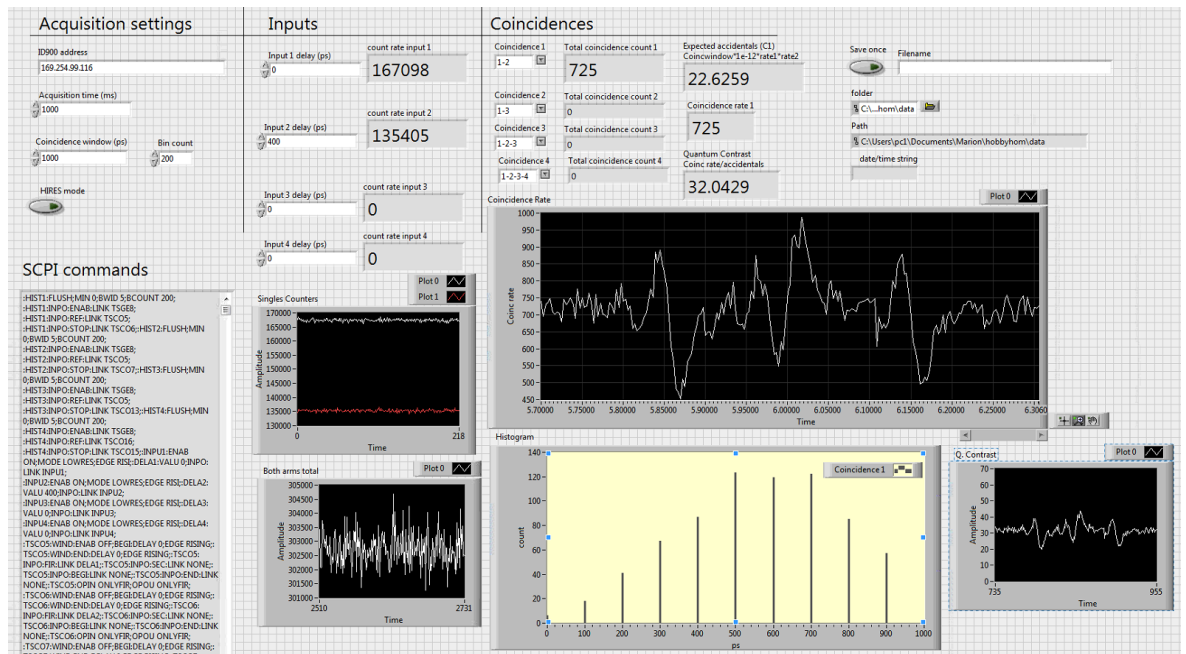
Figure 3.16: Screenshot of LabVIEW measurement. Three wiggly HOM dips can be seen in the coincidence measurements. The middle 'dip' is inverted compared to the side dip shapes. While the x axis for the coincidence graph is labelled 'Time' it is actually the HOM delay stage position in mm. The measurements here are taken with the coincidence machine in high speed mode rather than high resolution mode, which is why the histogram bins are 100 ps wide. In high resolution mode the smallest bin size is 13 ps.

nested Michelson didn't have good enough step precision to vary the path difference on a sub-wavelength level smoothly, and was also unstable and subject to vibrations, which blurred out the central interference features. So for better control of the middle interference feature, the Michelson stage was only used to vary the overall position of the dips on a μm scale, and to vary the phase a variable liquid crystal retarder (LCR) from Meadowlark Optics was employed. However the downside of the LCR over a free space distance delay is that the retardance is not linear with the applied voltage (see Figure 3.17) so the results require extra calibration. When no voltage is applied, the crystal has maximum retardance. As the voltage is increased, the retardance lessens to a minimum value. The LCR was placed in one of the Michelson arms and the slow axis aligned to the polarisation of the light passing through, to create a variable phase delay on the photons without altering the polarisation state. As the light passes through the crystal in each direction, the total retardance is double that of the crystal.

3.3 Results

3.3.1 Control of non-local interference

When the dips were separated by more than the single photon coherence length, the middle interference feature varied with phase in a way consistent with previous experiments and theory. Changing the LCR voltage changed the phase between the two
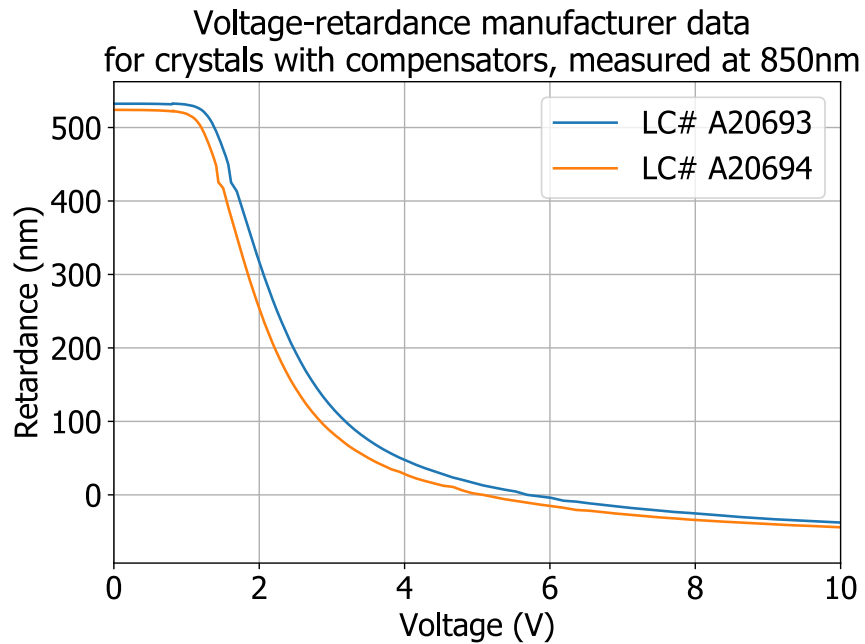
Figure 3.17: Voltage-retardance data for the liquid crystal retarders from Meadowlark Optics. Data supplied by the manufacturer. The decrease in retardance is not linear with increased voltage. #A20694 was used to vary the phase.
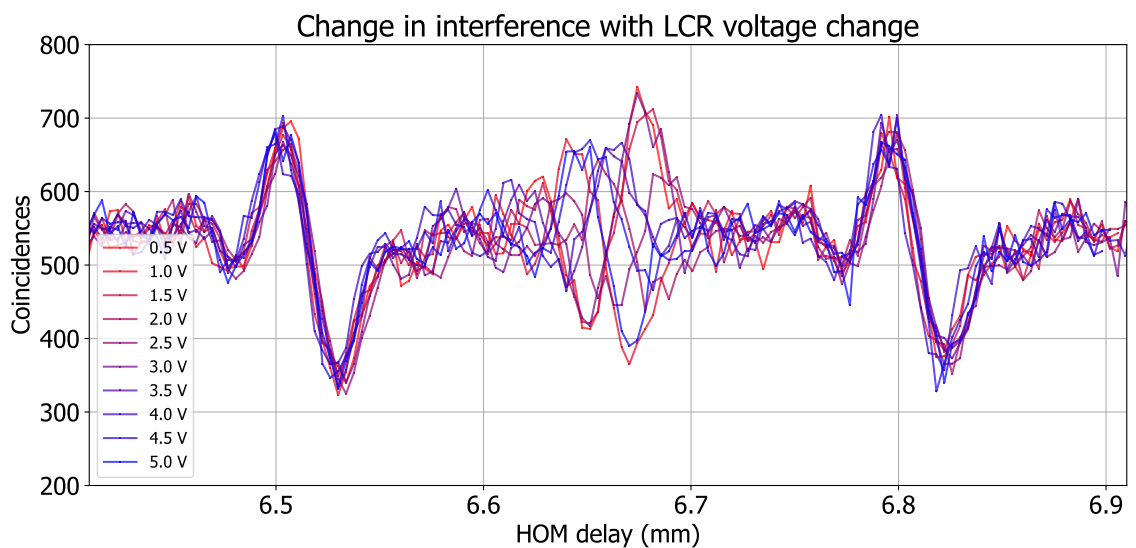
Figure 3.18: Variation of interference with LCR voltage. The shape of the middle interference inverts.
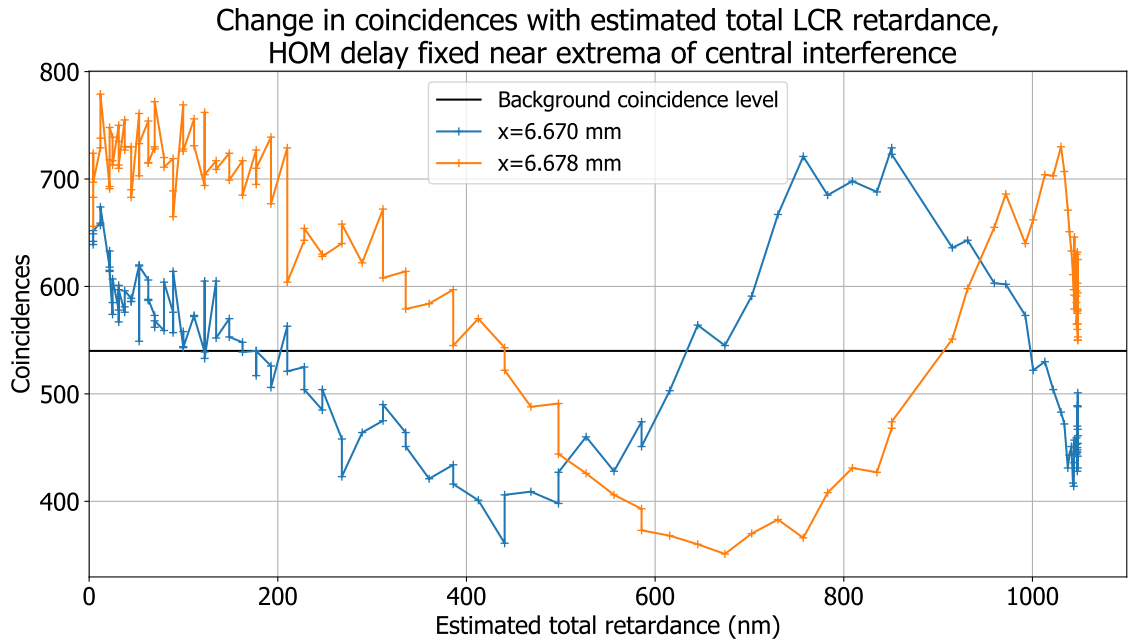
Figure 3.19: Coincidence variation of central dip with LCR delay, for two different positions near the extremum of the interference

nested Michelson interferometer arm lengths - the extra paths within the HOM. This changed the symmetry of the entangled photons so that at the HOM delay halfway between the short and long Michelson arms the interference changes. Figure 3.18 shows how changing the phase left the HOM dips at the delays matching each Michelson arm unchanged, but the central interference changed between matching the orientation of the two side dips, and being inverted. There also seems to be a slight displacement between the position of the minima of the dip and the corresponding maxima of the inverted peak, which was not expected, although this may be a spurious impression formed by noise. The phase sensitivity of the Michelson to vibrations from its surroundings did mean that the data was quite noisy, and the phase would drift a bit without actively changing the setup. Figure 3.19 shows how the extremal point of the central interference feature changes with reactance (roughly calibrated from a linearly decreasing voltage over time with the Figure 3.17 data), by fixing the HOM delay at that point. It shows an approximately sinusoidal variation, consistent with e.g. Figure 3.5d. Therefore we were able to control the symmetry of the state with the LCR voltage.

3.3.2   Coherence lengths in the system

This experiment allowed investigation of how the HOM interference that arises from extra nested paths within the system changes with how the nested path difference compares to the single photon coherence length and the biphoton coherence length which is inherited from the pump. Figure 3.20 shows how the coincidence measurements

for a scan over the HOM delay change for different dip separations. One of the dips is larger than the other because when aligning the Michelson to get the maximum total number of photons through, one of the arms of the Michelson interferometer has more loss than the other. This imbalance sadly degrades the relative visibility of the central interference because it becomes more likely that a photon detected at the output came from the arm with less loss, and so the interference isn't total.

3.3.2.1   Pump coherence

The pump laser spectrum in Figure 3.7 has a FWHM bandwidth $\Delta\lambda = 1.15$ nm and a centre wavelength of $\lambda = 402$ nm, which gives a frequency spread $\Delta\nu$ of about

$$\Delta\nu = \frac{c\Delta\lambda}{\lambda^2} = 2.13 \text{ THz} \tag{3.19}$$

gives us a value for the coherence length L_{coh} of the pump:

$$L_{coh} = \frac{c}{\pi\Delta\nu} = 44.8 \ \mu\text{m} \tag{3.20}$$

Olindo et al. [137] reported that their non-local interference dips disappeared when their cavity length was much larger than their pump pulse length (and theoretically should disappear when $\omega_p\tau_c \ll 1$ where τ_c was their cavity crossing time). Specifically, for a pump pulse FWHM of ~ 0.05 mm, they found the non-local interference was still partly present at a cavity length of 0.42 mm, but had disappeared completely with a cavity length of 0.62 mm (total dip separation of 1.24 mm).

We should expect similar. From Figure 3.18 we can see that with a dip separation of 0.3 mm the central interference is present, but at a similar visibility to the side dips, rather than being full visibility. From the data shown in Figure 3.20, the central interference has mostly disappeared at a nested stage position of 6.55 mm (the line at the bottom), which corresponds to a dip separation of 0.45 mm. When within the biphoton coherence length, the maximum visibility of the central interference (when the phase is 0 or π) should become greater than the side dips, and even theoretically reach 100% for a perfect experiment. The visibility of the central interference was sometimes observed to be higher than the side dips (although not by much) for the 40 nm filter (Figure 3.22) or with no bandwidth filter (Figure 3.23). However, this was not really observed with the 10 nm filter (Figure 3.20) and certainly not with the 3 nm filter (Figure 3.21). Because the pump coherence length was so short, it was hard to enter the regime of the pump coherence length being large in comparison to the dip separation without going into the realm of single photon interference.
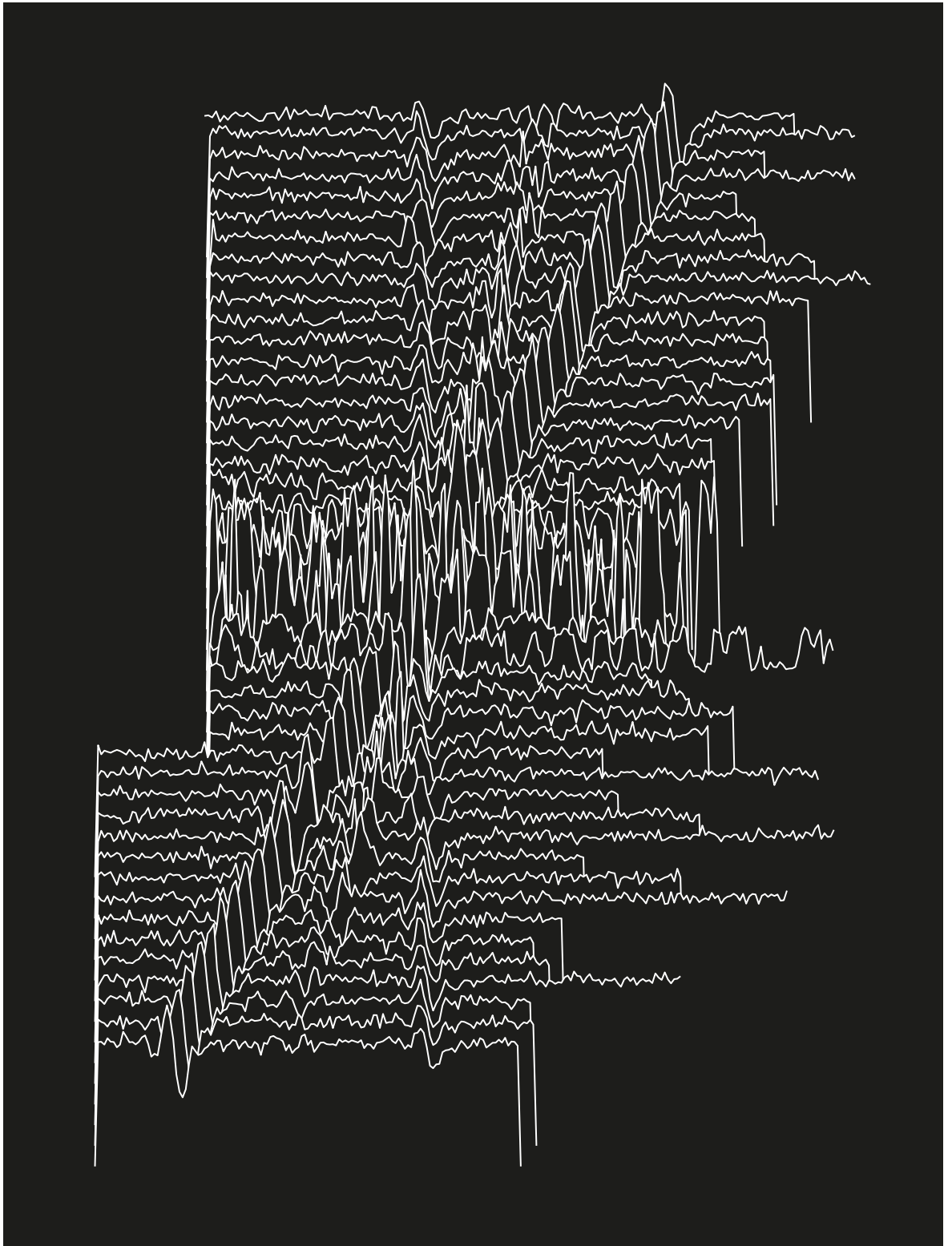
Figure 3.20: 'Unknown Wiggles'. Each horizontal line is a measurement of coincidences against HOM delay, and the nested delay controlling the dip separation is changed by an equal amount between each line. Nested stage position goes between 6.55 mm (bottom line) and 7.0 mm (top line). 10 nm bandwidth filter used. At large separations the middle interference feature loses visibility (moving outside the pump coherence length), at small separations within the single photon coherence length (when the two dips become one) large oscillations in the coincidence background occur as the total number of photons coming through the signal arm varies over the scan as the Michelson was not phase stable. Notice also this phase instability appears to warp the central dips as they can invert multiple times whilst being scanned over. If the acquisition times are long compared to the phase noise fluctuations in the system, then this can also average out the central non-local interference.
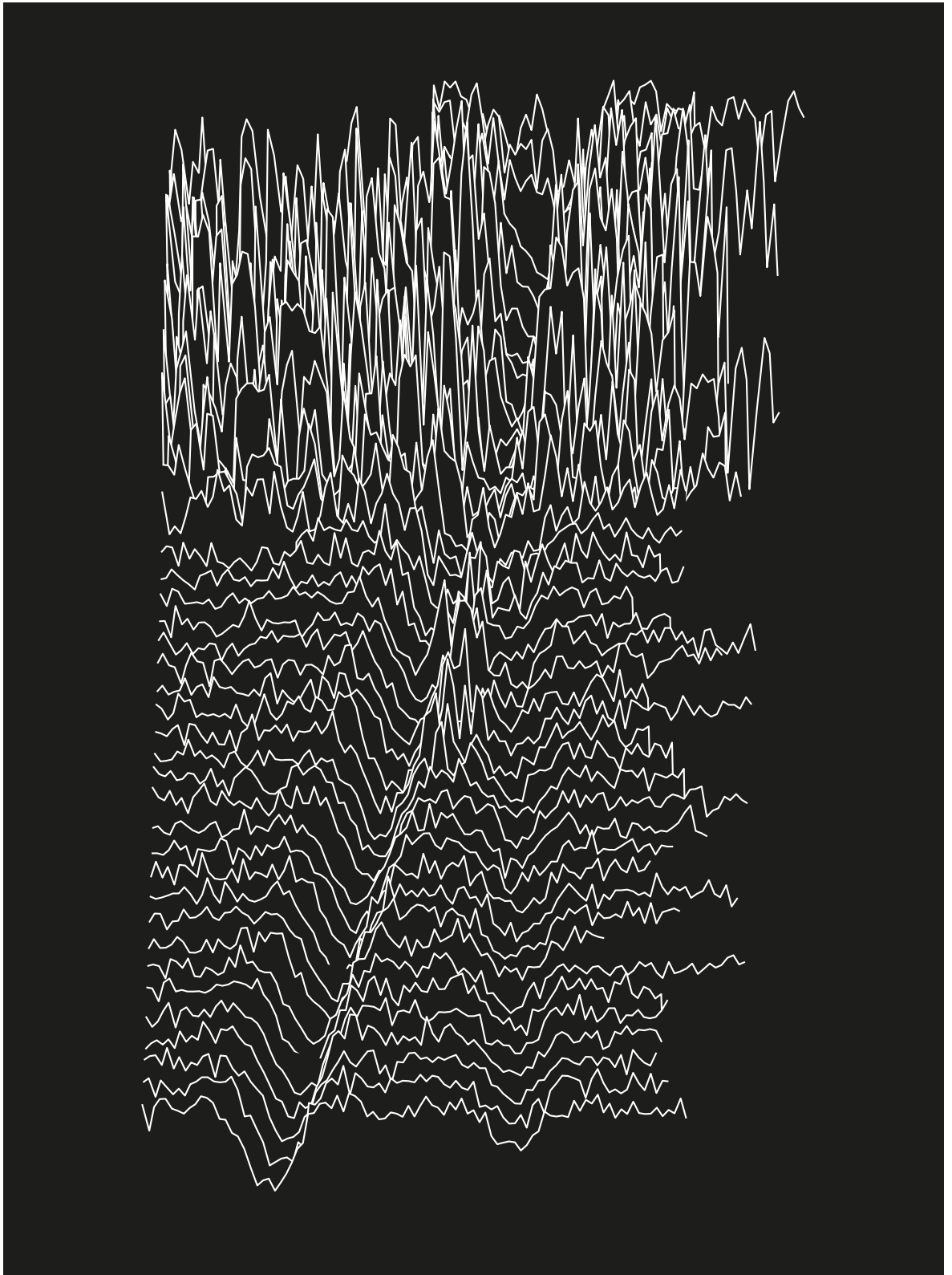
Figure 3.21: Each line is a measurement of coincidences against HOM delay, and the nested interferometer path difference that controls the dip separation is changed by an equal amount between each line. Nested stage position goes between 6.5 mm (bottom line) and 7.1 mm (top line). 3 nm bandwidth filter used. The dips need to be almost overlapping to observe a strong central interference peak (compare to Figure 3.20) with the narrower filter because the single photon coherence length is now larger (the dips are wider) and is now similar to the pump coherence length. The region over which the large fluctuations in the coincidence background occur is also longer for the same reason.
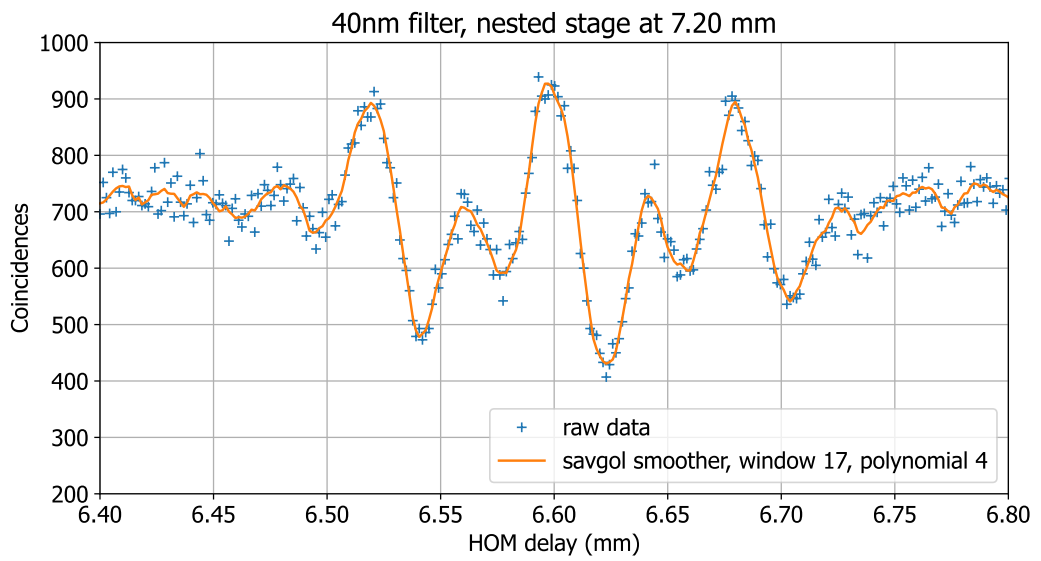
Figure 3.22: 40 nm nested HOM dips
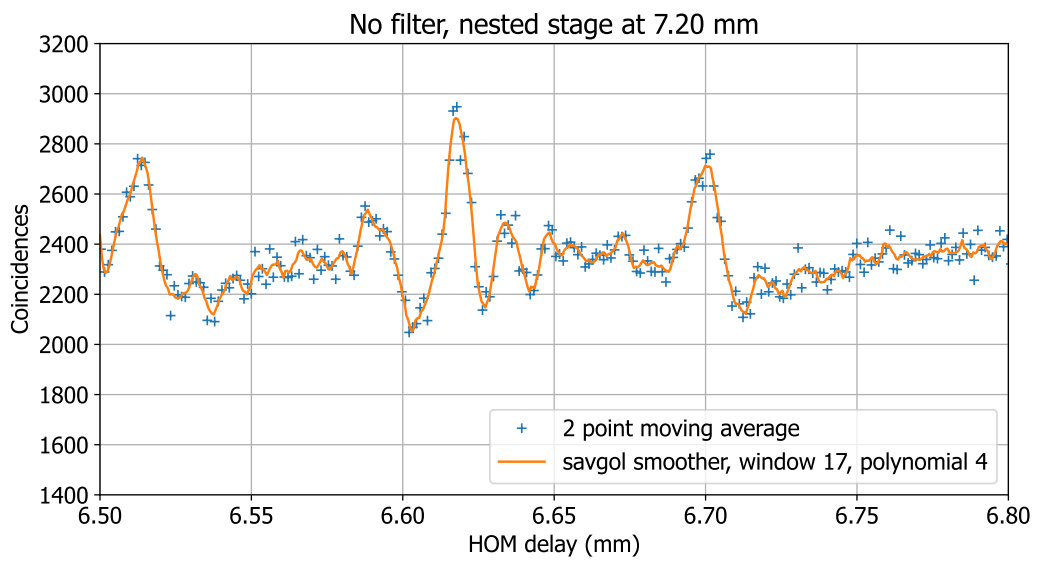
Figure 3.23: No filter nested HOM dips

3.3.2.2 Single Photon Interference

In Figures 3.20 and 3.21 we can see when the dips overlap and we enter the single photon coherence regime because the background coincidences start fluctuating by a large amount. This sadly just reveals the phase sensitivity of the experiment to vibrations from the environment when these measurements were taken - before it was slightly more effectively isolated (as for e.g. the Figure 3.19 measurements with the LCR). The phase between the two Michelson arms changed over the course of the scan, changing how much light passed through the signal arm, which is why the background oscillates in this region.

When the dips are overlapped (the balanced interferometer case), the flipping of the single dip present was not observed with a change of the phase between the two arms (Figure 3.24). Within the single photon coherence length, the total output of the Michelson interferometer towards the HOM beamsplitter depends on the phase between its two arms. Therefore the phase between the two arms is clear in Figure 3.24 from the singles counts (and also the background coincidence counts). However, as the phase changes the dip does not appear to invert. The maximum inversion is expected at the same phase where, in the balanced regime, there is maximum destructive interference between the Michelson arms. Not only that, in the balanced regime, the variance of the coincidences with the nested phase is no longer nicely evenly sinusoidal, it is predicted to have extremely sharp peaks instead (Figure 3.25). So while in *theory* these spikes could mean super sensitive phase measurements using the HOM effect, in *practice* to see an inversion of a dip, when photon counts are at their lowest, amongst both noise in the photon counts from accidentals and phase noise from a setup subject to vibrations from the environment was like looking for a needle in a haystack. (I did not find it.)

3.4 Conclusions

An experiment was built to investigate non-local interference in a HOM interferometer using a nested Michelson interferometer. This interference depends on the entanglement symmetry between the interfering photons, which can be controlled with the Michelson phase. We wanted to understand the underlying effect better and see how this interference would manifest in the balanced nested interferometer regime, as this linked back to our proposal to use rotation to change and reveal entanglement in a HOM experiment with a nested Sagnac interferometer. These are the lessons learned.

While the nested Michelson offered a way to control the phase, it was also prone to picking up phase noise from the environment, and keeping the system phase stable was a challenge. This should be less of an issue with a Sagnac experiment as the nested Sagnac interferometer is common path.

When one of the Michelson arms was more lossy than the other, this introduced distinguishing information that degraded the maximum visibility of the central inter-
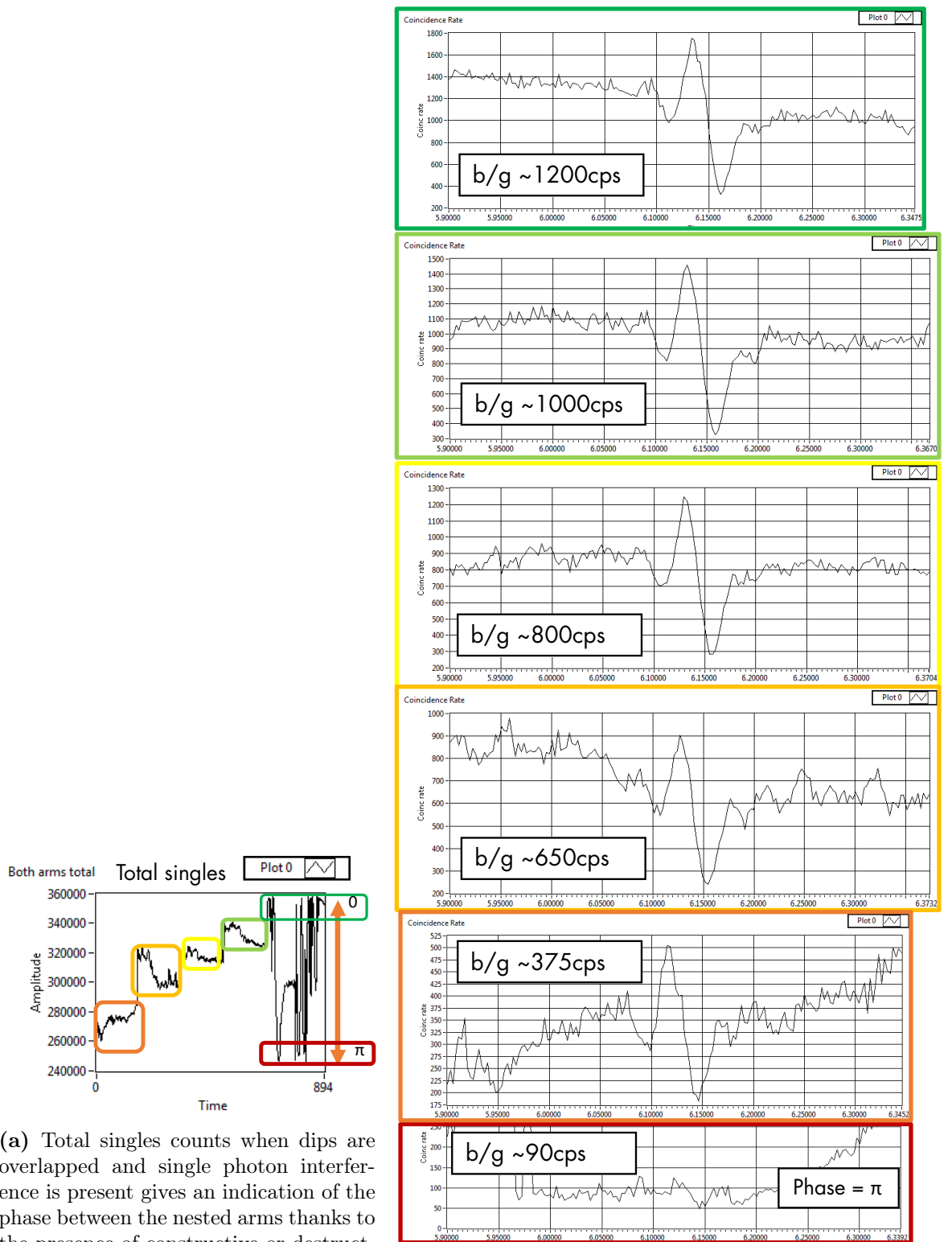
(a) Total singles counts when dips are overlapped and single photon interference is present gives an indication of the phase between the nested arms thanks to the presence of constructive or destructive interference at the output of the nested interferometer

(b) Coincidence measurements for different values of the phase between the two arms.

Figure 3.24: Balanced Michelson results. Singles counts indicate phase of Michelson interferometer. 1 s acquisition per point. Coloured boxes in a) anticlockwise from top right correspond to coloured boxes in b) from top to bottom.
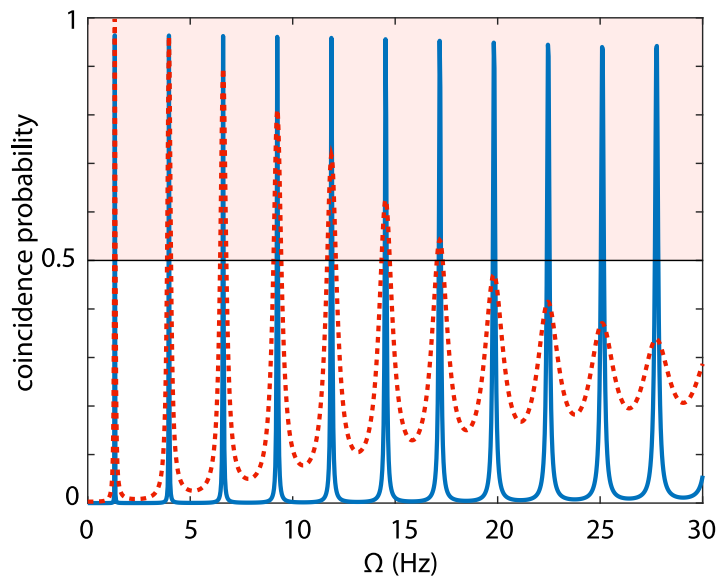
Figure 3.25: Coincidence plot for a HOM delay fixed in the centre of a HOM dip as a function of the angular frequency Ω. The phase difference depends linearly on Ω. This is Figure 4 from Ref. [1]: the theoretical proposal to alter and reveal photon entanglement with rotation using a HOM interferometer with a nested Sagnac interferometer. Two curves are shown for 800 nm photons with two different bandwidths, 5 nm (blue solid curve) and 40 nm (dashed red curve). In the shaded region measurement of anticoalescence implies photon entanglement. Reprinted with permission of the publisher.

ference. Again the common path configuration of the Sagnac should mean this will not be much of a concern, it should not be lossier in one direction that the other.

Within the single photon coherence length it is very difficult to meet the conditions required to see the theoretical inverted interference, due to it occurring when there is destructive single photon interference, and the presence of inversion being very sensitive to achieving exactly the right phase. This will also be the case in a Sagnac experiment. In practice, it is much easier to see inversion of the interference when the extra paths are unbalanced and the dips separated.

The coherence length of the pump needs to be taken into account. While the non-local interference perseveres until the dip separation is a few multiples of the pump coherence length, the visibility is degraded, and the best visibility is when the dip separation is smaller than the pump coherence length. But if the pump has a coherence length of similar magnitude to the single photon coherence length, it can be hard to achieve a high visibility before entering the range of single photon interference.

It's quantum, baby!

Keanu Reeves

4

Controlling Entanglement with Rotation
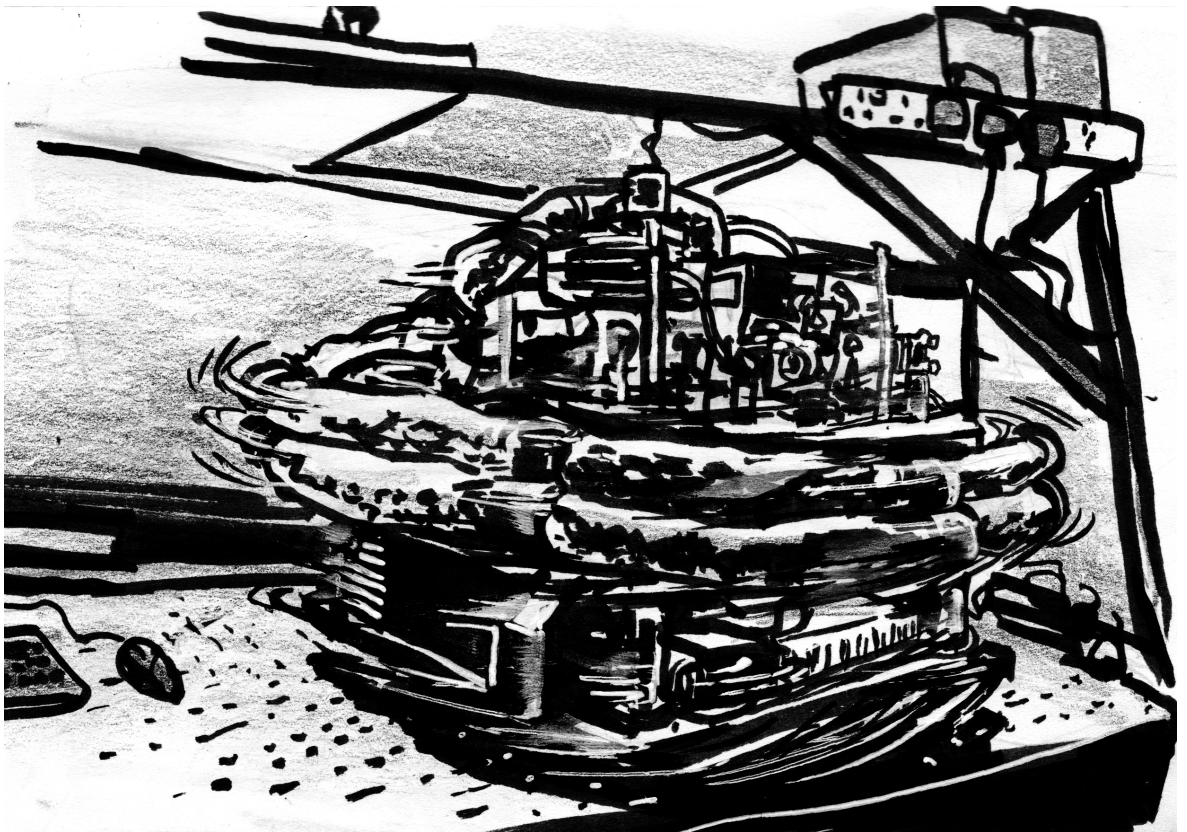
4.1 Introduction

As mentioned in the previous chapter, the overall goal of this part of my PhD was to use rotational motion to alter a quintessentially quantum property. In this way, through the equivalence of curved spacetime and non-inertial motion, these sorts of experiments could shed a bit of light on our murky understanding of a union between quantum mechanics and gravity.

As I was starting my PhD at the University of Glasgow, Sara Restuccia was finishing hers with an experiment probing the quantum Hong-Ou-Mandel effect with photons in a rotating frame. With classical light, the Sagnac effect creates a rotation-dependent phase difference between counter rotating light beams in a rotating frame. Sara's experiment would see how the effect would manifest if a HOM experiment was put in rotation, with one photon travelling with the rotation and the other travelling against the rotation before interfering at a beamsplitter. In this novel test of quantum optics in non-inertial frames, the rotation-induced time delay showed up as a shift of the HOM dip.

At the time, I was looking into the non-local HOM interference detailed in Section 3.1.5 and realised that rotation could be used to turn a HOM dip into a HOM peak through the Sagnac effect. By adapting the experimental setup of the rotating HOM experiment, we could do an experiment that goes a step further and probes entanglement within rotating frames. The initial theoretical proposal for this is set out in Ref. [1] (which also covers the theory underpinning the previous rotating HOM experiment). By nesting a Sagnac interferometer within one of the arms of a HOM interferometer, rotation can tune the entanglement symmetry of the SPDC photon pairs in the system. As only an antisymmetric biphoton state can produce the HOM entanglement witness of anticoalescence at the outputs of a lossless 50:50 beamsplitter, rotation can thus reveal and conceal the quantum entanglement present in the system.

As we were working on improving the previous rotating HOM experiment and about to include some work on adapting it for the new experiment, the first COVID-19 pandemic lockdown hit. Closure of labs and later restrictions to lab access meant I did not have access to the Optics lab with the rotating HOM experiment for 7 months. However, after 4 months I gained part-time access to the Extreme Light group labs in a different building. This factored into the decision to investigate the non-local HOM interference on a static HOM setup (Chapter 3) that I had there first, and then later alongside the rotating HOM experiment as access to the Optics lab was initially restricted to two days per week.

Better familiarity with the rotating setup and the lessons learned from the static experiment meant that there were some desired and required changes to the proposal in Ref. [1], which grew into the experimental design I used to show that rotation can alter entanglement, which culminated in the research paper I wrote up, reproduced here in Section 4.2.
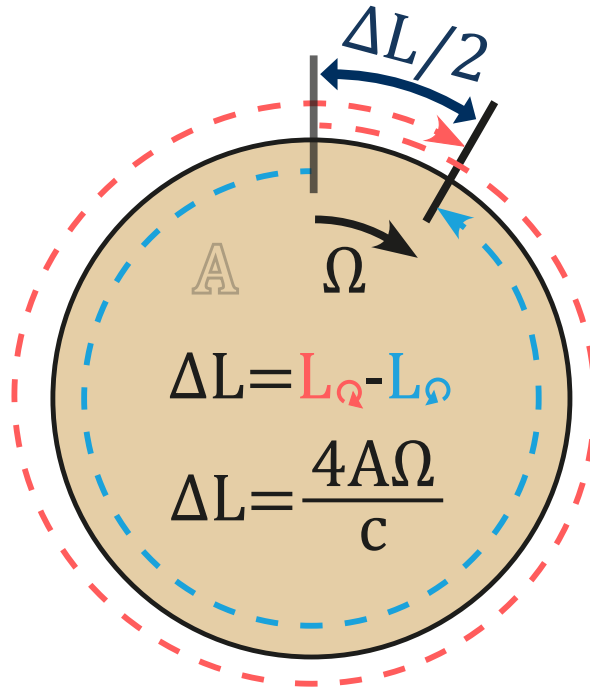
Figure 4.1: Intuitive diagram of the Sagnac effect. Two beams of light are sent opposite directions around a common path enclosing area A from the point at the top. If the system is rotating (at uniform angular frequency Ω), the light travelling in the same direction as the rotation (red) has further to go to complete one loop and return to its start point within the system which has moved away from it, whereas the light travelling against the rotation (blue) has less far to go because the end point has moved around to meet it. The $\Delta L/2$ distance indicated is an average, there are two different points in the inertial lab frame coordinates at which the counterpropagating beams complete one loop.

4.1.1 The Sagnac Effect

Funnily enough, Georges Sagnac considered his experiment to be a proof of the 'luminiferous aether':[1] the title of his 1913 paper is *L'éther lumineux démontré par l'effet du vent relatif d'éther dans un interféromètre en rotation uniforme*[2] [192]. Nevertheless, it is today seen as a special relativistic effect. While it can be derived to first order in several ways, which has lead to much debate around this, to do so to higher orders consistently between the rotating frame and the inertial lab frame requires relativistic transforms, see Ref. [193] for an overview.

If a light beam is spilt in two and each half made to follow the same path in opposite directions around a stationary circuit (for simplicity we consider a circular ring of radius r [194]), they take the same amount of time to circumnavigate the circuit (and then interfere). However if the system is rotating (with angular velocity Ω), from the perspective of the inertial laboratory frame the counter-rotating light will take a shorter time to complete one loop because the position of the end point has moved around by ΔL_{ac} to meet it, whilst the co-rotating light will take a longer time

---

[1]A medium considered at the time necessary to allow light to propagate as waves.

[2]*The luminiferous aether demonstrated by the effect of relative aether wind in a uniformly rotating interferometer*

as the end point has moved away (see Figure 4.1) by ΔL_{cw}:

$$t_{ac} = \frac{2\pi r}{c} - \frac{\Delta L_{ac}}{c} = \frac{\Delta L_{ac}}{r\Omega}, \tag{4.1}$$

$$t_{cw} = \frac{2\pi r}{c} + \frac{\Delta L_{cw}}{c} = \frac{\Delta L_{cw}}{r\Omega}. \tag{4.2}$$

Eliminating the ΔLs in Equations 4.1 and 4.2:

$$t_{ac} = \frac{2\pi r}{c} - \frac{t_{ac}r\Omega}{c} = \frac{2\pi r}{c + r\Omega}, \tag{4.3}$$

$$t_{cw} = \frac{2\pi r}{c} + \frac{t_{cw}r\Omega}{c} = \frac{2\pi r}{c - r\Omega}, \tag{4.4}$$

gives us the co-ordinate time difference

$$\Delta t_{Sagnac} = t_{cw} - t_{ac} = \frac{4\pi r^2 \Omega}{c^2(1 - (\frac{r\Omega}{c})^2)}. \tag{4.5}$$

Identifying the product $\pi r^2 \Omega$ with the more general projection of the area enclosed by the loop[3] onto the plane of rotation $\vec{A} \cdot \vec{\Omega}$, and assuming $r\Omega \ll c$ so relativistic effects are negligible we obtain the usual (first order) form of the Sagnac effect, which coincides for both the inertial frame and the rotating frame:

$$\Delta t_{Sagnac} = \frac{4\vec{A} \cdot \vec{\Omega}}{c^2}. \tag{4.6}$$

The Sagnac effect is usually measured from interference fringes as a phase difference between the exiting beams within a Sagnac interferometer [192]:

$$\Delta\phi_{Sagnac} = \frac{\omega 4\vec{A} \cdot \vec{\Omega}}{c^2}, \tag{4.7}$$

where ω is the frequency of the wave.

Because the Sagnac effect can be reduced down via relativity to pure geometry [195], it is quite universal, the phase shift holds for all kinds of waves: EM waves, acoustic waves, as well as particles (matter waves [196]), and the time difference also holds for macroscopic bodies, as long as the counterpropagating entities travel at the same speed with respect to the rotating system. It is also independent of any medium the wave is passing through, as long as the medium is rotating with the interferometer.[4] This means that the effect occurs in optical fibre, and is independent of any refractive index

---

[3]The shape of this circuit can be arbitrary, nor does the axis of rotation have to lie inside the shape. However, if the loop crosses itself, the area enclosed in different directions can cancel out. A symmetric figure of eight for example would create a zero-area interferometer.

[4]In fact, this version of the Sagnac effect (demonstrating its independence from refraction) was actually observed (and apparently to greater precision!) in 1911 before Sagnac did his famous experiment, by a PhD student Franz Harress - but he interpreted it as an inexplicable bias in his measurements of Fresnel-Fizeau drag of light by moving media. It was only in 1914 that the results were reinterpreted by Paul Harzer as what we now know as the Sagnac effect. [194]

or dispersion [193, 197]. This gives an easy way to increase the area enclosed in a Sagnac interferometer by using multiple turns of the fibre.

The Sagnac effect is the operating principle of high precision gyroscopes, usually ring lasers which pick up a beat frequency between counterrotating beams. These are used in inertial navigation systems, as well as being developed to precisely measure variations in the Earth's rotation, such as the variable length of a day and wobbles of the Earth's axis [198, 199, 200]. The application of the Sagnac effect to the rotation of the Earth (7.29×10^{-5} rad s^{-1}) has been a concern from its earliest days, Sagnac himself mentions it in the 1913 paper, and even before this in 1897 Sir Oliver Lodge hypothesised a large interferometer to measure the dragging of the ether by the rotation of the Earth[5] [11]. The first Sagnac interferometer capable of measuring the Earth's rotation was achieved in 1925 by Michelson and Gale [201], which managed to overcome the sticking point noted by Lodge that *"it does not seem possible to experimentally observe that shift, unless some method could be devised of making the observer and his apparatus independent of the rotation [of the Earth]"* ([11]), by including both a large area interferometer (0.21 km^2) and a small area one in the same experiment to provide a calibration.

State-of-the-art ring laser Sagnac interferometers have now reached record resolutions of 10^{-13} rad s^{-1} precision [202]. As the asymmetry of the propagation is a geometric effect, it depends on the spacetime in which the light moves. When gravity is fully taken into account, Eq. 4.6 picks up additional contributions from general relativity [203, 202]; a Lense-Thirring frame dragging (gravitomagnetic) term, and DeSitter geodetic precession. For an interferometer on the surface of the Earth, these effects are on the order of 10^{-14} rad s^{-1}, nine orders of magnitude smaller than the rotation rate of the Earth. Nevertheless, the GINGER (Gyroscopes IN GEneral Relativity) experiment proposes to use an Earth-based Sagnac interferometer to measure these GR contributions to high accuracy [204, 200]; a prototype - GINGERINO - is already in development [205]. Space-based Sagnacs could go even further in tests of fundamental physics. For example the proposed LAGRANGE experiment [206][207] - an interferometer between several Lagrange points in the Earth-Sun system - could measure the rotation of the Sun, as well as probe gravitomagnetic effects from the Milky Way galaxy.[6]

4.1.2 Original Rotating HOM experiment

Sara Restuccia et al. [133] performed a quantum version of Sagnac interferometry with entangled photon pairs from SPDC and the HOM effect (Section 3.1.3). By construct-

---

[5]He also notes that one could observe a phase shift in a rotating tabletop interferometer. Sagnac was neither the first to conceive the effect that bears his name, nor technically (thanks to Harress as mentioned previously) the first to observe it.

[6]Which would be a similar order of magnitude to the gravitomagnetic effects of the Earth in an Earth-based Sagnac.

Figure 4.2: Fibre configuration for previous rotating HOM experiment ([133]). Down-converted photon pairs produced in a nonlinear crystal are split by a knife-edge prism and coupled into a network of polarisation-maintaining fibre (PMF). Three beamsplitters are used. The left (L) and right (R) 50:50 beamsplitters are used to send the photon pair in opposite directions along the same 100 m fibre (between ports RT and L2), which is coiled to enclose an effective area of 22.7 m^2, and then interfere at the 50:50 HOM (H) beamsplitter, after which they are detected by fibre-coupled SPADs. The signal and idler paths each have 75% loss as a result of passing through the two extra beamsplitters, but the common path fibre reduces asymmetry between signal and idler photons due to temperature effects.

ing a HOM interferometer on a rotating platform, the effect of uniform rotation on the photon distinguishability could be investigated. Rotation created a time delay between the photons, which caused the HOM dip to shift from its zero rotation position, and the faster the rotation, the greater the shift in the dip, in concordance with the Sagnac effect.

A diagram of the optical fibre HOM interferometer is shown in Figure 4.2. 100 m of fibre was wound around the platform in a 0.908 m diameter loop, providing an area $A = 22.7$ m^2, and the experiment was rotated at a range of frequencies up to a few Hz. Instead of using separate fibres for the anticlockwise and clockwise directions and connecting the coupling optics directly to the 50:50 HOM beamsplitter, extra 50:50 beamsplitters are included to create a common path configuration. Using the same fibre for both the clockwise photon and the anticlockwise photons removes unwanted drifts of the dip which would occur if separate fibres were subject to different temperature-inflicted path-length variations. However, it does introduce extra loss, as a maximum of only 25% of the original photons can make it through to the HOM beamsplitter.

4.1.3 Theoretical proposal to reveal and conceal entanglement with rotation

Combining the rotating HOM experiment with the idea of controlling the coalescence or anticoalescence of photons at a beamsplitter (Section 3.1.5) we developed a proposal to reveal and conceal photon entanglement with rotation (Ref. [1]). Symmetrically entangled photon pairs would be sent through different input arms of a HOM interferometer. The idea was to split one of the arms of the HOM interferometer into a clockwise and anticlockwise path within a coiled fibre with a large enclosed area (Figure 3.14). When rotating, the phase between these two paths would be altered by the Sagnac effect, and therefore the entanglement symmetry of the two-photon state would be altered. The other arm of the HOM would need to match the total path length within the range of a HOM delay translation stage so a HOM dip could be observed. An antisymmetric state caused by the rotation would reveal itself as a HOM peak, an entanglement witness, thus revealing the entanglement with rotation. As rotation frequency increases, the HOM interference was calculated to cycle between dips and peaks (Figure 3.25). The idea to use the Sagnac effect to change the symmetry of the state and measure with the HOM effect was my own, the theoretical treatment of this idea in Ref. [1] was fleshed out by Marko Toroš.

4.1.4 Changes made for the experimental realisation

I made changes to the previous experimental setup (Figure 4.2) to achieve the aims of the theoretical proposal, but there were also practical deviations from the system imagined in the above-mentioned theoretical proposal (Ref. [1]) to minimise the overall alterations to the existing optics and to incorporate lessons learned from the HOM experiment with the nested Michelson interferometer (Chapter 3).

4.1.4.1 Separate fibres for signal and idler

Adding in an extra path option into one of the arms so that the signal photon could go both clockwise and anticlockwise would mean it would be difficult to keep the signal and idler photons in a common fibre for most of their propagation time (as in Figure 4.2) and still be able to separate them out again to interfere at the HOM beamsplitter. Instead we considered it the wiser option to use separate fibres for the signal and the idler. We were concerned with observing the HOM dip flip into a peak, rather than the position (or delay) of the HOM interference. It was much more important to keep the nested interferometer paths common path and phase stable, as this controlled the entanglement symmetry, than to keep the exact location of the interference with respect to the delay stage position the same. Some extra effective uncertainty in the delay stage position could be tolerated when what we care most about is whether the HOM interference is a dip or a peak.
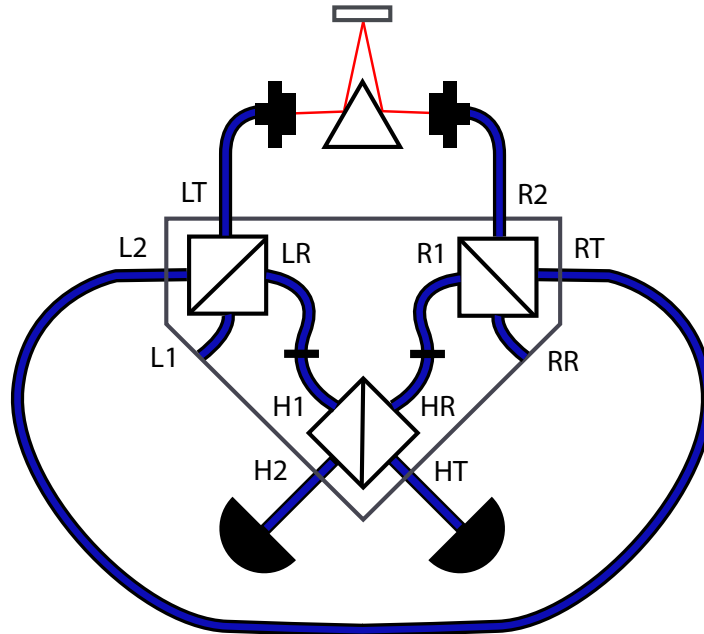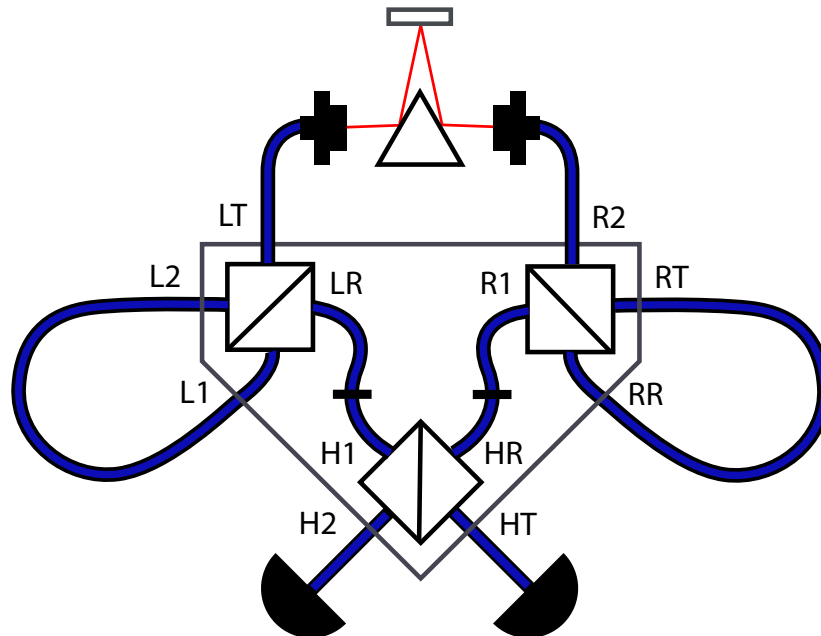
Figure 4.3: Fibre configuration for new rotating HOM experiment (Section 4.2). Down-converted photon pairs produced in a nonlinear crystal are split by a knife-edge prism and coupled into a network of polarisation-maintaining fibre (PMF). Three beamsplitters are used. The left (L) and right (R) 50:50 beamsplitters each form separate nested Sagnac interferometers, by looping 41 m of fibre between L1 and L2 ports (and between RT and RR ports). The photon pairs exiting the Sagnac interferometers then interfere at the 50:50 HOM (H) beamsplitter, after which they are detected by fibre-coupled SPADs. The signal and idler paths each have 50% loss on average as a result of passing through the Sagnac interferometers.

4.1.4.2 Unbalanced regime

From the difficulty I had observing an inversion of the HOM interference in the balanced nested interferometer regime (Chapter 3), I concluded it was pretty essential to operate in the unbalanced regime, as this would allow us to isolate the variable phase-sensitive biphoton interference, and the presence of anticoalescence would be more robust to noise. We needed to separate out the dips corresponding the clockwise and anticlockwise nested paths in time, within a Sagnac interferometer which is balanced *by design* as both directions share the same fibre. The method I developed to do this utilised the birefringence of the polarisation-maintaining fibre (PMF) used in the experiment (beat length ~ 1.1 mm). PMF has orthogonal slow and fast axes to stop light that is input with linear polarisation (along one of those axes) from coupling into other polarisation modes in the fibre. However, to use the birefringence of the whole 40 m of fibre (e.g. clockwise on slow axis, anticlockwise on fast axis) would firstly require changes to the optics of the setup to enforce this polarisation difference, and would create a large dip separation outwith the range of the HOM delay stage - it would be impractical to scan over the whole interference pattern. Such a large imbalance would also be prone to phase noise that could wash out the effect we were looking for, if the birefringence altered with temperature or movement. Instead, it would be best to have a dip separation 5-10 times the dip width (i.e. a few hundred micron), to achieve a

clear separation of the dips but minimising the time required to scan over the whole pattern. This was achieved by adding 1 m of effective birefringence between directions in the fibre. This required no changes to the inner optics of the experiment, just an additional length of custom PMF. This 1 m length of PMF was unusual in that it had its end connector keys aligned to different polarisation axes of the fibre. This meant that by connecting the fibre between the two normal 20 m PMFs that made up the Sagnac loop, the refractive index experienced by the photons would change partway round, when they entered or left the single mismatched connection (e.g. from the slow axis to the fast axis), but crucially this would be after a different propagation distance for the clockwise and anticlockwise directions (see Figure 4.5 for a diagram). For example, a clockwise photon would start on the slow axis and travel through 21 m of fibre before swapping to the fast axis for 20 m, and then out of the nested Sagnac. An anticlockwise photon would go through 20 m of fibre on the slow axis before 21 m of fast axis, and then out of the nested Sagnac. The propagation in the 20 m fibres cancels out and there is 1 m left of birefringent delay between the counterpropagating photons, which resulted in a dip separation of around 600 μm when scanning the HOM delay stage.

4.1.4.3 Two nested Sagnac interferometers

The issues I had in the static experiment (Chapter 3) in matching the fibre paths of a nested interferometer in one arm and a fibre of overall matching length in the other arm, even with just 1-2 m total fibre meant I was sceptical about matching the delays when there was $\sim$ 100 m of fibre involved. We already had four 20 m fibres that had been paired up to make two suitably matched 40 m lengths of fibres that were tried in the previous experiment before the 100 m common path fibre was adopted to remove the drift of the HOM dip with mismatched temperature variations. By adopting a symmetric configuration, with a nested 40 m Sagnac interferometer in each arm, we would not have to worry about path length matching, and it would be a minimally invasive change to the setup, as it would only require one fibre to be unplugged and the two 40 m lengths to be coiled around the platform and connected instead. However, two nested interferometers would add some additional complexity to the physics describing the experiment, extra loss, and potential new sources of noise (see Section A3 for the full equations incorporating potential asymmetry in the experiment). For example, asymmetric noise sources between each side meant the central dip of our five interference features (Figure 4.4b) - which should have always stayed a fully visible dip if both signal and idler underwent exactly the same conditions - also sometimes became a peak. If building the experiment from scratch, there would be less reason to choose this extra complication.

4.2 Controlling Photon Entanglement with Mechanical Rotation

This section reproduces the author's version of the manuscript submitted to *Physical Review Letters* as 'Controlling Photon Entanglement with Mechanical Rotation' by Marion Cromb, Sara Restuccia, Graham M. Gibson, Marko Toroš, Miles J. Padgett, and Daniele Faccio. Preprint version on arXiv DOI: 10.48550/arXiv.2210.05628 [3] The accompanying supplementary information file is reproduced in Section 4.3, with the exception of the detailed theoretical model which has been moved to the appendix (Section A3), since it is not required to follow the 10 pages of mathematics to understand the work.

The majority of the research and the writing of the paper was undertaken by myself. I performed all the measurements and data analysis included in the paper. Figures generated by myself. Early versions of the experimental set-up and LabVIEW code for data acquisition had already been built and developed by Sara Restuccia, Graham Gibson and Miles Padgett for a previous experiment to measure the temporal shift of a HOM dip due to rotation [133]. The adaptations to the experiment required to change the entanglement and to the code to measure this change were formulated and carried out by myself, with technical help from Sara Restuccia and Graham Gibson. The idea behind the experiment was conceived by myself, and developed with Daniele Faccio, Marko Toroš, Sara Restuccia, Graham Gibson and Miles Padgett, with the initial proposal included in Ref [1]. Theoretical model detailed in Section 4.3.1 was calculated by myself with help from Marko Toroš. Fruitful discussions with all authors happened throughout the undertaking of the research. I drafted and rewrote the paper, with edits and corrections provided by Daniele Faccio, Sara Restuccia, Marko Toroš and Graham Gibson.

Text included in { this format } indicates a comment not present in the original text, usually added where appropriate to explicitly indicate contributions of others.

4.2.1 Abstract

Understanding quantum mechanics within curved spacetime is a key stepping stone towards understanding the nature of spacetime itself. Whilst various theoretical models have been developed it is significantly more challenging to carry out actual experiments that probe quantum mechanics in curved spacetime. By adding Sagnac interferometers into the arms of a Hong-Ou-Mandel (HOM) interferometer that is placed on a mechanically rotating platform, we show that non-inertial motion modifies the symmetry of an entangled biphoton state. As the platform rotation speed is increased, we observe that HOM interference dips transform into HOM interference peaks. This indicates that the photons pass from perfectly indistinguishable (bosonic behaviour), to perfectly distinguishable (fermionic behavior), therefore demonstrating a mechanism for

how spacetime can affect quantum systems. The work is increasingly relevant in the real world as we move towards global satellite quantum communications, and paves the way for further fundamental research that could test the influence of non-inertial motion (and equivalently curved spacetime) on quantum entanglement.

4.2.2 Introduction

Quantum field theory in curved spacetime, a theoretical framework for quantum behaviour in background gravitational fields, indicates that motion and underlying spacetime will have non-trivial effects on quantum systems. It has had success in predicting new quantum effects such as Hawking radiation [42, 43] and the Unruh effect [208, 45]. However, so far only a few of these new effects have been shown, and only in analogue systems [54, 49, 51, 52, 53, 2, 55]. Understanding all the effects that spacetime can have on quantum states is also becoming increasingly technically relevant as quantum communications aim towards satellite networks, which will have to account for the curvature of spacetime around the Earth [209, 210].

An improvement over analogue systems, but a so far rarely exploited experimental approach, relies on the equivalence of curved spacetime to accelerating and non-inertial frames. It is generally easier to create accelerations in laboratory embodiments than to do space-based experiments, and allows access to regimes outside those found in our Solar System. Quantum technology is now sufficiently robust that we can start to test entanglement in various non-inertial frames. Fink et al. were able to place a bound on the (non-)effect of uniform acceleration on entanglement from 0.03g to 30g with a drop tower as well as on a centrifuge [70].

Non-inertial motion was also shown to influence the temporal distinguishability of photons by shifting the delay between them [133], combining the relativistic Sagnac effect [192, 194, 197] with Hong-Ou-Mandel (HOM) interference [132], and comparing the Sagnac effect between classical and quantum light.

Here we report an experiment using non-inertial motion to alter the form of quantum entanglement between two photons. By altering the rotation speed of a modified HOM interferometer we are able to change a Hong-Ou-Mandel interference dip into a peak, antisymmetrising the entangled state and changing bosonic photon behaviour into 'fermionic' behaviour. Non-inertial motion therefore affects photon indistinguishability, putting to experimental test the proposed mechanism by which the Sagnac effect alters the symmetry of quantum entangled states [1].

4.2.3 Hong-Ou-Mandel Interference

Hong-Ou-Mandel (HOM) biphoton interference [132] provides information about the distinguishability of photons. When two independent single photons cross at a lossless 50:50 beamsplitter, the unitarity of the beam splitter transformation, combined with

the photon bosonic commutation relations, results in an interference forcing indistinguishable photons to 'bunch' and exit the beamsplitter through the same port. A time delay between the input photons creates distinguishability between the photons. Counting coincident detections between single photon detectors in the two output paths, a dip in the coincidence rate is observed when the photons temporally overlap. The visibility of the dip indicates overall indistinguishability in all photon properties.

In an analogous experiment with fermions, the fermionic anti-commutation relations would suppress the bunching of independent fermions and a peak in the output coincidences would be observed instead. This 'fermionic' behaviour can also be observed with bosons if the particles are entangled in an antisymmetric state [134, 174, 173], which can be engineered in a number of ways [152, 176, 177, 136, 135, 179, 137, 180, 181].

4.2.4   Outline of the experiment

A schematic of the rotating Hong-Ou-Mandel (HOM) interferometer is shown in Fig. 4.4a. A pair of indistinguishable time-frequency entangled photons are produced in a nonlinear crystal and travel in separate arms (denoted with index 's', indicating the 'signal' photon, and 'i', indicating the 'idler' photon) until interfering at a final beamsplitter, after which they are detected in coincidence. In each of the arms, each photon is also split 50:50 into two directions, taking either a long path ($L_{\{s,i\}}$) travelling clockwise, or a short path ($S_{\{s,i\}}$) travelling anticlockwise. The extra paths are set so that the arms are symmetric, $L_s - S_s = L_i - S_i$. A variable overall delay δt is also added into the signal arm, which varies both S_s and L_s equally. There are three different settings of the overall delay at which photons cross the beamsplitter at the same time: when $S_s = L_i$, when $L_s = S_i$, and when both $L_s = L_i, S_s = S_i$. The various combinations of the extra paths therefore result in additional HOM dips in the coincidence measurements at different delays δt.

If the input light is entangled (rather than being two independent single photons), two additional interference features appear between these dips. These correspond to the delays at which $S_s = (L_i+S_i)/2, L_i = (L_s+S_s)/2$ and $L_s = (L_i+S_i)/2, S_i = (L_s+S_s)/2$. These additional interference features can be dips, but depending on the modulo 2π phase between paths S and L, they can disappear completely, or can flip to become peaks [136, 135, 179, 137, 180, 181].

The experiment is mounted on a rotating table. When the experiment is put into rotation at angular frequency Ω, the Sagnac effect changes the time it takes for light to travel with, or against the rotation direction

$$\Delta t_{\text{Sagnac}} = \frac{4A\Omega}{c^2} \tag{4.8}$$

Although the path lengths S and L are fixed, when rotating the Sagnac time delay

a)

b)
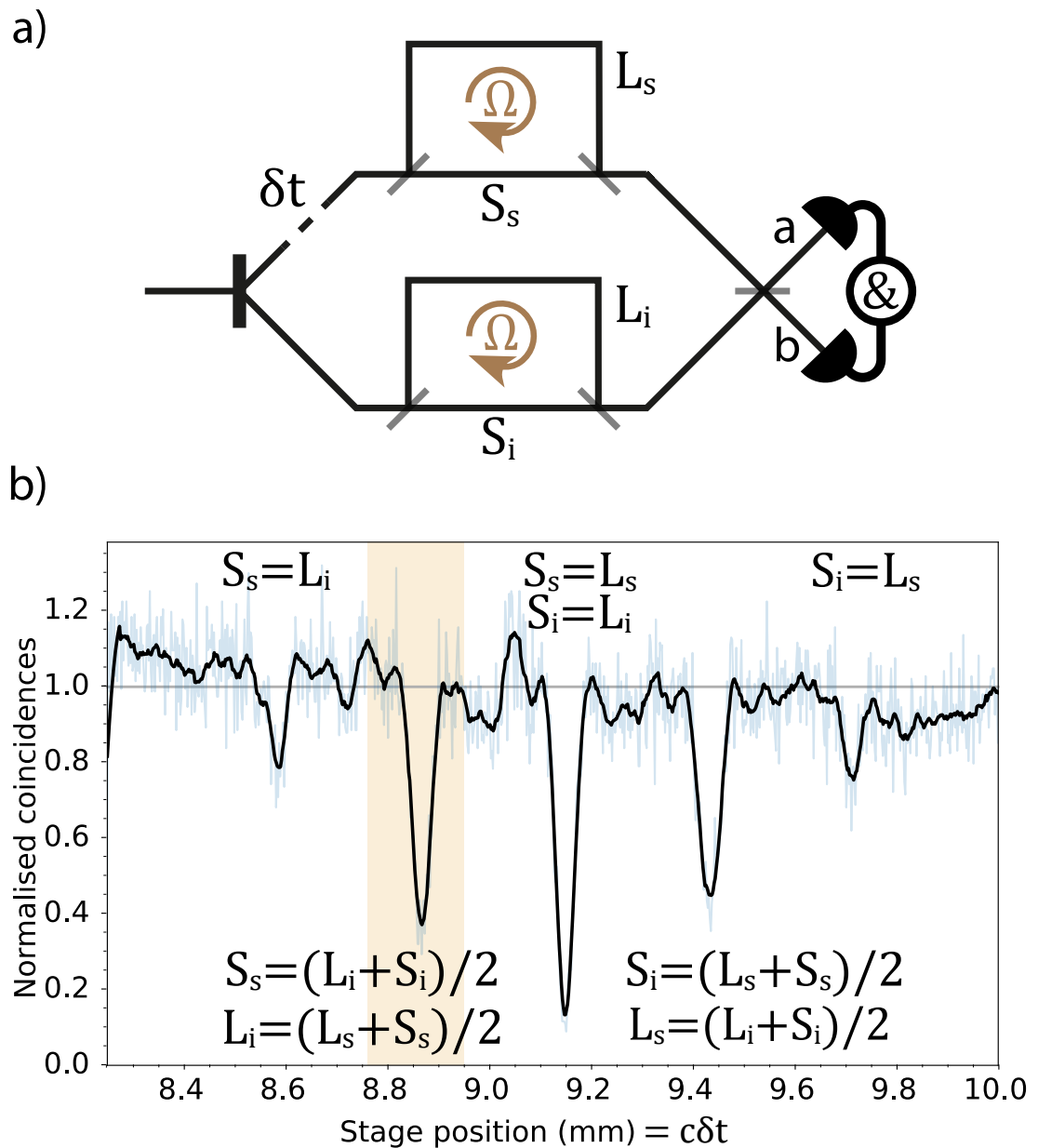
Figure 4.4: a) Schematic layout. Figurative diagram showing short S and long L path lengths (which travel against and with the rotation Ω direction) for the signal and idler photons in the system, along with the HOM delay δt that scans the delay of one arm with respect to the other, and the detection in coincidence after the HOM beamsplitter. **b) Experimental scan of dips while not rotating.** A graph of detected coincidences against the position of the stage, which is proportional to the HOM delay δt. Raw experimental data is shown in light blue, as well as a smoothed average in black. Five dips in the coincidences are present, corresponding to the different combinations of path lengths S_s, L_i etc. at which HOM interference can occur. The shaded region shows an example range over which the stage is scanned when the experiment is in rotation.
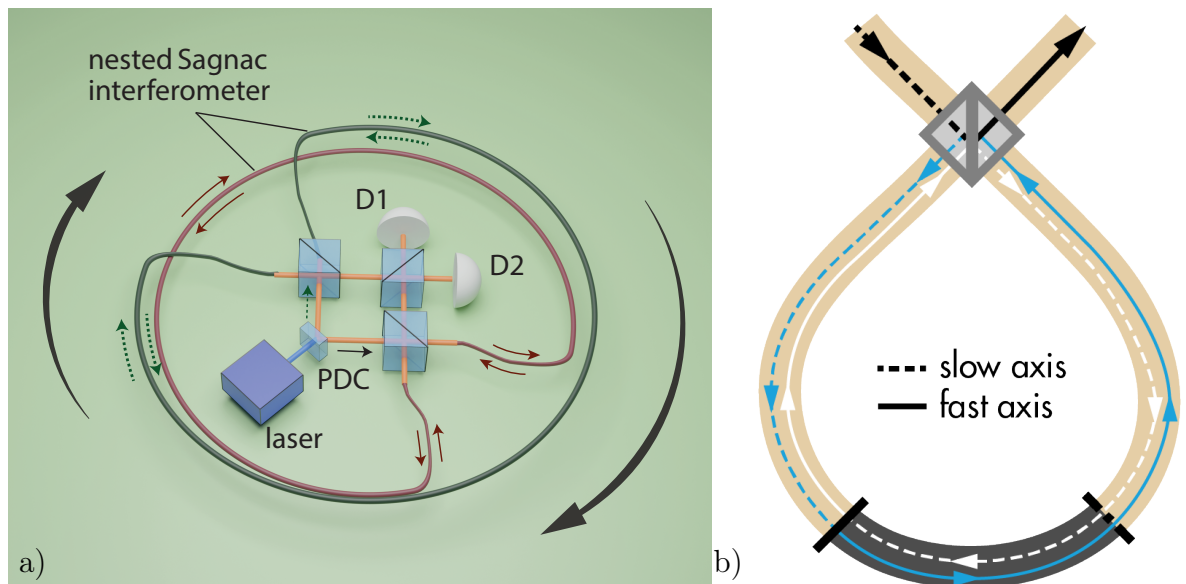
Figure 4.5: Diagram of experiment. aa) Rotating Hong-Ou-Mandel experiment with nested Sagnac interferometers that enclose the area of the rotating platform. A pump laser produces SPDC photon pairs at a nonlinear crystal which each pass through a Sagnac interferometer and then interfere at a beamsplitter. D1 and D2 are single photon detectors which can measure in coincidence. b) Detail of the 1 m birefringent delay between clockwise and anticlockwise directions created by the fibre loop in the nested Sagnac interferometers. This makes the HOM peaks easier to observe as a birefringent delay larger than the single photon coherence length ensures a consistent amount of light passing through the Sagnacs. Two 20 m polarisation-maintaining fibres are connected by a hybrid 1 m patch cord that flips the polarisation axis, so one direction in the Sagnac loop has 21 m of slow axis and 20 m of fast axis, the other has 21 m of fast axis and 20 m of slow axis.

changes the phase difference between them, scaling with the area A enclosed by the paths. Increasing the rotation frequency so that the Sagnac phase difference between S and L paths increases by π is therefore expected to flip these interferences from dips to peaks or vice versa, altering the entanglement symmetry and changing the indistinguishability of the photons as measured by the HOM - purely through non-inertial motion.

4.2.5 Theoretical Model

We follow a similar approach to Ref. [179]. For our input state we assume degenerate Type I spontaneous parametric down-conversion (SPDC) pumped by frequency ω_p and add a variable delay δt between the signal and idler photon arms:

$$|\psi\rangle = \int_0^{\omega_p} d\omega B(\omega) e^{-i\omega\delta t} a_i^\dagger(\omega) a_s^\dagger(\omega_p - \omega) |0\rangle, \qquad (4.9)$$

where $a_i^\dagger(\omega), a_s^\dagger(\omega_p - \omega)$ are the creation operators for modes of frequency $\omega, \omega_p - \omega$ for idler and signal photons, and $B(\omega)$ is the spectrum of the biphoton wavepacket.

Each arm contains a nested fibre Sagnac interferometer where the light hits a beamsplitter, splits into clockwise (cw) and anticlockwise (ac) directions, propagates in op-

posite directions through the same fibre loop for time $t_{\{cw,ac\}}$, and recombines when it hits the beamsplitter again upon exiting the nested Sagnac interferometer.

$$a_i^\dagger(\omega) \;\mapsto\; \frac{1}{2}\left(e^{-i\omega t_{i,cw}} - e^{-i\omega t_{i,ac}}\right) a_{i,out}^\dagger(\omega) \;+\; \frac{i}{2}\left(e^{-i\omega t_{i,cw}} + e^{-i\omega t_{i,ac}}\right) a_{i,back}^\dagger(\omega) \quad (4.10)$$

As well as the Sagnac delay created between clockwise and anticlockwise photons travelling in a total fibre length L_f, the polarisation maintaining fibre paths are constructed such that there is an additional constant birefringent delay from a mismatch between refractive indices n_{cw} and n_{ac} over a length $L_b \ll L_f$ (see Fig. 4.5b). This extra net delay is independent of rotation and creates the short S and long L paths in the Fig. 4.4a schematic, ensuring separation into a total of five interference features shown in Fig 4.4b. The total time delays are thus:

$$\begin{aligned}
t_{cw}(\Omega, n) &= \frac{L_b n_{cw}}{c} + \frac{L_f r\Omega}{c^2} \,, \\
t_{ac}(\Omega, n) &= \frac{L_b n_{ac}}{c} - \frac{L_f r\Omega}{c^2} \,.
\end{aligned} \qquad (4.11)$$

Here we assume that L_f, L_b and r are the same for signal and idler and thus $t_{i,cw} = t_{s,cw} = t_{cw}$ and $t_{i,ac} = t_{s,ac} = t_{ac}$ (for a more general approach, see Supplementary Material).

The light that exits the Sagnacs $(a_{i,out}, a_{s,out})$ interferes at the HOM beamsplitter, at which outputs (a, b) we find the final state:

$$\begin{aligned}
|\psi_{\text{final}}\rangle = \frac{1}{8}\int_0^{\omega_p} d\omega \, B(\omega) e^{-i\omega\delta t} \\
\left(e^{-i\omega t_{cw}} - e^{-i\omega t_{ac}}\right)\left(e^{-i(\omega_p-\omega)t_{cw}} - e^{-i(\omega_p-\omega)t_{ac}}\right) \\
\left(ia^\dagger(\omega) + b^\dagger(\omega)\right)\left(a^\dagger(\omega_p-\omega) + ib^\dagger(\omega_p-\omega)\right)|0\rangle. \quad (4.12)
\end{aligned}$$

The expected coincidences N_c, measured between two single photon detectors in the output arms, is calculated (details in Supplementary Material). Assuming a Gaussian spectrum for $B(\omega)$ of characteristic width $\Delta\omega$ we find

$$\begin{aligned}
N_c \propto C_b - e^{-\Delta\omega^2(\delta t+\Delta t)^2} - e^{-\Delta\omega^2(\delta t-\Delta t)^2} \\
+ 4\cos\left(\tfrac{\omega_p}{2}\Delta t\right)\left(e^{-\Delta\omega^2(\delta t+\frac{\Delta t}{2})^2} + e^{-\Delta\omega^2(\delta t-\frac{\Delta t}{2})^2}\right) \\
- 4e^{-\Delta\omega^2\delta t^2} - 2\cos(\omega_p\Delta t)e^{-\Delta\omega^2\delta t^2}, \quad (4.13)
\end{aligned}$$

where $\Delta t = t_{cw} - t_{ac}$. Eq. (4.13) contains a term that does not depend on the HOM delay δt and that forms the coincidence background

$$C_b \;=\; 4 \;-\; 8e^{-\frac{\Delta\omega^2}{4}(\Delta t)^2}\cos\left(\frac{\omega_p}{2}\Delta t\right) \;+\; 2\cos\left(\omega_p\Delta t\right) \;+\; 2e^{-\Delta\omega^2(\Delta t)^2}. \quad (4.14)$$

Of the terms in Eq. (4.13) that depend on δt and describe interference features, three describe 'fixed' HOM dips; a central dip and two smaller dips either side. There are then three oscillating terms, two which describe two fully oscillating dips/peaks in between the central 'fixed' dip and side dips, and another which can increase the depth of the central dip (essentially ensuring the central dip remains fully visible when the light is fully indistinguishable even as the background C_b fluctuates). From the periodicity of the fully oscillating dips (the $\cos\left(\frac{\omega_p}{2}\Delta t\right)$ term) we find that a change in rotation frequency of $c\lambda_p/(4\pi L_f r)$ Hz is required to fully flip a dip into a peak.

4.2.6   Experimental Apparatus

The experiment shown in Fig. 4.5 is mounted on a rotating table driven by a stepper motor (RS-PRO, 180-5292) run by a controller module (Geckodrive, G201X). A UV pump laser (355 nm, Coherent Genesis CX STM) produces degenerate down-converted photon pairs ($\lambda = 710$ nm) at a Type I BBO crystal. These (symmetrically) frequency-entangled photons are separated using a knife-edge prism, filtered (10 nm bandwidth), and each coupled into a polarisation maintaining fibre (PMF). One fibre coupler is mounted on a translation stage in order to scan the temporal delay δt. Each fibre arm contains a nested Sagnac interferometer, consisting of a beamsplitter with its reflection and transmission ports connected by a 41 m loop of PMF. This optical fibre link is secured around the rotating platform in loops of diameter 0.908 m. The 41 m fibre link is made up of three fibre optic cables connected in series: two 20 m lengths with a 1 m fibre in the middle which has one key aligned to the slow axis and the other key aligned to the fast axis (shown in Fig. 4.5). This 1 m fibre flips the polarisation axis as the light travels around, creating a fixed net 1 m birefringent delay (beat length ~ 1.1 mm) between light travelling in different directions around the loop, creating short and long path options. As the two Sagnac interferometers do not share the same optical fibre, any temperature fluctuations affecting one fibre and not the other can introduce unwanted noise. To minimise these issues, the two Sagnac fibres are looped alongside each other and thermally insulated. After the Sagnac interferometers, the light in each arm recombines at a final HOM beamsplitter and the photons at the outputs are detected by single-photon avalanche diodes (SPADs) which measure singles and coincidences within a coincidence window of 5 ns.

Measuring coincidences while scanning the delay δt resulted in the series of five HOM dips (shown in Fig. 4.4b) as expected from the different paths in the system and cross interference between the paths.

When the set-up is rotated at a constant speed, the Sagnac effect causes an additional phase shift between light travelling clockwise and anticlockwise around the loops, and with a large enough change in rotation speed this additional phase shift changes the symmetry of the entangled biphoton state such that the cross-interference features can flip from a dip to a peak and vice versa.
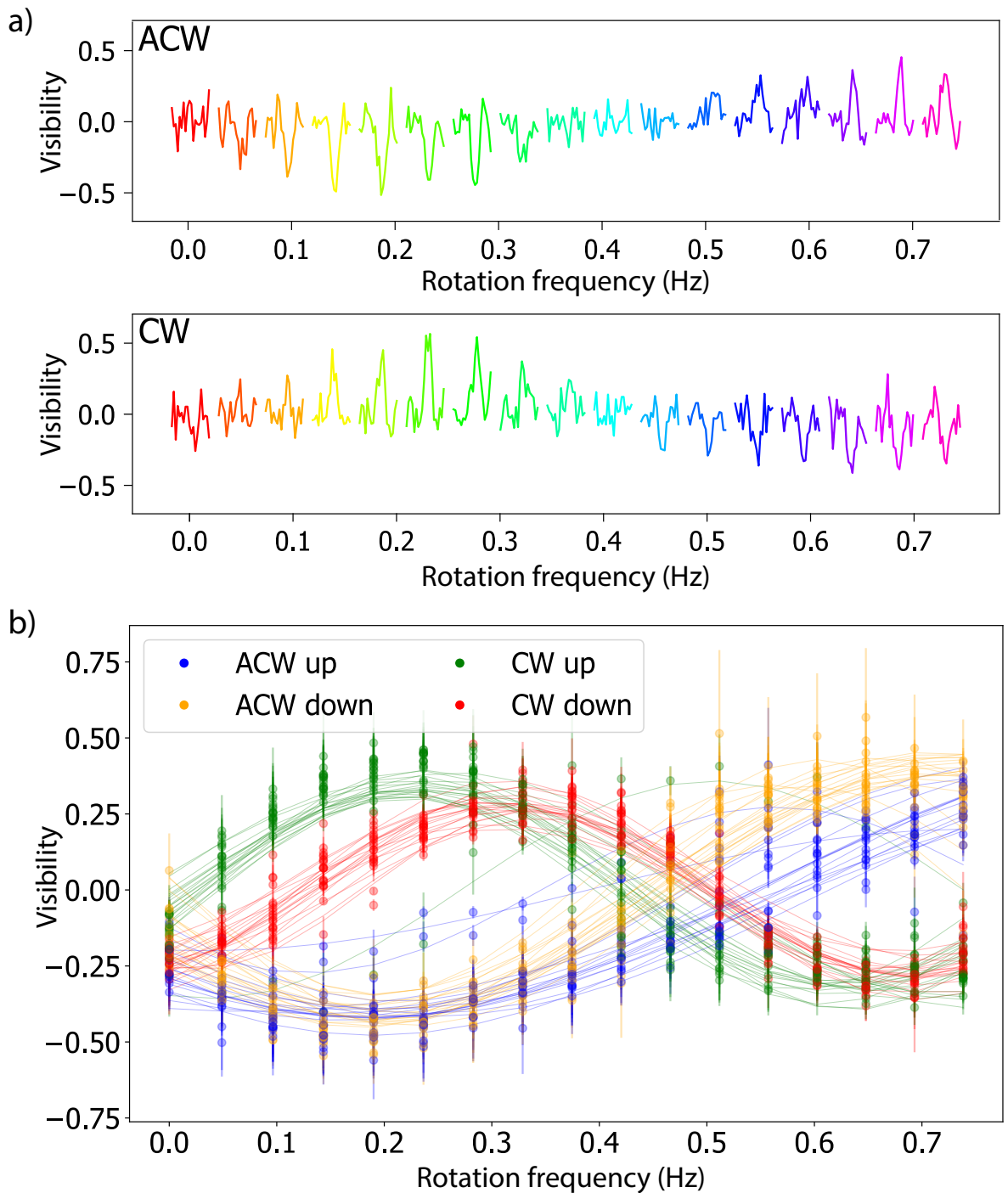
Figure 4.6: a) Dips inverting for clockwise and anticlockwise rotations. Each scan of the oscillating dip is taken at a set rotation frequency, the sequential discrete rotation frequencies used (from 0 to 0.735 Hz) are marked by colour. Contrasting adjacent clockwise and anticlockwise runs, to show how the effect depends on direction, consistent with the Sagnac effect. **b) Interference peak values with increasing rotation speed.** Data from a long overnight measurement run (~ 80 sequences). Plots peak height over background for each rotation speed (dots) and the best fit sinusoids for each 0-0.74 Hz ('up') or 0.74-0 Hz ('down') sequence. Each sequence took ~ 10 minutes. It is clear that clockwise and anticlockwise rotation move the peak in opposite directions from a similar starting phase.

The rotation speed of the apparatus was changed from 0 Hz to a maximum rotation speed (~ 0.735 Hz) in equally set steps (see in Supplementary Material for more information). It was then stepped back down again to 0 Hz. These sequences were repeated, alternating between rotating anticlockwise and clockwise. The maximum speed was set conservatively to ensure the experiment could be repeated consistently over several hours without damage to the equipment or changes to the alignment due to vibrations at higher rotation speeds.

At each rotation speed, the delay stage was used to scan over the second dip from the left (the shaded region in Fig. 4.4b) in equal steps; the singles and coincidences were measured at each delay stage position for a short acquisition time. Most of the data was taken with a 10 μm step size and a 1.5 s acquisition time. Background coincidence rates for these measurements were of the order 100 counts/s.

4.2.7 Results

The results in Fig. 4.6 clearly show that the rotation changed the biphoton state as predicted and that the HOM interference changed smoothly and sinusoidally from a dip to a peak and vice versa as the rotation was stepped up or down.

Depending on whether the experiment is spinning clockwise or anticlockwise, the Sagnac effect will either increase the phase between the nested paths or decrease it. As such, we expect that if we start from neither a dip nor a peak then rotating the experiment in one direction will turn it to a peak first as rotation speed increases, and the other direction will turn into a dip first as rotation speed increases. This can be seen in the experimental data, (Fig. 4.6). This dependence on rotation direction confirms that the main observed effect is due to the predicted Sagnac effect and is not due to spurious effects caused by centrifugal forces on the setup, which would not be dependent on the sense of rotation.

As the experiment consists of many metres of optical fibre, it was also sensitive to temperature changes [211] from the lab environment and from the operation of the electronics and the motor in the experiment. These temperature changes added extra phase drifts that changed over time, and thus also altered across measurement sequences precisely how many rotation steps were required to see a flip of the dip. To reduce these temperature noise effects, the measurements were performed in short time intervals whilst retaining an acceptable signal-to-noise ratio. We then averaged over 151 individual rotation sequences in order to average out small random changes and fluctuations in the environment. Some difference in periodicity might be anticipated between the clockwise and anticlockwise directions due to the g-force on the fibres mentioned above creating a common phase offset that in one direction works with, and in the other against, the Sagnac effect. Indeed, the mean of the 78 clockwise measurements was 0.41 Hz, and the mean of the 73 anticlockwise measurements was 0.53 Hz. Overall, averaging across all data, we measured a dip-to-peak rotation change (half

period) of mean $0.47^{+0.10}_{-0.11}$ Hz, and median 0.43 Hz, that matched well our theoretical expected value of 0.455 Hz.

4.2.8 Conclusions

We have shown that the statistics of biphoton interference can change depending on the non-inertial motion of the experimental frame. Non-inertial motion modifies the entanglement symmetry of the input biphoton state such that we observe Hong-Ou-Mandel interference dips ('bosonic' behaviour) change into peaks ('fermionic' behaviour) and vice versa, with changes in rotation speed of the set-up. This experimental change is consistent with the magnitude and directionality of the Sagnac effect mechanism at the heart of our theoretical model.

The dips that show this change do not appear in our simulations if we use two independent identical single photons as input; the mechanism for changing photon statistics acts on the frequency correlations between the photons that arise from the time-frequency entanglement of the photon pair.

We live in a rotating frame here on Earth, with its influence on the quantum mechanical phase of single particles already recorded [196, 212]. The fact that the underlying spacetime can have effects on photon entanglement may also have consequences for quantum communication technologies, particularly over long distances and using satellites.

This work shows the promising utility of combining photonic technologies and non-inertial motion for testing fundamental physics questions at the interface of quantum mechanics and general relativity. Taking these ideas and techniques further, it could be possible to create entanglement with rotational motion [4] or with other forms of non-inertial motion, particularly with non-uniform acceleration as indicated by theoretical research into quantum field theories in curved spacetimes [213, 214, 215].

4.2.9 Acknowledgements

4.3   Supplementary Information

Supplementary information file containing additional details of the calculations used to generate the theoretical simulations { Calculations moved to the appendix, Section A3 }, the turntable rotation calibration data and the distributions of the results data.

4.3.1   Extended Theoretical Model

{ The 10 pages of maths in this section, which includes my detailed theoretical analysis of the interferometer incorporating asymmetry between the arms and work by Marko Toroš which incorporates a non-monochromatic pump (and therefore a finite biphoton coherence length), has been moved to the appendix: Section A3. }

4.3.2   Rotation speed calibration

The rotation frequency that the motor was set to was not necessarily the actual rotation speed of the experimental turntable due to friction effects. To quantify this and calibrate the measurements accordingly, the time it took to complete a certain number of revolutions at each rotation step used in the experiment was recorded for both clockwise and anticlockwise directions, and used to estimate the real rotation frequency of the experiment. There was no significant difference in magnitude between clockwise and anticlockwise directions for the same set rotation. Both clockwise and anticlockwise measurements were averaged and that data is shown in Fig. 4.7, with a power law fit to the data and the ideal linear case for comparison.
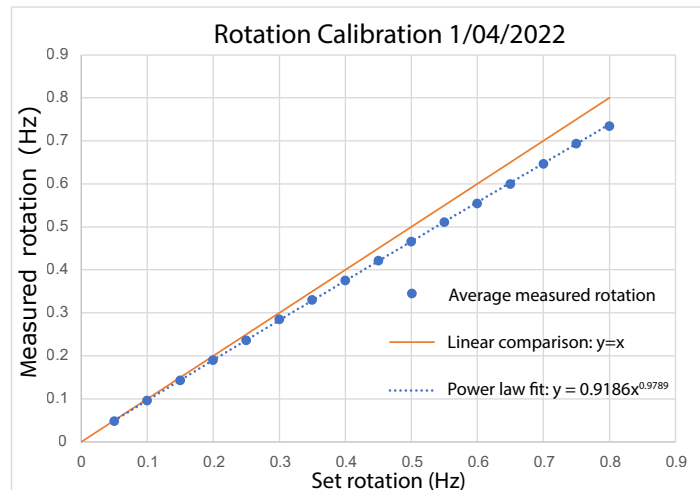
Figure 4.7: Calibration of rotation frequency. The dotted line is a power law fit to the measured rotation. Theoretical linear relationship is shown for comparison.

4.3.3 Histogram of measurements

It was expected for the oscillating dip to have a period of $\frac{2\pi c^2}{\omega_p L_f r}$ with respect to the angular frequency of Ω of the platform, with a corresponding change in rotation of $\frac{c\lambda_p}{4\pi L_f r}$ Hz required to fully flip a dip into a peak or vice versa. To find the change in rotation that caused a flip from a dip into a peak in our experiment, the amplitude of the centre of the peak (or dip) above the background was identified for each rotation speed setting within a sequence of 0 Hz-0.735 Hz (stepping either up or down). A sinusoid was then fit to the peak amplitude-rotation data, and if the fitting process converged well, the best fit parameter of the period of the curve was extracted. The half-periods (representing the rotation frequency change required to change a dip to a peak or vice versa) extracted from the data analysis are shown in Fig. 4.8.

Best-fit periods were extracted from 78 clockwise rotation sequences, and 73 anti-clockwise rotation sequences. The mean and the median from the clockwise data, the anticlockwise data, and the whole set are shown in Table 4.1. The mean and median of the whole set are also shown superimposed in Fig. 4.8b.

	Clockwise (78 runs)	Anticlockwise (73 runs)	Total (151 runs)
Mean	0.411	0.528	0.468
Median	0.396	0.530	0.427

Table 4.1: Mean and median of the dip-to peak rotation frequency change measurements (Hz)

(a)   (b)
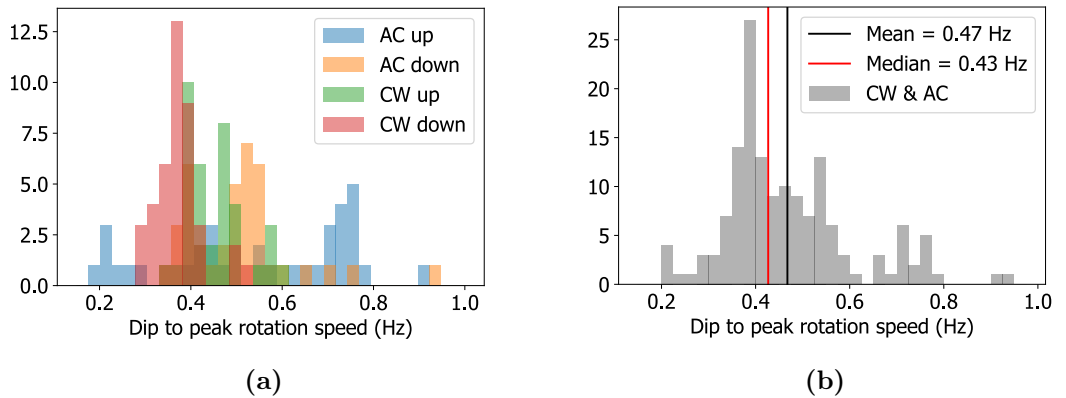
Figure 4.8: Histograms showing best fit rotation speed change required to fully flip from dip to peak (or vice versa). Data extracted from sinusoidal fits to 151 (0-0.735) Hz sequences. Sorted into sequence type (a), and also shown overall (b) with the mean and median of the set indicated.

4.4   Experimental limitations

It is unclear why the anticlockwise 0 increasing to 0.74 Hz (AC up) sequences have a significantly longer periodicity than the others (Figure 4.8a). The values peak at around 0.75 Hz, which was the maximum frequency used, so its likely the peak at that precise location is partly an artefact of trying to fit a sinusoid to data that is not periodic within the measured range. Nevertheless, the data is different to cause the convergence to fits of higher periodicity. It was not the case in all data sets but it was particularly true in the overnight data set (Figure 4.6b) which makes up around half of the measurements. As temperature fluctuations seemed to create noise in our measurements, we theorised that there could also be more systematic effects, from either heat dissipation of the equipment, or from the environment. A average difference in temperature between up and down (perhaps due to the time it takes for the experiment to heat or cool whilst spinning) could also explain the slight discrepancy between the clockwise up and down measurements. Since the effect was not the same across all data sets, it could also be that it was exacerbated when the periodicity of the measurements coincided with the fluctuations of the air-conditioning and heating in the room. Temperature measurements (Figure 4.9) showed that the motor powering the rotation of the platform, which was situated quite close to the optical fibre coils, was heating up by several degrees, and was also heating up the air around it, which the fibres were passing through. The hottest temperatures (near the motor at T1) coincided with the slowest rotation speeds (Figure 4.9a), so it seems likely the movement was dissipating the hot air. Measurements also showed a periodicity in the temperature of the environment, with a periodicity of around 15 minutes in Figure 4.9b, likely due to the air-conditioning unit. The data was taken during the day when the building heating and server room next door was active, so the temperature periodicity may be longer at night when the building is cooler.

Due to the limited time in which to finish a PhD, and since measuring the exact periodicity of the HOM interference inversion was secondary to the actual presence of the effect, further investigation into the relationship between temperature and the HOM interference was not pursued. However, if further experiments were done with the same equipment it would be a good idea to characterise the effect of temperature and to take more steps to isolate the experiment from heat sources and air currents.

4.5   Conclusions

The goal was to use rotational motion to alter a quantum property of photons. I achieved this by combining Hong-Ou-Mandel interference with the Sagnac effect in a new way, to alter the entanglement symmetry of a photon pair, and reveal the entanglement in our system by measuring increased photon anticoalescence at a beamsplitter. We have successfully shown a mechanism by which non-inertial motion can determine
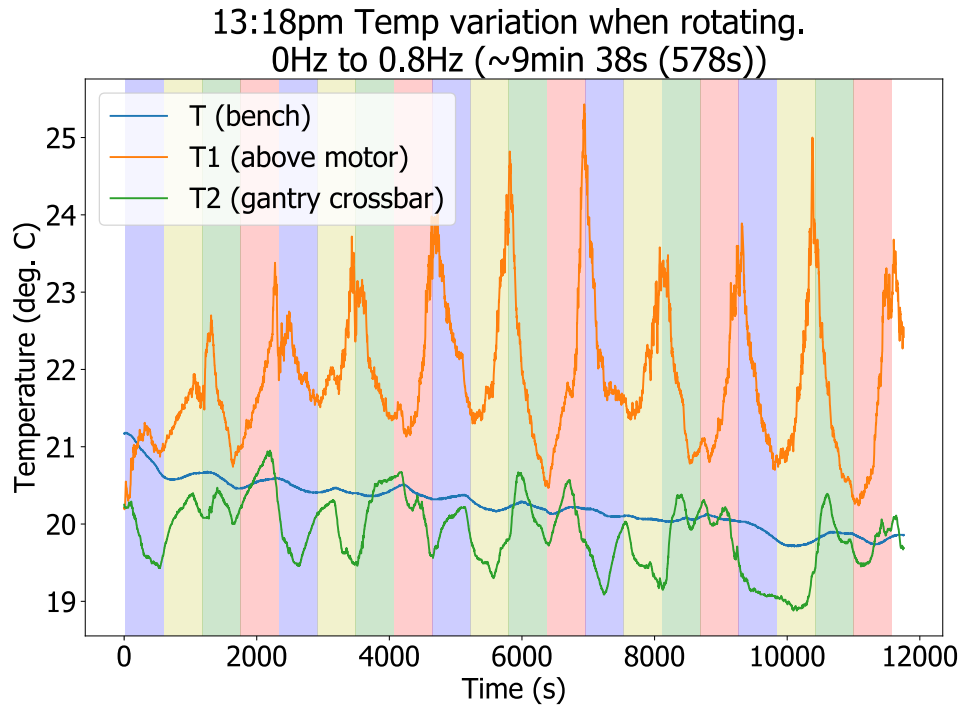
(a) Temperature data around the experiment whilst cycling through rotation sequences. Shading matches the colours used previously (in Figure 4.8a): The order is Blue - AC up, Yellow - AC down, Green - CW up, Red - CW down. Each takes about ten minutes, and is the same timings used to take the data in Figure 4.6b. Peaks in the temperature above the motor (T1) occur when the rotation of the experiment has slowed down to zero.
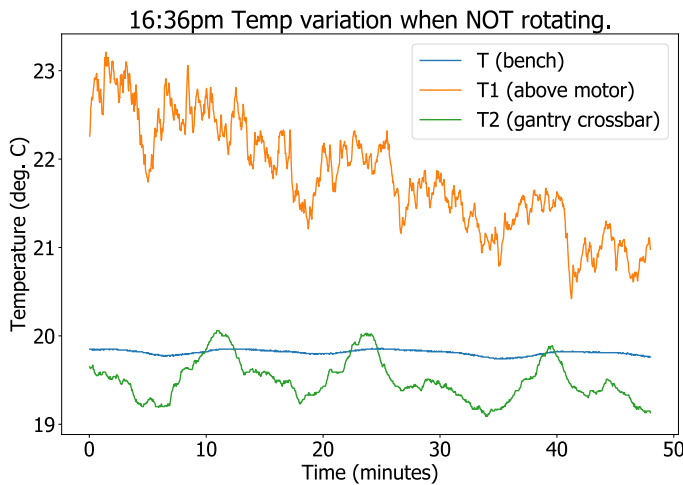
(b) Temperature data taken immediately after a), when the system was not rotating and the motor was off. The motor is cooling down slowly. Note that T2 is measuring a periodic temperature change from the environment (likely from the air-con unit which is situated on the ceiling above the experiment).
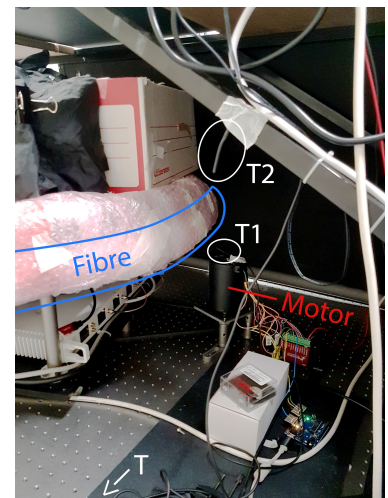
(c) Position of temperature sensors. T1 is just above the motor and just under the fibres. T2 in the foreground is on the gantry, above and to the side of the fibres. The T sensor is an internal sensor within the probe USB stick (Thorlabs TSP01), attached on the vertical front side of the optical bench, to be shielded partly from the airflow.

Figure 4.9: Temperature measurements. Taken during the day whilst the building heating system was on and the air-con in the room was running at a setting of 20 °C. One usual contribution to the heat landscape was missing - the computer within the rotating system that takes coincidence data had a failed power supply and was not working.
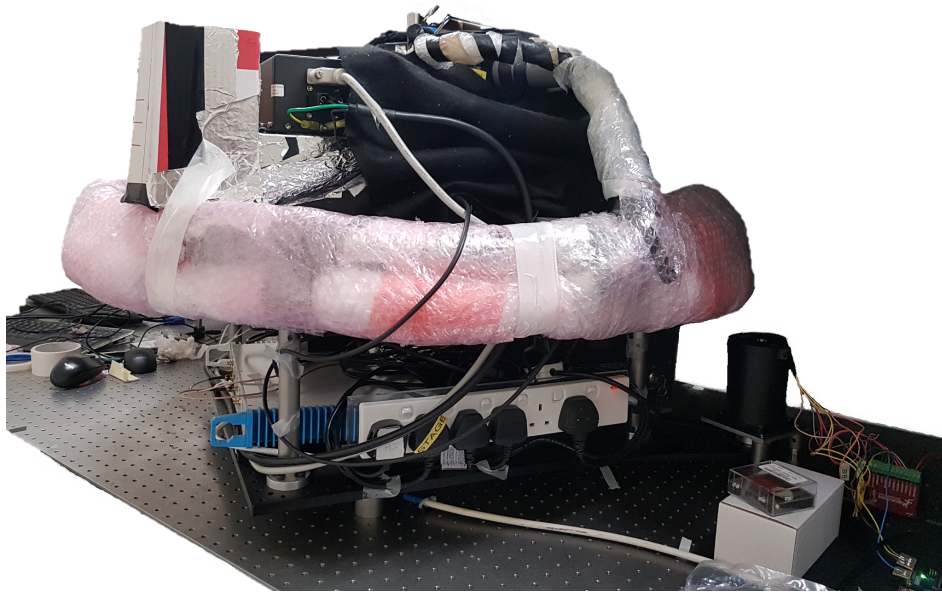
Figure 4.10: Photograph of the rotating HOM experiment.

quantum states. Quantum mechanics and quantum optics have mainly been tested in regimes where inertial frames are assumed. Yet we live in a rotating frame on the earth. This must be taken into account in global navigation satellites, which have to correct for the Sagnac effect in their classical communications to keep their timings precise [216]. As quantum communications scale up into quantum satellite networks, we have to consider how the spacetime around the Earth could affect quantum properties [209, 217]. Gaining a more thorough and robust understanding of quantum mechanics in all frames helps us to answer fundamental questions too. By testing quantum optics in regimes where special and general relativity need to be taken into account we can build new tools for increasing our understanding of quantum systems in curved spacetimes and potentially even for probing questions of quantum gravity. Already this research has sparked an idea for a new experiment, again making use of the Sagnac effect, that could actually generate photon entanglement through rotation (Ref. [4]), as well as other ideas in Chapter 5. As Sagnac interferometers act as a probe of underlying spacetime symmetries, and can also pick up general relativistic effects [203, 202], I hope this work inspires more experiments combining quantum mechanics and relativity in new ways. For example, matter waves increase the sensitivity of Sagnac interferometry [196], by a factor of $mc^2/(\hbar\omega)$ over a interferometer using photons of frequency ω [212] increasing the feasibility of sensing GR effects in tabletop experiments. [7]

---

[7]The area of Werner, Staudenmann and Colella's neutron Sagnac interferometer for a phase shift due to the Earth's rotation that varied by 180° with the varied orientation of the apparatus was just 8.8 cm^2 in area [196]. The area of Gustavson et al.'s atom interferometer also able to measure the Earth's rotation rate was just 22 mm^2 [212].

There is nothing so big nor so crazy that one out of a million technological societies may not feel itself driven to do, provided it is physically possible

Freeman Dyson, 1966 [218, p. 643]

5

Future Directions

The research presented in this thesis has sparked new evolutions of these ideas and new directions to take. This is particularly true of the most recent work, the control of entanglement through non-inertial motion, which can be built upon in many ways.

5.1 The Electromagnetic Zel'dovich effect

As mentioned in Section 2.4.2, it has been proposed to measure electromagnetic Zel'dovich amplification from a rotating levitating microsphere [128]. Such a system could even measure Zel'dovich amplification from the vacuum. The levitated optomechanics techniques required to control the rotating microsphere could also be applied to other fundamental physics problems, such as the existence of quantum friction [219], the construction of closed timelike curves necessary to allow time travel [220], and gravitational radiation damping [221, 222] (or not [223]).

5.2 Control of polarisation entanglement through rotation

With polarisation entangled photons it should also be possible to change the symmetry of a *polarisation* entangled state through rotation in a similar way to Chapter 4. For example, in Ref [161] waveplates are used to change from symmetric Bell state $|\Psi^+\rangle$ to antisymmetric Bell state $|\Psi^-\rangle$ and go from coalescence to anticoalescence. Using uniform rotation in place of the half-wave plate to change the phase delay between H and V photons and go from $|\Psi^+\rangle$ to $|\Psi^-\rangle$ should also be possible.

Start with this polarisation entangled state:

$$|\Psi\rangle = \frac{1}{\sqrt{2}}(|H\rangle_1 |V\rangle_2 + e^{i\phi} |V\rangle_1 |H\rangle_2).$$ (5.1)

The phase between the two terms gives us the symmetric ($e^{i\phi} = 1$) or antisymmetric ($e^{i\phi} = -1$) Bell states. Changing the phase between the H and V photons in a single arm with a PBS and a Sagnac would change this phase with rotation $e^{i\phi(\Omega)}$. This variant on the experiment in Chapter 4 extends the effect to another entanglement degree of freedom.

However, for a fibre Sagnac interferometer the birefringence of the fibre (assuming a use of PMF to keep the polarisations maintained) would create a much larger delay in a long fibre. This could provide distinguishing which-path information and so degrade the entanglement and the interference visibility. Perhaps adopting a symmetric setup with a Sagnac in each arm, set so e.g. the H photon goes against the rotation in one and with it in the other, could be able to change the state symmetry and counter the entanglement degradation that would occur with an asymmetric setup where the relative delay would provide which-path information. It would also produce an overall

π phase shift with half the rotation speed required. Another approach could be to again use a PMF axis swapping trick- instead of using a hybrid cable to shorten the effective birefringent delay as in Section 4.1.4.2, two cables, one with connector keys both aligned to the fast axis, the other with both keys aligned to the slow axis, might be used to cancel the birefringent delays in the fibre Sagnac loop.

5.3 Earth's rotation to reveal entanglement

Here on the Earth, we already live in a rotating frame. Instead of using a rotating platform, it should be possible (although not *easy*) to create an experiment similar to Chapter 4 or Ref [1] (Figure 4.2) that is sensitive to the rotation of the Earth. As the angular frequency of the Earth is extremely slow (7.29×10^{-5} rad s^{-1}), to achieve a phase shift on the order of half a wavelength in order to turn a HOM dip into a peak would need a large effective Sagnac area. Back in 1925, the free-space Sagnac interferometer Albert A. Michelson and Henry Gale built in Illinois was 0.61 km long by 0.34 km wide. The Sagnac effect gives this formula for the expected displacement in fringes for a loop at latitude ϕ_{lat}, on a planet spinning at frequency Ω enclosing area A, using light wavelength λ at speed c:

$$d = \frac{4A\Omega \sin(\phi_{lat})}{\lambda c}. \tag{5.2}$$

With an area of 0.21 km^2, at latitude 41.78° and light of 570 nm wavelength, Michelson and Gale observed a fringe shift of 0.230±0.005 fringes, compatible with the expected value of 0.236 fringes.

To get a π phase shift ($d = 0.5$), this area would need to be doubled. For different wavelengths, again the area would need to be adjusted. The area required is given by re-arranging Eq. 5.2:

$$A = \frac{d\lambda c}{4\Omega \sin(\phi_{lat})}. \tag{5.3}$$

As we used fibres for our Sagnac loops in the experiment in Chapter 4, we can consider how the area required could be achieved in fibre, here in Glasgow (latitude 55.865°). Using the same SPDC wavelength (710 nm) as the light on the rotating platform would require an area of 0.44 km^2 (just smaller than Glasgow Green, which is about 0.5 km^2), which would require a minimum length[1] of 2.3 km. Of course, one may not have access to an area the size of Glasgow Green. The same effective area could be achieved by looping the fibre multiple times around a smaller area, for example 39 times around the OVO Hydro (120 m diameter, 0.011 km^2 area). However, total length of fibre required scales inversely with the radius, this would then require a minimum of 14.7 km of fibre. With large lengths of optical fibre, loss can be a problem.

The area required may scale linearly with wavelength λ, but due to the Rayleigh

---

[1]Corresponding to a circular loop.

scattering limit, loss α through fibre scales as λ^4:

$$\alpha(\lambda) = \alpha_0 \left(\frac{\lambda_0}{\lambda}\right)^4 \qquad\qquad \alpha_0 = 1.7 \text{ dB/km at } \lambda_0 = 0.85 \ \mu\text{m}, \qquad (5.4)$$

dB loss relates to power P in and out like so:

$$\text{Loss}_{dB} = 10 \log \frac{P_{out}}{P_{in}}. \qquad (5.5)$$

For a single 2.3 km loop of fibre, the output power would be 16% of the 710 nm light that is coupled in. For 14.7 km of fibre, you're screwed, the most you get out is 7×10^{-6} of the input. When measuring in coincidences, a factor γ loss for both signal and idler results in a factor γ^2 loss of coincidence counts, e.g. if in the signal arm you have 1% of the original photons remaining, and the idler arm also 1% remaining then you only get 0.01% of the original coincidences. To ensure there are still photon pairs to measure, it might be worth using telecoms wavelengths (1550 nm or 1310 nm) which have much lower loss through fibre, even if the areas required are slightly larger.

If a down-conversion wavelength of 1550 nm was used, then an area of 0.96 km^2 would be required - roughly the three times the size of Kelvingrove Park. For a single circular loop, that is 3.5 km of fibre, and roughly 90% of the light in each fibre is retained. Looping around the Hydro would require 85 loops and a total length 32 km, but could still retain about 30% of the light through the fibre. With telecoms wavelengths, large area fibre networks have the advantage of already existing for the Internet. Such a communications network has already been used as a Sagnac interferometer to detect the earth's rotation by Clivati et al. [224], although using one to manipulate and measure photon pair entanglement without losing it completely would be a bigger challenge.

Considering the difficulty of keeping the 41 m of fibre used in our rotating platform experiment (Chapter 4) phase stable for our HOM measurements due to thermally induced non-reciprocity [211], increasing the fibre length by a factor of 100 or 1000 would be a problem. Finding a way to do the experiment with both signal and idler in a common path would be likely essential for keeping the path lengths equal to within the mm required for HOM interferometry, and the noise sources cancelled to first order. This might be a case where free space propagation and vacuum chambers are required, as used in Michelson and Gale's experiment, although the methods Hilweg et al. [225] propose to reduce fibre noise sources to measure the gravitational effect of the Earth on a single photon with a Mach-Zehnder interferometer could also provide a solution.

It would be a technically ambitious task to show an altering of entanglement by the Earth's rotation (and nothing else!), but the underlying physics is solid, as the results of Chapter 4 has proved. If one could use beams of entangled matter particle pairs (a far less mature technology) rather than photons, then the area requirements would be reduced by huge orders of magnitude [196, 212].

5.4 Generating entanglement with rotation

We have shown that quantum entanglement can be altered with mechanical rotation, but could it actually be created? We[2] have proposed an experiment where inputting a separable single photon state, maximal path-polarisation entanglement can be generated at the output of a Sagnac interferometer system when the system is put into rotation. Full details can be found in Ref. [4].

There are two different configurations outlined in Ref [4] that can both result in entanglement generation from the separable single photon input state:

$$|\psi_i\rangle \sim \frac{1}{2}\Big(|a\rangle + |b\rangle\Big)\Big(|H\rangle + |V\rangle\Big), \tag{5.6}$$

where a, b denote path and H, V denote polarisation.

The configuration in the main body of the paper (reproduced in Figure 5.1a) involves a single photon of angular optical frequency ω in a polarisation and path superposition across two looped Sagnac interferometers of different radii r_a, r_b but the same total path length l, which creates an output state:

$$|\psi_{\text{final}}\rangle = \frac{1}{2}\Big(|a\rangle \left[e^{-i\phi_a} |H\rangle + e^{i\phi_a} |V\rangle\right] + |b\rangle \left[e^{-i\phi_b} |H\rangle + e^{i\phi_b} |V\rangle\right]\Big), \tag{5.7}$$

where

$$\phi_j \equiv \frac{\Omega r_j l \omega}{c^2}, \ (j = a, b). \tag{5.8}$$

When there is no rotation ($\Omega = 0$), the state remains separable. The state becomes maximally entangled at rotations

$$\Omega_{\text{Bell}} \equiv \frac{(2k+1)\pi c^2}{2\omega \Delta r l}, \quad (k \in \mathbb{Z}), \tag{5.9}$$

where $\Delta r = r_b - r_a$. As both the radius and the rotation vector Ω affect the metric of the curved space the photon probability amplitude travels through, the recombined state, and thus the amount of entanglement, depends on the difference in curvature. The mathematics could equally well describe the inverted case of the *spacetime itself* being in superposition. These are interesting new ways of thinking about the interplay between quantum mechanics and spacetime.[3]

A slightly different configuration (Figure 5.1b) is set out in the supplementary material of Ref [4]. This uses a single Sagnac loop (of area A) rather than two, using optical circulators to both input and output light from the same ports. From the same

---

[2]Marko Toroš, myself, Mauro Paternostro and Daniele Faccio. Marko did most of the work on this.

[3]A similar scheme by Chiara Marletto and Vlatko Vedral [72] proposes a way to create single particle entanglement in a modified matter wave Sagnac interferometer as a test of quantum gravity. However the scheme requires *actually* creating a macroscopic superposition of rotations - putting the whole experiment into a superposition of rotations which is far beyond experimental capability. Although the authors point out that for electrons in an atom such things might be possible.
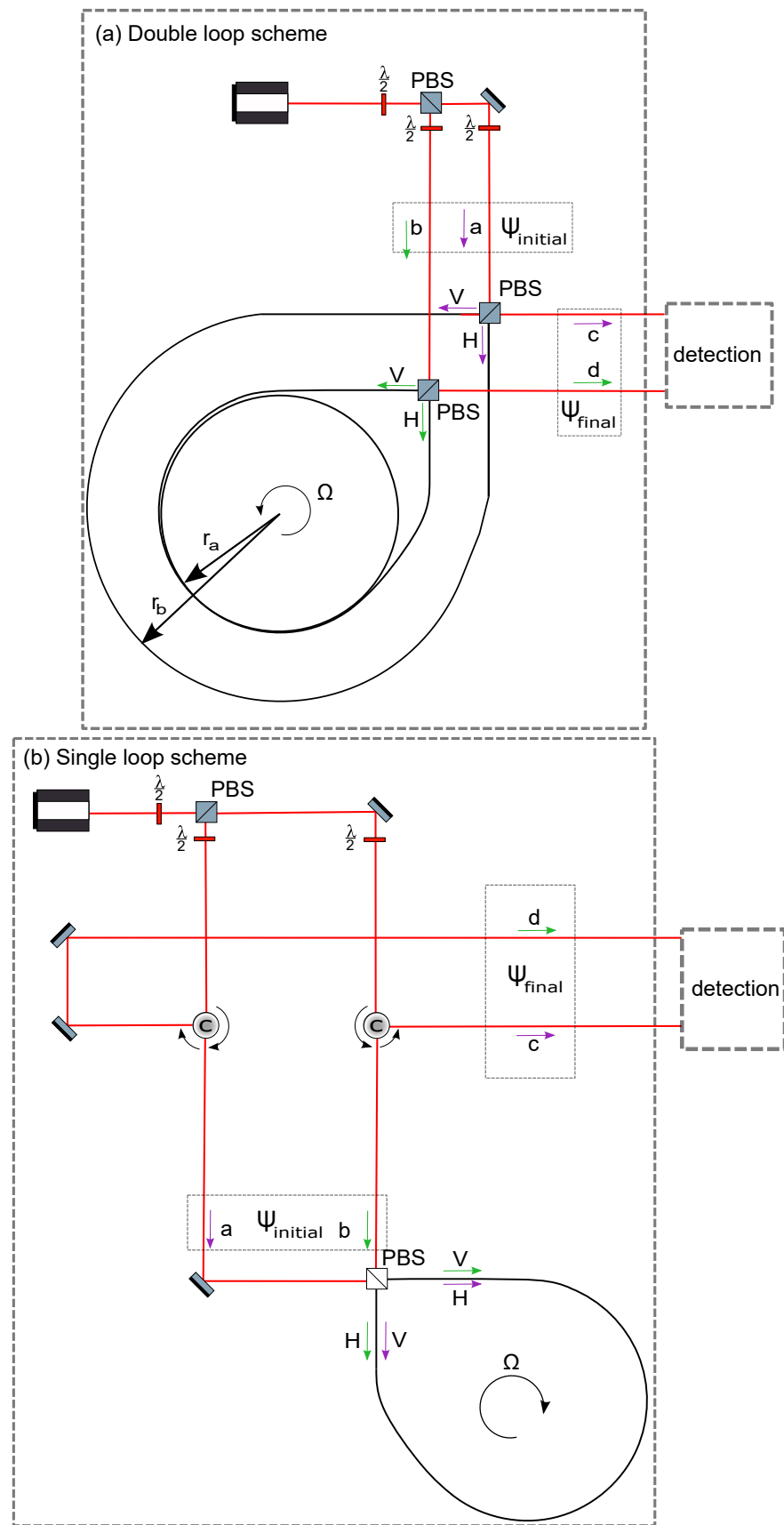
Figure 5.1: Schemes to generate entanglement with rotation, reproduced from Ref [4]. The schemes consist of a single photon source, polarising beamsplitters (PBSs), and half-wave plates (HWPs) denoted by $\lambda/2$ (with the fast axis oriented at $\pi/8$ which rotates the polarization by $\pi/4$). The experimental setup is placed on a platform which can be set in rotation with frequency Ω. The purple and green arrows indicate the paths a, b, while the polarisation is denoted by H, V. (a) double loop scheme (b) single loop scheme.

initial state Eq. 5.6, a slightly different output state

$$|\phi_{f,\text{Sagnac}}\rangle \sim \frac{1}{2} \left(|a\rangle \left[e^{-i\phi_s/2} |H\rangle + e^{+i\phi_s/2} |V\rangle \right] + |b\rangle \left[e^{+i\phi_s/2} |H\rangle + e^{-i\phi_s/2} |V\rangle \right] \right) \quad (5.10)$$

is obtained where ϕ_s is the Sagnac phase:

$$\phi_s = \frac{4\Omega\omega A}{c^2}. \tag{5.11}$$

Again, no entanglement is present for $\Omega = 0$, and maximum entanglement is obtained for certain rotation speeds:

$$\Omega_{\text{Bell}} \equiv \frac{(2k+1)\pi c^2}{8\omega A} \quad (k \in \mathbb{Z}). \tag{5.12}$$

For similar choices of the wavelength, fibre length, and fibre loop radius to our experiment in Chapter 4, the rotation speeds required for maximal entanglement generation[4] for both the single loop and double loop case are within a similar range (0 - 2 Hz) to those explored in Chapter 4. This makes performing the experiment feasible, particularly the single loop scheme which would be more robust against environmental noise. Although the required control of polarisation will have additional technical considerations, for example of how the fibre birefringence can affect the state.

Combining this idea with use of the Earth's rotation as above (Section 5.3) raises the possibility also of using the Earth's rotation to generate entanglement.

5.5 Generating entanglement with gravitational waves

One can also generalise the entanglement generating scheme of the previous section (Section 5.4), to be sensitive to other changes in spacetime. For example, to gravitational waves, which stretch and squeeze spacetime perpendicular to their propagation as they pass. Consider the separable single photon input state in Eq. 5.6 from Ref [4].

Instead of a Sagnac interferometer to sense the gravitational wave,[5] replace the Sagnac loop of Figure 5.1 with something like LIGO - a very large Michelson interferometer with arms L_1, L_2 - although using a polarising beam splitter (PBS). For no gravitational wave, we take the path lengths to be equal $L_1 = L_2 = L$. Consider the simple, optimal case of a gravitational wave of magnitude h passing through that is propagating in a direction orthogonal to the axes of the two interferometer arms, with polarisation aligned with the interferometer arms $\vec{h} = h\vec{e}_+$ [231]. As the wave passes

---

[4]This *intraparticle* entanglement - between the different degrees of freedom of a single particle, could be misconstrued as being purely classical non-separability, however it is a quantum effect. The quantumness lies in the discrete, indivisible single particle nature [226, 227]. Correspondingly intraparticle entanglement can be used as a quantum resource, and can be converted into *inter*particle entanglement between spatially separated particles with only unitary operations [228].

[5]Although zero-area Sagnac interferometers have actually been proposed for next generation gravitational wave detectors [229, 230].

the stretch and squeeze of spacetime means the arm lengths will oscillate between:

$$L_1 = L - \Delta L, \qquad L_2 = L + \Delta L, \tag{5.13}$$

and

$$L_1 = L + \Delta L, \qquad L_2 = L - \Delta L, \tag{5.14}$$

where

$$\frac{\Delta L}{L} = \frac{h}{2} \tag{5.15}$$

The input states to the PBS transform to the output states like so:

$$
\begin{aligned}
|a\rangle |H\rangle &\mapsto |a\rangle |H\rangle \, e^{i\pi} e^{-i2kL_2} \\
|a\rangle |V\rangle &\mapsto |a\rangle |V\rangle \, e^{i\pi} e^{i\pi} e^{i\pi} e^{-i2kL_1} \\
|b\rangle |H\rangle &\mapsto |b\rangle |H\rangle \, e^{i\pi} e^{-i2kL_1} \\
|b\rangle |V\rangle &\mapsto |b\rangle |V\rangle \, e^{i\pi} e^{i\pi} e^{i\pi} e^{-i2kL_2},
\end{aligned}
\tag{5.16}
$$

where phases of $e^{i\pi}$ are picked up upon reflection from the PBS and the mirrors, but are common factors that can be ignored. For simplicity we consider a moment of maximum amplitude of the wave in one direction, Eq. 5.13. There is also a common phase factor e^{-i2kL} which also can be ignored, leaving a final state of:

$$
\begin{aligned}
|\psi_{f,\mathrm{GW}}\rangle &= \frac{1}{2}(|a\rangle |H\rangle \, e^{-i2k\Delta L} + |a\rangle |V\rangle \, e^{+i2k\Delta L} + |b\rangle |H\rangle \, e^{+i2k\Delta L} |b\rangle |V\rangle \, e^{-i2k\Delta L}) \\
&= \frac{1}{2}(|a\rangle \, [e^{-i2k\Delta L} |H\rangle + e^{+i2k\Delta L} |V\rangle] + |b\rangle \, [e^{+i2k\Delta L} |H\rangle + e^{-i2k\Delta L} |V\rangle])
\end{aligned}
\tag{5.17}
$$

which is the same as Eq. 5.10, except with $2k\Delta L$ instead of $\phi_s/2$.

Such a scenario should therefore lead to generation of entanglement as in Section 5.4. As the wave passes, the amount of entanglement should oscillate as the arm lengths oscillate.

However, typical detectable gravitational wave strains are on the order $h = 10^{-21}$ [231], corresponding to a change on the order 10^{-18} m between the 4 km length arms. Using beam recycling, LIGO increases the effective arm lengths to 1600 km [232], for a total effective length difference detected between the arms of 10^{-15} m. Naturally, for optical wavelengths ($\approx 10^{-7}$ m) this is still a minuscule phase shift, and would be a correspondingly minuscule amount of entanglement generated. As entanglement is in general much more laborious to detect and verify than a phase shift, to prove gravitational waves had generated entanglement in this manner, *at a single photon level*, would be an immense technical challenge. But not totally impossible. And who knows, as quantum technologies advance it may be that we find new ways of detecting entanglement - entanglement witnessing [59] - that offer advantages over more direct sensing of e.g. a phase shift.

We never experiment with just one electron or atom or (small) molecule. In thought experiments we sometimes assume that we do; this invariably entails ridiculous consequences [...] In the first place it is fair to state that we are not experimenting with single particles, any more than we can raise Ichthyosauria in the zoo. [...] We can never reproduce the same single-particle-event under planned varied conditions; and this is the typical procedure of the experimenter.

Erwin Schrödinger, 1952 [233]

There are more things in Heaven and Earth, Horatio, than are dreamt of in your philosophy

Hamlet, Act I Scene V of *Hamlet* by William Shakespeare

6

Conclusions

The research in this thesis was motivated by the rather broad question: how do rotating frames affect quantum systems? This fits into wider questions of how quantum systems are affected by inertial frames and curved spacetimes, questions entangled[1] with the biggest unsolved problem in fundamental physics - how to unite quantum physics with general relativity. One cannot expect, within the course of a PhD, or likely even in the course of an entire career, to *completely* answer this question. Nevertheless, we can pick out ways forward, gaps in the literature waiting to be filled, natural extensions to existing work.

To that end, I have verified a 50 year old prediction that waves can be amplified through interaction with a rotating absorber, albeit in the more initially achievable case of a classical, rather than quantum, system. I have also investigated how to detect and manipulate quantum entanglement in Hong-Ou-Mandel interferometry, to enable and verify the successful control of photon pair entanglement symmetry with mechanical rotation.

First, I showed an effect of a rotating frame on a classical system. Secondly, I investigated a quantum effect in an inertial frame. Finally, I explored how this quantum effect could be controlled by rotation.

Zel'dovich predicted in 1971 [75, 76] that an absorber when rotating should be able to amplify waves scattered from it. As in the quantum world any stimulated emission should have have a spontaneous counterpart, he also predicted that even in the absence of incident waves, such a rotating body should amplify quantum vacuum fluctuations

---

[1]Excuse the pun.

into real radiation. Such a picture should also apply to rotating black holes - Penrose had shown that energy could be extracted from rotating black holes [83, 84], and this work by Zel'dovich suggested they should spontaneously radiate away their energy. Initially unconvinced by this, Hawking did his own calculations and found that non-rotating black holes should also radiate, the famous Hawking radiation [42]. These linked curved-spacetime effects of Penrose superradiance and Hawking radiation have been verified in generalised forms in analogue gravity experiments [50, 49, 51, 52, 53, 55], but Zel'dovich amplification was neglected, because the configuration set out in his proposal was difficult to realise. However, recent theoretical treatments allowed a simplification of the geometry; the effect should also occur for waves incident and reflected along the rotation axis of the object, rather than perpendicular to it [78]. Using sound waves should also produce the classical effect, with conditions easier to meet than with EM waves [80]. Other theoretical work showed the effect should also appear in transmission, and also in a sub-wavelength regime [79]. This meant the absorber could be much thinner than the wavelengths used. Recent experimental work by Gibson et al. [81] had demonstrated an extreme rotational Doppler shift into negative frequencies, also for sound waves, these negative frequencies being key to meeting the conditions for the Zel'dovich effect. By adding and measuring absorption into the experimental system, we could test the Zel'dovich effect.

Section 2.2 shows our direct demonstration of amplification of waves due to a rotating absorber, in acoustics [2]. The calibre of the work was recognised by the IOP as 2020's *"best paper [in physical acoustics] by a PhD student at a UK university"* ([117]). A particular strength of our experiment was the experimental elegance [116]. The simplicity of the design has allowed the system to be replicated by researchers at Zhejiang University [118], to apply the idea of amplification from rotation to the field of acoustic OAM communications. This example shows impact of the research in the academic community, and reminds us that fundamental physics motivated research can feed into technical applications in unexpected ways! The work also caught the imagination of the press and the public [121], due to its link to black hole physics.

However there are obvious limitations to this particular experiment with respect to our aims in exploring quantum effects of rotating frames. The use of an acoustic system not an electromagnetic one, while a more achievable experiment due to the slower wave propagation speed, is unable to probe the quantum nature of the effect and observe any amplification from the quantum vacuum. Yet, the theoretical flexibility of the effect with regard to geometry [78, 80, 79] - with experimental proof provided here - that relaxes some of the original requirements has made an electromagnetic test much more feasible. A new configuration has been proposed that could test the effect with electromagnetic circuits [128], and in theory should also be suitable for observing spontaneous amplification from the quantum vacuum due to the rotation of an object.

To explore quantum effects in rotating frames, I was inspired by the experiment by

Restuccia et al. [133], which measured the shift of a Hong-Ou-Mandel dip due to the time delay between photons induced by the Sagnac effect in a rotating frames. This was already a bit quantum due to the use of photon pairs and HOM interference, I wanted to see if we could make it even more quantum. There was existing research that had explored how HOM interference can act as an entanglement witness [134, 174, 173], if a HOM peak is observed instead of a dip. To see if this could be combined with the rotating HOM set up, it was desirable to replicate the HOM peak effect for frequency entangled photons [136, 135, 179, 180, 181], to understand in what regimes the effect appeared and could be easily controlled, using a static experiment. To use a Michelson interferometer specifically to introduce and control additional interference features was a novel approach, and enabled easy control over which coherence regime the experiment was in. I replicated the result [137] that the cross-interference disappeared when the dip separation was much greater than the pump coherence length, using a continuous-wave, rather than pulsed, pump beam. The relevance of this work was mostly in enabling the evolution of the rotating experiment, rather than any wider impact. While some control of the cross-interference with phase was achieved, it was severely limited by the phase (in)stability of the Michelson interferometer which created a lot of noise. The realities of experimental work were brought into focus, so while we had proposed (Ref. [1]) to work in the single-photon interference (balanced-interferometer) regime to observe the anti-coalescence appear with rotation, this work made it obvious that working in such a regime would be an almost unwinnable battle against noise and low signal. The more achievable option is to work in the sweet spot outside the single-photon coherence length but within the biphoton interference length inherited from the pump.

Building (quite literally![2]) on the previous experiment by Restuccia et al. [133] measuring photon temporal indistinguishability in rotating frames, we have shown it is possible to alter and control photon entanglement solely by changing the uniformly rotating frame the photons propagate in. The entanglement of the photon pairs was revealed through Hong-Ou-Mandel interferometric measurements, for a specific change in rotation speed of the experimental apparatus, a HOM dip (photon coalescence) turned into a HOM peak (photon anti-coalescence), the signature of a change from a symmetric to an antisymmetric entangled wavefunction, akin to a difference between bosons and fermions. We have experimentally demonstrated a mechanism by which non-inertial frames, and curved space(time) can alter quantum states.

This work is distinct from, and does not contradict but complements, the work by Fink et al. [70], which showed how the magnitude of uniform acceleration does not change the degree of quantum entanglement. That work used a centrifuge to subject to large g-forces an impressively robust optical setup measuring the degree of polarisation entanglement of photon pairs. Firstly the change in our experiment is in

---

[2]The fibres used for the nested Sagnac interferometers were mounted directly over the 100 m fibre used for the previous experiment.

the symmetry of the entanglement, not the total amount. Moreover, the work by Fink et al. explores a local effect in a rotating frame - the centrifugal acceleration at one location - whereas our work hinges on a global effect - the Sagnac effect - that occurs when a closed loop is formed. It is the way in which entangled systems experience non-inertial motion that is key. As such, by building on this work with the Sagnac effect, we have also proposed a way by which rotation should actually generate (path-polarisation) entanglement [4], which would be a natural next step for experiment. The Sagnac effect can also be generalised as a probe of underlying spacetime symmetries; a full treatment requires general relativistic terms [203, 202]; which hints at true general relativistic effects on quantum systems. These gravitational effects should in principle induce changes in HOM interference [234, 235]. Extensions to the work could also consider how non-uniform circular acceleration affects entanglement, as non-uniform linear accelerations in theory should alter the degree of entanglement [213, 214, 215]. Further work could also be done to address the limitations of this experiment, the timeline of PhD completion within 4 years[3] meant that there was not time to properly characterise the effect of temperature on the system, and confirm any hypothesis about the variance in the periodicities across different measurement sequences (Section 4.4).

How non-inertial frames and curved spacetimes affect the quantum world are important avenues of research, both for fundamental physics to build a bridge between quantum mechanics and general relativity, but also for quantum technologies. Quantum cryptography protocols and quantum communication methods have been built on a background of flat spacetime, but if the quantum resources they require to work are altered by their reference frame, then this needs to be taken into account [217]. Quantum communications are being scaled up into long-distance and satellite networks, so the rotating frame of the Earth [209] and its curved spacetime is a practical consideration today. The influence of the rotating earth on the quantum mechanical phase of single particles is already recorded [196, 212], and understanding better these effects could even lead to ways to exploit non-inertial frames to enhance quantum technologies further. On the other side of the coin, the fact these quantum technologies are so advanced that these effects are now practical considerations also means these technologies are ready to do fundamental physics tests in these regimes. Both in branching out into space experiments, but also being robust [70] and sensitive enough to do experiments in labs here on the ground.

By testing quantum mechanics in new reference frames we move into uncharted territory. We may expect to see results consistent with current theories of quantum mechanics and relativity, but it can't be guaranteed. Null results could trigger a new revolution in our understanding of physics, as how the Michelson-Morley experiment [10] and subsequent experiments failing to detect the aether ushered in special relativity. Alternatively, turning philosophy and prediction into validated experiment [236] can

---

[3]Combined with equipment failure of the computer running the measurements...

also open up groundbreaking new fields, as realisations of Bell tests [237, 238, 239, 64] showing extra strong correlations did with quantum optics. To do the same with quantum gravity could open up opportunities we could hardly dream of now. We should not fall into the pessimistic trap of assuming that the natural scales of quantum gravity are so extreme that quantum gravity effects can never be tested. Measurement sensitivities are continually improving, enabling new experiments. In 1903 Michelson said that in *"such extreme refinement"*,

> *the greater part of all future discovery must lie. The more important fundamental laws and facts of physical science have all been discovered, and these are now so firmly established that the possibility of their ever being supplanted in consequence of new discoveries is exceedingly remote. [...] our future discoveries must be looked for in the sixth place of decimals. It follows that every means which facilitates accuracy in measurement is a possible factor in a future discovery. ([240])*

While this importance of measurement precision - the *"romance of the next decimal place"* ([241]) - is undeniable, working at the extreme limits of technology is not necessarily required to make progress. The research work on effects in rotating frames presented here is by no means breaking records for sensitivity, quite on the contrary. Indirect tests of quantum gravity may be well within our current capabilities, as long as clever methods are found. Last but not least, the fact Michelson states this just two years before the formulation of special relativity is a reminder that nor should we fall into the biased trap of assuming that because we now know more than ever before (as has been true for almost[4] every point in history), that our current understanding of the universe cannot be overturned and 'supplanted'. Certainly there are enough mysteries left to permit another fundamental physics revolution!

---

[4]The aftermath of the burning of the library of Alexandria perhaps the only exception.

A

Appendix

A1 Two coherent states interfering at a beamsplitter

Coherent states enter beamsplitter ports a and b:

$$
\begin{aligned}
|\Psi_i\rangle &= |\alpha\rangle_a \, |\alpha\rangle_b \, |0\rangle_c \, |0\rangle_d \\
&= e^{\alpha a^\dagger - \alpha^* a} \, |0\rangle_a \, e^{\alpha b^\dagger - \alpha^* b} \, |0\rangle_b \, |0\rangle_c \, |0\rangle_d
\end{aligned}
\tag{A1}
$$

Beamsplitter transformation (symmetric phase: Eq. 3.7):

$$
\begin{aligned}
|\Psi_f\rangle &= e^{\alpha \frac{1}{\sqrt{2}}(c^\dagger + i d^\dagger) - \alpha^* \frac{1}{\sqrt{2}}(c - id)} \, |0\rangle_a \, e^{\alpha \frac{1}{\sqrt{2}}(ic^\dagger + d^\dagger) - \alpha^* \frac{1}{\sqrt{2}}(-ic + d)} \, |0\rangle_b \, |0\rangle_c \, |0\rangle_d \\
&= |0\rangle_a \, |0\rangle_b \, e^{\frac{1}{\sqrt{2}}(\alpha c^\dagger - \alpha^* c + i\alpha d^\dagger + i\alpha^* d + i\alpha c^\dagger + \alpha d^\dagger + i\alpha^* c - \alpha^* d)} \, |0\rangle_c \, |0\rangle_d \\
&= |0\rangle_a \, |0\rangle_b \, e^{\frac{1}{\sqrt{2}}((1+i)\alpha c^\dagger - (1-i)\alpha^* c + (1+i)\alpha d^\dagger - (1-i)\alpha^* d)} \, |0\rangle_c \, |0\rangle_d \\
&= |0\rangle_a \, |0\rangle_b \, e^{\frac{1}{\sqrt{2}}(\sqrt{2}e^{\frac{i\pi}{4}}\alpha c^\dagger - \sqrt{2}e^{\frac{-i\pi}{4}}\alpha^* c)} e^{\frac{1}{\sqrt{2}}(\sqrt{2}e^{\frac{i\pi}{4}}\alpha d^\dagger - \sqrt{2}e^{\frac{-i\pi}{4}}\alpha^* d)} \, |0\rangle_c \, |0\rangle_d \\
&= |0\rangle_a \, |0\rangle_b \, \left| e^{\frac{i\pi}{4}}\alpha \right\rangle_c \left| e^{\frac{i\pi}{4}}\alpha \right\rangle_d
\end{aligned}
\tag{A2}
$$

Or beamsplitter transformation (using asymmetric (Eq. 3.8) instead):

$$
\begin{aligned}
|\Psi_f\rangle &= e^{\alpha \frac{1}{\sqrt{2}}(c^\dagger + d^\dagger) - \alpha^* \frac{1}{\sqrt{2}}(c + d)} \, |0\rangle_a \, e^{\alpha \frac{1}{\sqrt{2}}(c^\dagger - d^\dagger) - \alpha^* \frac{1}{\sqrt{2}}(c - d)} \, |0\rangle_b \, |0\rangle_c \, |0\rangle_d \\
&= |0\rangle_a \, |0\rangle_b \, e^{\frac{1}{\sqrt{2}}(\alpha c^\dagger - \alpha^* c + \alpha c^\dagger - \alpha^* c + \alpha d^\dagger - \alpha^* d - \alpha d^\dagger + \alpha^* d)} \, |0\rangle_c \, |0\rangle_d \\
&= |0\rangle_a \, |0\rangle_b \, e^{\frac{1}{\sqrt{2}}(2\alpha c^\dagger - 2\alpha^* c)} \, |0\rangle_c \, |0\rangle_d \\
&= |0\rangle_a \, |0\rangle_b \, \left| \sqrt{2}\alpha \right\rangle_c \, |0\rangle_d
\end{aligned}
\tag{A3}
$$

A2 Entanglement

Quantum entanglement is a physical phenomenon in which the state of a system of two or more particles cannot be represented as the product of quantum states of the individual components.

$$|\Psi\rangle_{AB} \neq |\psi\rangle_A \otimes |\phi\rangle_B \tag{A4}$$

In other words, the components cannot be described independently, even if they are physically separated. In quantum optics, this is usually a system of photons. Measurements on entangled photons are found to be correlated in any basis used for those properties which are entangled, e.g energy, momentum, polarisation. In performing a measurement on one photon a measurement is performed on the system as a whole, causing the state of the other photon(s) to collapse into a complementary state.

A2.0.1 Bell States

Bell states are four maximally entangled states of two qubits. Qubits are a two-state quantum system - the quantum analogue of a classical binary bit. The Bell states provide the simplest example of quantum entangled states, and together form a maximally entangled basis (the Bell basis) for the 4D Hilbert space for two qubits.

$$\begin{aligned}
\left|\Phi^{\pm}\right\rangle &= \frac{1}{\sqrt{2}}(|0\rangle_A \otimes |0\rangle_B \pm |1\rangle_A \otimes |1\rangle_B) \\
\left|\Psi^{\pm}\right\rangle &= \frac{1}{\sqrt{2}}(|0\rangle_A \otimes |1\rangle_B \pm |1\rangle_A \otimes |0\rangle_B)
\end{aligned} \tag{A5}$$

Note that $|\Phi^+\rangle$ is the **same** state as:

$$\left|\Phi^+\right\rangle = \frac{1}{\sqrt{2}}(|+\rangle_A \otimes |+\rangle_B + |-\rangle_A \otimes |-\rangle_B) \tag{A6}$$

where $|+\rangle = \frac{1}{\sqrt{2}}(|0\rangle + |1\rangle)$ and $|-\rangle = \frac{1}{\sqrt{2}}(|0\rangle - |1\rangle)$.

An example of a qubit is the polarisation of a single photon. For example $|0\rangle = |H\rangle$ (horizontal), $|1\rangle = |V\rangle$ (vertical).

A3   Extended Theoretical Model

{ This section reproduces the detailed theoretical model from the supplementary information file which accompanies the paper in Ref [3]. The paper is reproduced in Section 4.2, and the remaining sections of the supplementary file are reproduced in Section 4.3 }

In this section we present a detailed theoretical analysis of the interferometer. We first define the initial state (Sec. (A3.1)), followed by the general analysis of the interference when we have asymmetry between the arms (Sec. (A3.2)), and finally show that the coincidence probability, in the considered experimental regime, is not affected by the biphoton width (Sec. A3.3).

A3.1   Initial biphoton state

{This subsection with biphoton spread explicitly stated from here until Eq. A11 to was contributed by Marko Toroš.}

For our input state we assume degenerate Type I SPDC pumped by frequency ω_p. We represent a single signal photon in one arm and a single idler photon in the other arm as creation mode operators $a_s^\dagger, a_i^\dagger$ acting on the vacuum $|0\rangle$. The initial state is given by

$$|\psi_\mathrm{i}\rangle = \int d\omega_1 d\omega_2 \psi_\mathrm{i}(\omega_1, \omega_2) a_i^\dagger(\omega_1) a_s^\dagger(\omega_2)|0\rangle, \tag{A7}$$

the biphoton spectrum is

$$\psi_\mathrm{i}(\omega_1, \omega_2) = \frac{1}{\mathcal{N}_\mathrm{i}} e^{-\frac{(\mu-\omega_1)^2}{4\Delta\omega^2}} e^{-\frac{(\mu-\omega_2)^2}{4\Delta\omega^2}} e^{-\frac{(\omega_1+\omega_2-2\mu)^2}{4\sigma_p^2}}, \tag{A8}$$

and the normalization is

$$\mathcal{N}_\mathrm{i} = \sqrt{\frac{2\pi\Delta\omega}{\sqrt{\frac{1}{\Delta\omega^2} + \frac{2}{\sigma_p^2}}}}. \tag{A9}$$

The behaviour of two-photon interference depends on three parameters of the initial state: the mean photon frequency $\mu = \omega_p/2$, the single photon frequency spread $\Delta\omega$, and the biphoton frequency spread σ_p.

We now first discuss in detail the case $\sigma_p \ll \Delta\omega$, providing a full derivation (section A3.2). We will then validate this approximation by considering the more general analysis with a finite σ_p which can be performed using similar steps (section A3.3).

A3.2   Derivation of the number of coincidences

In this section we present a more general and detailed treatment of the interferometer, allowing for asymmetry between the arms. In the experiment, fluctuation in the middle dip - even flipping as well - was sometimes observed, which can only be explained by

this more general model, caused by an imbalance between the birefringent delays in one arm compared to the other, exacerbated and changed by noise.

To obtain a simple expression with a Gaussian spectrum we divide Eq. (A7) by $\sqrt{4\pi\sigma_p}\sqrt[4]{2\sigma^2 + \sigma_p^2}$ to find:

$$|\psi\rangle = \int d\omega_1 d\omega_2 \left[\frac{1}{\sqrt{2\pi(\sqrt{2}\sigma_p)^2}} e^{-\frac{(\omega_1 + \omega_2 - 2\mu)^2}{2(\sqrt{2}\sigma_p)^2}} \right] \left[\frac{1}{\sqrt{2\pi\sigma^2}} e^{-\frac{(\mu-\omega_1)^2}{4\Delta\omega^2}} e^{-\frac{(\mu-\omega_2)^2}{4\Delta\omega^2}} \right] a_i^\dagger(\omega_1) a_s^\dagger(\omega_2)|0\rangle.$$

$$(A10)$$

The term in the first square bracket of Eq. (A10) is a Gaussian which can be approximated with a Dirac delta function $\delta(\omega_1 + \omega_2 - 2\mu)$ in the limit $\sigma_p \to 0$ (see Sec. A3.3 for the general model with a finite σ_p). Performing the integration over ω_2, and relabelling $\omega_1 \to \omega$, we obtain:

$$|\psi\rangle = \int_0^{\omega_p} d\omega B(\omega) a_i^\dagger(\omega) a_s^\dagger(\omega_p - \omega) |0\rangle , \qquad (A11)$$

where the spectrum of the biphoton wavepacket $B(\omega)$ is a gaussian centred at $\mu = \omega_p/2$ and frequency spread $\Delta\omega$ (which depends on the filters used in the experiment). We now follow analogous steps as discussed in Ref [179], applied to the experimental setting presented in the main text.

We include a variable delay δt between the signal and idler photon arms, to represent the scannable HOM delay:

$$|\psi\rangle = \int_0^{\omega_p} d\omega B(\omega) e^{-i\omega\delta t} a_i^\dagger(\omega) a_s^\dagger(\omega_p - \omega) |0\rangle . \qquad (A12)$$

Each arm contains a nested fibre Sagnac interferometer, formed of a beamsplitter with the reflection and transmission ports connected by looped optical fibre. Upon entering the Sagnac interferometer, the mode splits into clockwise (cw) and anticlockwise (ac) directions:

$$a_i^\dagger(\omega) \mapsto \frac{1}{\sqrt{2}} \left(a_{i,cw}^\dagger(\omega) + i a_{i,ac}^\dagger(\omega) \right). \qquad (A13)$$

Afterwards, these modes propagate in opposite directions through the same fibre for a time $t_{cw,ac}$ and so pick up a phase $\phi_{cw}(\omega) = \omega t_{cw}(\Omega, n)$ that changes with rotation speed Ω:

$$a_i^\dagger(\omega) \mapsto \frac{1}{\sqrt{2}} \left(e^{-i\phi_{i,cw}} a_{i,cw}^\dagger(\omega) + e^{-i\phi_{i,ac}} i a_{i,ac}^\dagger(\omega) \right). \qquad (A14)$$

As well as the Sagnac delay created between clockwise and anticlockwise photons travelling in a total fibre length L_f looped in radius r on a platform rotating clockwise at Ω, the fibre paths are constructed such that there is an additional constant birefringent

delay from a mismatch between refractive indices n_{cw} and n_{ac} over a length $L_b \ll L_f$:

$$
\begin{aligned}
t_{cw} &= \frac{L_b n_{cw}}{c} + \frac{L_f r \Omega}{c^2}, \\
t_{ac} &= \frac{L_b n_{ac}}{c} - \frac{L_f r \Omega}{c^2}.
\end{aligned}
\tag{A15}
$$

Here we continue with a more experimentally-realistic generality that any or all of L_f, L_b and r could be slightly different for signal and idler, and thus in general $t_{i,cw} \neq t_{s,cw}$ etc.

The clockwise and anticlockwise paths interfere as they pass the beamsplitter again:

$$
\begin{aligned}
a_{i,cw}^\dagger(\omega) &\mapsto \frac{1}{\sqrt{2}} \left(a_{i,out}^\dagger(\omega) + i a_{i,back}^\dagger(\omega) \right), \\
a_{i,ac}^\dagger(\omega) &\mapsto \frac{1}{\sqrt{2}} \left(i a_{i,out}^\dagger(\omega) + a_{i,back}^\dagger(\omega) \right).
\end{aligned}
\tag{A16}
$$

Combining Eqs. (A14) and (A16) gives:

$$
a_i^\dagger(\omega) \mapsto \frac{1}{2} \left(e^{-i\phi_{i,cw}(\omega)} - e^{-i\phi_{i,ac}(\omega)} \right) a_{i,out}^\dagger(\omega) + \frac{i}{2} \left(e^{-i\phi_{i,cw}(\omega)} + e^{-i\phi_{i,ac}(\omega)} \right) a_{i,back}^\dagger(\omega),
\tag{A17}
$$

and similarly for the signal mode we find:

$$
\begin{aligned}
a_s^\dagger(\omega_p - \omega) \mapsto \frac{1}{2} &\left(e^{-i\phi_{s,cw}(\omega_p-\omega)} - e^{-i\phi_{s,ac}(\omega_p-\omega)} \right) a_{s,out}^\dagger(\omega_p - \omega) \\
&+ \frac{i}{2} \left(e^{-i\phi_{s,cw}(\omega_p-\omega)} + e^{-i\phi_{s,ac}(\omega_p-\omega)} \right) a_{s,back}^\dagger(\omega_p - \omega).
\end{aligned}
\tag{A18}
$$

We only consider light that exits the Sagnac towards the HOM beamsplitter $(a_{i,out}, a_{s,out})$:

$$
\begin{aligned}
|\psi_{\text{Sagnacs}}\rangle = \frac{1}{4} \int_0^{\omega_p} d\omega\, B(\omega) e^{-i\omega\delta t} &\left(e^{-i\phi_{i,cw}(\omega)} - e^{-i\phi_{i,ac}(\omega)} \right) a_{i,out}^\dagger(\omega) \\
&\left(e^{-i\phi_{s,cw}(\omega_p-\omega)} - e^{-i\phi_{s,ac}(\omega_p-\omega)} \right) a_{s,out}^\dagger(\omega_p - \omega) |0\rangle.
\end{aligned}
\tag{A19}
$$

At the HOM beamsplitter there is the last mode transformation (input $(a_{i,out}, a_{s,out})$, output (a, b)):

$$
a_{i,out}^\dagger \mapsto \frac{1}{\sqrt{2}} \left(i a^\dagger + b^\dagger \right) \qquad\qquad a_{s,out}^\dagger \mapsto \frac{1}{\sqrt{2}} \left(a^\dagger + i b^\dagger \right).
\tag{A20}
$$

Then from Eqs. (A19) and (A20) we finally find:

$$
\begin{aligned}
|\psi_{\text{final}}\rangle = \frac{1}{8} \int_0^{\omega_p} d\omega\, B(\omega) e^{-i\omega\delta t} &\left(e^{-i\phi_{i,cw}(\omega)} - e^{-i\phi_{i,ac}(\omega)} \right) \left(e^{-i\phi_{s,cw}(\omega_p-\omega)} - e^{-i\phi_{s,ac}(\omega_p-\omega)} \right) \\
&\left(i a^\dagger(\omega) + b^\dagger(\omega) \right) \left(a^\dagger(\omega_p - \omega) + i b^\dagger(\omega_p - \omega) \right) |0\rangle.
\end{aligned}
\tag{A21}
$$

For the state of the electromagnetic field exiting the beamsplitter, we want to find

the expected number of coincidences N_c. A coincidence detection is detecting one photon at one detector, and another photon at the other detector within a small, finite coincidence window τ_f. Specifically, we define the coincidence probability as the probability of detecting a photon in detector a at time t and a photon in detector b at time $t + \tau$ is given by $P(\tau)$.

$$N_c = \int_{-\tau_f}^{\tau_f} d\tau P(\tau), \tag{A22}$$

$$P(\tau) = \langle \psi_{\text{final}} | E_a^-(t) E_b^-(t+\tau) E_b^+(t+\tau) E_a^+(t) | \psi_{\text{final}} \rangle, \tag{A23}$$

$$E_a^+(t) = \int d\omega e^{-i\omega t} a(\omega), \qquad E_b^+(t) = \int d\omega e^{-i\omega t} b(\omega). \tag{A24}$$

Let us now evaluate Eq. (A23). We first calculate $E_b^+(t+\tau) E_a^+(t) | \psi_{\text{final}} \rangle$:

$$E_b^+(t+\tau) E_a^+(t) | \psi_{\text{final}} \rangle = \frac{1}{8} \int d\omega_2 \int d\omega_1 \int_0^{\omega_p} d\omega e^{-i\omega_2(t+\tau)} b(\omega_2) e^{-i\omega_1 t} a(\omega_1) e^{-i\omega \delta t} B(\omega)$$
$$\left(e^{-i\phi_{i,cw}(\omega)} - e^{-i\phi_{i,ac}(\omega)} \right) \left(e^{-i\phi_{s,cw}(\omega_p - \omega)} - e^{-i\phi_{s,ac}(\omega_p - \omega)} \right)$$
$$\left(i a^\dagger(\omega) a^\dagger(\omega_p - \omega) - a^\dagger(\omega) b^\dagger(\omega_p - \omega) + b^\dagger(\omega) a^\dagger(\omega_p - \omega) + i b^\dagger(\omega) b^\dagger(\omega_p - \omega) \right) | 0 \rangle. \tag{A25}$$

The $a^\dagger(\omega) a^\dagger(\omega_p - \omega)$ and $b^\dagger(\omega) b^\dagger(\omega_p - \omega)$ terms are bunching terms (not coincidences) and give a contribution of zero. The only non-zero contributions to the coincidence count comes from the $a^\dagger(\omega) b^\dagger(\omega_p - \omega)$ and $b^\dagger(\omega) a^\dagger(\omega_p - \omega)$ terms when $\omega_1 = \omega, \omega_2 = \omega_p - \omega$ or when $\omega_1 = \omega_p - \omega, \omega_2 = \omega$. Eq. (A25) thus simplifies to:

$$E_b^+(t+\tau) E_a^+(t) | \psi_{\text{final}} \rangle =$$
$$\frac{1}{8} \int_0^{\omega_p} d\omega e^{-i\omega \delta t} B(\omega) \left(e^{-i\phi_{i,cw}(\omega)} - e^{-i\phi_{i,ac}(\omega)} \right) \left(e^{-i\phi_{s,cw}(\omega_p - \omega)} - e^{-i\phi_{s,ac}(\omega_p - \omega)} \right)$$
$$\left(e^{-i\omega(t+\tau)} e^{-i(\omega_p - \omega)t} - e^{-i(\omega_p - \omega)(t+\tau)} e^{-i\omega t} \right) (1 + \delta(\omega_p - 2\omega)) | 0 \rangle. \tag{A26}$$

The $\delta(\omega_p - 2\omega)$ term in Eq. (A26) evaluates to zero:

$$\frac{1}{8} \int_0^{\omega_p} d\omega e^{-i\omega \delta t} B(\omega) \left(e^{-i\phi_{i,cw}(\omega)} - e^{-i\phi_{i,ac}(\omega)} \right) \left(e^{-i\phi_{s,cw}(\omega_p - \omega)} - e^{-i\phi_{s,ac}(\omega_p - \omega)} \right)$$
$$\left(e^{-i(\omega_p - \omega)(t+\tau)} e^{-i\omega t} - e^{-i\omega(t+\tau)} e^{-i(\omega_p - \omega)t} \right) \delta(\omega_p - 2\omega) | 0 \rangle$$
$$= \frac{1}{8} e^{-i\frac{\omega_p}{2} \delta t} B(\frac{\omega_p}{2}) \left(e^{-i\phi_{i,cw}(\frac{\omega_p}{2})} - e^{-i\phi_{i,ac}(\frac{\omega_p}{2})} \right) \left(e^{-i\phi_{s,cw}(\frac{\omega_p}{2})} - e^{-i\phi_{s,ac}(\frac{\omega_p}{2})} \right)$$
$$\left(e^{-i(\frac{\omega_p}{2})(t+\tau)} e^{-i\frac{\omega_p}{2} t} - e^{-i\frac{\omega_p}{2}(t+\tau)} e^{-i(\frac{\omega_p}{2})t} \right) | 0 \rangle = 0. \tag{A27}$$

The global phase $(e^{-i\omega_p t})$ in the remaining term of Eq. (A26) can be factored out,

resulting in:

$$
E_b^+(t+\tau)E_a^+(t)\,|\psi_{final}\rangle = \frac{1}{8}e^{-i\omega_p t}\int_0^{\omega_p}d\omega\, e^{-i\omega\delta t}B(\omega)\left(e^{-i\phi_{i,cw}(\omega)}-e^{-i\phi_{i,ac}(\omega)}\right)
$$

$$
\left(e^{-i\phi_{s,cw}(\omega_p-\omega)}-e^{-i\phi_{s,ac}(\omega_p-\omega)}\right)\left(e^{-i\omega(t+\tau)}e^{+i\omega t}-e^{-i\omega_p\tau}e^{+i\omega(t+\tau)}e^{-i\omega t}\right)|0\rangle
$$

$$
=\frac{1}{8}e^{-i\omega_p t}\int_0^{\omega_p}d\omega\, e^{-i\omega\delta t}B(\omega)\left(e^{-i\phi_{i,cw}(\omega)}-e^{-i\phi_{i,ac}(\omega)}\right)
$$

$$
\left(e^{-i\phi_{s,cw}(\omega_p-\omega)}-e^{-i\phi_{s,ac}(\omega_p-\omega)}\right)\left(e^{-i\omega\tau}-e^{-i\omega_p\tau}e^{+i\omega\tau}\right)|0\rangle. \quad \text{(A28)}
$$

We do a change of variables $\omega \mapsto (\omega+\omega_p/2)$; $\omega = \omega - \omega_p/2$, and factor out global phases that won't contribute to the final probability. From Eq. (A28) we thus find:

$$
E_b^+(t+\tau)E_a^+(t)\,|\psi_{final}\rangle = \frac{1}{8}e^{-i\omega_p t}e^{-i\frac{\omega_p}{2}\delta t}e^{-i\frac{\omega_p}{2}\tau}\int_{-\omega_p/2}^{\omega_p/2}d\omega\, e^{-i\omega\delta t}B(\omega+\omega_p/2)
$$

$$
\left(e^{-i\phi_{i,cw}(\omega+\omega_p/2)}-e^{-i\phi_{i,ac}(\omega+\omega_p/2)}\right)
$$

$$
\left(e^{-i\phi_{s,cw}(\omega_p/2-\omega)}-e^{-i\phi_{s,ac}(\omega_p/2-\omega)}\right)\left(e^{-i\omega\tau}-e^{+i\omega\tau}\right)|0\rangle. \quad \text{(A29)}
$$

Multiplying Eq. (A29) by the conjugate transpose to get $P(\tau)$ we thus find:

$$
P(\tau) = \frac{1}{16}\int_{-\omega_p/2}^{\omega_p/2}d\omega\int_{-\omega_p/2}^{\omega_p/2}d\omega'\, e^{+i\omega'\delta t}e^{-i\omega\delta t}B^*(\omega'+\omega_p/2)B(\omega+\omega_p/2)
$$

$$
\left(e^{+i\omega'\tau}-e^{-i\omega'\tau}\right)\left(e^{-i\omega\tau}-e^{+i\omega\tau}\right)
$$

$$
\left(e^{+i\phi_{i,cw}(\omega'+\omega_p/2)}-e^{+i\phi_{i,ac}(\omega'+\omega_p/2)}\right)\left(e^{-i\phi_{i,cw}(\omega+\omega_p/2)}-e^{-i\phi_{i,ac}(\omega+\omega_p/2)}\right)
$$

$$
\left(e^{+i\phi_{s,cw}(\omega_p/2-\omega')}-e^{+i\phi_{s,ac}(\omega_p/2-\omega')}\right)\left(e^{-i\phi_{s,cw}(\omega_p/2-\omega)}-e^{-i\phi_{s,ac}(\omega_p/2-\omega)}\right). \quad \text{(A30)}
$$

We now insert Eq. (A30) into Eq. (A22) to obtain the number of coincidences. The integration over τ can be simplified by assuming τ is the longest timescale in the system, so that the limits can be taken to infinity and we can use $\int_{-\infty}^{\infty}d\tau e^{i(\omega_1+\omega_2)\tau} = 2\pi\delta(\omega_1+\omega_2)$. Hence the time integration can be carried out analytically and we find:

$$
\int_{-\infty}^{\infty}d\tau\left(e^{+i\omega'\tau}-e^{-i\omega'\tau}\right)\left(e^{-i\omega\tau}-e^{+i\omega\tau}\right) = 4\pi(\delta(\omega'-\omega)-\delta(\omega'+\omega)). \quad \text{(A31)}
$$

The expression for the number of coincidences thus reduces to:

$$N_c = \frac{4\pi}{16} \int_{-\omega_p/2}^{\omega_p/2} d\omega \bigg[e^{+i\omega\delta t} e^{-i\omega\delta t} B^*(\omega + \omega_p/2) B(\omega + \omega_p/2)$$

$$\left(e^{+i\phi_{i,cw}(\omega+\omega_p/2)} - e^{+i\phi_{i,ac}(\omega+\omega_p/2)} \right) \left(e^{-i\phi_{i,cw}(\omega+\omega_p/2)} - e^{-i\phi_{i,ac}(\omega+\omega_p/2)} \right)$$

$$\left(e^{+i\phi_{s,cw}(\omega_p/2-\omega)} - e^{+i\phi_{s,ac}(\omega_p/2-\omega)} \right) \left(e^{-i\phi_{s,cw}(\omega_p/2-\omega)} - e^{-i\phi_{s,ac}(\omega_p/2-\omega)} \right)$$

$$- e^{-i2\omega\delta t} B^*(-\omega + \omega_p/2) B(\omega + \omega_p/2)$$

$$\left(e^{+i\phi_{i,cw}(-\omega+\omega_p/2)} - e^{+i\phi_{i,ac}(-\omega+\omega_p/2)} \right) \left(e^{-i\phi_{i,cw}(\omega+\omega_p/2)} - e^{-i\phi_{i,ac}(\omega+\omega_p/2)} \right)$$

$$\left(e^{+i\phi_{s,cw}(\omega_p/2+\omega)} - e^{+i\phi_{s,ac}(\omega_p/2+\omega)} \right) \left(e^{-i\phi_{s,cw}(\omega_p/2-\omega)} - e^{-i\phi_{s,ac}(\omega_p/2-\omega)} \right) \bigg]. \quad (A32)$$

Assuming symmetry of B around $\omega_p/2$ we see the emergence of two parts, one that does not depend on the HOM delay δt (the coincidence background), and one that does, that gives rise to dips (or peaks) at specific delays:

$$N_c = \frac{4\pi}{16} \int_{-\omega_p/2}^{\omega_p/2} d\omega |B(\omega + \omega_p/2)|^2 \bigg[\left(e^{+i\phi_{i,cw}(\omega+\omega_p/2)} - e^{+i\phi_{i,ac}(\omega+\omega_p/2)} \right)$$

$$\left(e^{-i\phi_{i,cw}(\omega+\omega_p/2)} - e^{-i\phi_{i,ac}(\omega+\omega_p/2)} \right)$$

$$\left(e^{+i\phi_{s,cw}(\omega_p/2-\omega)} - e^{+i\phi_{s,ac}(\omega_p/2-\omega)} \right) \left(e^{-i\phi_{s,cw}(\omega_p/2-\omega)} - e^{-i\phi_{s,ac}(\omega_p/2-\omega)} \right)$$

$$- e^{-i2\omega\delta t} \left(e^{+i\phi_{i,cw}(-\omega+\omega_p/2)} - e^{+i\phi_{i,ac}(-\omega+\omega_p/2)} \right) \left(e^{-i\phi_{i,cw}(\omega+\omega_p/2)} - e^{-i\phi_{i,ac}(\omega+\omega_p/2)} \right)$$

$$\left(e^{+i\phi_{s,cw}(\omega_p/2+\omega)} - e^{+i\phi_{s,ac}(\omega_p/2+\omega)} \right) \left(e^{-i\phi_{s,cw}(\omega_p/2-\omega)} - e^{-i\phi_{s,ac}(\omega_p/2-\omega)} \right) \bigg]. \quad (A33)$$

From Eq. (A33) using the linearity of the phase shifts $\phi_{cw}(\omega) = \omega t_{cw}(\Omega, n), \phi_{ac}(\omega) = \omega t_{ac}(\Omega, n)$, we find:

$$N_c = \frac{4\pi}{16} \int_{-\omega_p/2}^{\omega_p/2} d\omega |B(\omega + \omega_p/2)|^2 \bigg[\left(2 - 2\cos\left((\omega + \omega_p/2)(t_{i,cw} - t_{i,ac})\right)\right)$$

$$\left(2 - 2\cos\left((\omega_p/2 - \omega)(t_{s,cw} - t_{s,ac})\right)\right)$$

$$- e^{-i2\omega\delta t} \left(e^{-i2\omega t_{i,cw}} + e^{-i2\omega t_{i,ac}} - 2\cos\left(\frac{\omega_p}{2}(t_{i,cw} - t_{i,ac})\right) e^{-i\omega(t_{i,cw}+t_{i,ac})} \right)$$

$$\left(e^{+i2\omega t_{s,cw}} + e^{+i2\omega t_{s,ac}} - 2\cos\left(\frac{\omega_p}{2}(t_{s,cw} - t_{s,ac})\right) e^{+i\omega(t_{s,cw}+t_{s,ac})} \right) \bigg]. \quad (A34)$$

We now insert the Gaussian for $B(\omega + \omega_p/2)$, and in addition assuming the Gaussian spread $\delta\omega << \frac{\omega_p}{2}$ we can extend the integration limits to infinity. Eq. (A34) simplifies

to:

$$N_c = \frac{4\pi}{16} \int_{-\infty}^{\infty} d\omega \frac{1}{2\pi(\Delta\omega)^2} e^{-\frac{\omega^2}{(\Delta\omega)^2}} \Big[4\left(1 - \cos\left((\omega + \omega_p/2)(t_{i,cw} - t_{i,ac})\right)\right)$$

$$\left(1 - \cos\left((\omega_p/2 - \omega)(t_{s,cw} - t_{s,ac})\right)\right)$$

$$- e^{-i2\omega\delta t}\left(e^{-i2\omega t_{i,cw}} + e^{-i2\omega t_{i,ac}} - 2\cos\left(\tfrac{\omega_p}{2}(t_{i,cw} - t_{i,ac})\right)e^{-i\omega(t_{i,cw}+t_{i,ac})}\right)$$

$$\left(e^{+i2\omega t_{s,cw}} + e^{+i2\omega t_{s,ac}} - 2\cos\left(\tfrac{\omega_p}{2}(t_{s,cw} - t_{s,ac})\right)e^{+i\omega(t_{s,cw}+t_{s,ac})}\right)\Big]. \quad \text{(A35)}$$

We can evaluate the integral in Eq. (A35) using

$$\int_{-\infty}^{\infty} d\omega\, e^{-a\omega^2 + b\omega + c} = \sqrt{\frac{\pi}{a}} e^{\frac{b^2}{4a}+c}, \tag{A36}$$

$$\int_{-\infty}^{\infty} d\omega\, e^{-a\omega^2 + ik\omega} = \sqrt{\frac{\pi}{a}} e^{-\frac{k^2}{4a}} \tag{A37}$$

$$\text{and } \int_{-\infty}^{\infty} d\omega \cos(a\omega) = Re\left[\int_{-\infty}^{\infty} d\omega\, e^{ia\omega}\right]. \tag{A38}$$

Using Eqs. ((A36) - (A38)) in Eq. (A35) we find an analytic expression for the coincidences N_c:

$$N_c = \frac{\sqrt{\pi}}{8(\Delta\omega)} \Bigg[\left(4 - 4e^{-\frac{\Delta\omega^2}{4}(t_{iac}-t_{icw})^2} \cos\left(\frac{\omega_p}{2}(t_{iac} - t_{icw})\right)\right.$$

$$- 4e^{-\frac{\Delta\omega^2}{4}(t_{sac}-t_{scw})^2} \cos\left(\frac{\omega_p}{2}(t_{sac} - t_{scw})\right)$$

$$+ 2e^{-\frac{\Delta\omega^2}{4}(t_{iac}-t_{icw}-t_{sac}+t_{scw})^2} \cos\left(\frac{\omega_p}{2}(t_{iac} - t_{icw} + t_{sac} - t_{scw})\right)$$

$$\left.+ 2e^{-\frac{\Delta\omega^2}{4}(t_{iac}-t_{icw}+t_{sac}-t_{scw})^2} \cos\left(\frac{\omega_p}{2}(t_{iac} - t_{icw} - t_{sac} + t_{scw})\right)\right)$$

$$+ \left(-e^{-\Delta\omega^2(\delta t+t_{icw}-t_{scw})^2} - e^{-\Delta\omega^2(\delta t+t_{icw}-t_{sac})^2} - e^{-\Delta\omega^2(\delta t+t_{iac}-t_{scw})^2} - e^{-\Delta\omega^2(\delta t+t_{iac}-t_{sac})^2}\right.$$

$$+ 2\cos\left(\tfrac{\omega_p}{2}(t_{scw} - t_{sac})\right)\left(e^{-\frac{\Delta\omega^2}{4}(2\delta t+2t_{icw}-t_{scw}-t_{sac})^2} + e^{-\frac{\Delta\omega^2}{4}(2\delta t+2t_{iac}-t_{scw}-t_{sac})^2}\right)$$

$$+ 2\cos\left(\tfrac{\omega_p}{2}(t_{icw} - t_{iac})\right)\left(e^{-\frac{\Delta\omega^2}{4}(2\delta t-2t_{scw}+t_{icw}+t_{iac})^2} + e^{-\frac{\Delta\omega^2}{4}(2\delta t-2t_{sac}+t_{icw}+t_{iac})^2}\right)$$

$$\left.- 4\cos\left(\tfrac{\omega_p}{2}(t_{scw} - t_{sac})\right)\cos\left(\tfrac{\omega_p}{2}(t_{icw} - t_{iac})\right)e^{-\frac{\Delta\omega^2}{4}(2\delta t+t_{icw}+t_{iac}-t_{scw}-t_{sac})^2}\right)\Bigg]. \quad \text{(A39)}$$

In an ideal experiment, to simplify the effect, the differences between corresponding signal and idler paths should be zero, i.e. $t_{sac} = t_{iac} = t_{ac}$ and $t_{scw} = t_{icw} = t_{cw}$. Which

further simplifies Eq. (A39) to:

$$N_c = \frac{\sqrt{\pi}}{8(\Delta\omega)} \left[\left(4 - 8e^{-\frac{\Delta\omega^2}{4}(t_{ac}-t_{cw})^2} \cos\left(\frac{\omega_p}{2}(t_{ac}-t_{cw})\right) \right. \right.$$
$$\left. + 2\cos\left(\omega_p(t_{ac}-t_{cw})\right) + 2e^{-\Delta\omega^2(t_{ac}-t_{cw})^2} \right)$$
$$+ \left(-2e^{-\Delta\omega^2\delta t^2} - e^{-\Delta\omega^2(\delta t+t_{cw}-t_{ac})^2} - e^{-\Delta\omega^2(\delta t+t_{ac}-t_{cw})^2} \right.$$
$$+ 4\cos\left(\frac{\omega_p}{2}(t_{ac}-t_{cw})\right) \left(e^{-\Delta\omega^2(\delta t-\frac{t_{ac}-t_{cw}}{2})^2} + e^{-\Delta\omega^2(\delta t+\frac{t_{ac}-t_{cw}}{2})^2} \right)$$
$$\left. \left. - 4\cos^2\left(\frac{\omega_p}{2}(t_{ac}-t_{cw})\right)e^{-\Delta\omega^2\delta t^2} \right) \right]. \quad (A40)$$

To reach the form in the main paper, we can designate the background coincidence level C_b:

$$C_b = 4 - 8e^{-\frac{\Delta\omega^2}{4}\Delta t^2} \cos\left(\frac{\omega_p}{2}\Delta t\right) + 2\cos\left(\omega_p\Delta t\right) + 2e^{-\Delta\omega^2\Delta t^2}, \quad (A41)$$

where we have defined $\Delta t = t_{cw} - t_{ac}$. In addition we re-write the middle dip terms to isolate the oscillatory part:

$$4\cos^2\left(\frac{\omega_p}{2}\Delta t\right)e^{-\Delta\omega^2\delta t^2} = 2\cos(\omega_p\Delta t)e^{-\Delta\omega^2\delta t^2} + 2e^{-\Delta\omega^2\delta t^2}. \quad (A42)$$

From Eq. (A3.2) we then find:

$$N_c = \frac{\sqrt{\pi}}{8\Delta\omega} \left[C_b - e^{-\Delta\omega^2(\delta t+\Delta t)^2} - e^{-\Delta\omega^2(\delta t-\Delta t)^2} \right.$$
$$\left. + 4\cos\left(\frac{\omega_p}{2}\Delta t\right) \left(e^{-\Delta\omega^2(\delta t+\frac{\Delta t}{2})^2} + e^{-\Delta\omega^2(\delta t-\frac{\Delta t}{2})^2} \right) - 4e^{-\Delta\omega^2\delta t^2} - 2\cos(\omega_p\Delta t)e^{-\Delta\omega^2\delta t^2} \right],$$
$$(A43)$$

which matches Eq. (6) in the main text. The coincidence landscape plotted from the simulation, where the arms are symmetric (Eq. (A43)), is shown in Figure A1.

A3.3   Effect of biphoton frequency spread

{This subsection with biphoton spread explicitly considered was contributed by Marko Toroš.}

In this section we discuss the general case with a finite biphoton spread σ_p. The analysis is analogous to the one discussed in detail in Sec. A3.2 but due to the significantly longer expressions we report only the final results.

The final state (i.e., the state at the input of the final beamsplitter) is given by

$$|\psi_f\rangle = \int d\omega_1 d\omega_2 \psi_f(\omega_1, \omega_2)\hat{a}^\dagger(\omega_1)\hat{b}^\dagger(\omega_2)|0\rangle, \quad (A44)$$
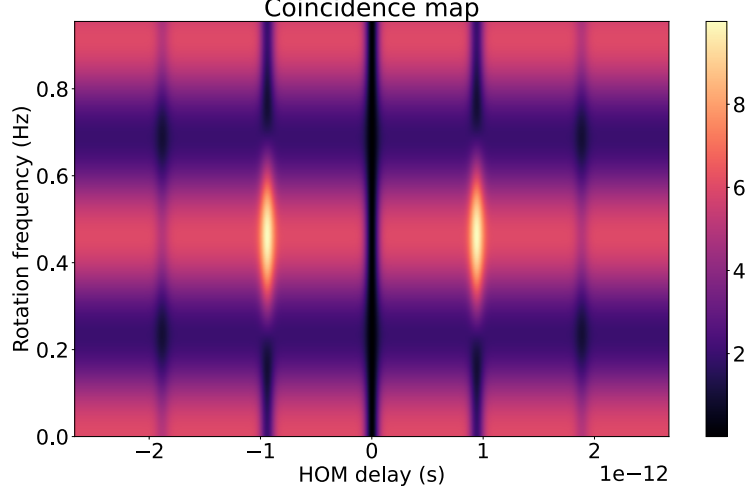
Figure A1: Simulation results. Plots Equation (A43) using $\lambda_p = 355$nm, $L_f = 41$m, $r = 0.454$m, $L_b = 1$m, $\Delta\omega = 1.19 \times 10^{13}$, $n_{cw} - n_{ac} = 5.641 \times 10^{-4}$. Shows how coincidences are expected to change with rotation and delay. The changing dips go from maximum visibility dips (with respect to the background) to maximum visibility peaks with a 0.455 Hz rotation change. The background also changes with rotation.

where the biphoton spectrum is

$$\psi_{\mathrm{f}}(\omega_1, \omega_2) = \frac{1}{\mathcal{N}_{\mathrm{f}}} e^{-\frac{(\mu-\omega_1)^2}{4\Delta\omega^2}} e^{-\frac{(\mu-\omega_2)^2}{4\Delta\omega^2}} e^{-\frac{(\omega_1+\omega_2-2\mu)^2}{4\sigma_p^2}} \sin^2\left(\frac{\omega_1\Delta t}{2}\right) \sin^2\left(\frac{\omega_2\Delta t}{2}\right), \quad \text{(A45)}$$

and the normalization is given by

$$\mathcal{N}_{\mathrm{f}} = \frac{\pi\Delta\omega^2\sigma_p e^{-\Delta\omega^2\Delta t^2}}{\sqrt{2\Delta\omega^2 + \sigma_p^2}} \left(1 - 4\cos(\mu\Delta t)\exp\left(\frac{\Delta\omega^2\left(3\Delta\omega^2 + \sigma_p^2\right)\Delta t^2}{2\left(2\Delta\omega^2 + \sigma_p^2\right)}\right)\right.$$
$$\left. + \cos(2\mu\Delta t)e^{\frac{2\Delta\omega^4\Delta t^2}{2\Delta\omega^2+\sigma_p^2}} + 2e^{\Delta\omega^2\Delta t^2}\right). \quad \text{(A46)}$$

In the first part of Eq. (A45) we recognize the initial state defined in Eq. (A7), while the last two factors contain the interference contribution due to the imbalanced paths.

The probability of preparing the final state in Eq. (A44) is given by:

$$P_{\mathrm{f}} = \frac{1}{8}\left[2 - 4\cos(\mu\Delta t)\exp\left(\frac{\Delta\omega^2\left(3\Delta\omega^2 + \sigma_p^2\right)\Delta t^2}{2\left(2\Delta\omega^2 + \sigma_p^2\right)} - \sigma^2\Delta t^2\right)\right.$$
$$\left. + \cos(2\mu\Delta t)\exp\left(\frac{2\Delta\omega^4\Delta t^2}{2\Delta\omega^2 + \sigma_p^2} - \Delta\omega^2\Delta t^2\right) + e^{-\Delta\omega^2\Delta t^2}\right], \quad \text{(A47)}$$

as only the input modes of the final beamsplitter contribute to the final coincidence probability (for more details see the derivation leading up to Eq. (A19)).

The coincidence probability can be computed using the formula [174]:

$$P_{\mathrm{c}} = \frac{1}{2} - \frac{1}{2}\int\int \psi_{\mathrm{f}}^*(\omega_1, \omega_2)\psi_{\mathrm{f}}(\omega_2, \omega_1)d\omega_1 d\omega_2. \quad \text{(A48)}$$

Inserting Eqs. (A45) in (A48) and performing the integrations we find:

$$P_c(\delta t, \Delta t, \mu, \Delta\omega, \sigma_p) = \frac{1}{2}\left(1 - \frac{I_1 + I_2 + I_3 + I_4}{S}\right), \tag{A49}$$

where the interference is quantified by

$$I_1 = 4e^{-\Delta\omega^2(\delta t + \Delta t)(\delta t - \Delta t)} + e^{-\delta t \Delta\omega^2(\delta t + 2\Delta t)} + e^{-\delta t \Delta\omega^2(\delta t - 2\Delta t)}, \tag{A50}$$

$$I_2 = -4\cos(\mu\Delta t)\exp\left(\frac{\Delta\omega^2\sigma_p^2\left(-2\delta t^2 - 2\delta t\Delta t + \Delta t^2\right) + \Delta\omega^4(-2\delta t - 3\Delta t)(2\delta t - \Delta t)}{2\left(2\Delta\omega^2 + \sigma_p^2\right)}\right), \tag{A51}$$

$$I_3 = -4\cos(\mu\Delta t)\exp\left(\frac{\Delta\omega^2\sigma_p^2\left(-2\delta t^2 + \Delta t(\Delta t + 2\delta t)\right) + \Delta\omega^4(-2\delta t - \Delta t)(2\delta t - 3\Delta t)}{2\left(2\Delta\omega^2 + \sigma_p^2\right)}\right), \tag{A52}$$

$$I_4 = 2\cos(2\mu\Delta t)\exp\left(\frac{2\Delta\omega^4\Delta t^2}{2\Delta\omega^2 + \sigma_p^2} - \delta t^2\Delta\omega^2\right), \tag{A53}$$

and

$$S = 2 - 8\cos(\mu\Delta t)\exp\left(\frac{\Delta\omega^2\left(3\Delta\omega^2 + \sigma_p^2\right)\Delta t^2}{2\left(2\Delta\omega^2 + \sigma_p^2\right)}\right) + 2\cos(2\mu\Delta t)e^{\frac{2\Delta\omega^4\Delta t^2}{2\Delta\omega^2 + \sigma_p^2}} + 4e^{\Delta\omega^2\Delta t^2}. \tag{A54}$$

The number of counts (with unit incoming photon rate) is thus given by:

$$N_c = P_f P_c, \tag{A55}$$

where P_f and P_c are given in Eqs. (A47) and (A49), respectively. We recover Eq. (A43) from Eq. (A55) by multiplying it with the normalization factor $4\sqrt{\pi}/\Delta\omega$ and taking the limit $\sigma_p \to 0$.

We find that when $\sigma_p/2\pi \leq 2 \times 10^{10}$ Hz, which is the experimental parameter, the model predicts that the coincidence count N_c is not significantly different from the one found for the case $\sigma_p \to 0$. On the other hand, by increasing the value of σ_p to values close to the single-photon frequency spread $\Delta\omega$, the model predicts a loss of visibility of the two invertible HOM dips, which arise due the entangled nature of the biphoton state, as the degree of entanglement starts to decrease, as well as we start to move out of the biphoton coherence time.

Bibliography

[1]   Marko Toroš et al. *"Revealing and Concealing Entanglement with Noninertial Motion"*. In: *Physical Review A* 101.4 (Apr. 2020), p. 043837. DOI: 10.1103/PhysRevA.101. 043837 (cit. on pp. x, 42, 60, 61, 72, 74, 79, 82, 83, 99, 107).

[2]   Marion Cromb et al. *"Amplification of Waves from a Rotating Body"*. In: *Nature Physics* (June 2020). DOI: 10.1038/s41567-020-0944-3. URL: https://www.nature.com/articles/ s41567-020-0944-3 (visited on 22/06/2020) (cit. on pp. x, xi, 16, 18, 25, 83, 106).

[3]   Marion Cromb et al. *Controlling Photon Entanglement with Mechanical Rotation*. Oct. 2022. DOI: 10.48550/arXiv.2210.05628. arXiv: 2210.05628 [physics, physics:quant-ph]. URL: http://arxiv.org/abs/2210.05628 (visited on 12/10/2022) (cit. on pp. x, xi, 16, 82, 112).

[4]   Marko Toroš et al. *"Generation of Entanglement from Mechanical Rotation"*. In: *Physical Review Letters* 129.26 (Dec. 2022), p. 260401. DOI: 10.1103/PhysRevLett.129. 260401. URL: https://link.aps.org/doi/10.1103/PhysRevLett.129.260401 (visited on 21/12/2022) (cit. on pp. x, 91, 96, 101–103, 108).

[5]   Gennady E. Gorelik and Victor Ya. Frenkel. *Matvei Petrovich Bronstein and Soviet Theoretical Physics in the Thirties*. Basel: Birkhäuser, 1994. DOI: 10.1007/978-3-0348-8488-4. URL: http://link.springer.com/10.1007/978-3-0348-8488-4 (visited on 17/08/2022) (cit. on pp. 1, 7).

[6]   A. Einstein. *"Über Einen Die Erzeugung Und Verwandlung Des Lichtes Betreffenden Heuristischen Gesichtspunkt"*. In: *Annalen der Physik* 322.6 (1905), pp. 132–148. DOI: 10.1002/andp.19053220607. URL: https://onlinelibrary.wiley.com/doi/abs/10.1002/ andp.19053220607 (visited on 21/09/2022) (cit. on p. 2).

[7]   Alain Aspect, Jean Dalibard and Gérard Roger. *"Experimental Test of Bell's Inequalities Using Time-Varying Analyzers"*. In: *Physical Review Letters* 49.25 (Dec. 1982), pp. 1804–1807. DOI: 10.1103/PhysRevLett.49.1804. URL: https://link.aps.org/doi/10. 1103/PhysRevLett.49.1804 (visited on 11/10/2022) (cit. on p. 3).

[8]   Gregor Weihs et al. *"Violation of Bell's Inequality under Strict Einstein Locality Conditions"*. In: *Physical Review Letters* 81.23 (Dec. 1998), pp. 5039–5043. DOI: 10.1103/ PhysRevLett.81.5039. URL: https://link.aps.org/doi/10.1103/PhysRevLett.81.5039 (visited on 11/10/2022) (cit. on p. 3).

[9]   Galileo Galilei. *Dialogue Concerning the Two Chief World Systems-Ptolemaic & Copernican*. Trans. by Stillman Drake. University of California Press, 1967 (cit. on p. 3).

[10]   A. A. Michelson and E. W. Morley. *"On the Relative Motion of the Earth and the Luminiferous Ether"*. In: *American Journal of Science* s3-34.203 (Nov. 1887), pp. 333–345. DOI: 10.2475/ajs.s3-34.203.333. URL: https://www.ajsonline.org/content/s3-34/203/333 (visited on 22/09/2022) (cit. on pp. 3, 108).

[11]   Oliver Lodge. *"VI. Experiments on the Absence of Mechanical Connexion between Ether and Matter"*. In: *Philosophical Transactions of the Royal Society of London. Series A, Containing Papers of a Mathematical or Physical Character* 189 (Dec. 1897), pp. 149–166. DOI: 10.1098/rsta.1897.0006. URL: https://royalsocietypublishing.org/doi/10.1098/rsta.1897.0006 (visited on 12/09/2022) (cit. on pp. 3, 77).

[12]   Hendrik Lorentz. *"The Relative Motion of the Earth and the Aether"*. In: *Zittingsverlag Akad. V. Wet.* (1892) (cit. on p. 3).

[13]   Henri Poincaré. *"Sur La Dynamique de l'électron"*. In: *Comptes rendus hebdomadaires des séances de l'Académie des sciences* (1905) (cit. on p. 3).

[14]   Max Born. *Physics In My Generation*. PERGAMON PRESS, 1956. URL: http://archive.org/details/physucsinmygener006567mbp (visited on 30/08/2022) (cit. on p. 4).

[15]   A. Einstein. *"Zur Elektrodynamik Bewegter Körper"*. In: *Annalen der Physik* 322.10 (1905), pp. 891–921. DOI: 10.1002/andp.19053221004. URL: https://onlinelibrary.wiley.com/doi/abs/10.1002/andp.19053221004 (visited on 30/08/2022) (cit. on p. 4).

[16]   Hermann Minkowski. *"Space and Time"*. 1909 (cit. on p. 4).

[17]   Albert Einstein. *"The Field Equations of Gravitation"*. In: *Preussische Akademie der Wissenschaften, Sitzungsberichte* (1915), pp. 844–847 (cit. on p. 4).

[18]   P. J. E. Peebles and Bharat Ratra. *"The Cosmological Constant and Dark Energy"*. In: *Reviews of Modern Physics* 75.2 (Apr. 2003), pp. 559–606. DOI: 10.1103/RevModPhys.75.559. URL: https://link.aps.org/doi/10.1103/RevModPhys.75.559 (visited on 11/10/2022) (cit. on pp. 4, 7).

[19]   Frank Watson Dyson, Arthur Stanley Eddington and C. Davidson. *"IX. A Determination of the Deflection of Light by the Sun's Gravitational Field, from Observations Made at the Total Eclipse of May 29, 1919"*. In: *Philosophical Transactions of the Royal Society of London. Series A, Containing Papers of a Mathematical or Physical Character* 220.571-581 (Jan. 1920), pp. 291–333. DOI: 10.1098/rsta.1920.0009. URL: https://royalsocietypublishing.org/doi/10.1098/rsta.1920.0009 (visited on 29/08/2022) (cit. on pp. 5, 6).

[20]   A. Einstein. *"Die Grundlage Der Allgemeinen Relativitätstheorie"*. In: *Annalen der Physik* 354.7 (1916), pp. 769–822. DOI: 10.1002/andp.19163540702. URL: https://onlinelibrary.wiley.com/doi/abs/10.1002/andp.19163540702 (visited on 23/09/2022) (cit. on p. 6).

[21]   R. V. Pound and G. A. Rebka. *"Apparent Weight of Photons"*. In: *Physical Review Letters* 4.7 (Apr. 1960), pp. 337–341. DOI: 10.1103/PhysRevLett.4.337. URL: https://link.aps.org/doi/10.1103/PhysRevLett.4.337 (visited on 23/09/2022) (cit. on p. 6).

[22] Rudolf L. Mössbauer. *"Kernresonanzfluoreszenz von Gammastrahlung in Ir191"*. In: *Zeitschrift für Physik* 151.2 (Apr. 1958), pp. 124–143. DOI: 10.1007/BF01344210. URL: https://doi.org/10.1007/BF01344210 (visited on 12/10/2022) (cit. on p. 6).

[23] Kip S. Thorne and Stephen Hawking. *Black Holes and Time Warps: Einstein's Outrageous Legacy*. W.W. Norton, 1994 (cit. on pp. 6, 8, 18, 21).

[24] Michio Kaku. *Physics of the Impossible: A Scientific Exploration of the World of Phasers, Force Fields, Teleportation and Time Travel*. Penguin UK, 2009 (cit. on p. 7).

[25] Ya B Zel'dovich. *"THE COSMOLOGICAL CONSTANT AND THE THEORY OF ELEMENTARY PARTICLES"*. In: *Soviet Physics Uspekhi* 11.3 (1968), pp. 381–393 (cit. on p. 7).

[26] Muon g-2 Collaboration et al. *"Measurement of the Positive Muon Anomalous Magnetic Moment to 0.46 Ppm"*. In: *Physical Review Letters* 126.14 (Apr. 2021), p. 141801. DOI: 10.1103/PhysRevLett.126.141801. URL: https://link.aps.org/doi/10.1103/PhysRevLett.126.141801 (visited on 11/10/2022) (cit. on p. 7).

[27] CDF COLLABORATION et al. *"High-Precision Measurement of the W Boson Mass with the CDF II Detector"*. In: *Science* 376.6589 (Apr. 2022), pp. 170–176. DOI: 10.1126/science.abk1781. URL: https://www.science.org/doi/10.1126/science.abk1781 (visited on 11/10/2022) (cit. on p. 7).

[28] John Stachel. *"The Early History of Quantum Gravity (1916–1940)"*. In: *Black Holes, Gravitational Radiation and the Universe: Essays in Honor of C.V. Vishveshwara*. Ed. by Bala R. Iyer and Biplab Bhawal. Fundamental Theories of Physics. Dordrecht: Springer Netherlands, 1999, pp. 525–534. DOI: 10.1007/978-94-017-0934-7_31. URL: https://doi.org/10.1007/978-94-017-0934-7_31 (visited on 08/08/2022) (cit. on p. 7).

[29] W. Heisenberg and W. Pauli. *"Zur Quantendynamik der Wellenfelder"*. In: *Zeitschrift für Physik* 56.1 (Jan. 1929), pp. 1–61. DOI: 10.1007/BF01340129. URL: https://doi.org/10.1007/BF01340129 (visited on 17/08/2022) (cit. on p. 7).

[30] Kip S Thorne. *"Spacetime Warps and the Quantum World: Speculations about the Future"*. In: *The Future of Spacetime*. New York: Norton, 2002, p. 32 (cit. on p. 7).

[31] Matvei Bronstein. *"Republication of: Quantum Theory of Weak Gravitational Fields"*. In: *General Relativity and Gravitation* 44.1 (Jan. 2012), pp. 267–283. DOI: 10.1007/s10714-011-1285-4. URL: http://link.springer.com/10.1007/s10714-011-1285-4 (visited on 17/08/2022) (cit. on p. 8).

[32] Albert Einstein. *"On the Generalized Theory of Gravitation"*. In: *Scientific American* 182.4 (1950), pp. 13–17. URL: https://www.jstor.org/stable/24967425 (visited on 24/09/2022) (cit. on p. 8).

[33] Helge Kragh. *On Arthur Eddington's Theory of Everything*. Oct. 2015. DOI: 10.48550/arXiv.1510.04046. arXiv: 1510.04046 [physics]. URL: http://arxiv.org/abs/1510.04046 (visited on 29/08/2022) (cit. on p. 8).

[34] Tilman Sauer. *"Field Equations in Teleparallel Space–Time: Einstein's Fernparallelismus Approach toward Unified Field Theory"*. In: *Historia Mathematica*. Special Issue on Geometry and Its Uses in Physics, 1900-1930 33.4 (Nov. 2006), pp. 399–439. DOI: 10.1016/j.hm.2005.11.005. URL: https://www.sciencedirect.com/science/article/pii/S0315086005001060 (visited on 11/10/2022) (cit. on p. 8).

[35] Carlo Rovelli. *Notes for a Brief History of Quantum Gravity*. Jan. 2001. DOI: 10.48550/arXiv.gr-qc/0006061. arXiv: gr-qc/0006061. URL: http://arxiv.org/abs/gr-qc/0006061 (visited on 08/08/2022) (cit. on pp. 8, 10, 12).

[36] Giovanni Amelino-Camelia. *"Quantum-Spacetime Phenomenology"*. In: *Living Reviews in Relativity* 16.1 (June 2013), p. 5. DOI: 10.12942/lrr-2013-5. URL: https://doi.org/10.12942/lrr-2013-5 (visited on 25/09/2022) (cit. on p. 11).

[37] Ian C. Percival and Walter T. Strunz. *"Detection of Spacetime Fluctuation by a Model Interferometer"*. In: *Proceedings of the Royal Society of London. Series A: Mathematical, Physical and Engineering Sciences* 453.1957 (Feb. 1997), pp. 431–446. DOI: 10.1098/rspa.1997.0025. URL: https://royalsocietypublishing.org/doi/10.1098/rspa.1997.0025 (visited on 17/08/2022) (cit. on p. 11).

[38] Giovanni Amelino-Camelia. *"Are We at the Dawn of Quantum-Gravity Phenomenology?"* In: *Towards Quantum Gravity*. Ed. by Jerzy Kowalski-Glikman. Lecture Notes in Physics. Berlin, Heidelberg: Springer, 2000, pp. 1–49. DOI: 10.1007/3-540-46634-7_1 (cit. on p. 11).

[39] G. Amelino-Camelia et al. *"Tests of Quantum Gravity from Observations of γ-Ray Bursts"*. In: *Nature* 393.6687 (June 1998), pp. 763–765. DOI: 10.1038/31647. URL: https://www.nature.com/articles/31647 (visited on 17/08/2022) (cit. on p. 11).

[40] R. Colella, A. W. Overhauser and S. A. Werner. *"Observation of Gravitationally Induced Quantum Interference"*. In: *Physical Review Letters* 34.23 (June 1975), pp. 1472–1474. DOI: 10.1103/PhysRevLett.34.1472 (cit. on p. 11).

[41] J. J. Sakurai. *Modern Quantum Mechanics*. 1994. URL: http://archive.org/details/ModernQuantumMechanicsJ.J.Sakurai (visited on 26/09/2022) (cit. on p. 11).

[42] S. W. Hawking. *"Black Hole Explosions?"* In: *Nature* 248.5443 (Mar. 1974), pp. 30–31. DOI: 10.1038/248030a0 (cit. on pp. 12, 23, 83, 106).

[43] S. W. Hawking. *"Particle Creation by Black Holes"*. In: *Communications in Mathematical Physics* 43.3 (Aug. 1975), pp. 199–220. DOI: 10.1007/BF02345020 (cit. on pp. 12, 83).

[44] Steven Carlip et al. *"Quantum Gravity: A Brief History of Ideas and Some Prospects"*. In: *International Journal of Modern Physics D* 24.11 (Oct. 2015), p. 1530028. DOI: 10.1142/S0218271815300281. arXiv: 1507.08194 [gr-qc]. URL: http://arxiv.org/abs/1507.08194 (visited on 08/08/2022) (cit. on p. 12).

[45] W. G. Unruh. *"Notes on Black-Hole Evaporation"*. In: *Physical Review D* 14.4 (Aug. 1976), pp. 870–892. DOI: 10.1103/PhysRevD.14.870 (cit. on pp. 12, 83).

[46] W. G. Unruh. *"Experimental Black-Hole Evaporation?"* In: *Physical Review Letters* 46.21 (May 1981), pp. 1351–1353. DOI: 10.1103/PhysRevLett.46.1351. URL: https://link.aps.org/doi/10.1103/PhysRevLett.46.1351 (visited on 23/08/2022) (cit. on p. 12).

[47] Carlos Barceló, Stefano Liberati and Matt Visser. *"Analogue Gravity"*. In: *Living Reviews in Relativity* 14.1 (May 2011), p. 3. DOI: 10.12942/lrr-2011-3. URL: https://doi.org/10.12942/lrr-2011-3 (visited on 23/08/2022) (cit. on p. 12).

[48] Yuval Rosenberg. *"Optical Analogues of Black-Hole Horizons"*. In: *arXiv:2002.04216 [gr-qc, physics:physics]* (Feb. 2020). arXiv: 2002.04216 [gr-qc, physics:physics]. URL: http://arxiv.org/abs/2002.04216 (visited on 18/02/2020) (cit. on p. 12).

[49] Silke Weinfurtner et al. *"Measurement of Stimulated Hawking Emission in an Analogue System"*. In: *Physical Review Letters* 106.2 (Jan. 2011), p. 021302. DOI: 10.1103/PhysRevLett.106.021302 (cit. on pp. 12, 18, 23, 26, 83, 106).

[50] Theo Torres et al. *"Rotational Superradiant Scattering in a Vortex Flow"*. In: *Nature Physics* 13.9 (Sept. 2017), pp. 833–836. DOI: 10.1038/nphys4151 (cit. on pp. 12, 23, 26, 106).

[51] Jeff Steinhauer. *"Observation of Self-Amplifying Hawking Radiation in an Analogue Black-Hole Laser"*. In: *Nature Physics* 10.11 (Nov. 2014), pp. 864–869. DOI: 10.1038/nphys3104 (cit. on pp. 12, 18, 23, 26, 83, 106).

[52] Jeff Steinhauer. *"Observation of Quantum Hawking Radiation and Its Entanglement in an Analogue Black Hole"*. In: *Nature Physics* 12.10 (Oct. 2016), pp. 959–965. DOI: 10.1038/nphys3863 (cit. on pp. 12, 18, 23, 26, 83, 106).

[53] Juan Ramón Muñoz de Nova et al. *"Observation of Thermal Hawking Radiation and Its Temperature in an Analogue Black Hole"*. In: *Nature* 569.7758 (May 2019), pp. 688–691. DOI: 10.1038/s41586-019-1241-0 (cit. on pp. 12, 18, 23, 26, 83, 106).

[54] Thomas G. Philbin et al. *"Fiber-Optical Analog of the Event Horizon"*. In: *Science* 319.5868 (Mar. 2008), pp. 1367–1370. DOI: 10.1126/science.1153625. URL: https://www.science.org/doi/10.1126/science.1153625 (visited on 05/10/2022) (cit. on pp. 12, 18, 23, 83).

[55] Maria Chiara Braidotti et al. *"Measurement of Penrose Superradiance in a Photon Superfluid"*. In: *Physical Review Letters* 128.1 (Jan. 2022), p. 013901. DOI: 10.1103/PhysRevLett.128.013901. URL: https://link.aps.org/doi/10.1103/PhysRevLett.128.013901 (visited on 05/10/2022) (cit. on pp. 12, 18, 23, 83, 106).

[56] Grace Field. *"The Latest Frontier in Analogue Gravity: New Roles for Analogue Experiments"*. In: (), p. 27 (cit. on p. 12).

[57] Gerald T. Moore. *"Quantum Theory of the Electromagnetic Field in a Variable-Length One-Dimensional Cavity"*. In: *Journal of Mathematical Physics* 11.9 (Sept. 1970), pp. 2679–2691. DOI: 10.1063/1.1665432. URL: http://aip.scitation.org/doi/10.1063/1.1665432 (visited on 27/09/2022) (cit. on p. 13).

[58] C. M. Wilson et al. *"Observation of the Dynamical Casimir Effect in a Superconducting Circuit"*. In: *Nature* 479.7373 (Nov. 2011), pp. 376–379. DOI: 10.1038/nature10561. arXiv: 1105.4714. URL: http://arxiv.org/abs/1105.4714 (visited on 24/04/2019) (cit. on p. 13).

[59] Ryszard Horodecki et al. *"Quantum Entanglement"*. In: *Reviews of Modern Physics* 81.2 (June 2009), pp. 865–942. DOI: 10.1103/RevModPhys.81.865. URL: https://link.aps.org/doi/10.1103/RevModPhys.81.865 (visited on 30/09/2022) (cit. on pp. 13, 104).

[60] C. Marletto and V. Vedral. *"Gravitationally Induced Entanglement between Two Massive Particles Is Sufficient Evidence of Quantum Effects in Gravity"*. In: *Physical Review Letters* 119.24 (Dec. 2017), p. 240402. DOI: 10.1103/PhysRevLett.119.240402. URL: https://link.aps.org/doi/10.1103/PhysRevLett.119.240402 (visited on 27/09/2022) (cit. on p. 13).

[61] Sougato Bose et al. *"Spin Entanglement Witness for Quantum Gravity"*. In: *Physical Review Letters* 119.24 (Dec. 2017), p. 240401. DOI: 10.1103/PhysRevLett.119.240401 (cit. on p. 13).

[62] Marco Di Mauro, Salvatore Esposito and Adele Naddeo. *"A Road Map for Feynman's Adventures in the Land of Gravitation"*. In: *The European Physical Journal H* 46.1 (Aug. 2021), p. 22. DOI: 10.1140/epjh/s13129-021-00028-3. URL: https://doi.org/10.1140/epjh/s13129-021-00028-3 (visited on 27/09/2022) (cit. on p. 13).

[63] *The Nobel Prize in Physics 2022*. 2022. URL: https://www.nobelprize.org/prizes/physics/2022/press-release/ (visited on 13/10/2022) (cit. on p. 13).

[64] Stuart J. Freedman and John F. Clauser. *"Experimental Test of Local Hidden-Variable Theories"*. In: *Physical Review Letters* 28.14 (Apr. 1972), pp. 938–941. DOI: 10.1103/PhysRevLett.28.938. URL: https://link.aps.org/doi/10.1103/PhysRevLett.28.938 (visited on 05/10/2022) (cit. on pp. 13, 109).

[65] Alain Aspect, Philippe Grangier and Gérard Roger. *"Experimental Realization of Einstein-Podolsky-Rosen-Bohm Gedankenexperiment: A New Violation of Bell's Inequalities"*. In: *Physical Review Letters* 49.2 (July 1982), pp. 91–94. DOI: 10.1103/PhysRevLett.49.91. URL: https://link.aps.org/doi/10.1103/PhysRevLett.49.91 (visited on 04/12/2018) (cit. on p. 13).

[66] Dik Bouwmeester et al. *"Experimental Quantum Teleportation"*. In: *Nature* 390.6660 (Dec. 1997), pp. 575–579. DOI: 10.1038/37539. URL: https://www.nature.com/articles/37539 (visited on 13/10/2022) (cit. on p. 13).

[67] Gaspard-Gustave Coriolis. *"Sur Les Équations Du Mouvement Relatif Des Systèmes de Corps"*. In: *Journal de l'Ecole Royale Polytechnique* 15 (1835), pp. 144–154 (cit. on p. 15).

[68] *"Propagation of Light in Non-Inertial Reference Frames"*. In: *Relativity and the Nature of Spacetime*. Ed. by Vesselin Petkov. The Frontiers Collection. Berlin, Heidelberg: Springer, 2005, pp. 191–223. DOI: 10.1007/3-540-27700-5_8. URL: https://doi.org/10.1007/3-540-27700-5_8 (visited on 28/09/2022) (cit. on p. 15).

[69] Dennis Lehmkuhl. *"Why Einstein Did Not Believe That General Relativity Geometrizes Gravity"*. In: *Studies in History and Philosophy of Science Part B: Studies in History and Philosophy of Modern Physics* 46 (May 2014), pp. 316–326. DOI: 10.1016/j.shpsb.2013.08.002. URL: https://www.sciencedirect.com/science/article/pii/S1355219813000695 (visited on 27/09/2022) (cit. on p. 15).

[70] Matthias Fink et al. *"Experimental Test of Photonic Entanglement in Accelerated Reference Frames"*. In: *Nature Communications* 8.1 (May 2017), p. 15304. DOI: 10.1038/ncomms15304 (cit. on pp. 15, 83, 107, 108).

[71] John R. Letaw. *"Stationary World Lines and the Vacuum Excitation of Noninertial Detectors"*. In: *Physical Review D* 23.8 (Apr. 1981), pp. 1709–1714. DOI: 10.1103/PhysRevD.23.1709. URL: https://link.aps.org/doi/10.1103/PhysRevD.23.1709 (visited on 04/10/2022) (cit. on p. 15).

[72] Chiara Marletto and Vlatko Vedral. *"Sagnac Interferometer and the Quantum Nature of Gravity"*. In: *Journal of Physics Communications* 5.5 (May 2021), p. 051001. DOI: 10.1088/2399-6528/abfd43. URL: https://doi.org/10.1088/2399-6528/abfd43 (visited on 12/10/2022) (cit. on pp. 15, 101).

[73] Jacob D. Bekenstein and Marcelo Schiffer. *"The Many Faces of Superradiance"*. In: *Physical Review D* 58.6 (Aug. 1998), p. 064014. DOI: 10.1103/PhysRevD.58.064014 (cit. on pp. 16, 21).

[74] Charles Vernon Boys. *Soap-Bubbles and the Forces That Mould Them.* 1896. URL: https://www.gutenberg.org/files/33370/33370-h/33370-h.htm (visited on 13/10/2022) (cit. on p. 17).

[75] Ya.B. Zel'dovich. *"Generation of Waves by a Rotating Body"*. In: *JETP letters* 14 (1971), pp. 180–181. URL: http://www.jetpletters.ru/ps/1604/article_24607.shtml (cit. on pp. 18, 21, 26, 105).

[76] Ya.B. Zel'dovich. *"Amplification of Cylindrical Electromagnetic Waves Reflected from a Rotating Body"*. In: *JETP* 35.6 (1972), p. 1085. URL: http://www.jetp.ras.ru/cgi-bin/e/index/e/35/6/p1085?a=list (cit. on pp. 18, 21, 23, 26, 105).

[77] Carla Rodrigues Almeida. *"The Thermodynamics of Black Holes: From Penrose Process to Hawking Radiation"*. In: *The European Physical Journal H* 46.1 (Aug. 2021), p. 20. DOI: 10.1140/epjh/s13129-021-00022-9. URL: https://doi.org/10.1140/epjh/s13129-021-00022-9 (visited on 19/08/2022) (cit. on pp. 18, 22).

[78] Cisco Gooding, Silke Weinfurtner and William G. Unruh. *"Reinventing the Zel'Dovich Wheel"*. In: *Physical Review A* 101.6 (June 2020), p. 063819. DOI: 10.1103/PhysRevA.101.063819. URL: https://link.aps.org/doi/10.1103/PhysRevA.101.063819 (visited on 22/07/2022) (cit. on pp. 18, 24, 27, 34, 106).

[79] D. Faccio and E. M. Wright. *"Superradiant Amplification of Acoustic Beams via Medium Rotation"*. In: *Physical Review Letters* 123.4 (2019), p. 044301. DOI: 10.1103/PhysRevLett.123.044301 (cit. on pp. 18, 24, 25, 27, 29, 34, 36, 106).

[80] Cisco Gooding, Silke Weinfurtner and William G. Unruh. *"Superradiant Scattering of Orbital Angular Momentum Beams"*. In: *Physical Review Research* 3.2 (June 2021), p. 023242. DOI: 10.1103/PhysRevResearch.3.023242. URL: https://link.aps.org/doi/10.1103/PhysRevResearch.3.023242 (visited on 03/10/2022) (cit. on pp. 18, 24, 106).

[81] Graham M. Gibson et al. *"Reversal of Orbital Angular Momentum Arising from an Extreme Doppler Shift"*. In: *Proceedings of the National Academy of Sciences* 115.15 (Apr. 2018), pp. 3800–3803. DOI: 10.1073/pnas.1720776115 (cit. on pp. 18, 24, 25, 27–30, 36, 38, 106).

[82] Ridley Scott. *Alien*. Horror, Sci-Fi. Sept. 1979 (cit. on p. 18).

[83] R Penrose. *"Gravitational Collapse: The Role of General Relativity"*. In: *Rivista del Nuovo Cimento* Numero Speziale I.Numero Speziale I (1969), pp. 257–276 (cit. on pp. 18, 20, 26, 106).

[84] R. Penrose and R. M. Floyd. *"Extraction of Rotational Energy from a Black Hole"*. In: *Nature Physical Science* 229.6 (Feb. 1971), pp. 177–179. DOI: 10.1038/physci229177a0 (cit. on pp. 18, 106).

[85] Freeman J. Dyson. *Disturbing the Universe*. Harper & Row, 1979 (cit. on p. 19).

[86] Freeman J. Dyson. *"Search for Artificial Stellar Sources of Infrared Radiation"*. In: *Science* 131.3414 (June 1960), pp. 1667–1668. DOI: 10.1126/science.131.3414.1667. URL: https://www.science.org/doi/10.1126/science.131.3414.1667 (visited on 19/08/2022) (cit. on p. 19).

[87] Roy P. Kerr. *"Gravitational Field of a Spinning Mass as an Example of Algebraically Special Metrics"*. In: *Physical Review Letters* 11.5 (Sept. 1963), pp. 237–238. DOI: 10.1103/PhysRevLett.11.237 (cit. on p. 19).

[88] Christopher M Hirata. *"Lecture XXVI: Kerr Black Holes: I. Metric Structure and Regularity of Particle Orbits"*. In: (), p. 6 (cit. on p. 19).

[89] Demetrios L. Christodoulou. *"Investigations in Gravitational Collapse and the Physics of Black Holes."* PhD thesis. Jan. 1971. URL: https://ui.adsabs.harvard.edu/abs/1971PhDT........75C (visited on 20/08/2022) (cit. on p. 21).

[90] Reva Kay Williams. *"Extracting x Rays, \ensuremath{\gamma} Rays, and Relativistic ${\mathit{e}}\^{\mathrm{\ensuremath{-}}}$${\mathit{e}}\^{+}$ Pairs from Supermassive Kerr Black Holes Using the Penrose Mechanism"*. In: *Physical Review D* 51.10 (May 1995), pp. 5387–5427. DOI: 10.1103/PhysRevD.51.5387. URL: https://link.aps.org/doi/10.1103/PhysRevD.51.5387 (visited on 06/10/2022) (cit. on p. 21).

[91] Reva Kay Williams. *"Collimated Escaping Vortical Polar e–E+ Jets Intrinsically Produced by Rotating Black Holes and Penrose Processes"*. In: *The Astrophysical Journal* 611.2 (Aug. 2004), p. 952. DOI: 10.1086/422304. URL: https://iopscience.iop.org/article/10.1086/422304/meta (visited on 06/10/2022) (cit. on p. 21).

[92] Reva Kay Williams. *A Word from a Black Female Relativistic Astrophysicist: Setting the Record Straight on Black Holes.* Apr. 2004. DOI: 10.48550/arXiv.physics/0404029. arXiv: physics / 0404029. URL: http : / / arxiv . org / abs / physics / 0404029 (visited on 09/10/2022) (cit. on p. 21).

[93] Erin G. Teich et al. *"Citation Inequity and Gendered Citation Practices in Contemporary Physics"*. In: *Nature Physics* 18.10 (Oct. 2022), pp. 1161–1170. DOI: 10.1038/ s41567- 022- 01770- 1. URL: http : / / www . nature . com / articles / s41567- 022- 01770- 1 (visited on 09/10/2022) (cit. on p. 21).

[94] Maxwell A. Bertolero et al. *Racial and Ethnic Imbalance in Neuroscience Reference Lists and Intersections with Gender.* Oct. 2020. DOI: 10 . 1101 / 2020 . 10 . 12 . 336230. URL: https : / / www . biorxiv . org / content / 10 . 1101 / 2020 . 10 . 12 . 336230v1 (visited on 09/10/2022) (cit. on p. 21).

[95] Joan Mason. *"Hertha Ayrton (1854-1923) and the Admission of Women to the Royal Society of London"*. In: *Notes and Records of the Royal Society of London* 45.2 (July 1991), pp. 201–220. DOI: 10.1098/rsnr.1991.0019. URL: http://royalsocietypublishing. org/doi/10.1098/rsnr.1991.0019 (visited on 09/10/2022) (cit. on p. 21).

[96] Claire Denis. *High Life.* 2018 (cit. on p. 21).

[97] Ya. B. Zel'dovich, L. V. Rozhanskii and A. A. Starobinskii. *"Rotating Bodies and Electrodynamics in a Rotating Coordinate System"*. In: *Radiophysics and Quantum Electronics* 29.9 (Sept. 1986), pp. 761–768. DOI: 10.1007/BF01034472 (cit. on pp. 21, 26).

[98] C. W. Misner. *"Interpretation of Gravitational-Wave Observations"*. In: *Physical Review Letters* 28.15 (Apr. 1972), pp. 994–997. DOI: 10.1103/PhysRevLett.28.994. URL: https://link.aps.org/doi/10.1103/PhysRevLett.28.994 (visited on 22/08/2022) (cit. on p. 22).

[99] A A Starobinskii. *"Amplification of Waves during Reflection from a Rotating Black Hole"*. In: *JETP* 37.1 (1973), p. 5 (cit. on p. 22).

[100] W. Israel. *"Entropy and Black-Hole Dynamics"*. In: *Lettere al Nuovo Cimento (1971-1985)* 6.7 (Feb. 1973), pp. 267–269. DOI: 10.1007/BF02746447. URL: https://doi.org/ 10.1007/BF02746447 (visited on 19/08/2022) (cit. on p. 22).

[101] Jacob D. Bekenstein. *"Black Holes and Entropy"*. In: *Physical Review D* 7.8 (Apr. 1973), pp. 2333–2346. DOI: 10.1103/PhysRevD.7.2333. URL: https://link.aps.org/doi/ 10.1103/PhysRevD.7.2333 (visited on 25/08/2022) (cit. on p. 23).

[102] Ted Jacobson. *"Thermodynamics of Spacetime: The Einstein Equation of State"*. In: *Physical Review Letters* 75.7 (Aug. 1995), pp. 1260–1263. DOI: 10.1103/PhysRevLett. 75.1260. URL: https://link.aps.org/doi/10.1103/PhysRevLett.75.1260 (visited on 13/10/2022) (cit. on p. 23).

[103] D. J. Acheson. *"On Over-Reflexion"*. In: *Journal of Fluid Mechanics* 77.3 (1976), 433?472 (cit. on p. 26).

[104] F. Belgiorno et al. *"Hawking Radiation from Ultrashort Laser Pulse Filaments"*. In: *Physical Review Letters* 105.20 (Nov. 2010), p. 203901. DOI: 10.1103/PhysRevLett. 105.203901. URL: https://link.aps.org/doi/10.1103/PhysRevLett.105.203901 (cit. on p. 26).

[105] Jonathan Drori et al. *"Observation of Stimulated Hawking Radiation in an Optical Analogue"*. In: *Physical Review Letters* 122.1 (Jan. 2019), p. 010404. DOI: 10.1103/ PhysRevLett.122.010404. URL: https://link.aps.org/doi/10.1103/PhysRevLett.122. 010404 (cit. on p. 26).

[106] L. Allen et al. *"Orbital Angular Momentum of Light and the Transformation of Laguerre-Gaussian Laser Modes"*. In: *Physical Review A: Atomic, Molecular, and Optical Physics* 45.11 (June 1992), pp. 8185–8189. DOI: 10.1103/PhysRevA.45.8185 (cit. on p. 26).

[107] David L. Andrews and Mohamed Babiker. *The Angular Momentum of Light.* Cambridge University Press, 2013 (cit. on p. 26).

[108] Miles Padgett, Johannes Courtial and Les Allen. *"Light's Orbital Angular Momentum"*. In: *Physics Today* 57.5 (May 2004), pp. 35–40. DOI: 10.1063/1.1768672 (cit. on p. 26).

[109] Robert Fickler et al. *"Quantum Entanglement of Angular Momentum States with Quantum Numbers up to 10,010"*. In: *Optics Letters* 113.48 (2016), pp. 13642–13647 (cit. on p. 27).

[110] Daniele Faccio and Ewan M. Wright. *"Nonlinear Zel'dovich Effect: Parametric Amplification from Medium Rotation"*. In: *Physical Review Letters* 118.9 (Feb. 2017), p. 093901. DOI: 10.1103/PhysRevLett.118.093901. URL: https://link.aps.org/doi/10.1103/ PhysRevLett.118.093901 (visited on 01/05/2020) (cit. on p. 27).

[111] Cisco Gooding, Silke Weinfurtner and William G. Unruh. *"Superradiant Scattering of Orbital Angular Momentum Beams"*. In: *arXiv:1809.08235 [physics]* (Feb. 2020). arXiv: 1809.08235 [physics]. URL: http://arxiv.org/abs/1809.08235 (visited on 01/05/2020) (cit. on pp. 27, 34).

[112] Cisco Gooding. *"Dynamics Landscape for Acoustic Superradiance"*. In: *arXiv:2002.05605 [physics]* (Feb. 2020). arXiv: 2002.05605 [physics] (cit. on pp. 27, 34).

[113] J. Courtial et al. *"Rotational Frequency Shift of a Light Beam"*. In: *Physical Review Letters* 81.22 (Nov. 1998), pp. 4828–4830. DOI: 10.1103/PhysRevLett.81.4828 (cit. on p. 27).

[114] Iwo Bialynicki-Birula and Zofia Bialynicka-Birula. *"Rotational Frequency Shift"*. In: *Physical Review Letters* 78.13 (1997), p. 4 (cit. on p. 27).

[115] R.W. Boyd. *Nonlinear Optics.* New York: Academic Press, 2008 (cit. on p. 28).

[116] Bruce W. Drinkwater. *"An Acoustic Black Hole"*. In: *Nature Physics* 16.10 (Oct. 2020), pp. 1010–1011. DOI: 10.1038/s41567-020-0954-1. URL: https://www.nature.com/ articles/s41567-020-0954-1 (visited on 19/08/2022) (cit. on pp. 39, 106).

[117] *Bob Chivers Prize in Physical Acoustics.* URL: https://www.iop.org/physics-community/ special-interest-groups/physical-acoustics-group/bob-chivers-prize (visited on 22/08/2022) (cit. on pp. 39, 106).

[118] Lianyun Liu et al. *"Experimental Study of Acoustic Superradiance from a Rotating Absorber"*. In: *Journal of Applied Physics* 131.16 (Apr. 2022), p. 164901. DOI: 10.1063/5.0086043. URL: https://aip.scitation.org/doi/10.1063/5.0086043 (visited on 19/08/2022) (cit. on pp. 39, 106).

[119] Chengzhi Shi et al. *"High-Speed Acoustic Communication by Multiplexing Orbital Angular Momentum"*. In: *Proceedings of the National Academy of Sciences* 114.28 (July 2017), pp. 7250–7253. DOI: 10.1073/pnas.1704450114. URL: https://www.pnas.org/doi/full/10.1073/pnas.1704450114 (visited on 19/08/2022) (cit. on p. 39).

[120] Marion Cromb. *Amplification of Twisted Sound Waves*. June 2020. URL: https://www.youtube.com/watch?v=ES2VxhRAkUM (visited on 28/07/2022) (cit. on p. 39).

[121] Bendoris. *Black Holes Star Trek Theory Proven by Glasgow University Research Team*. June 2020. URL: https://www.thescottishsun.co.uk/tvandshowbiz/5730625/black-holes-star-trek-glasgow-university/ (visited on 22/08/2022) (cit. on pp. 39, 106).

[122] Tom Fish. *Black Hole Bombshell: 50-Year-Old Theory PROVES How Aliens Could Exploit a Black Hole*. June 2020. URL: https://www.express.co.uk/news/science/1300263/black-hole-theory-proves-aliens-exploit-black-hole-space-news (visited on 22/08/2022) (cit. on p. 39).

[123] Ellena Cruse. *Black Hole Energy Theory 'verified' by Scottish Scientists*. June 2020. URL: https://www.standard.co.uk/news/uk/black-hole-energy-theory-verified-roger-penrose-scottish-scientists-a4476191.html (visited on 22/08/2022) (cit. on p. 39).

[124] Alfredo Carpineti. *It Is Possible To Get Energy Out Of A Black Hole, Lab Experiment Shows*. June 2020. URL: https://iflscience.com/it-is-possible-to-get-energy-out-of-a-black-hole-lab-experiment-shows-56477 (visited on 22/08/2022) (cit. on p. 39).

[125] *Covid -19 and Children*. July 2020. URL: https://www.bbc.co.uk/programmes/w3cszh0j (visited on 28/07/2022) (cit. on p. 39).

[126] Daniele Faccio and Marion Cromb. *"Could We Extract Energy from a Black Hole? Our Experiment Verifies Old Theory"*. In: *The Conversation* (June 2020). URL: http://theconversation.com/could-we-extract-energy-from-a-black-hole-our-experiment-verifies-old-theory-141464 (visited on 28/07/2022) (cit. on p. 40).

[127] Po-Cheng Lin, Graham M. Gibson and Miles J. Padgett. *"Real-Time Visualisation and Optimisation of Acoustic Waves Carrying Orbital Angular Momentum"*. In: *Journal of Physics A: Mathematical and Theoretical* 55.26 (June 2022), p. 264007. DOI: 10.1088/1751-8121/ac717f. URL: https://doi.org/10.1088/1751-8121/ac717f (visited on 22/08/2022) (cit. on p. 40).

[128] Maria Chiara Braidotti et al. *"Zel'dovich Amplification in a Superconducting Circuit"*. In: *Physical Review Letters* 125.14 (Oct. 2020), p. 140801. DOI: 10.1103/PhysRevLett.125.140801. URL: https://link.aps.org/doi/10.1103/PhysRevLett.125.140801 (visited on 22/07/2022) (cit. on pp. 40, 98, 106).

[129] *"Optical Test of Quantum Mechanics"*. In: *Introductory Quantum Optics*. Ed. by Christopher Gerry and Peter Knight. Cambridge: Cambridge University Press, 2004, pp. 213–237. DOI: 10.1017/CBO9780511791239.009. URL: https://www.cambridge.org/core/books/introductory-quantum-optics/optical-test-of-quantum-mechanics/77425FEDA18B30BFBD09190720377717 (visited on 07/10/2022) (cit. on pp. 42, 44, 45).

[130] Peter Shadbolt et al. *"Testing Foundations of Quantum Mechanics with Photons"*. In: *Nature Physics* 10.4 (Apr. 2014), pp. 278–286. DOI: 10.1038/nphys2931. URL: https://www.nature.com/articles/nphys2931/ (visited on 07/10/2022) (cit. on p. 42).

[131] Zhen-Sheng Yuan et al. *"Entangled Photons and Quantum Communication"*. In: *Physics Reports* 497.1 (Dec. 2010), pp. 1–40. DOI: 10.1016/j.physrep.2010.07.004. URL: https://www.sciencedirect.com/science/article/pii/S0370157310001833 (visited on 07/10/2022) (cit. on p. 42).

[132] C. K. Hong, Z. Y. Ou and L. Mandel. *"Measurement of Subpicosecond Time Intervals between Two Photons by Interference"*. In: *Physical Review Letters* 59.18 (Nov. 1987), pp. 2044–2046. DOI: 10.1103/PhysRevLett.59.2044. URL: https://link.aps.org/doi/10.1103/PhysRevLett.59.2044 (visited on 19/10/2018) (cit. on pp. 42, 45, 83).

[133] Sara Restuccia et al. *"Photon Bunching in a Rotating Reference Frame"*. In: *Physical Review Letters* 123.11 (Sept. 2019), p. 110401. DOI: 10.1103/PhysRevLett.123.110401 (cit. on pp. 42, 77, 78, 82, 83, 107).

[134] Kaige Wang and Shiyao Zhu. *"Two-Photon Anti-Coalescence Interference: The Signature of Two-Photon Entanglement"*. In: *Europhysics Letters (EPL)* 64.1 (Oct. 2003), pp. 22–28. DOI: 10.1209/epl/i2003-00503-6. URL: http://stacks.iop.org/0295-5075/64/i=1/a=022?key=crossref.dd3b7403537ec4f3d238a63b89bfe95a (visited on 19/10/2018) (cit. on pp. 42, 50, 51, 54, 84, 107).

[135] M. A. Sagioro et al. *"Time Control of Two-Photon Interference"*. In: *Physical Review A* 69.5 (May 2004). DOI: 10.1103/PhysRevA.69.053817. URL: https://link.aps.org/doi/10.1103/PhysRevA.69.053817 (visited on 08/10/2018) (cit. on pp. 42, 50, 52, 84, 107).

[136] D. V. Strekalov, T. B. Pittman and Y. H. Shih. *"What We Can Learn about Single Photons in a Two-Photon Interference Experiment"*. In: *Physical Review A* 57.1 (Jan. 1998), pp. 567–570. DOI: 10.1103/PhysRevA.57.567. URL: https://link.aps.org/doi/10.1103/PhysRevA.57.567 (visited on 31/10/2018) (cit. on pp. 42, 50, 51, 84, 107).

[137] C. Olindo et al. *"Erasing Nonlocal like Two Photon Interference"*. In: *Optics Communications* 357 (Dec. 2015), pp. 58–62. DOI: 10.1016/j.optcom.2015.08.091. URL: http://www.sciencedirect.com/science/article/pii/S0030401815300845 (visited on 15/11/2018) (cit. on pp. 42, 50, 53, 66, 84, 107).

[138] S. E. Harris, M. K. Oshman and R. L. Byer. *"Observation of Tunable Optical Parametric Fluorescence"*. In: *Physical Review Letters* 18.18 (May 1967), pp. 732–734. DOI: 10.1103/PhysRevLett.18.732. URL: https://link.aps.org/doi/10.1103/PhysRevLett.18.732 (visited on 07/10/2022) (cit. on p. 43).

[139] Douglas Magde and Herbert Mahr. *"Study in Ammonium Dihydrogen Phosphate of Spontaneous Parametric Interaction Tunable from 4400 to 16 000 \AA{}"*. In: *Physical Review Letters* 18.21 (May 1967), pp. 905–907. DOI: 10.1103/PhysRevLett.18.905. URL: https://link.aps.org/doi/10.1103/PhysRevLett.18.905 (visited on 07/10/2022) (cit. on p. 43).

[140] R. Ghosh and L. Mandel. *"Observation of Nonclassical Effects in the Interference of Two Photons"*. In: *Physical Review Letters* 59.17 (Oct. 1987), pp. 1903–1905. DOI: 10.1103/PhysRevLett.59.1903. URL: https://link.aps.org/doi/10.1103/PhysRevLett.59.1903 (visited on 19/10/2018) (cit. on p. 43).

[141] Y. H. Shih and C. O. Alley. *"New Type of Einstein-Podolsky-Rosen-Bohm Experiment Using Pairs of Light Quanta Produced by Optical Parametric Down Conversion"*. In: *Physical Review Letters* 61.26 (Dec. 1988), pp. 2921–2924. DOI: 10.1103/PhysRevLett.61.2921. URL: https://link.aps.org/doi/10.1103/PhysRevLett.61.2921 (visited on 07/10/2022) (cit. on p. 43).

[142] Robert W. Boyd. *Nonlinear Optics*. Academic Press, Mar. 2020 (cit. on p. 43).

[143] Matthias Bock et al. *"Highly Efficient Heralded Single-Photon Source for Telecom Wavelengths Based on a PPLN Waveguide"*. In: *Opt. Express, OE* 24.21 (Oct. 2016), pp. 23992–24001. DOI: 10.1364/OE.24.023992. URL: https://www.osapublishing.org/oe/abstract.cfm?uri=oe-24-21-23992 (visited on 02/05/2019) (cit. on p. 43).

[144] Z. Y. Ou, J.-K. Rhee and L. J. Wang. *"Observation of Four-Photon Interference with a Beam Splitter by Pulsed Parametric Down-Conversion"*. In: *Physical Review Letters* 83.5 (Aug. 1999), pp. 959–962. DOI: 10.1103/PhysRevLett.83.959. URL: https://link.aps.org/doi/10.1103/PhysRevLett.83.959 (visited on 07/10/2022) (cit. on p. 43).

[145] Hugues De Riedmatten et al. *"Two Independent Photon Pairs versus Four-Photon Entangled States in Parametric down Conversion"*. In: *Journal of Modern Optics* (July 2009). URL: https://www.tandfonline.com/doi/abs/10.1080/09500340408232478 (visited on 07/10/2022) (cit. on p. 43).

[146] David C. Burnham and Donald L. Weinberg. *"Observation of Simultaneity in Parametric Production of Optical Photon Pairs"*. In: *Physical Review Letters* 25.2 (July 1970), pp. 84–87. DOI: 10.1103/PhysRevLett.25.84. URL: https://link.aps.org/doi/10.1103/PhysRevLett.25.84 (visited on 07/10/2022) (cit. on p. 43).

[147] B. Ya. Zel'Dovich and D. N. Klyshko. *"Field Statistics in Parametric Luminescence"*. In: *JETP letters* 9 (Jan. 1969), p. 40. URL: http://www.jetpletters.ru/ps/1639/article_25275.shtml (visited on 07/10/2022) (cit. on p. 44).

[148] P. A. Franken and J. F. Ward. *"Optical Harmonics and Nonlinear Phenomena"*. In: *Reviews of Modern Physics* 35.1 (Jan. 1963), pp. 23–39. DOI: 10.1103/RevModPhys.35.23. URL: https://link.aps.org/doi/10.1103/RevModPhys.35.23 (visited on 02/05/2019) (cit. on p. 44).

[149] Dr Rüdiger Paschotta. *Temporal Walk-off*. URL: https://www.rp-photonics.com/temporal_walk_off.html (visited on 07/10/2022) (cit. on p. 44).

[150] Dr Rüdiger Paschotta. *Spatial Walk-off*. URL: https://www.rp-photonics.com/spatial_walk_off.html (visited on 07/10/2022) (cit. on p. 45).

[151] Paul G. Kwiat et al. *"New High-Intensity Source of Polarization-Entangled Photon Pairs"*. In: *Physical Review Letters* 75.24 (Dec. 1995), pp. 4337–4341. DOI: 10.1103/PhysRevLett.75.4337. URL: https://link.aps.org/doi/10.1103/PhysRevLett.75.4337 (visited on 20/11/2018) (cit. on p. 45).

[152] T. B. Pittman et al. *"Can Two-Photon Interference Be Considered the Interference of Two Photons?"* In: *Physical Review Letters* 77.10 (Sept. 1996), pp. 1917–1920. DOI: 10.1103/PhysRevLett.77.1917 (cit. on pp. 45, 84).

[153] Paul G. Kwiat et al. *"Ultrabright Source of Polarization-Entangled Photons"*. In: *Physical Review A: Atomic, Molecular, and Optical Physics* 60.2 (Aug. 1999), R773–R776. DOI: 10.1103/PhysRevA.60.R773. URL: https://link.aps.org/doi/10.1103/PhysRevA.60.R773 (visited on 28/11/2018) (cit. on p. 45).

[154] Heonoh Kim, Osung Kwon and Han Seb Moon. *"Pulsed Sagnac Source of Polarization-Entangled Photon Pairs in Telecommunication Band"*. In: *Scientific Reports* 9.1 (Mar. 2019), p. 5031. DOI: 10.1038/s41598-019-41633-z. URL: https://www.nature.com/articles/s41598-019-41633-z (visited on 02/05/2019) (cit. on p. 45).

[155] H. Fearn and R. Loudon. *"Quantum Theory of the Lossless Beam Splitter"*. In: *Optics Communications* 64.6 (Dec. 1987), pp. 485–490. DOI: 10.1016/0030-4018(87)90275-6. URL: https://www.sciencedirect.com/science/article/pii/0030401887902756 (visited on 07/10/2022) (cit. on p. 45).

[156] Zhe-Yu Jeff Ou. *Multi-Photon Quantum Interference*. New York: Springer, 2007 (cit. on pp. 45, 48–50, 58).

[157] I. Abram et al. *"Direct Observation of the Second-Order Coherence of Parametrically Generated Light"*. In: *Physical Review Letters* 57.20 (Nov. 1986), pp. 2516–2519. DOI: 10.1103/PhysRevLett.57.2516. URL: https://link.aps.org/doi/10.1103/PhysRevLett.57.2516 (visited on 07/10/2022) (cit. on p. 45).

[158] Anton Zeilinger, Herbert J. Bernstein and M.A. Horne. *"Information Transfer with Two-state Two-particle Quantum Systems"*. In: *Journal of Modern Optics* 41.12 (Dec. 1994), pp. 2375–2384. DOI: 10.1080/09500349414552211. URL: https://doi.org/10.1080/09500349414552211 (visited on 03/02/2023) (cit. on p. 46).

[159] Emilio Pisanty. *Answer to "Phase Added on Reflection at a Beam Splitter?"* Jan. 2019. URL: https://web.archive.org/web/20220730133333/https://physics.stackexchange.com/questions/185155/phase-added-on-reflection-at-a-beam-splitter (visited on 30/07/2022) (cit. on p. 46).

[160] Benjamin Vest et al. *"Anti-Coalescence of Bosons on a Lossy Beam Splitter"*. In: *Science (New York, N.Y.)* 356.6345 (June 2017), pp. 1373–1376. DOI: 10.1126/science.aam9353 (cit. on p. 47).

[161] Anton N. Vetlugin et al. *"Anti-Hong-Ou-Mandel Effect with Entangled Photons"*. In: *arXiv:2105.05444 [quant-ph]* (May 2021). arXiv: 2105.05444 [quant-ph] (cit. on pp. 47, 50, 98).

[162] Christopher Gerry and Peter Knight. *Introductory Quantum Optics*. Cambridge: Cambridge University Press, 2004. DOI: 10.1017/CBO9780511791239. URL: https://www.cambridge.org/core/books/introductory-quantum-optics/B9866F1F40C45936A81D03AF7617C (visited on 07/10/2022) (cit. on p. 47).

[163] Daryl Achilles et al. *"Photon-Number-Resolving Detection Using Time-Multiplexing"*. In: *Journal of Modern Optics* 51.9-10 (June 2004), pp. 1499–1515. DOI: 10.1080/09500340408235288. URL: https://doi.org/10.1080/09500340408235288 (visited on 07/10/2022) (cit. on p. 48).

[164] Jan Provazník et al. *"Benchmarking Photon Number Resolving Detectors"*. In: *Optics Express* 28.10 (May 2020), pp. 14839–14849. DOI: 10.1364/OE.389619. URL: https://opg.optica.org/oe/abstract.cfm?uri=oe-28-10-14839 (visited on 07/10/2022) (cit. on p. 48).

[165] Simanraj Sadana et al. *"Near-100% Two-Photon-like Coincidence-Visibility Dip with Classical Light and the Role of Complementarity"*. In: *Physical Review A* 100.1 (July 2019), p. 013839. DOI: 10.1103/PhysRevA.100.013839 (cit. on p. 48).

[166] Nicolas Fabre et al. *The Hong-Ou-Mandel Experiment: From Photon Indistinguishability to Continuous Variables Quantum Computing*. June 2022. DOI: 10.48550/arXiv.2206.01518. arXiv: 2206.01518 [quant-ph] (cit. on p. 48).

[167] Toshiki Kobayashi et al. *"Frequency-Domain Hong-Ou-Mandel Interference"*. In: *Nature Photonics* 10.7 (July 2016), pp. 441–444. DOI: 10.1038/nphoton.2016.74. arXiv: 1601.00739. URL: http://arxiv.org/abs/1601.00739 (visited on 11/03/2019) (cit. on p. 49).

[168] Yoon-Ho Kim. *"Two-Photon Interference without Bunching Two Photons"*. In: *Physics Letters A* 315.5 (Sept. 2003), pp. 352–357. DOI: 10.1016/S0375-9601(03)01114-9. URL: http://www.sciencedirect.com/science/article/pii/S0375960103011149 (visited on 15/11/2018) (cit. on p. 49).

[169] R. C. Liu et al. *"Quantum Interference in Electron Collision"*. In: *Nature* 391.6664 (Jan. 1998), pp. 263–265. DOI: 10.1038/34611 (cit. on p. 49).

[170] E. Bocquillon et al. *"Coherence and Indistinguishability of Single Electrons Emitted by Independent Sources"*. In: *Science* 339.6123 (Mar. 2013), pp. 1054–1057. DOI: 10.1126/science.1232572. URL: https://www.science.org/doi/10.1126/science.1232572 (visited on 03/08/2022) (cit. on p. 49).

[171] V. Freulon et al. *"Hong-Ou-Mandel Experiment for Temporal Investigation of Single-Electron Fractionalization"*. In: *Nature Communications* 6.1 (Apr. 2015), p. 6854. DOI: 10.1038/ncomms7854. URL: https://www.nature.com/articles/ncomms7854 (visited on 03/08/2022) (cit. on p. 49).

[172] Yuan Liang Lim and Almut Beige. *"Generalized Hong–Ou–Mandel Experiments with Bosons and Fermions"*. In: *New Journal of Physics* 7 (July 2005), pp. 155–155. DOI: 10.1088/1367-2630/7/1/155 (cit. on p. 49).

[173] Alessandro Fedrizzi et al. *"Anti-Symmetrization Reveals Hidden Entanglement"*. In: *New Journal of Physics* 11.10 (Oct. 2009), p. 103052. DOI: 10.1088/1367-2630/11/10/103052. URL: http://stacks.iop.org/1367-2630/11/i=10/a=103052?key=crossref.add7c9c91107f1bc2624d1465a0437df (visited on 08/10/2018) (cit. on pp. 49, 51, 84, 107).

[174] Kaige Wang. *"Quantum Theory of Two-Photon Wavepacket Interference in a Beamsplitter"*. In: *Journal of Physics B: Atomic, Molecular and Optical Physics* 39.18 (Sept. 2006), R293–R324. DOI: 10.1088/0953-4075/39/18/R01. URL: http://stacks.iop.org/0953-4075/39/i=18/a=R01?key=crossref.0bf3638e0ffa5cc7e79fbd6ac13f64c4 (visited on 08/10/2018) (cit. on pp. 50, 51, 54, 84, 107, 120).

[175] H. P. Specht et al. *"Shaping the Phase of a Single Photon"*. In: *Nature Photonics* 3.8 (Aug. 2009), pp. 469–472. DOI: 10.1038/nphoton.2009.115. arXiv: 0905.4583 (cit. on p. 50).

[176] Paul G. Kwiat, Aephraim M. Steinberg and Raymond Y. Chiao. *"Observation of a "Quantum Eraser": A Revival of Coherence in a Two-Photon Interference Experiment"*. In: *Physical Review A* 45.11 (June 1992), pp. 7729–7739. DOI: 10.1103/PhysRevA.45.7729 (cit. on pp. 50, 84).

[177] S. P. Walborn et al. *"Multimode Hong-Ou-Mandel Interference"*. In: *Physical Review Letters* 90.14 (Apr. 2003). DOI: 10.1103/PhysRevLett.90.143601. URL: https://link.aps.org/doi/10.1103/PhysRevLett.90.143601 (visited on 19/10/2018) (cit. on pp. 50, 84).

[178] Andreas Eckstein and Christine Silberhorn. *"Broadband Frequency Mode Entanglement in Waveguided Parametric Downconversion"*. In: *Optics Letters* 33.16 (Aug. 2008), p. 1825. DOI: 10.1364/OL.33.001825. URL: https://opg.optica.org/abstract.cfm?URI=ol-33-16-1825 (visited on 20/06/2022) (cit. on pp. 50, 58).

[179] C. Olindo et al. *"Hong-Ou-Mandel Interferometer with Cavities: Theory"*. In: *Physical Review A* 73.4 (Apr. 2006), p. 043806. DOI: 10.1103/PhysRevA.73.043806 (cit. on pp. 50, 53, 84, 86, 107, 113).

[180] Ayman F. Abouraddy et al. *"Quantum-Optical Coherence Tomography with Dispersion Cancellation"*. In: *Physical Review A* 65.5 (May 2002), p. 053817. DOI: 10.1103/PhysRevA.65.053817 (cit. on pp. 50, 84, 107).

[181] Magued B. Nasr et al. *"Demonstration of Dispersion-Canceled Quantum-Optical Coherence Tomography"*. In: *Physical Review Letters* 91.8 (Aug. 2003), p. 083601. DOI: 10.1103/PhysRevLett.91.083601 (cit. on pp. 50, 84, 107).

[182] T. R. Judge and P. J. Bryanston-Cross. *"A Review of Phase Unwrapping Techniques in Fringe Analysis"*. In: *Optics and Lasers in Engineering* 21.4 (Jan. 1994), pp. 199–239. DOI: 10.1016/0143-8166(94)90073-6. URL: https://www.sciencedirect.com/science/article/pii/0143816694900736 (visited on 07/10/2022) (cit. on p. 50).

[183] Dr Rüdiger Paschotta. *Pockels Cells*. URL: https://www.rp-photonics.com/pockels_cells.html (visited on 07/10/2022) (cit. on p. 52).

[184] J. D. Franson. *"Bell Inequality for Position and Time"*. In: *Physical Review Letters* 62.19 (May 1989), pp. 2205–2208. DOI: 10.1103/PhysRevLett.62.2205. URL: https://link.aps.org/doi/10.1103/PhysRevLett.62.2205 (visited on 04/09/2022) (cit. on p. 53).

[185] P. H. Tomlins and R. K. Wang. *"Theory, Developments and Applications of Optical Coherence Tomography"*. In: *Journal of Physics D: Applied Physics* 38.15 (July 2005), pp. 2519–2535. DOI: 10.1088/0022-3727/38/15/002. URL: https://doi.org/10.1088/0022-3727/38/15/002 (visited on 16/09/2021) (cit. on p. 54).

[186] J. Lavoie, R. Kaltenbaek and K. J. Resch. *"Quantum-Optical Coherence Tomography with Classical Light"*. In: *Optics Express* 17.5 (Mar. 2009), pp. 3818–3826. DOI: 10.1364/OE.17.003818 (cit. on p. 54).

[187] Tomohiro Shirai and Ari T. Friberg. *"Intensity-Interferometric Spectral-Domain Optical Coherence Tomography with Dispersion Cancellation"*. In: *JOSA A* 31.2 (Feb. 2014), pp. 258–263. DOI: 10.1364/JOSAA.31.000258 (cit. on p. 54).

[188] Tomohiro Shirai and Ari T. Friberg. *"Practical Implementation of Spectral-Intensity Dispersion-Canceled Optical Coherence Tomography with Artifact Suppression"*. In: *Journal of Optics* 20.4 (Mar. 2018), p. 045610. DOI: 10.1088/2040-8986/aab245 (cit. on p. 54).

[189] R. Kaltenbaek et al. *"Quantum-Inspired Interferometry with Chirped Laser Pulses"*. In: *Nature Physics* 4.11 (Nov. 2008), pp. 864–868. DOI: 10.1038/nphys1093 (cit. on p. 54).

[190] Masayuki Okano et al. *"Dispersion Cancellation in High-Resolution Two-Photon Interference"*. In: *Physical Review A* 88.4 (Oct. 2013), p. 043845. DOI: 10.1103/PhysRevA.88.043845. URL: https://link.aps.org/doi/10.1103/PhysRevA.88.043845 (visited on 01/09/2022) (cit. on p. 58).

[191] Zeudi Mazzotta et al. *"High-Order Dispersion Effects in Two-Photon Interference"*. In: *Physical Review A* 94.6 (Dec. 2016), p. 063842. DOI: 10.1103/PhysRevA.94.063842. URL: https://link.aps.org/doi/10.1103/PhysRevA.94.063842 (visited on 01/09/2022) (cit. on pp. 58, 60).

[192] Georges Sagnac. *"L'éther Lumineux Démontré"*. In: *Comptes rendus hebdomadaires des séances de l'Académie des sciences* 157 (1913), pp. 708–710 (cit. on pp. 75, 76, 83).

[193] Grigorii B. Malykin. *"The Sagnac Effect: Correct and Incorrect Explanations"*. In: *Physics-Uspekhi* 43.12 (Dec. 2000), p. 1229. DOI: 10.1070/PU2000v043n12ABEH000830. URL: https://iopscience.iop.org/article/10.1070/PU2000v043n12ABEH000830/meta (visited on 13/09/2022) (cit. on pp. 75, 77).

[194] E. J. Post. *"Sagnac Effect"*. In: *Reviews of Modern Physics* 39.2 (Apr. 1967), pp. 475–493. DOI: 10.1103/RevModPhys.39.475 (cit. on pp. 75, 76, 83).

[195] Angelo Tartaglia and Matteo Luca Ruggiero. *"The Sagnac Effect and Pure Geometry"*. In: *American Journal of Physics* 83.5 (May 2015), pp. 427–432. DOI: 10.1119/1.4904319. URL: http://aapt.scitation.org/doi/10.1119/1.4904319 (visited on 17/06/2022) (cit. on p. 76).

[196]   S. A. Werner, J. -L. Staudenmann and R. Colella. *"Effect of Earth's Rotation on the Quantum Mechanical Phase of the Neutron"*. In: *Physical Review Letters* 42.17 (Apr. 1979), pp. 1103–1106. DOI: 10.1103/PhysRevLett.42.1103 (cit. on pp. 76, 91, 96, 100, 108).

[197]   H. J. Arditty and H. C. Lefèvre. *"Sagnac Effect in Fiber Gyroscopes"*. In: *Optics Letters* 6.8 (Aug. 1981), pp. 401–403. DOI: 10.1364/OL.6.000401. URL: https://www.osapublishing.org/ol/abstract.cfm?uri=ol-6-8-401 (cit. on pp. 77, 83).

[198]   R. Anderson, H. R. Bilger and G. E. Stedman. *""Sagnac" Effect: A Century of Earth-rotated Interferometers"*. In: *American Journal of Physics* 62.11 (Nov. 1994), pp. 975–985. DOI: 10.1119/1.17656. URL: https://aapt.scitation.org/doi/10.1119/1.17656 (visited on 12/09/2022) (cit. on p. 77).

[199]   Karl Ulrich Schreiber and Jon-Paul R. Wells. *"Invited Review Article: Large Ring Lasers for Rotation Sensing"*. In: *Review of Scientific Instruments* 84.4 (Apr. 2013), p. 041101. DOI: 10.1063/1.4798216. URL: https://aip.scitation.org/doi/full/10.1063/1.4798216 (visited on 16/09/2022) (cit. on p. 77).

[200]   Di Virgilio and Angela D. V. *"Sagnac Gyroscopes and the GINGER Project"*. In: *Frontiers in Astronomy and Space Sciences* 7 (2020). DOI: 10.3389/fspas.2020.00049. URL: https://www.frontiersin.org/articles/10.3389/fspas.2020.00049/full (visited on 27/04/2021) (cit. on p. 77).

[201]   A A Michelson and Henry G Gale. *"The Effect of the Earth's Rotation on the Velocity of Light Part II"*. In: *Astrophysical Journal* LXI.3 (1925), pp. 140–145 (cit. on p. 77).

[202]   Angelo Tartaglia et al. *"Testing General Relativity by Means of Ring Lasers"*. In: *The European Physical Journal Plus* 132.2 (Feb. 2017), p. 73. DOI: 10.1140/epjp/i2017-11372-5. URL: https://doi.org/10.1140/epjp/i2017-11372-5 (visited on 12/09/2022) (cit. on pp. 77, 96, 108).

[203]   M. O. Scully, M. S. Zubairy and M. P. Haugan. *"Proposed Optical Test of Metric Gravitation Theories"*. In: *Physical Review A* 24.4 (Oct. 1981), pp. 2009–2016. DOI: 10.1103/PhysRevA.24.2009. URL: https://link.aps.org/doi/10.1103/PhysRevA.24.2009 (visited on 13/10/2022) (cit. on pp. 77, 96, 108).

[204]   F. Bosi et al. *"Measuring Gravitomagnetic Effects by a Multi-Ring-Laser Gyroscope"*. In: *Physical Review D* 84.12 (Dec. 2011), p. 122002. DOI: 10.1103/PhysRevD.84.122002. URL: https://link.aps.org/doi/10.1103/PhysRevD.84.122002 (visited on 17/06/2022) (cit. on p. 77).

[205]   Angela D. V. Di Virgilio et al. *"Underground Sagnac Gyroscope with Sub-Prad/s Rotation Rate Sensitivity: Toward General Relativity Tests on Earth"*. In: *Physical Review Research* 2.3 (Sept. 2020), p. 032069. DOI: 10.1103/PhysRevResearch.2.032069. URL: https://link.aps.org/doi/10.1103/PhysRevResearch.2.032069 (visited on 12/09/2022) (cit. on p. 77).

[206]   A. Tartaglia et al. *"How to Use the Sun–Earth Lagrange Points for Fundamental Physics and Navigation"*. In: *General Relativity and Gravitation* 50.1 (Dec. 2017), p. 9. DOI: 10.1007/s10714-017-2332-6. URL: https://doi.org/10.1007/s10714-017-2332-6 (visited on 12/09/2022) (cit. on p. 77).

[207]   Angelo Tartaglia. *"Detecting the Angular Momentum of the Galactic Dark Halo"*. In: *Advances in Space Research* 64.2 (July 2019), pp. 545–550. DOI: 10.1016/j.asr.2019.04.031. URL: https://www.sciencedirect.com/science/article/pii/S0273117719303072 (visited on 12/09/2022) (cit. on p. 77).

[208]   Stephen A. Fulling. *"Nonuniqueness of Canonical Field Quantization in Riemannian Space-Time"*. In: *Physical Review D* 7.10 (May 1973), pp. 2850–2862. DOI: 10.1103/PhysRevD.7.2850 (cit. on p. 83).

[209]   Jan Kohlrus et al. *"Quantum Communications and Quantum Metrology in the Spacetime of a Rotating Planet"*. In: *EPJ Quantum Technology* 4.1 (Dec. 2017), p. 7. DOI: 10.1140/epjqt/s40507-017-0061-0 (cit. on pp. 83, 96, 108).

[210]   Roy Barzel et al. *"Observer Dependence of Photon Bunching: The Influence of the Relativistic Redshift on Hong-Ou-Mandel Interference"*. In: *Physical Review D* 105.10 (May 2022), p. 105016. DOI: 10.1103/PhysRevD.105.105016 (cit. on p. 83).

[211]   D. M. Shupe. *"Thermally Induced Nonreciprocity in the Fiber-Optic Interferometer"*. In: *Applied Optics* 19.5 (Mar. 1980), pp. 654–655. DOI: 10.1364/AO.19.000654 (cit. on pp. 90, 100).

[212]   T. L. Gustavson, P. Bouyer and M. A. Kasevich. *"Precision Rotation Measurements with an Atom Interferometer Gyroscope"*. In: *Physical Review Letters* 78.11 (Mar. 1997), pp. 2046–2049. DOI: 10.1103/PhysRevLett.78.2046 (cit. on pp. 91, 96, 100, 108).

[213]   David Edward Bruschi, Ivette Fuentes and Jorma Louko. *"Voyage to Alpha Centauri: Entanglement Degradation of Cavity Modes Due to Motion"*. In: *Physical Review D* 85.6 (Mar. 2012), p. 061701. DOI: 10.1103/PhysRevD.85.061701 (cit. on pp. 91, 108).

[214]   Nicolai Friis et al. *"Motion Generates Entanglement"*. In: *Physical Review D* 85.8 (Apr. 2012). DOI: 10.1103/PhysRevD.85.081701. URL: https://link.aps.org/doi/10.1103/PhysRevD.85.081701 (visited on 22/04/2019) (cit. on pp. 91, 108).

[215]   Paul M. Alsing and Ivette Fuentes. *"Observer Dependent Entanglement"*. In: *Classical and Quantum Gravity* 29.22 (Nov. 2012), p. 224001. DOI: 10.1088/0264-9381/29/22/224001. arXiv: 1210.2223. URL: http://arxiv.org/abs/1210.2223 (visited on 22/04/2019) (cit. on pp. 91, 108).

[216]   Neil Ashby. *"Relativity in the Global Positioning System"*. In: *Living Reviews in Relativity* 6.1 (Jan. 2003), p. 1. DOI: 10.12942/lrr-2003-1. URL: https://doi.org/10.12942/lrr-2003-1 (visited on 14/10/2022) (cit. on p. 96).

[217]   Qasem Exirifard, Eric Culf and Ebrahim Karimi. *"Towards Communication in a Curved Spacetime Geometry"*. In: *Communications Physics* 4.1 (July 2021), pp. 1–6. DOI: 10.1038/s42005-021-00671-8. URL: http://www.nature.com/articles/s42005-021-00671-8 (visited on 04/10/2022) (cit. on pp. 96, 108).

[218] Freeman Dyson. *"The Search for Extraterrestrial Technology"*. In: *Perspectives in Modern Physics. Essays in Honor of Hans A. Bethe on the Occasion of His 60th Birthday.* Ed. by Robert Eugene Marshak. 1966, pp. 641–655. URL: https://ui.adsabs.harvard. edu/abs/1966pmp..book..641D (visited on 09/10/2022) (cit. on p. 97).

[219] Rongkuo Zhao et al. *"Rotational Quantum Friction"*. In: *Physical Review Letters* 109.12 (Sept. 2012), p. 123604. DOI: 10.1103/PhysRevLett.109.123604. URL: https://link.aps. org/doi/10.1103/PhysRevLett.109.123604 (visited on 19/09/2022) (cit. on p. 98).

[220] W. B. Bonnor and B. R. Steadman. *"Exact Solutions of the Einstein-Maxwell Equations with Closed Timelike Curves"*. In: *General Relativity and Gravitation* 37.11 (Nov. 2005), pp. 1833–1844. DOI: 10.1007/s10714-005-0163-3. URL: https://doi.org/10.1007/s10714- 005-0163-3 (visited on 11/09/2022) (cit. on p. 98).

[221] James C. Keith. *"Gravitational Radiation and Aberrated Centripetal Force Reactions in Relativity Theory"*. In: *Revista Mexicana de Física* 12.1 (Jan. 1963), pp. 1–25. URL: https://rmf.smf.mx/ojs/index.php/rmf/article/view/836 (visited on 27/09/2022) (cit. on p. 98).

[222] J. K. Fremerey. *"Significant Deviation of Rotational Decay from Theory at a Reliability in the ${10}\hat{ }{\ensuremath{-}12}$ ${\mathrm{sec}}\hat{ }{\ensuremath{-}1}$ Range"*. In: *Physical Review Letters* 30.16 (Apr. 1973), pp. 753–757. DOI: 10.1103/PhysRevLett. 30.753. URL: https://link.aps.org/doi/10.1103/PhysRevLett.30.753 (visited on 27/09/2022) (cit. on p. 98).

[223] M. Reinhardt and A. Rosenblum. *"The Nonexistence of a Relativistic Effect Proposed by Keith"*. In: *Lettere al Nuovo Cimento (1971-1985)* 6.5 (Feb. 1973), pp. 189–191. DOI: 10.1007/BF02827274. URL: https://doi.org/10.1007/BF02827274 (visited on 28/09/2022) (cit. on p. 98).

[224] C. Clivati et al. *"Large-Area Fiber-Optic Gyroscope on a Multiplexed Fiber Network"*. In: *Optics Letters* 38.7 (Apr. 2013), pp. 1092–1094. DOI: 10.1364/OL.38.001092 (cit. on p. 100).

[225] Christopher Hilweg et al. *"Gravitationally Induced Phase Shift on a Single Photon"*. In: *New Journal of Physics* 19.3 (Mar. 2017), p. 033028. DOI: 10.1088/1367-2630/ aa638f. URL: https://doi.org/10.1088%5C%2F1367-2630%5C%2Faa638f (visited on 09/06/2020) (cit. on p. 100).

[226] Andrei Khrennikov. *"Quantum Versus Classical Entanglement: Eliminating the Issue of Quantum Nonlocality"*. In: *Foundations of Physics* 50.12 (Dec. 2020), pp. 1762–1780. DOI: 10.1007/s10701-020-00319-7. URL: https://doi.org/10.1007/s10701-020-00319-7 (visited on 31/01/2023) (cit. on p. 103).

[227] Hai-Woong Lee and Jaewan Kim. *"Quantum Teleportation and Bell's Inequality Using Single-Particle Entanglement"*. In: *Physical Review A* 63.1 (Dec. 2000), p. 012305. DOI: 10.1103/PhysRevA.63.012305. URL: https://link.aps.org/doi/10.1103/PhysRevA.63. 012305 (visited on 31/01/2023) (cit. on p. 103).

[228] S. Adhikari et al. *"Swapping Path-Spin Intraparticle Entanglement onto Spin-Spin Interparticle Entanglement"*. In: *EPL (Europhysics Letters)* 89.1 (Jan. 2010). Comment: 5 pages, 1 Figure, p. 10005. DOI: 10.1209/0295-5075/89/10005. arXiv: 0909.0425 [quant-ph]. URL: http://arxiv.org/abs/0909.0425 (visited on 31/01/2023) (cit. on p. 103).

[229] Ke-Xun Sun et al. *"Sagnac Interferometer for Gravitational-Wave Detection"*. In: *Physical Review Letters* 76.17 (Apr. 1996), pp. 3053–3056. DOI: 10.1103/PhysRevLett.76. 3053. URL: https://link.aps.org/doi/10.1103/PhysRevLett.76.3053 (visited on 30/09/2022) (cit. on p. 103).

[230] Tobias Eberle et al. *"Quantum Enhancement of the Zero-Area Sagnac Interferometer Topology for Gravitational Wave Detection"*. In: *Physical Review Letters* 104.25 (June 2010), p. 251102. DOI: 10.1103/PhysRevLett.104.251102. URL: https://link.aps.org/doi/10.1103/PhysRevLett.104.251102 (visited on 30/09/2022) (cit. on p. 103).

[231] Barry C Barish. *"THE SCIENCE AND DETECTION OF GRAVITATIONAL WAVES"*. Talk. Lake Louise Winter Insitute, University of Alberta, Feb. 2000. URL: https://labcit.ligo.caltech.edu/~BCBAct/talks00/talks00.html (cit. on pp. 103, 104).

[232] *LIGO's Interferometer*. URL: https://www.ligo.caltech.edu/page/ligos-ifo (visited on 30/09/2022) (cit. on p. 104).

[233] E. Schrödinger. *"Are There Quantum Jumps? Part II"*. In: *The British Journal for the Philosophy of Science* 3.11 (Nov. 1952), pp. 233–242. DOI: 10.1093/bjps/III.11.233. URL: https://www.journals.uchicago.edu/doi/10.1093/bjps/III.11.233 (visited on 07/10/2022) (cit. on p. 105).

[234] Anthony J. Brady and Stav Haldar. *"Frame Dragging and the Hong-Ou-Mandel Dip: Gravitational Effects in Multiphoton Interference"*. In: *Physical Review Research* 3.2 (Apr. 2021), p. 023024. DOI: 10.1103/PhysRevResearch.3.023024. URL: https://link.aps.org/doi/10.1103/PhysRevResearch.3.023024 (visited on 25/07/2022) (cit. on p. 108).

[235] Roy Barzel et al. *Gravitationally Induced Entanglement Dynamics of Photon Pairs and Quantum Memories*. Sept. 2022. DOI: 10.48550/arXiv.2209.02099. arXiv: 2209.02099 [gr-qc, physics:quant-ph]. URL: http://arxiv.org/abs/2209.02099 (visited on 13/10/2022) (cit. on p. 108).

[236] Philip Ball [@philipcball]. *Let's Hear It for John Bell Though. I Mean Christ, Really. It Was Thanks to Him That Quantum Foundations Became Experimental Physics and Not Philosophy. (Nothing against Philosophy, but It's Good to Get Answers Sometimes.)* Tweet. Oct. 2022. URL: https://web.archive.org/web/20221013115914/https://twitter.com/philipcball/status/1577341235307679744 (visited on 13/10/2022) (cit. on p. 108).

[237] J. S. Bell. *"On the Einstein Podolsky Rosen Paradox"*. In: *Physics Physique Fizika* 1.3 (Nov. 1964), pp. 195–200. DOI: 10.1103/PhysicsPhysiqueFizika.1.195. URL: https://link.aps.org/doi/10.1103/PhysicsPhysiqueFizika.1.195 (visited on 01/05/2019) (cit. on p. 109).

[238] John S. Bell. *"On the Problem of Hidden Variables in Quantum Mechanics"*. In: *Reviews of Modern Physics* 38.3 (July 1966), pp. 447–452. DOI: 10.1103/RevModPhys.38.447. URL: https://link.aps.org/doi/10.1103/RevModPhys.38.447 (visited on 01/05/2019) (cit. on p. 109).

[239] John F. Clauser et al. *"Proposed Experiment to Test Local Hidden-Variable Theories"*. In: *Physical Review Letters* 23.15 (Oct. 1969), pp. 880–884. DOI: 10.1103/PhysRevLett.23.880. URL: https://link.aps.org/doi/10.1103/PhysRevLett.23.880 (visited on 30/04/2019) (cit. on p. 109).

[240] Albert Abraham Michelson. *Light Waves and Their Uses*. University of Chicago Press, 1903. URL: https://en.wikisource.org/wiki/Light_waves_and_their_uses (cit. on p. 109).

[241] F. K. Richtmyer. *"The Romance of the Next Decimal Place"*. In: *Science* 75.1931 (Jan. 1932), pp. 1–5. DOI: 10.1126/science.75.1931.1. URL: http://www.science.org/doi/10.1126/science.75.1931.1 (visited on 12/10/2022) (cit. on p. 109).

[242] George Marx. *"The Neutrinos Grow Up"*. In: *Nuclear Physics B - Proceedings Supplements*. Neutrino 94 38.1 (Jan. 1995), pp. 518–523. DOI: 10.1016/0920-5632(94)00786-U. URL: https://www.sciencedirect.com/science/article/pii/092056329400786U (visited on 14/10/2022) (cit. on p. 110).